

## ABSTRACT

Title of Document: BIOORGANIC CHEMISTRY OF  
PRODIGIOSENES: ANION TRANSPORT,  
BASICITY, CONFORMATION AND  
G-QUADRUPLEX DNA BINDING.

Soumya Rastogi, Doctor of Philosophy, 2015

Directed By: Professor Jeffery T. Davis,  
Department of Chemistry and Biochemistry

Naturally occurring prodigiosenes are produced by microorganisms such as *Streptomyces* and *Serratia marcescens*. Prodigiosenes are fascinating for their wide range of biological activities in the form of anti-cancer, immunosuppressive, and antimicrobial agents. Some of the analogs, such as prodigiosin, are currently undergoing preclinical and clinical trials. Despite such widespread interest, the origin of prodigiosin's biological activity has not been established unambiguously. Based on biological studies, it is known that prodigiosin plays a physiologically relevant role and has several cellular targets. The work described in this thesis explores some of the chemistry that may help explain prodigiosenes' biological activity.

A new series of analogs of prodigiosin bearing an additional methyl and a carbonyl group at the C-ring were evaluated as transmembrane anion transporters. The effect of C-ring modifications in these new prodigiosenes on their basicity, transmembrane anion transport ability and their *in vitro* anticancer activity was

assessed. The ability of prodigiosenes to facilitate co-transport of  $\text{H}^+\text{Cl}^-$  leading to alteration of intracellular pH, and catalyze anion exchange across lipid bilayers has been proposed to be one of the cause of its anti-cancer activity. It has been suggested that the prodigiosenes bind anions in their protonated state at physiological pH. Prodigiosene analogs with modified B-ring demonstrated that the electronic nature of the substituent on the B-ring influences the basicity of these analogs, and consequently, their anion transport efficiency is also affected.

A study of the conformations of prodigiosin and its analogs was performed to learn about how the ligands orient in different solvents. This information could potentially link the preferred conformational states of these compounds and their observed biological activities. Lastly, we confirmed that prodigiosin binds at the 3' end of a G-quadruplex DNA. The results from this chapter are significant as they widen the scope of developing prodigiosenes as G-quadruplex binding ligands or telomerase inhibiting agents. Further, they lead the way to revealing another possible mechanism to explain the anti-cancer activity of prodigiosenes.

BIOORGANIC CHEMISTRY OF PRODIGIOSENES: ANION TRANSPORT,  
BASICITY, CONFORMATION AND G-QUADRUPLEX DNA BINDING.

By

Soumya Rastogi

Thesis submitted to the Faculty of the Graduate School of the  
University of Maryland, College Park, in partial fulfillment  
of the requirements for the degree of  
Doctor of Philosophy  
2015

Advisory Committee:  
Professor Jeffery T. Davis, Chair  
Professor Marco Colombini  
Professor Daniel E. Falvey  
Professor Lyle Isaacs  
Associate Professor Herman Sintim

© Copyright by  
Soumya Rastogi  
2015

## DEDICATION

To my parents.

## ACKNOWLEDGEMENTS

I would like to thank Professor Jeffery T. Davis for his invaluable guidance, enthusiasm, patience and constant support. I have learnt so much from you. Thank you for maintaining an environment that encouraged ideas and opportunities for professional development. As an international student, sometimes the learning curves were steep, thank you for keeping patience and your sense of humor. I would like to thank my committee members for their support, encouragement and valuable input during the course of my degree. I am especially thankful to Professor Herman Sintim for his insightful discussions, guidance and useful suggestions on research and career opportunities. I would also like to thank Professor Marco Colombini for agreeing to be the Dean's representative on my committee.

I thank our collaborators - Professor Alison Thompson, Dr. Estelle Marchal from Dalhousie University, Canada and Ms. Maria Garcia Valverde, Professor Roberto Quesada from the University of Burgos, Spain for their enthusiasm and willingness to exchange and work on ideas. A sincere thanks to Dr. Yiu-Fai Lam and Dr. Yinde Wang for helping out with NMR and the instruments. Thank you Dr. Lam for your kindness and enjoyable conversations. Thank you Dr. Daoning Zhang for doing a wonderful job with the DNA project. It was a pleasure working with you.

I am thankful to the business and graduate office for their help and taking care of things effortlessly. Thank you Bill Griffin and Levi Gayatao of Chemistry Stores and Chemistry Receiving for your cheerful conduct and willingness to help.

A special and warm thanks goes out to the past and present Davis group members. Thank you Yomi, Will, Monique and Jin for making me feel welcome into

the group when I first started out. It really paved the way for the remaining journey. Thanks Will for the encouragement and helpful suggestions. Thank you Yomi for being my friend, for teaching me all about liposomes and for being somebody I can always turn to. I thank the post-docs – Brian and Ning for engaging discussions. Thank you Gretchen for the ‘group lunches’ and the elusive happy-hours. Thank you Brooke, Luke, Taylor, Keith and Songjun for making it fun working in the lab.

Graduate school just won’t be the same without you Karina. Thank you for making me laugh with your incredible impersonations and simply, for always being there. Thank you Anna and Romina for being such wonderful friends. Thanks Roger, Shiva, Mani, Srav and Mr. M for being such excellent friends and good listeners.

Lastly, I would like to thank my parents-in-law for having so much confidence and faith in me. Adapting a quote from one of my favorite authors, I feel thanking my parents, my brother Soumitra and my husband Rishabh would be like giving elementary school sticker prizes to people who actually deserve the Nobel. I am thankful for having the greatest support system in the world. Thank you Pa for never letting me lose my focus, for your unconditional love and immeasurable support. Thank you Ma for laughing at all my bad jokes, for being my strength and my voice of reason. Thank you Bhai for being the best-est brother. Rishabh, you have been a friend, a pillar of strength and a confidant all these years. Life is a happy circle with you around. Thank you for tirelessly and unconditionally supporting me in all my antics.

## TABLE OF CONTENTS

|   |           |
|---|-----------|
| List of Tables .....  | x         |
| List of Figures .....   | xi        |
| <b>Chapter 1: A Background on Prodigiosenes .....</b>   | <b>1</b>  |
| <b>BACKGROUND:</b>  |           |
| 1.1 Introduction.....   | 1         |
| 1.2 Thesis Organization .....   | 2         |
| 1.3 Introduction on Prodigiosenes .....   | 6         |
| 1.4 Proposed Mechanisms for Anti-Cancer Properties of Prodigiosenes .....   | 8         |
| 1.4.1 Oxidative DNA Cleavage by Prodigiosene•Cu <sup>2+</sup> Complexes .....   | 8         |
| 1.4.2 H <sup>+</sup> /Cl <sup>-</sup> Co-Transport Triggers Apoptosis .....   | 9         |
| 1.4.2.1 Prodigiosenes can Inhibit Proton Pump Activity.....   | 10        |
| 1.4.2.2 H <sup>+</sup> Cl <sup>-</sup> Co-Transport by Prodigiosenes can Lead to Apoptosis.....   | 13        |
| 1.5 Prodigiosenes and Transmembrane Anion Transport.....  | 16        |
| 1.5.1 Anti-Cancer Activity Correlates with the Anion Transport Rates.....   | 19        |
| 1.5.2 Prodigiosin Catalyzes Anion Exchange Across Bilayer .....   | 20        |
| 1.5.3 Prodigiosin Facilitates Transmembrane Movement of HCO <sub>3</sub> <sup>-</sup> .....   | 23        |
| 1.5.4 Prodigiosin <b>1</b> can Target Anions Other than Cl <sup>-</sup> .....   | 25        |
| 1.6 Some Examples of Gating Anion Transport.....  | 27        |
| 1.6.1 Gating Influenced by Conformational Changes in ClC Channel.....   | 27        |
| 1.6.2 Photoresponsive Ion Gating.....   | 28        |
| 1.6.3 Voltage-Gated Anion Transport .....   | 30        |
| 1.6.4 Inhibition of Ion Activity by Formation of Inclusion Complexes .....  | 32        |
| 1.6.5 Effect of Intramolecular Hydrogen Bonding on Anion Transport<br>Property.....   | 36        |
| 1.6.6 Ion-Gating in Nanochannels .....  | 38        |
| 1.6.7 pH Tunable Thiosquaramides as Anion Transporters .....  | 41        |
| 1.7 Summary.....  | 44        |
| <b>Chapter 2: Synthetic Prodigiosenes and the Influence of C-Ring Substitution on<br/>Transmembrane Chloride Transport and Basicity .....</b> | <b>46</b> |
| <b>BACKGROUND:</b>  |           |
| 2.1 Introduction.....   | 46        |
| 2.2 Previous Work with C-Ring Modified Prodigiosenes .....  | 47        |
| 2.2.1 Earlier Examples of C-Ring Modified Prodigiosenes .....   | 48        |



|   |  |    |
|---|--|----|
| 2.2.1.1   | Boger's Prodigiosene <b>25</b> .....   | 48 |
| 2.2.1.2   | Prodigiosin 25-C .....   | 49 |
| 2.2.1.3   | Indole-Based Prodigiosenes by Wasserman .....  | 50 |
| 2.2.1.4   | C-Ring Functionalized Prodigiosenes by Thompson .....  | 51 |
| 2.2.2   | Rationale for Studying Influence of C-Ring Substitution on Transmembrane Chloride Transport and Basicity .....   | 52 |
| <b>RESULTS:</b>   |  |    |
| 2.3   | Study of Transmembrane Anion Transport Activity of Prodigiosin <b>1</b> , Ester Analog <b>2</b> and <b>24</b> .....  | 53 |
| 2.3.1   | EC <sub>50</sub> Values for Cl <sup>-</sup> /NO <sub>3</sub> <sup>-</sup> Exchange Process Demonstrate the Effect of C-Ring Modifications in Prodigiosenes ..... | 54 |
| 2.3.2   | Ester Chain Length Affects the Ability to Transport Cl <sup>-</sup> Across Bilayers .....  | 57 |
| 2.4   | <sup>1</sup> H NMR Competition Experiment Proves that Prodigiosin <b>1</b> is More Basic than Ester Analog <b>2e</b> .....                                       | 63 |
| 2.5   | Determination of pK <sub>a</sub> of Ester Analog <b>2f</b> and Prodigiosin <b>1</b> .....  | 66 |
| 2.6   | Transmembrane Anion Transport as a Function of pH .....  | 68 |
| 2.7   | <i>In vitro</i> Anticancer Activity of C-Ring Functionalized Prodigiosenes .....   | 70 |
| 2.8   | Conclusions .....  | 72 |
| <b>Chapter 3: Influence of B-Ring Modifications on Proton Affinity, Transmembrane Anion Transport and Anti-Cancer Properties of Synthetic Prodigiosenes</b> ..... |  |    |
| <b>BACKGROUND:</b>  |  |    |
| 3.1   | Introduction .....   | 74 |
| 3.2   | Earlier Work with B-Ring Modified Prodigiosenes .....  | 75 |
| 3.2.1   | Rationale for Studying the Anion Transport Activity by B-Ring Modified Aryl Prodigiosenes .....  | 76 |
| 3.2.2   | Examples of Previous B-Ring Modified Prodigiosenes .....   | 78 |
| 3.2.2.1   | Desmethoxyprodigiosin by Boger .....   | 78 |
| 3.2.2.2   | Sessler's B-Ring Modified Prodigiosene .....   | 80 |
| 3.2.2.3   | PNU-156804 by D'Alessio .....  | 80 |
| <b>RESULTS:</b>   |  |    |
| 3.3   | Novel Phenyl Analogs <b>3</b> and a Comparison of their Basicity .....   | 81 |
| 3.3.1   | Determination of Apparent pK <sub>a</sub> Values for Synthetic Prodigiosenes .....   | 82 |
| 3.4   | Correlation Between Anion Transport Rates and Transporter Basicity .....   | 85 |
| 3.5   | <i>In Vitro</i> Anti-Cancer Properties .....   | 88 |
| 3.6   | Conclusions .....  | 91 |

|  |            |
|--|------------|
| <b>Chapter 4: Conformations and Anion Binding Properties of Prodigiosenes .....</b>                        | <b>93</b>  |
| <b>BACKGROUND:</b>   |            |
| 4.1 Introduction.....  | 93         |
| 4.2 Previous Work on Conformations of Prodigiosenes.....   | 94         |
| 4.2.1 Work with $\alpha$ -Conformation by McNab.....   | 95         |
| 4.2.2 Kinetics of $\alpha,\beta$ -Rotamer Interconversion by Rizzo .....                                   | 96         |
| 4.2.3 Conformational Analysis of Prodigiosene-Anion Complexes by Quesada.....                              | 99         |
| <b>RESULTS:</b>  |            |
| 4.3 Using NH Protons to Analyze Anion Binding Patterns in $\alpha$ and $\beta$ Isomers .....               | 103        |
| 4.3.1 NMR Titrations Reveal $\alpha,\beta$ Conformations of Phenyl Analog <b>3b</b> .....                  | 104        |
| 4.3.2 NOESY Data Shows Presence of $\alpha$ Conformation in CDCl <sub>3</sub> Solution.                    | 106        |
| 4.3.3 NH Protons of Prodigiosin <b>1</b> and Ester <b>2e</b> Reveal Anion Binding Patterns.....            | 108        |
| 4.4 Evidence for CH $\cdots$ Anion Hydrogen-Bonding by $\alpha$ -Isomer of Prodigiosenes .....             | 113        |
| 4.4.1 CH Hydrogen Assisted Anion Binding by Tambjamines.....   | 114        |
| 4.4.2 The $\alpha$ -H1" Hydrogen on Prodigiosenes <b>1</b> and <b>2e</b> Binds Anions.....                 | 115        |
| 4.5 Factors Affecting $\alpha/\beta$ Conformational Ratio .....  | 120        |
| 4.5.1 Anions Affect the $\alpha/\beta$ Conformational Ratio.....   | 120        |
| 4.5.1.1 Binding Energies of $\alpha$ and $\beta$ Conformations of <b>2e</b> •HCl.....                      | 123        |
| 4.5.2 Water Influences Population of $\alpha$ Isomer in Solution.....                                      | 125        |
| 4.6 Conclusions.....   | 130        |
| <b>Chapter 5: Prodigiosin as a G-Quadruplex DNA Binding Ligand .....</b>                                   | <b>133</b> |
| <b>BACKGROUND:</b>   |            |
| 5.1 Introduction.....  | 133        |
| 5.2 A background on G-Quadruplex DNA.....  | 133        |
| 5.2.1 Examples of G-Quadruplex Binding Ligands.....  | 135        |
| 5.3 Characterizing Ligand-Quadruplex Interactions.....   | 138        |
| 5.3.1 UV-vis Spectroscopy .....  | 138        |
| 5.3.2 Circular Dichroism.....  | 140        |
| 5.3.3 Fluorescence Spectroscopy.....   | 140        |
| 5.3.4 NMR Spectroscopy.....  | 142        |
| 5.4 Rationale for Studying the Binding Interactions Between Prodigiosin <b>1</b> and G-Quadruplex DNA..... | 144        |

|  |   |            |
|--|---|------------|
| 5.4.1  | Prodigiosin Intercalates Preferably at AT-Rich Sites in Duplex DNA.   | 147        |
| 5.4.2  | Prodigiosin Inhibits Topoisomerases I and II .....  | 148        |
| 5.4.3  | Prodigiosin Partially Intercalates into ct-DNA .....  | 150        |
| <b>RESULTS:</b>  |   |            |
| 5.5  | G-Quadruplex $K^+ \cdot d[TG_4T]_4$ Increases Solubility of Prodigiosin <b>1</b> in Water .....                   | 151        |
| 5.6  | Fluorescence Studies Indicate Interactions Between G-Quadruplex and Prodigiosin .....                             | 154        |
| 5.7  | NMR Experiments Reveal that Prodigiosin <b>1</b> Binds the G-Quadruplex $K^+ \cdot d[TG_4T]_4$ at its 3' End..... | 156        |
| 5.7.1  | Characterization of the $d[TG_4T]_4$ Quadruplex in Solution by $^1H$ NMR  | 156        |
| 5.7.2  | NMR Experiments Probing Binding of Prodigiosin <b>1</b> to $K^+ \cdot d[TG_4T]_4$                                 | 158        |
| 5.7.2.1  | Titration with Prodigiosin <b>1</b> in 90% $H_2O$ -10% $D_2O$ .....   | 159        |
| 5.7.2.2  | NMR Control Experiments with $d_6$ -DMSO and $K^+ \cdot d[TG_4T]_4$ .....   | 162        |
| 5.7.2.3  | $^{31}P$ NMR to Investigate Groove Binding by Prodigiosin .....   | 164        |
| 5.7.3  | Prodigiosin Does Not Bind to Single-Stranded DNA.....   | 166        |
| 5.8  | NMR Experiments in Mixed Solvent Systems .....  | 168        |
| 5.8.1  | NMR Titration in $d_6$ -DMSO: 90% $H_2O$ -10% $D_2O$ (1:1) Mixture .....  | 168        |
| 5.8.2  | Saturation Transfer Difference Experiments Confirm Interaction Between Prodigiosin and G-Quadruplex DNA.....      | 172        |
| 5.9  | Molecular Model Showing End-Stacking by Prodigiosin .....   | 174        |
| 5.10   | Conclusions.....  | 176        |
| <b>Chapter 6: Conclusions and Future Directions .....</b>                  |   | <b>177</b> |
| <b>Chapter 7: Experimental Procedures and Supporting Information .....</b> |   | <b>183</b> |
| 7.1  | General Experimental .....  | 183        |
| 7.2  | Experimental Procedures for <b>Chapter 2</b> .....  | 185        |
| 7.2.1  | Anion Exchange Transport Assays .....   | 185        |
| 7.2.2  | NMR Titrations .....  | 190        |
| 7.2.3  | Determination of $pK_a$ Values for Prodigiosin <b>1</b> and Prodigiosene Ester <b>2f</b> .....                    | 190        |
| 7.3  | Experimental Procedures for <b>Chapter 3</b> .....  | 191        |
| 7.3.1  | Determination of $pK_a$ Values for Prodigiosenes <b>3b</b> , <b>3d-f</b> and <b>3h</b> .....                      | 191        |
| 7.3.2  | Anion Exchange Transport Assays .....   | 193        |
| 7.4  | Experimental Procedures for <b>Chapter 4</b> .....  | 194        |
| 7.4.1  | NMR Titrations .....  | 194        |

|       |  |     |
|-------|--|-----|
| 7.5   | Experimental Procedures for <b>Chapter 5</b> ..... | 196 |
| 7.5.1 | UV-vis titration .....                             | 197 |
| 7.5.2 | Fluorescence titration.....                        | 197 |
| 7.5.3 | <sup>1</sup> H-NMR titration .....                 | 197 |
|       | Bibliography .....                                 | 199 |

## LIST OF TABLES

|   |    |
|---|----|
| <b>Table 2.1.</b> The <i>in-vitro</i> activity of prodigiosenes <b>27-29</b> over 60 cancer cell lines.....   | 52 |
| <b>Table 2.2.</b> EC <sub>50</sub> values for the transmembrane anion transport abilities of <b>1, 2e</b> and <b>24</b> . .....   | 56 |
| <b>Table 2.3.</b> Mean in vitro activity of prodigiosenes over 59 cancer cell lines.....  | 71 |
| <b>Table 3.1.</b> The <i>in vitro</i> cytotoxic activity (IC <sub>50</sub> ) of prodigiosin <b>1</b> and desmethoxyprodigiosin <b>30</b> against four cancer cell lines - leukemia (L1210 mouse), melanoma (B16 mouse), 9PS (P388 mouse) and human epidermoid carcinoma of the nasopharynx (9KB). ..... | 79 |
| <b>Table 3.2.</b> The pK <sub>a</sub> values for synthetic prodigiosenes <b>3b, 3d-f</b> and <b>3h</b> with different – OAr groups on the B-ring. ....  | 85 |
| <b>Table 3.3.</b> The pK <sub>a</sub> values, transmembrane anion exchange rates and half-life of the anion transport process for prodigiosenes <b>3b, 3d-f</b> and <b>3h</b> with different – OAr groups on the B-ring. ....   | 87 |
| <b>Table 3.4.</b> <i>In vitro</i> activity of prodigiosenes <b>1, 3a-3b, 3d</b> and <b>3h</b> over the NCI60 cancer cell lines. Values are a mean of two experiments. ....  | 89 |

## LIST OF FIGURES

|   |    |
|---|----|
| <b>Figure 1.1.</b> Structure of natural product prodigiosin <b>1</b> .....  | 1  |
| <b>Figure 1.2.</b> Structures of natural product <b>1</b> and synthetic prodigiosenes - ester analog <b>2</b> and phenyl analog <b>3</b> .....  | 4  |
| <b>Figure 1.3.</b> Different conformations of the protonated form of prodigiosin <b>1•H<sup>+</sup></b> - $\alpha$ , $\beta$ , $\gamma$ and $\delta$ are in equilibrium with each other in solution. The $\alpha$ conformation of <b>1•H<sup>+</sup></b> binds $\text{MeSO}_3^-$ ion using a CH hydrogen .....                              | 5  |
| <b>Figure 1.4.</b> Structures of some of the commonly known prodigiosenes <b>1</b> and <b>4-8</b> .....   | 6  |
| <b>Figure 1.5.</b> Structures of prodigiosenes <b>1</b> , <b>4</b> and <b>7</b> .....   | 11 |
| <b>Figure 1.6.</b> The proposed lipophilic ion pair <b>1•H<sup>+</sup>Cl<sup>-</sup></b> formed between prodigiosin <b>1</b> and $\text{H}^+/\text{Cl}^-$ ions that promotes proton movement across the liposomal membrane. ....  | 13 |
| <b>Figure 1.7.</b> Structure of cycloprodigiosin hydrochloride <b>9</b> .....   | 14 |
| <b>Figure 1.8.</b> Effect of <b>PG-L-1</b> on cellular and nuclear morphology in U937 Cells. U937 cells ( $6 \times 10^5$ cells/dish) were treated with 0 mg/ml ( <b>A</b> , <b>E</b> ), 0.1 mg/ml ( <b>B</b> , <b>F</b> ), 1.5 mg/ml ( <b>C</b> , <b>G</b> ), and 50 mg/ml ( <b>D</b> , <b>H</b> ) of <b>PG-L-1</b> at 37 °C for 3 h. .... | 15 |
| <b>Figure 1.9.</b> Compound <b>10</b> developed by Yang and her group for treatment of CF. ..   | 18 |
| <b>Figure 1.10.</b> Structure of the prodigiosenes <b>11</b> and <b>12</b> . Two views of the X-ray crystal structure of the complex formed between protonated prodigiosin <b>11</b> and $\text{Cl}^-$ ion. ....  | 19 |
| <b>Figure 1.11.</b> Anion exchange mediated by prodigiosin <b>1•H<sup>+</sup></b> across a lipid bilayer. <b>1•H<sup>+</sup></b> can bind $\text{Cl}^-$ or $\text{NO}_3^-$ anions and diffuse them through the membrane. .  | 20 |
| <b>Figure 1.12.</b> Chloride gradient assays on 100 nm EYPC liposomes in 10 mM sodium phosphate (pH 6.4) containing either 75 mM $\text{Na}_2\text{SO}_4$ ( <b>A</b> and <b>B</b> ) or 100 mM $\text{NaNO}_3$ ( <b>C</b> and <b>D</b> ). ....   | 22 |
| <b>Figure 1.13.</b> Proposed structure of a complex between $\text{HCO}_3^-$ and prodigiosin <b>1•H<sup>+</sup></b> . The H5 proton on ring A and the methyl group on ring C are highlighted in red.....  | 23 |
| <b>Figure 1.14.</b> $^{13}\text{C}$ NMR experiments demonstrate that prodigiosin <b>1</b> is able to facilitate chloride/bicarbonate antiport. Titration sequence for monitoring the  |    |

|   |    |
|---|----|
| transmembrane transport of bicarbonate ions in $\text{H}^{13}\text{CO}_3^-$ loaded EYPC liposomes by prodigiosin <b>1</b> and DMSO. ....  | 24 |
| <b>Figure 1.15.</b> Schematic drawing of the closed and opened conformation of a Cl <sup>-</sup> chloride channel. ....   | 28 |
| <b>Figure 1.16.</b> Structure of compound <b>13</b> . <b>a)</b> Schematic representation of the light-regulated ion channel-transport. <b>b)</b> Transport activity measured based on fluorescence of safranin O dye for <i>cis</i> and <i>trans</i> isomer. ....   | 29 |
| <b>Figure 1.17.</b> Structure of pillarenes <b>14</b> . Schematic presentation for the voltage-driven channel insertion and exit from the lipid bilayer. ....   | 31 |
| <b>Figure 1.18.</b> <b>a)</b> Structure of imidazolium salt <b>15</b> <b>b)</b> Schematic representation of the formation of inclusion complexes of <b>15</b> with CB7 and $\alpha$ -CD and displacement of the transporter from the bilayer. <b>c)</b> Relative activity of compound <b>15</b> . ....  | 33 |
| <b>Figure 1.19.</b> <b>a)</b> Structure of amphiphilic thread <b>16</b> and pyridyl containing macrocycle <b>17</b> . <b>b)</b> Schematic representation of the formation of inclusion complexes between <b>16</b> and <b>17</b> . <b>c)</b> Relative anion transport activity of compounds <b>16</b> , <b>17</b> , their complex and the pre-formed rotaxane in the LG-based assay. .... | 35 |
| <b>Figure 1.20.</b> <b>a)</b> and <b>b)</b> show structures of thiourea <b>18</b> and acylthiourea <b>19</b> . <b>c)</b> Chloride efflux mediated by receptors <b>18</b> and <b>19</b> from POPC vesicles. ....   | 37 |
| <b>Figure 1.21.</b> Non-covalent functionalization of viologen <b>20</b> modified nanopores with negatively charged donor, pyranine <b>21</b> , to switch the gating properties of the nanopores from anion selective ( $[\text{Fe}(\text{CN})_6]_3^-$ ) to cation selective ( $[\text{Ru}(\text{NH}_3)_6]^{3+}$ ). ....  | 39 |
| <b>Figure 1.22.</b> Cyclic voltammograms corresponding to coronene tetracarboxylate <b>22</b> bound MF-V in the presence of 1 mM $[\text{Ru}(\text{NH}_3)_6]^{3+}$ (red trace) and 1 mM $[\text{Fe}(\text{CN})_6]_3^-$ (blue trace) at different pH conditions. ....  | 40 |
| <b>Figure 1.23.</b> <b>a)</b> Schematic representation showing ON/OFF switching of anion transport by thiosquaramide <b>23</b> . <b>b)</b> Chloride efflux from POPC vesicles. ....   | 42 |
| <b>Figure 2.1.</b> Natural product prodigiosin ( <b>1</b> ) and C-ring modified synthetic analogs – ester ( <b>2a-j</b> ) and <b>24</b> . ....  | 47 |
| <b>Figure 2.2.</b> Structures of prodigiosene <b>25</b> and prodigiosin 25-C ( <b>7</b> ). ....   | 49 |
| <b>Figure 2.3.</b> Structures of indoloprodigiosin <b>26</b> and prodigiosenes <b>27-29</b> . ....  | 51 |

|   |    |
|---|----|
| <b>Figure 2.4.</b> Structures of compounds <b>1</b> , <b>2e</b> and <b>24</b> . Anion exchange assay for the natural product prodigiosin <b>1</b> relative to synthetic analogs <b>2e</b> and <b>24</b> .....   | 55 |
| <b>Figure 2.5.</b> Anion exchange assay for prodigiosenes <b>2a-d</b> , <b>2g</b> and <b>2i-j</b> , relative to <b>24</b> . Anion exchange in EYPC liposomes.....   | 58 |
| <b>Figure 2.6.</b> Anion exchange assay for prodigiosenes <b>2f</b> , <b>2g</b> , <b>2h</b> , relative to <b>24</b> in EYPC liposomes. ....   | 60 |
| <b>Figure 2.7.</b> The long <sup>14</sup> C chain on prodigiosene <b>2h</b> will tend to promote formation of aggregates in an aqueous solution.....  | 61 |
| <b>Figure 2.8.</b> Anion exchange assay for prodigiosene <b>2h</b> in EYPC liposomes. ....  | 62 |
| <b>Figure 2.9.</b> A 1:1 mixture of prodigiosin <b>1</b> and C5 ester analog <b>2e•HCl</b> was taken. The <sup>1</sup> H NMR of the 1:1 mixture (top trace) showed that prodigiosin was in the protonated form ( <b>1•HCl</b> ), while the ester was in the free-base form ( <b>2e</b> ).<br>.....  | 64 |
| <b>Figure 2.10.</b> <sup>1</sup> H NMR spectra showing the B-ring -OCH <sub>3</sub> signals during titration of a 1:1 mixture of prodigiosin <b>1</b> and ester <b>2e</b> at 1 mM concentration with MeSO <sub>3</sub> H in CD <sub>3</sub> CN at 25 °C. ....   | 65 |
| <b>Figure 2.11.</b> The $\alpha$ and $\beta$ isomers of prodigiosene <b>2f</b> in free-base and protonated form are in equilibrium with each other in solution. The apparent pK <sub>a</sub> values were calculated for the equilibrium mixture of $\alpha$ and $\beta$ isomers of protonated prodigiosene <b>2f•H<sup>+</sup></b> . .... | 67 |
| <b>Figure 2.12.</b> UV-vis absorbance spectra for <b>a</b> ) prodigiosin <b>1</b> and <b>b</b> ) ester <b>2f</b> as a function of pH in 1:1 CH <sub>3</sub> CN/H <sub>2</sub> O (v/v) at 25 °C (0.1 M NaCl).....  | 68 |
| <b>Figure 2.13.</b> Experimental procedure for the pH variation experiments performed with octyl ester analog <b>2g</b> . Chloride influx promoted by 0.05 mol % of ester <b>2g</b> as a function of extravesicular pH.. ....   | 69 |
| <b>Figure 3.1.</b> Structures of B-ring modified prodigiosenes <b>3a-h</b> . ....   | 75 |
| <b>Figure 3.2.</b> Protonation of prodigiosin <b>1</b> and subsequent binding of chloride anion by <b>1•H<sup>+</sup></b> . The schematic at the right depicts the protonated prodigiosin <b>1•H<sup>+</sup></b> catalyzing the exchange of anions across a lipid bilayer.....  | 77 |
| <b>Figure 3.3.</b> Structures of prodigiosenes ester analog <b>2f</b> and phenyl analog <b>3</b> .....  | 78 |
| <b>Figure 3.4.</b> Structures of prodigiosenes <b>30</b> , <b>31</b> and PNU-156804 ( <b>7</b> ).....   | 78 |
| <b>Figure 3.5.</b> Structures of B-ring modified prodigiosenes <b>3a-h</b> . ....   | 81 |



|   |     |
|---|-----|
| <b>Figure 3.6.</b> The $\alpha$ and $\beta$ isomers of prodigiosene <b>3d</b> in free-base and protonated form are in equilibrium with each other in solution. The apparent $pK_a$ values were calculated for the equilibrium mixture of $\alpha$ and $\beta$ isomers of protonated prodigiosene <b>3d</b> •H <sup>+</sup> .....  | 83  |
| <b>Figure 3.7.</b> UV-vis absorbance spectra for <b>a) 3d</b> and <b>b) 3f</b> as a function of pH in 1:1 CH <sub>3</sub> CN–H <sub>2</sub> O (v/v) at 25 °C (0.1 M NaCl).....  | 84  |
| <b>Figure 3.8.</b> Anion exchange assay for analogs <b>3b</b> , <b>3d-f</b> and <b>3h</b> in EYPC liposomes at 25°C.....  | 86  |
| <b>Figure 3.9.</b> Anion exchange assay for prodigiosin <b>1</b> and analog <b>3d</b> in EYPC liposomes at 25°C.....  | 88  |
| <b>Figure 3.10.</b> GI <sub>50</sub> concentrations (half maximal growth inhibition concentrations) of some synthetic prodigiosenes <b>3a</b> , <b>3b</b> , <b>3d</b> and <b>3h</b> against 60 human cancer cell lines representing 9 different cancer types. ....  | 90  |
| <b>Figure 4.1.</b> <b>a)</b> Structure of prodigiosene <b>12</b> . Two molecules of <b>12</b> bind non-covalently to form a dimer. <b>b)</b> Perspective drawing of solid state structure of Zn•( <b>1</b> ) <sub>2</sub> . Zinc atom is represented by the green sphere. <b>c)</b> Proposed ORTEP plot of solid state structure from reaction of <b>1</b> with CuCl <sub>2</sub> ..... | 94  |
| <b>Figure 4.2.</b> Structure of compound <b>32</b> . Crystal structure of compound <b>32</b> from <b>a)</b> front and <b>b)</b> top.....  | 96  |
| <b>Figure 4.3.</b> The $\alpha$ and $\beta$ conformations of ( <b>8</b> •MeSO <sub>3</sub> H). ....   | 97  |
| <b>Figure 4.4.</b> Structure of the methanesulfonate salt of PNU-156804 ( <b>8</b> •MeSO <sub>3</sub> H) in its $\beta$ conformation. Selective NOESY cross-peaks are indicated with blue colored double-headed arrows.....   | 98  |
| <b>Figure 4.5.</b> Structure of prodigiosene derivative <b>33</b> . Tautomer <b>I</b> is shown as $\alpha$ , $\beta$ , $\gamma$ and $\delta$ isomers for the computational study of a neutral prodigiosene <b>33</b> .....  | 100 |
| <b>Figure 4.6.</b> Isomer <b>IV</b> $\gamma$ can bind Cl <sup>-</sup> and MeSO <sub>3</sub> <sup>-</sup> anions to give four possible complexes each. Binding energies were calculated in kcal/mol for each complex .....   | 101 |
| <b>Figure 4.7.</b> <sup>1</sup> H NMR for the phenyl analog <b>3b</b> •HCl in CDCl <sub>3</sub> shows a single set of peaks belonging to the $\beta$ isomer. ....   | 104 |
| <b>Figure 4.8.</b> $\beta$ and $\alpha$ conformational isomers of prodigiosene <b>3b</b> •H <sup>+</sup> . Both the major $\beta$ and minor $\alpha$ isomers should be able to bind anions. ....  | 105 |

- Figure 4.9.**  $^1\text{H}$  NMR spectra in  $\text{CDCl}_3$  for the pyrrolic NH region of: (a) **3b•HCl**; (b) after addition of 6 eq. of  $\text{MeSO}_3\text{H}$  to sample **a**; two sets of NH signals were resolved for each  $\alpha$  (●) and  $\beta$  (\*) conformer; (c) after addition of 1 eq. of tetrabutylammonium chloride (TBACl) to sample **b**. ..... 106
- Figure 4.10.** A region of the NOESY spectrum of **3b•MeSO<sub>3</sub>H** in  $\text{CDCl}_3$  shows a NOE between one of the “minor” pyrrole NH protons and C2 methyl hydrogens... ..... 107
- Figure 4.11.** Structures of  $\alpha$  and  $\beta$  isomers of **1•H<sup>+</sup>A<sup>-</sup>** are illustrated at the top to show the interaction between NH protons and anion  $\text{A}^-$ .  $^1\text{H}$  NMR spectra shows the changes in conformations for (a) prodigiosin **1•H<sup>+</sup>** and (b) ester **2e•H<sup>+</sup>** based on the chemical shifts of the NH protons ..... 109
- Figure 4.12.**  $^1\text{H}$  NMR spectra of  $\alpha$  and  $\beta$  conformations of **2e•HCl** shows the changes in chemical shifts of NH protons as TBACl is added to the sample in  $\text{CD}_3\text{CN}$  at  $-10^\circ\text{C}$ . Shifting of signals has been highlighted by red dashed lines for  $\alpha$  isomer and black dashed lines for  $\beta$  isomer. .... 111
- Figure 4.13.** Structures of  $\alpha$  and  $\beta$  conformations of **2e•MeSO<sub>3</sub>H** and **2e•HCl** complexes. The  $\alpha$  and  $\beta$  isomers are in slow equilibrium with each other for both anion complexes of the ester compound..... 112
- Figure 4.14.** Examples of receptors that can bind anions using CH hydrogens. .... 113
- Figure 4.15.** Stack plot of  $^1\text{H}$  NMR titration of **36** with TBACl in  $d_6$ -DMSO  $-0.5\text{H}_2\text{O}$ ..... 115
- Figure 4.16.** The H1" (highlighted in red) in **a2e•MeSO<sub>3</sub>H** complex is involved in binding  $\text{MeSO}_3^-$  anion in addition to the two NH protons on rings A and B. .... 115
- Figure 4.17.** Proposed structure depicts the involvement of  $\alpha$ -H1" (highlighted in red) proton in **1•MeSO<sub>3</sub>H** complex for binding  $\text{MeSO}_3^-$  anion, in addition to the two NH protons on rings A and B.  $^1\text{H}$  NMR spectra shows the changes in chemical shift for H1" proton on  $\alpha$  isomer of prodigiosin **1•H<sup>+</sup>** ..... 117
- Figure 4.18.** Structures showing the H1" (highlighted in red) in  $\alpha$  isomer of **2e•MeSO<sub>3</sub>H** complex, involved in binding  $\text{MeSO}_3^-$  in addition to the two NH protons on rings A and B ..... 119
- Figure 4.19.**  $^1\text{H}$  NMR spectra shows the changes in conformer ratios for (a) prodigiosin **1•H<sup>+</sup>** with respect to aromatic CH protons as  $\text{MeSO}_3\text{H}$  and TBACl are titrated into the NMR sample in  $\text{CD}_3\text{CN}$  at  $25^\circ\text{C}$ . The results for prodigiosin have been contrasted with results obtained from ester **2e•H<sup>+</sup>** (b). ..... 122

|   |     |
|---|-----|
| <b>Figure 4.20.</b> The $\gamma 2e \cdot H^+$ cation can bind $Cl^-$ to give four possible isomers. Energies were calculated in kcal/mol for each chloride ( $Cl^-$ ) complex in gas phase and acetonitrile (in parentheses).....   | 124 |
| <b>Figure 4.21.</b> Structures of the $\alpha$ and $\beta$ conformations of <b>1</b> •MeSO <sub>3</sub> H. <sup>1</sup> H NMR spectra of prodigiosin <b>1</b> •MeSO <sub>3</sub> H in presence of 3 equivalents of MeSO <sub>3</sub> H in CD <sub>3</sub> CN (bottom) and 1:1 mixture of CD <sub>3</sub> CN:D <sub>2</sub> O (top) at 25 °C. ....   | 126 |
| <b>Figure 4.22.</b> DOSY NMR of prodigiosin <b>1</b> •MeSO <sub>3</sub> H with 3 equivalents of MeSO <sub>3</sub> H in a 1:1 mixture of CD <sub>3</sub> CN:D <sub>2</sub> O at 25 °C. Only one set of DOSY signals were observed for all aromatic protons. ....   | 127 |
| <b>Figure 4.23.</b> 2D COSY NMR of prodigiosin <b>1</b> •MeSO <sub>3</sub> H with 3 equivalents of MeSO <sub>3</sub> H in a 1:1 mixture of CD <sub>3</sub> CN:D <sub>2</sub> O at 25 °C. The signals for aromatic protons could be segregated for the two isomers. ....   | 128 |
| <b>Figure 5.1.</b> <b>a)</b> A G-quartet showing hydrogen bonds between the Hoogsteen and Watson-Crick faces of guanosine bases. <b>b)</b> Depiction of a intermolecular G-quadruplex 5'-d[TG <sub>4</sub> T] <sub>4</sub> formed by assembly of four strands aligned parallel to each other. <b>c)</b> Depiction of an anti-parallel intramolecular G-quadruplex formed by the folding of a single-strand of DNA. .... | 134 |
| <b>Figure 5.2.</b> Structure of G-quadruplex binding Thioflavin T <b>37</b> . ....  | 136 |
| <b>Figure 5.3.</b> Structures of quadruplex binding drugs – Telomestatin <b>38</b> , Distamycin A <b>39</b> and TMPyP4 <b>40</b> . ....   | 137 |
| <b>Figure 5.4.</b> UV-vis spectra of TMPyP4 <b>40</b> in absence (solid line) and presence (dashed line) of d[T <sub>4</sub> G <sub>4</sub> ] <sub>4</sub> at a [porphyrin]/[DNA quadruplex] ratio of 8.33 .....  | 139 |
| <b>Figure 5.5.</b> Structure of thiazole orange (TO) <b>41</b> .....  | 141 |
| <b>Figure 5.6.</b> <sup>1</sup> H NMR stack plot illustrating the slow exchange for single-stranded and G-quadruplex forms of d[TG <sub>4</sub> T]. ....  | 143 |
| <b>Figure 5.7.</b> The cation-templated self-assembly of 16 equivalents of 5'-silyl-2',3'-O-isopropylidene guanosine ( <b>42</b> ) gives a lipophilic G-quadruplex ( <b>42</b> ) <sub>16</sub> •3K <sup>+</sup> •4DNP in the solid state and in solution .....  | 145 |
| <b>Figure 5.8.</b> A <sup>1</sup> H NMR stack plot of <b>a)</b> Prodigiosin <b>1</b> (5 mM), <b>b)</b> G-quadruplex ( <b>42</b> ) <sub>16</sub> •3K <sup>+</sup> •4DNP (5 mM) and <b>c)</b> Prodigiosin <b>1</b> : ( <b>42</b> ) <sub>16</sub> •3K <sup>+</sup> •4DNP:MeSO <sub>3</sub> H in 1:1:1 ratio in a 1:1 mixture of CD <sub>2</sub> Cl <sub>2</sub> :CD <sub>3</sub> CN.. ....                                 | 146 |

- Figure 5.9.** a) UV-Vis spectra of prodigiosin **1** (4  $\mu\text{M}$ ) in absence (solid line) and presence (dashed line) of 10 bp equivalents of poly d[A-T]<sub>2</sub> in 10 mM NaCl-50 mM MES buffer at pH 6.5. b) Fluorescence intensity of prodigiosin **1** (4  $\mu\text{M}$ ) in the presence of 10 bp equivalent of poly d[A-T]<sub>2</sub> (1), ct-DNA (2) and poly d[G-C]<sub>2</sub> (3)..... 147
- Figure 5.10.** Prodigiosin-induced ds breakage of genomic DNA independent of the apoptotic process. MCF7 cells untreated (A), or treated with 2  $\mu\text{M}$  prodigiosin for 3h (B) were dual stained with primary antibodies directed against apoptosis inducing factor (AIF) and p-H2AX (bar = 20  $\mu\text{m}$ )... 150
- Figure 5.11.** An illustration showing formation of G-quadruplex d[**TG<sub>4</sub>T**]<sub>4</sub> from hexanucleotide 5'-d[**TG<sub>4</sub>T**]-3' in presence of K<sup>+</sup> cations..... 151
- Figure 5.12.** A CD spectrum showing the characteristic peak for d[**TG<sub>4</sub>T**]<sub>4</sub> in presence of K<sup>+</sup> at 45 °C ..... 152
- Figure 5.13.** A UV-Vis titration plot between prodigiosin **1•H<sup>+</sup>** (~50  $\mu\text{M}$ ) and variable equivalents of a) K<sup>+</sup>•d[**TG<sub>4</sub>T**]<sub>4</sub> b) Li<sup>+</sup>•d[**TG<sub>4</sub>T**]<sub>4</sub> at 37 °C ..... 153
- Figure 5.14.** A fluorescence titration plot between 50  $\mu\text{M}$  prodigiosin **1•H<sup>+</sup>** and variable equivalents of a) K<sup>+</sup>•d[**TG<sub>4</sub>T**]<sub>4</sub> b) 50  $\mu\text{M}$  prodigiosin and variable equivalents of KCl buffer at 37 °C..... 155
- Figure 5.15.** A portion of the <sup>1</sup>H NMR of d[**TG<sub>4</sub>T**]<sub>4</sub> quadruplex in 90% H<sub>2</sub>O-10% D<sub>2</sub>O at 45 °C showing six peaks in the aromatic region, corresponding to the H8 proton on four guanosines and H6 proton on two thymine bases ..... 157
- Figure 5.16.** A 2D NOESY spectrum of K<sup>+</sup>•d[**TG<sub>4</sub>T**]<sub>4</sub> correlating the aromatic protons on the bases (top) with the H1' protons on sugars (left) in 90% H<sub>2</sub>O-10% D<sub>2</sub>O at 45 °C..... 158
- Figure 5.17.** <sup>1</sup>H NMR stack plot showing titration of K<sup>+</sup>•d[**TG<sub>4</sub>T**]<sub>4</sub> with varying equivalents of prodigiosin **1•H<sup>+</sup>** in 90% H<sub>2</sub>O-10% D<sub>2</sub>O at 45 °C..... 160
- Figure 5.18.** A 2D NOESY spectrum of K<sup>+</sup>•d[**TG<sub>4</sub>T**]<sub>4</sub> with “4.5 eq” of prodigiosin **1•H<sup>+</sup>** in 90% H<sub>2</sub>O-10% D<sub>2</sub>O at 45 °C. .... 161
- Figure 5.19.** An illustration showing interaction between protonated form of prodigiosin **1•H<sup>+</sup>** and G-quadruplex K<sup>+</sup>•d[**TG<sub>4</sub>T**]<sub>4</sub>. Prodigiosin binds at the 3' end. .... 162
- Figure 5.20.** <sup>1</sup>H NMR stack plot showing titration of K<sup>+</sup>•d[**TG<sub>4</sub>T**]<sub>4</sub> with *d*<sub>6</sub>-DMSO in 90% H<sub>2</sub>O-10% D<sub>2</sub>O at 45 °C. The only changes in chemical shifts observed were for H6 protons of thymines..... 163

- Figure 5.21.**  $^{31}\text{P}$  NMR stack plot showing titration of  $\text{K}^+\cdot\text{d}[\text{TG}_4\text{T}]_4$  with **a)** prodigiosin  $\mathbf{1}\cdot\text{H}^+$  and **b)**  $d_6$ -DMSO in 90%  $\text{H}_2\text{O}$ -10%  $\text{D}_2\text{O}$  at 45  $^\circ\text{C}$ . The  $^{31}\text{P}$  NMR spectrum in both cases looked the same..... 165
- Figure 5.22.** A 2D  $^1\text{H}$ - $^{31}\text{P}$  HSQC spectrum of  $\text{K}^+\cdot\text{d}[\text{TG}_4\text{T}]_4$  in 90%  $\text{H}_2\text{O}$ -10%  $\text{D}_2\text{O}$  at 45  $^\circ\text{C}$ . This spectrum correlates the sugar protons (H3', H4', H5' and H5'' on top) with the phosphate groups (left). ..... 166
- Figure 5.23.**  $^1\text{H}$  NMR stack plot showing titration of  $\text{Li}^+\cdot\text{d}[\text{TG}_4\text{T}]$  with prodigiosin  $\mathbf{1}\cdot\text{H}^+$  in 90%  $\text{H}_2\text{O}$ -10%  $\text{D}_2\text{O}$  at 45  $^\circ\text{C}$ . ..... 168
- Figure 5.24.** TOCSY NMR showing correlations between ring A resonances (H3, H4 and H5) in prodigiosin (1 mM) in a 1:1 mixture of  $d_6$ -DMSO and 90%  $\text{H}_2\text{O}$ -10%  $\text{D}_2\text{O}$  at 45  $^\circ\text{C}$ ..... 169
- Figure 5.25.**  $^1\text{H}$  NMR stack plot showing titration of prodigiosin  $\mathbf{1}\cdot\text{H}^+$  (1 mM) with different eq of  $\text{K}^+\cdot\text{d}[\text{TG}_4\text{T}]_4$  in 1:1 mixture of  $d_6$ -DMSO and 90%  $\text{H}_2\text{O}$ -10%  $\text{D}_2\text{O}$  at 45  $^\circ\text{C}$ . ..... 171
- Figure 5.26.** A STD NMR of 1:20 sample of G-quadruplex  $\text{K}^+\cdot\text{d}[\text{TG}_4\text{T}]_4$  DNA and prodigiosin  $\mathbf{1}\cdot\text{H}^+$  in a 1:1 mixture of  $d_6$ -DMSO and 90%  $\text{H}_2\text{O}$ -10%  $\text{D}_2\text{O}$ ..... 173
- Figure 5.27.** Molecular models generated for G-quadruplex  $\text{d}[\text{TTAGGGT}]_4$  and prodigiosin  $\mathbf{1}\cdot\text{H}^+$  complex from G-quadruplex ligands database (G4LDB).<sup>194</sup> The model can be seen from **a)** top and **b)** side..... 175
- Figure 6.1.** Structures of proposed prodigiosene analogs **43-45** and ester **2a**. ..... 179
- Figure 6.2.** Structure of the hexapyrrole **46** $\cdot\mathbf{2HCl}$  shows two  $\text{Cl}^-$  anions bound to a planar S-shaped conformation. **b)** Schematic representation of a S-shaped **46** $\cdot\mathbf{2HCl}$  stacking over a G-quartet. .... 180
- Figure 6.3.** Compound **47** reacts with  $\text{Cu}^{2+}$  to give prodigiosene-metal complex **47** $\cdot\text{Cu}^{2+}$ . **a)** Top and **b)** side views of the crystal structure of copper(II) complex ..... 181
- Figure 6.4.** The  $\alpha$  and  $\beta$  conformations of  $\mathbf{1}\cdot\text{HA}$  are shown. Different factors such as water and counter-anion can affect the  $\alpha/\beta$  conformational ratio..... 182
- Figure 7.1.** Determination of the Stern-Volmer constant. .... 187
- Figure 7.2.** EC<sub>50</sub> dose response curve for prodigiosin **1** at 150 s. EC<sub>50</sub> value was calculated by plotting the percentage of chloride efflux at 150 s vs. the natural log of concentration of prodigiosin **1** and then fitting to Hill equation. .... 187

- Figure 7.3.** EC50 dose response curve for ester **2e** at 150 s. EC<sub>50</sub> value was calculated by plotting the percentage of chloride efflux at 150 s vs. the natural log of concentration of prodigiosin **2e** and then fitting to Hill equation. .... 188
- Figure 7.4.** EC50 dose response curve for ester **24** at 150 s. EC<sub>50</sub> value was calculated by plotting the percentage of chloride efflux at 150 s vs. the natural log of concentration of prodigiosin **24** and then fitting to Hill equation. .... 188
- Figure 7.5.** A plot of log (ionization ratio) vs. pH for prodigiosin **1** and ester analog **2f**. .... 191
- Figure 7.6.** Absorbance spectra and ionization plot for **3e** (X = NMe<sub>2</sub>) as a function of pH. .... 191
- Figure 7.7.** Absorbance spectra and ionization plot for **3h** (X = Cl) as a function of pH. .... 192
- Figure 7.8.** Absorbance spectra and ionization plot for **3b** (X = H) as a function of pH. .... 192
- Figure 7.9.** Ionization plots for a) **3d** (X = OMe) and b) **3f** (X = CF<sub>3</sub>) as a function of pH. .... 192
- Figure 7.10.** a) Full and b) expanded NOESY spectrum of **3b•MeSO<sub>3</sub>H** in CDCl<sub>3</sub>. .... 195

# 1 Chapter 1: A Background on Prodigiosenes

## 1.1 Introduction

The work described in this thesis centers around a natural product called prodigiosin **1** (**Figure 1.1**). Prodigiosin is the parent compound of the tripyrrolic natural products known as the prodigiosenes.<sup>1</sup> It is a remarkable molecule as it has been found useful for its anti-cancer,<sup>2-4</sup> immunosuppressive,<sup>5,6</sup> anti-malarial,<sup>7</sup> and antimicrobial activities.<sup>8</sup> Undoubtedly, there's a huge interest in developing synthetic analogs of prodigiosin for therapeutic purposes.<sup>1,2,6,9-11</sup> In fact, a few of its derivatives such as Obtaoclax are undergoing preclinical and clinical trials.<sup>5,12-15</sup>

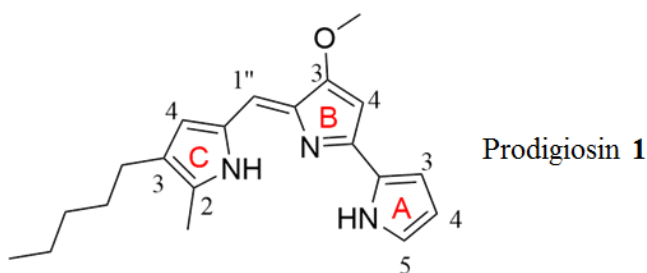


**Figure 1.1.** Structure of natural product prodigiosin **1**.

Naturally occurring prodigiosenes are produced by microorganisms such as *Streptomyces* and *Serratia marcescens*. They were first isolated in 1929.<sup>16</sup> However, prodigiosin's complete structure was not elucidated until the 1960s.<sup>17,18</sup> Very soon, scientists realized that prodigiosin has promising biological activity. Multiple groups undertook the investigation of the cytotoxic and immunosuppressive properties of prodigiosin.<sup>19,20</sup> Although there have been several studies done since then to evaluate

the full spectrum of the biological activities exhibited by the prodigiosenes,<sup>21-25</sup> the origin of this activity has not been established unambiguously yet.

There are multiple mechanisms put forth to explain prodigiosin's biological activity, such as the ability to inhibit phosphorylation and activate JAK-3, a cytoplasmic tyrosine kinase that may give rise to prodigiosin's immunosuppressive properties.<sup>26</sup> The ability to facilitate co-transport of HCl,<sup>10,22,27-30</sup> and catalyze anion exchange across lipid bilayers,<sup>10,31,32</sup> has been proposed to be the cause of prodigiosin's anti-cancer activity. Another theory attributes prodigiosin's anti-cancer activity to the formation of prodigiosene-copper complexes that mediate cleavage of double stranded DNA.<sup>33-35</sup> Obviously, the full spectrum of medicinal applications of prodigiosenes has ensured a steady interest in this particular group of natural products. A lot is known about the biological significance of prodigiosenes, whereas comparatively little is known about the chemistry behind these biological applications.<sup>9-11,24,36-38</sup> In this thesis, I have made an effort to explore some of the chemistry that may help explain prodigiosin's biological activity.

## **1.2 Thesis Organization**

This thesis is organized into seven chapters. The initial goal of the collaborative research between our group and that of Dr. Alison Thompson, some of which is described in this thesis, was to develop synthetic analogs of prodigiosin **1** (**Figure 1.2**) that would exhibit greater efficiency in anion transport across lipid bilayers, but would have reduced cytotoxicity. Further, we wanted to develop analogs with properties that could be exploited for regulation of transmembrane anion transport. These goals were



accomplished as described in the following chapters. Additionally, efforts were made to study some of the solution properties of prodigiosenes such as their basicity, conformation in solution and the modes of binding with anions (like  $\text{Cl}^-$ ,  $\text{MeSO}_3^-$ ). Taking our studies a step further, we also explored the interactions between prodigiosin and another anion, DNA. There are thumbprints of prodigiosin's biological relevance in the literature describing the ability of **1** to intercalate with duplex DNA.<sup>39-41</sup> These studies point towards the possibility of an important role of prodigiosin as a therapeutic agent for treating cancer. We wanted to explore the possibility of prodigiosin acting as a ligand for G-quadruplex DNA.

**Chapter 1** gives a description about prodigiosenes. It also describes the journey undertaken by scientists to elucidate the biological mechanism behind the anti-cancer activity observed for prodigiosin **1**. The initial studies that led to the discovery of prodigiosin **1** being able to catalyze  $\text{H}^+/\text{Cl}^-$  symport across cellular membranes are explained.<sup>10,22,27-30</sup> A description of the work done to study the anion-exchange process across bilayers, as catalyzed by prodigiosin is explained as well.<sup>10,31,32</sup>

**Chapter 2** is a description of efforts to study synthetic "C-ring" analogs of prodigiosin **1**. Some of the analogs showed improved ability to execute anion transport across lipid membranes. The ester derivatives **2** (**Figure 1.2**), also demonstrated that installation of an ester group on the C-ring can allow for a greater control over the transmembrane anion transport activity of prodigiosenes. The last finding paved our way for the research described in **Chapter 3**.

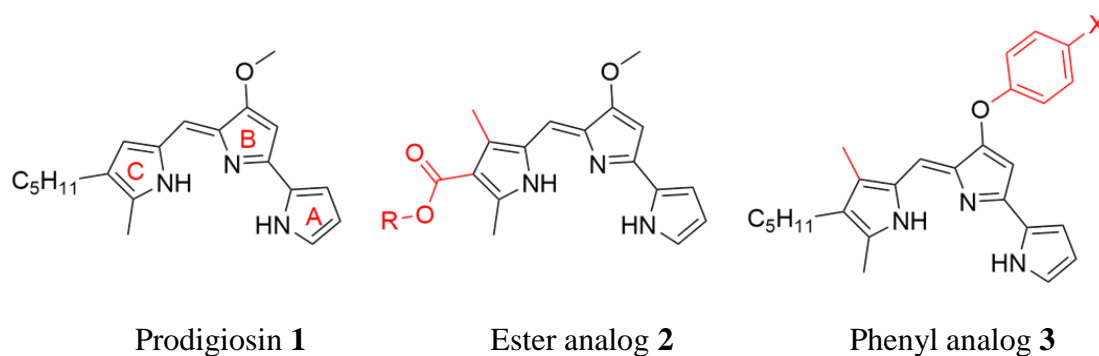


**Figure 1.2.** Structures of natural product **1** and synthetic prodigiosenes - ester analog **2e** and phenyl analog **3**.

In **Chapter 3**, a series of B-ring modified prodigiosenes **3** were designed and developed to study the impact of electronic effects on the basicity, and consequently, on the anion transport abilities of prodigiosenes (**Figure 1.2**). Different electron withdrawing and electron donating groups were installed on the prodigiosin scaffold. When the resultant set of new prodigiosenes **3** were tested for their anion transport activity, a correlation between the  $pK_a$  of a prodigiosene and its ability to move anions across lipid membranes was found. This finding revealed the significance of protonation of prodigiosenes in the process of moving anions across lipid membranes, which led us to the research performed in **Chapter 4**.

**Chapter 4** deals with studies done to investigate the conformation of prodigiosenes in solution (**Figure 1.3**). The anion binding patterns specific to different conformations were identified. Additionally, for the first time, it was shown that prodigiosenes can bind anions by using CH hydrogen (**Figure 1.3**). The C-H $\cdots$ A $^-$  binding is an unconventional type of H-bonding. Therefore, this result may be a significant addition to the topic of receptor-anion interactions in the ion transport field.

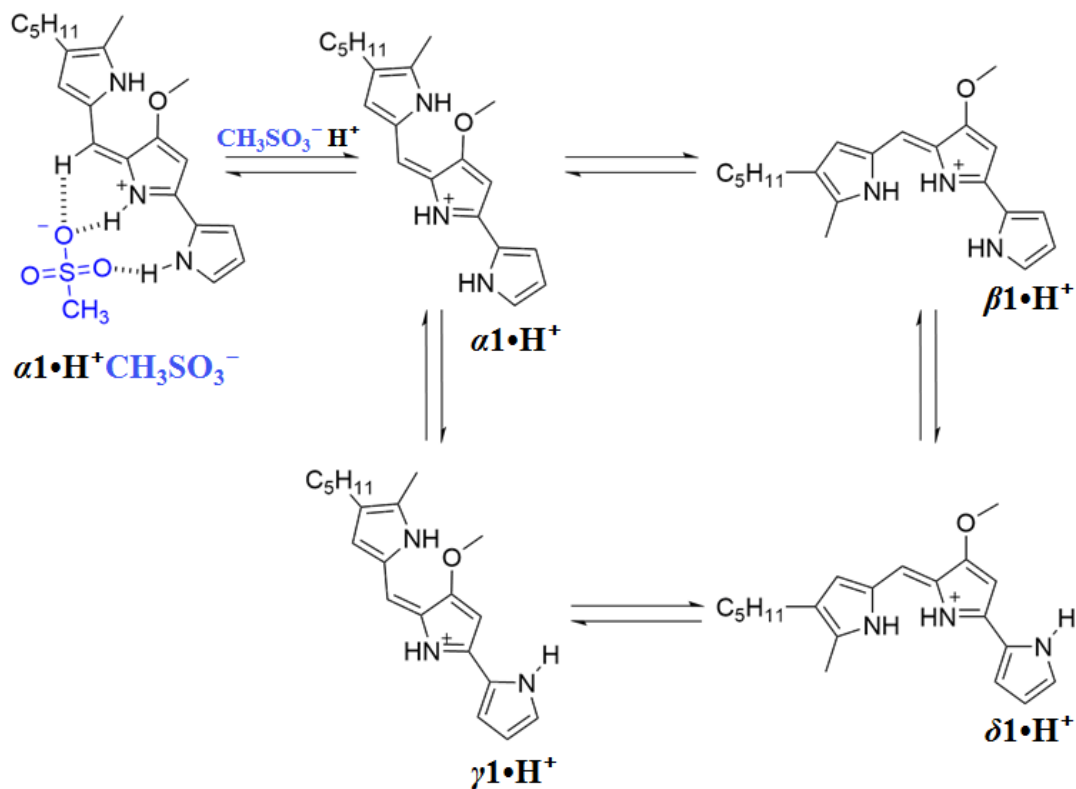


**Figure 1.3.** Different conformations of the protonated form of prodigiosin  $1 \cdot H^+$  -  $\alpha$ ,  $\beta$ ,  $\gamma$  and  $\delta$  are in equilibrium with each other in solution. The  $\alpha$  conformation of  $1 \cdot H^+$  binds MeSO<sub>3</sub><sup>-</sup> ion using a CH hydrogen.

DNA is a polyanion and can exist in different higher order structures - duplex, triplex and tetraplex forms. Since prodigiosin **1** has been shown to bind anions, **Chapter 5** describes the experiments performed to probe the binding interactions between prodigiosin **1** and an anionic sequence d[TG<sub>4</sub>T] that forms a G-quadruplex d[TG<sub>4</sub>T]<sub>4</sub>. Results showed that prodigiosin **1** is a G-quadruplex DNA binding ligand. This result opens up new possibilities to develop prodigiosenes as G-quadruplex stabilizing ligands, and therefore, as potential telomerase inhibitors, and anti-cancer agents.

**Chapter 6** summarizes major conclusions of this research and suggests some future directions, while the experimental protocols used for the research described in **Chapters 2-5** are described in **Chapter 7**.

### 1.3 Introduction on Prodigiosenes

Prodigiosenes are a family of naturally-occurring red pigments produced by microorganisms such as *Streptomyces* and *Serratia marcescens* (*Bacillus prodigiosus*), a bacterium found in damp and warm conditions.<sup>9,42</sup> These compounds are bacterial secondary metabolites with a characteristic pyrrolylpyromethene skeleton, a B-ring methoxy group and different alkyl substituents arranged either in an acyclic or cyclic manner. **Figure 1.4** lists some naturally-occurring prodigiosenes (**1**, **4** and **5**) as well as some synthetic analogs (**6-8**).

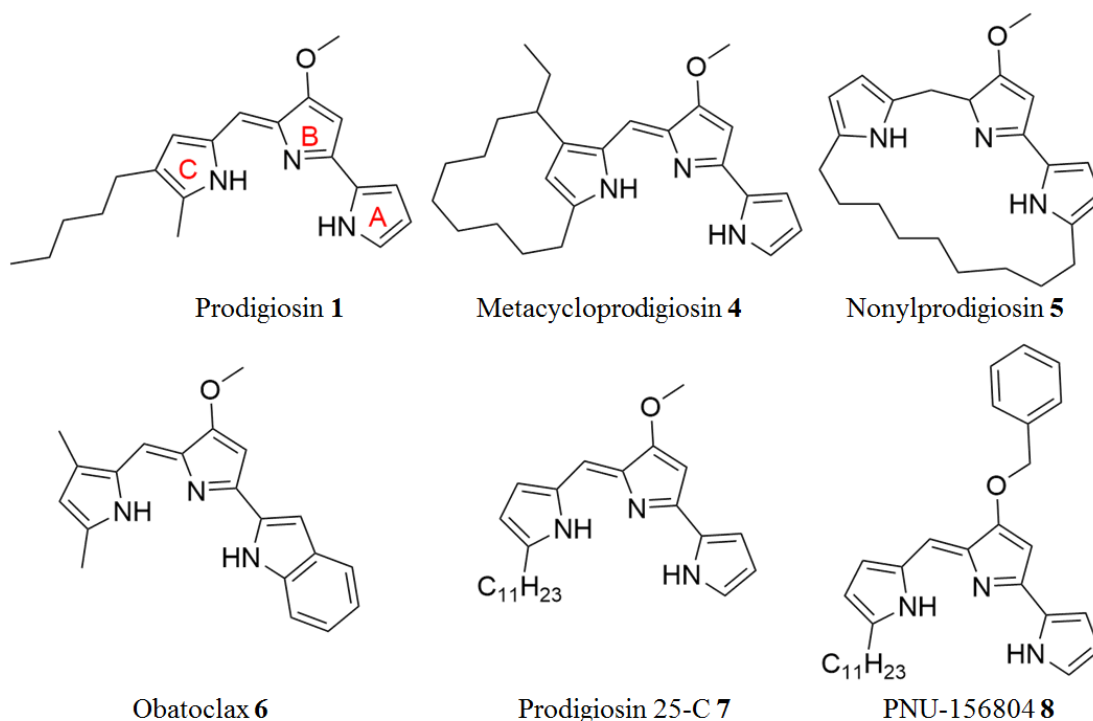


**Figure 1.4.** Structures of some of the commonly known prodigiosenes **1** and **4-8**.

Prodigiosin **1** was the first prodigiosene to be isolated in 1929,<sup>16</sup> but its full synthesis was not elucidated until 1962.<sup>17,18</sup> Initially, prodigiosenes were found to be too cytotoxic and were not pursued for any pharmacological purposes. However, over the last two decades, there has been a renewed interest in these natural products because some of the derivatives have been found to possess potent antimicrobial, antimalarial, anti-cancer, and immunosuppressive activities.<sup>14,24,43</sup> At non-toxic concentrations, the potential immunosuppressive activity was found to be significant.<sup>44</sup> Therefore, synthetic analogs of prodigiosin **1** were developed as immunosuppressive agents.<sup>5</sup> Prodigiosenes have been examined for their anti-cancer properties by the National Cancer Institute (NCI).<sup>45</sup> These compounds induce apoptosis and are active against breast,<sup>21,46</sup> haematopoietic,<sup>23,47</sup> and colon cancer cell lines.<sup>48</sup> They also showed activity in hepatocellular carcinoma xenografts and in B-cell chronic lymphocytic leukemia in 32 patients.<sup>22,49</sup>

The therapeutic relevance of prodigiosenes has made sure that new, less toxic but more effective derivatives of prodigiosenes are pursued for treatments of various anomalies. In this ongoing pursuit, a number of derivatives have been selected for clinical and pre-clinical trials. Prodigiosin **1** is in preclinical trials for treatment of pancreatic cancer.<sup>14,50</sup> The mesylate salt of obatoclax (GX15-070) **6** has undergone Phase I clinical trials for leukemia treatment.<sup>12,13</sup> PNU-156804 (**8**) has been used as an anti-rejection compound in organ transplants due to its immunosuppressive properties.<sup>5,15</sup>

Despite the keen interest in biological activity of prodigiosenes, their main mechanism of action for cancer treatment has not been identified unambiguously. There are two proposed mechanisms to explain the anti-cancer activity shown by prodigiosenes that have been described in more detail in the next sections. Before describing my research, some background on the two proposed mechanisms used to explain the anti-cancer properties of prodigiosenes is provided.

#### **1.4 Proposed Mechanisms for Anti-Cancer Properties of Prodigiosenes**

For developing any compound as a potential therapeutic, it is essential to understand its mode of action. By knowing the details of the mechanism, one can fine-tune the properties of the compound to extract maximum efficacy. In this regard, Manderville and colleagues reported on the ability of prodigiosenes to facilitate cleavage of dsDNA in the presence of copper(II).<sup>51</sup> This mechanism has been discussed in brief in the **Section 1.4.1**. In the second mechanism put forth to explain prodigiosenes anti-cancer activity, the research groups of Nakashima and Yamamoto pointed out the ability of prodigiosenes to catalyze symport of  $H^+/Cl^-$  ions across cellular membranes. This second mechanism is described in detail in **Section 1.4.2**.

##### **1.4.1 Oxidative DNA Cleavage by Prodigiosene•Cu<sup>2+</sup> Complexes**

Bipyrroles are known to undergo one-electron oxidation leading to the formation of a dimeric species. The resulting dimer can donate two electrons and trigger oxidative damage of biopolymers and cause oxidative stress.<sup>52,53</sup> Based on this knowledge, Manderville *et. al.* rationalized that prodigiosenes, in the presence of a suitable redox-active metal ion, should be able to facilitate a similar oxidative damage

of DNA. They tested their hypothesis by monitoring mixtures of supercoiled plasmid DNA (Form I) with prodigiosin **1** and different metal cations, such as Cu(II), Fe(III) and Ni(II) by agarose gel electrophoresis.<sup>51</sup> Following a 20-40 minute incubation time, the single-stranded nicked circular form of DNA was visible on the gel in the presence of Cu(II). This observation is classical evidence for a dsDNA cleavage event.<sup>54</sup> Also, dsDNA cleavage is a known mechanism of apoptosis.<sup>55</sup> Catalase is an enzyme that lowers the solution concentrations of hydrogen peroxide (H<sub>2</sub>O<sub>2</sub>). When catalase was added to the original mixture of dsDNA, prodigiosin and Cu(II) it completely inhibited the DNA cleavage reaction. This confirmed the oxidative nature of DNA cleavage as catalyzed by prodigiosin **1**.

In the absence of copper(II), prodigiosin has been shown to intercalate with calf thymus-DNA, particularly at AT rich regions.<sup>39,40</sup> The prodigiosin-DNA interaction study is discussed in more detail in **Chapter 5**. Collectively, these studies inspired us to explore the binding interactions between prodigiosin **1** and G-quadruplex DNA.

#### **1.4.2 H<sup>+</sup>/Cl<sup>-</sup> Co-Transport Triggers Apoptosis**

The second mechanism proposed for prodigiosenes anti-cancer activity evolved out of multiple studies done by different research groups. Discussion of these studies is arranged into two sets. The first set involves studies done to establish the role of prodigiosenes in altering intracellular pH, due to the apparent movement of H<sup>+</sup> and Cl<sup>-</sup> ions across membranes. The second set of studies involves work done with prodigiosenes and cancer cells to confirm whether these compounds induce apoptosis in tumor cells.

### 1.4.2.1 Prodigiosenes can Inhibit Proton Pump Activity

Vacuolar H<sup>+</sup>-ATPase (or V-ATPase) are enzymes found in eukaryotes that catalyze the hydrolysis of adenosine triphosphate (ATP) into adenosine diphosphate (ADP) and a phosphate ion. The hydrolysis reaction is an exergonic reaction and the energy produced by this reaction helps V-ATPase to transport protons against the gradient across intracellular and plasma membranes. Maintenance of intracellular pH is essential for smooth functioning of cells, and V-ATPase is responsible for maintaining a low internal pH in certain cell types and intracellular organelles such as Golgi apparatus, lysosomes and other vacuoles.<sup>56</sup>

Kataoka and colleagues published two important papers that demonstrated the ability of prodigiosin 25-C (undecylprodigiosin) **7** to neutralize acidic organelles in cytotoxic T cells and baby hamster kidney (BHK) cells (**Figure 1.5**).<sup>19,57</sup> In the first study, the authors showed that **7** reversed the activity of V-ATPase by increasing the pH of certain organelles present inside T-cells.<sup>19</sup> By neutralizing the acidic organelles, compound **7** also successfully negated the cytotoxicity of T cells. This result was one of the first studies done to explain the immunosuppressive properties of prodigiosenes.

In a second publication, Kataoka and group showed that even though prodigiosin 25-C inhibited the proton pump activity of V-ATPase with an IC<sub>50</sub> value of 30 nM in BHK cells, it did not interfere with the ATP hydrolysis reaction.<sup>57</sup> Concentrations as high as 1 μM of prodigiosin 25-C did not affect the ATP hydrolysis process. Further, specific organelles such as Golgi apparatus and mitochondria in BHK cells were monitored using transmission electron micrographs. It was noted that



addition of **7** was followed by swelling of these organelles. The swelling in organelles correlated with the initial observations. By neutralizing the acidic pH of these organelles, prodigiosin 25-C increased their internal pH. As a result, an osmotic imbalance was generated which, was rectified by inflow of water into the organelles, and led to the swelling of these intracellular organelles.

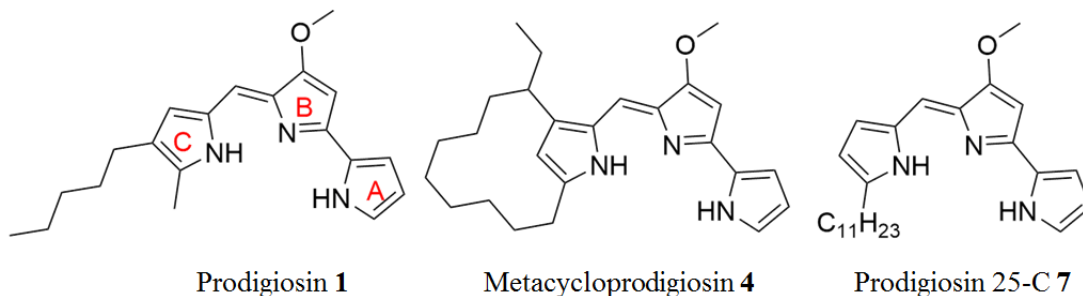


**Figure 1.5.** Structures of prodigiosenes **1**, **4** and **7**.

Similar observations were made in different cell types such as osteoclasts and bovine cells.<sup>27,58</sup> In both cases, metacycloprodigiosin **4** and prodigiosin 25-C **7** inhibited the proton pump activity of V-ATPase. The study by Wasserman and colleagues was especially important as it helped in narrowing down the molecular mechanism to some extent.<sup>27</sup> The authors first showed that prodigiosin **1**, metacycloprodigiosin **4** and prodigiosin 25-C **7** reversed the activity of V-ATPase enzyme in bovine cells in the presence of chloride anion (**Figure 1.5**). No potential difference across the membranes was detected, which means that the movement of ions is an electroneutral process such that it involved either the symport of H<sup>+</sup>/Cl<sup>-</sup> ions or the functionally equivalent antiport of OH<sup>-</sup>/Cl<sup>-</sup> ions.

Next, to prove that the ion movement was dependent on the presence of  $\text{Cl}^-$ , Wasserman and his group performed some experiments with liposomes loaded with a pH-sensitive fluorescent dye pyranine. Liposomes are small vesicles with a bilayer membrane devoid of any ion conducting proteins.<sup>27</sup> Thus, no ions can diffuse through the membrane unless assisted by an ion transporter. Activity of prodigiosenes was tested by changing two variables – dose and time-dependence. The general observation was that when the concentration of extravesicular  $\text{Cl}^-$  ion was in excess, as compared to the concentration in internal solution of liposomes, addition of prodigiosenes reduced the intravesicular pH (measured in terms of fluorescence of pyranine). This pH drop was presumably due to influx of  $\text{H}^+$  and  $\text{Cl}^-$  ions into the vesicle. In the reverse case, when the intravesicular concentration of  $\text{Cl}^-$  was increased, then the addition of prodigiosenes led to an increase in the intravesicular pH due to efflux of  $\text{H}^+$  and  $\text{Cl}^-$  ions. This was indirect evidence to indicate the involvement of  $\text{Cl}^-$  in the  $\text{H}^+$  translocation process catalyzed by prodigiosenes.<sup>25, 27</sup>

Taking their experiments a step further, the authors used radioactive  $^{36}\text{Cl}$  in the external buffer to gather direct evidence for transmembrane  $\text{Cl}^-$  movement.<sup>27</sup> The uptake of  $^{36}\text{Cl}^-$  into the liposomes was measured by liquid-scintillation counter, while the changes in intravesicular pH were monitored by measuring fluorescence of pyranine. Initially, the extravesicular pH was lower than the pH inside the liposomes. It was reported that prodigiosin **1**, metacycloprodigiosin **4** and prodigiosin 25-C **7** promoted the uptake of radioactive  $^{36}\text{Cl}$  from the external buffer into the liposomes, accompanied by a decrease in the intravesicular pH.

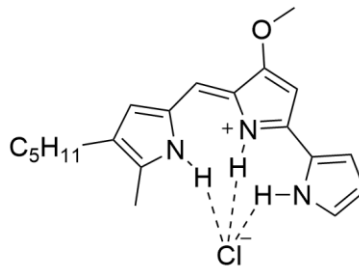


**Figure 1.6.** The proposed lipophilic ion pair  $1 \cdot \text{H}^+ \text{Cl}^-$  formed between prodigiosin **1** and  $\text{H}^+/\text{Cl}^-$  ions that promotes proton movement across the liposomal membrane.

Thus, based on the above experiments, Wasserman and colleagues proposed a lipophilic ion pair formation between prodigiosenes and  $\text{H}^+/\text{Cl}^-$  (**Figure 1.6**). The lipophilic ion pair  $1 \cdot \text{H}^+ \text{Cl}^-$  should be able to diffuse through the liposomal membrane, promoting  $\text{H}^+$  and  $\text{Cl}^-$  movement across the membrane.

There were other studies performed with plant vacuoles that further established that the process of alteration of pH inside cells was only possible in the presence of  $\text{Cl}^-$  and not with other anions such as the hydrophilic  $\text{SO}_4^{2-}$  anion.<sup>59,60</sup> The next important development was the finding that the  $\text{H}^+ \text{Cl}^-$  co-transport catalyzed by prodigiosenes leads to apoptosis in cancer cells.

#### 1.4.2.2 $\text{H}^+ \text{Cl}^-$ Co-Transport by Prodigiosenes can Lead to Apoptosis

A few years after Kataoka and colleagues connected the ability of prodigiosenes to inhibit the proton pump activity of V-ATPase in presence of  $\text{Cl}^-$  ions,<sup>27,57</sup> two publications examining the impact of prodigiosenes on cancer cells were reported.<sup>22,61</sup>

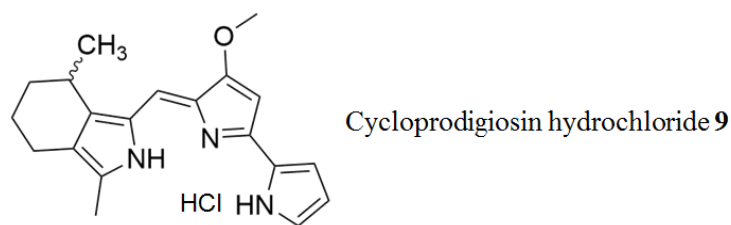


**Figure 1.7.** Structure of cycloprodigiosin hydrochloride **9**.

Yamamoto and colleagues found that cycloprodigiosin hydrochloride **9** can inhibit the growth of six different types of liver cancer cells, depending on dosage and duration of incubation (structure shown in **Figure 1.7**).<sup>22</sup> The same effect was not observed on normal rat hepatocytes. When Huh-7 liver cancer cells were treated with **9** *in vitro*, cell proliferation decreased drastically. By using cell cytometry, it was found that the intracellular pH ( $\text{pH}_i$ ) decreased from 7.3 to 6.8 after treatment of Huh-7 cells with cycloprodigiosin hydrochloride **9**. A change in intracellular pH can lead to cell death as has been shown by different studies.<sup>62</sup> In an *in vivo* study, **9** was also tested on mice xenografted with Huh-7 cells. In a treatment that lasted 14 days, tumor growth was found to be significantly reduced on day 8. Based on a histological examination, it was found that the tumor cells had undergone apoptosis. Although the molecular mechanism could not be comprehended, the authors advocated the potential application of cycloprodigiosin as an anti-cancer agent.

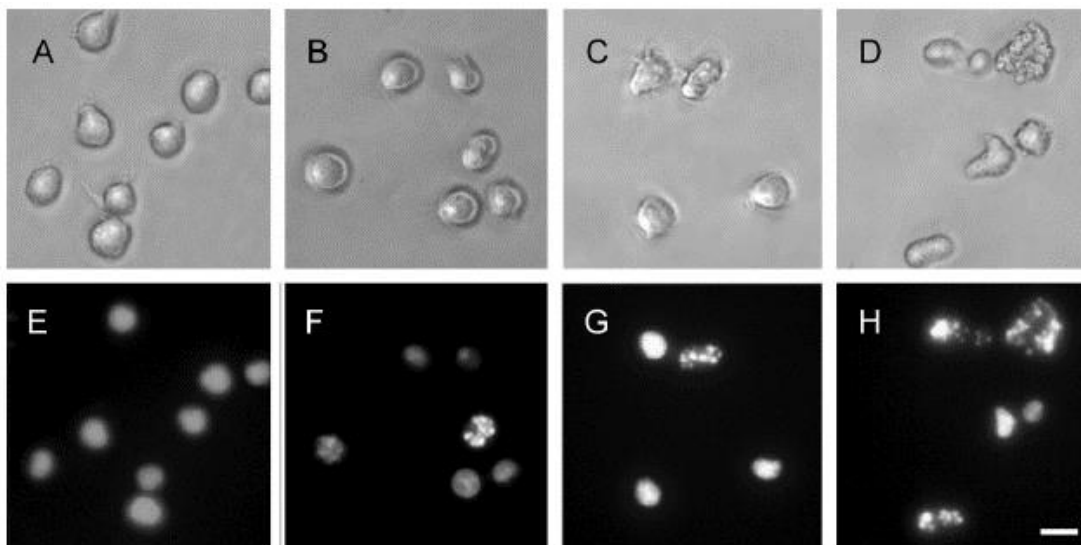


**Figure 1.8.** Effect of **PG-L-1** on cellular and nuclear morphology in U937 Cells. U937 cells ( $6 \times 10^5$  cells/dish) were treated with 0 mg/ml (**A, E**), 0.1 mg/ml (**B, F**), 1.5 mg/ml (**C, G**), and 50 mg/ml (**D, H**) of **PG-L-1** at 37 °C for 3 h. Then, the cells were observed under a phase contrast microscope (**A, B, C, D**), or a fluorescence microscope (**E, F, G, H**) after staining with Hoechst 33258 (40 mM) for 10 min. The bar indicates 10 mm. Reprinted with permission from *Biol. Pharm. Bull.* **2005**, 28 (12), 2289-2295. Copyright (2005) Pharmaceutical Society of Japan.<sup>61</sup>

Another significant finding was made by Nakashima and colleagues who used **PG-L-1**, a prodigiosene extracted from a bacterial strain for *in vitro* studies with human myeloid leukemia (U937) cells.<sup>61</sup> **PG-L-1** was reported to induce apoptotic nuclear morphological changes in U937 cells (**Figure 1.8**). Further, it was found that in the treated U937 cells, the acidic compartment such as lysosomes disintegrated, suggesting that **PG-L-1** induced a change in intracellular pH of these cell organelles that then triggered an apoptotic signal.

Some cancer cells have an alkaline intracellular pH, which is essential for the growth, transformation and metabolism of the cells.<sup>63</sup> Therefore, a possible cancer treatment therapy can take advantage of the ability of prodigiosenes to alter pH inside cancer cells and trigger apoptosis.<sup>64</sup> The research described in this section culminates together to provide evidence for this possibility. But, the prodigiosenes could possibly be used for other therapeutic purposes as well. Their ability to move anions across membranes might be used for treatment of abnormalities caused due to misregulation or malfunctioning of natural ion channels or proteins. The next section describes the significance of anion transport in physiological system and the work done with prodigiosenes to investigate their ability to catalyze anion exchange across membranes.

### **1.5 Prodigiosenes and Transmembrane Anion Transport**

In all living organisms, movement of gases (O<sub>2</sub>, CO<sub>2</sub>, N<sub>2</sub>), polar molecules (amino acids, sugars) and ions (Cl<sup>-</sup>, K<sup>+</sup>, Na<sup>+</sup>) across the membrane of a cell and its organelles is an integral part of biological processes. Most hydrophobic and small uncharged solutes can diffuse through a lipid membrane. However, specific membrane proteins or ion channels are required for the movement of larger molecules and ions through the membrane. Nature being the original innovator, has a large array of ionophores in the form of ion channels,<sup>65,66</sup> proteins,<sup>67</sup> or ion carriers<sup>68</sup> to move ions across membranes. Just like a transistor in an electronic circuit, these channels open and close when signaled to create a hydrophilic passage through a hydrophobic membrane that enables the movement of charged ions. This catalytic process is mostly governed by external factors such as an imbalance in pH or ion concentration, potential

difference on either side of the membrane, osmosis or specific messengers. Therefore, movement of ions becomes an important step in processes like respiration, signaling pathways, regulating cell pH and osmotic balance. Interestingly, ion movement across channels makes use of certain non-covalent interactions (such as H-bonding, electrostatic interactions, anion- $\pi$ ) that form the same foundation pillars of the supramolecular chemistry field.

One example of a membrane embedded protein is the cystic fibrosis transmembrane conductance regulator (CFTR) located in the epithelial tissue. This channel regulates the flow of  $\text{Cl}^-$  and  $\text{HCO}_3^-$  ions and is controlled by protein kinase A. There are more than 1800 mutations that can disrupt the flow of  $\text{Cl}^-$ ,  $\text{HCO}_3^-$  and water molecules across the CFTR channel.<sup>69</sup> These mutations result in thickening of mucus in lungs, pancreas and intestines. The resulting condition is an autosomal recessive disease known as cystic fibrosis (CF). Thickened mucus in lungs leads to frequent respiratory infections.<sup>70</sup> Conditions resulting due to CF can severely risk the health of a patient and can be fatal. There are other diseases like Bartter syndrome and Dent's disease that are also caused due to misregulation of  $\text{K}^+$  or  $\text{Cl}^-$  ions.<sup>71-73</sup>

It is widely understood that by applying supramolecular concepts of reversible non-covalent binding, synthetic channels or small compounds may ultimately be used to alleviate some of these disorders. In this regard, scientists have been actively working on developing anion receptors. The synthetic anion receptors should be able to mimic natural transport systems and be capable of moving anions across hydrophobic membranes.<sup>74,75</sup> One excellent example in recent times is that of molecule

**10** developed by Yang and colleagues (**Figure 1.9**). They successfully demonstrated the ability of **10** to form chloride channels that restore  $\text{Cl}^-$  movement in epithelial cells affected by cystic fibrosis.<sup>76</sup> Using whole-cell patch clamp technique, currents were detected in CuFi-8 cells upon application of compound **10**. The CuFi-8 cells were obtained from the bronchial epithelia of a patient suffering from CF. A gradual increase in whole-cell currents was observed initially, after which the currents stabilized.

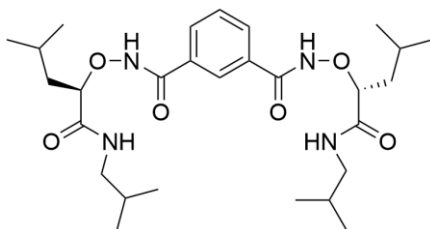


**Figure 1.9.** Compound **10** developed by Yang and her group for treatment of CF.

The work done by the Yang group is an important milestone in the field of anion transport. More and more research groups are trying to explore the biological aspects of their work. Similarly, a number of interesting transmembrane anion transport studies have been done with prodigiosin **1** and its derivatives.<sup>2,9,77</sup> There are 3 publications that are most significant. Two of these studies showed that the natural product prodigiosin **1** can transport  $\text{Cl}^-$ ,  $\text{NO}_3^-$  and  $\text{HCO}_3^-$  across liposomal membrane.<sup>31,32</sup> The third study correlated the anion transport rates of synthetic prodigiosenes with their anti-cancer activity.<sup>10</sup> These studies are described below.



### 1.5.1 Anti-Cancer Activity Correlates with the Anion Transport Rates

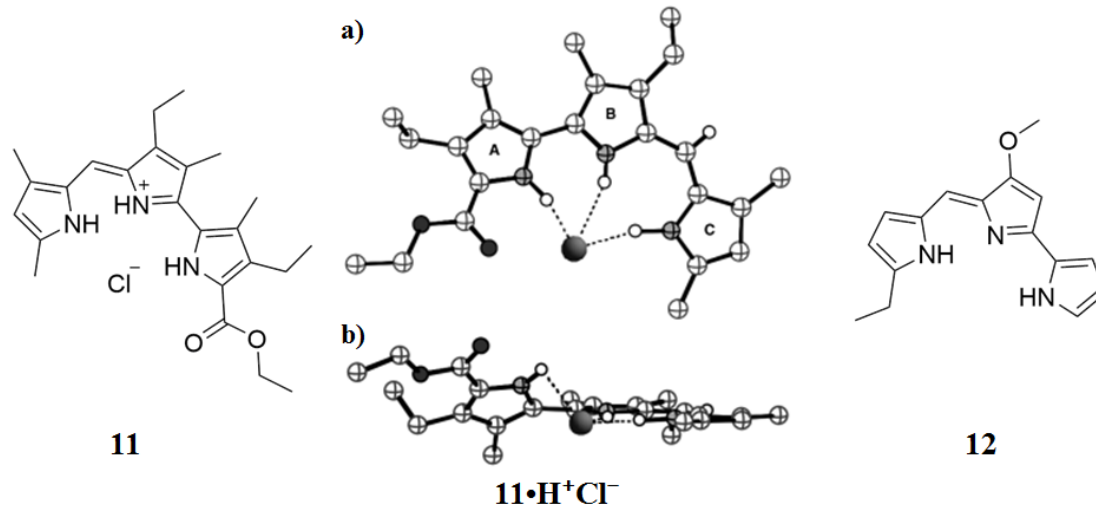


**Figure 1.10.** Structure of the prodigiosenes **11** and **12**. Two views of the X-ray crystal structure of the complex formed between protonated prodigiosin **11** and Cl<sup>-</sup> ion. Reprinted with permission from *Angew. Chem. Int. Ed.* **2005**, *44* (37), 5989-5992. Copyright © 2005 Wiley-VCH Verlag GmbH & Co. KGaA, Weinheim.<sup>10</sup>

Sessler's work with synthetic prodigiosenes was an important piece of work that correlated the anion transport activity of synthetic prodigiosenes with their *in vitro* anti-cancer activity.<sup>10</sup> A series of synthetic derivatives of prodigiosin **1** were synthesized and tested for their anion binding, transmembrane transport and *in vitro* anti-cancer activity. An X-ray crystal structure of compound **11** showed a Cl<sup>-</sup> anion bound by the three NH protons on the pyrrole rings in solid state (**Figure 1.10**). After establishing binding interactions between prodigiosene **11** and Cl<sup>-</sup>, they tested these synthetic derivatives for their Cl<sup>-</sup> transport activity using phospholipid liposomes. A chloride ion selective electrode was used to monitor the efflux of Cl<sup>-</sup> from liposomes.

Compound **12**, with a structure closest to prodigiosin **1**, was most efficient at transporting  $\text{Cl}^-$  ions out of the liposomes and into the extravesicular solution.

*In vitro* cell proliferation studies were also performed with the synthetic analogs.<sup>10</sup> The compounds were tested against two cell lines – A549 human lung cancer and PC3 human prostate cancer cells. All of the compounds exhibited 100% inhibition of cell proliferation at concentrations of 40  $\mu\text{M}$ . When the data from anti-cancer activity and transmembrane anion transport experiments were compared, it was found that the results from both studies correlated well. Further, this correlation supported the  $\text{H}^+/\text{Cl}^-$  co-transport mechanism proposed by Wasserman, Ohkuma and colleagues.<sup>27</sup>

### 1.5.2 Prodigiosin Catalyzes Anion Exchange Across Bilayer

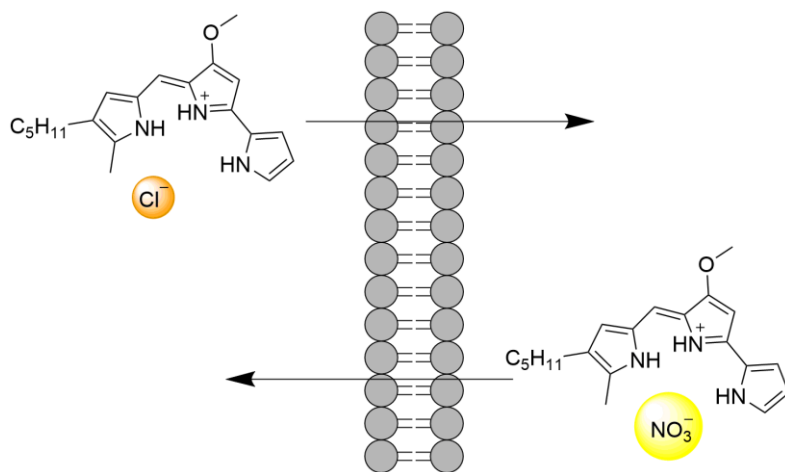


**Figure 1.11.** Anion exchange mediated by prodigiosin  $1\cdot\text{H}^+$  across a lipid bilayer. Prodigiosin  $1\cdot\text{H}^+$  can bind  $\text{Cl}^-$  or  $\text{NO}_3^-$  anions and diffuse them through the membrane.

Wasserman proposed a  $\text{H}^+/\text{Cl}^-$  co-transport or  $\text{OH}^-/\text{Cl}^-$  antiport mechanism while rationalizing the ability of prodigiosenes to alter intravesicular pH.<sup>27</sup> Studies done by the Davis group demonstrated that prodigiosin could indeed exchange anions

across lipid bilayers.<sup>31</sup> In a study done by Seganish and Davis, it was shown that prodigiosin can catalyze exchange of anions –  $\text{Cl}^-$  and  $\text{NO}_3^-$  across a lipid bilayer (**Figure 1.11**). The anion transport experiments were done with liposomes encapsulating, either  $\text{NaNO}_3$  or  $\text{Na}_2\text{SO}_4$  buffer. A chloride gradient was applied by adding a pulse of  $\text{NaCl}$ . The internal pH of the liposomes was monitored by loading the vesicles with a pH sensitive fluorescent pyranine dye. Influx of  $\text{Cl}^-$  was measured by monitoring the change in fluorescence of the  $\text{Cl}^-$  sensitive lucigenin (LG) dye.<sup>78</sup>

For the first case, liposomes were loaded with  $\text{Na}_2\text{SO}_4$ , which is a hydrophilic anion ( $\Delta G_{\text{hyd}} = -1080$  kJ/mol). Addition of prodigiosin **1** led to an immediate drop in the intravesicular pH (**Figure 1.12B**) whereas a  $\text{Cl}^-$  influx occurred to only 20% of the value that would be expected for complete equilibrium (**Figure 1.12A**). In the second case, liposomes were loaded with  $\text{NaNO}_3$  on the inside.  $\text{NaNO}_3$  is a less hydrophilic anion ( $\Delta G_{\text{hyd}} = -300$  kJ/mol). When prodigiosin **1** was added to the liposome solution, a rapid increase in  $\text{Cl}^-$  influx was observed (**Figure 1.12C**) accompanied by no change in the internal pH of liposomes (**Figure 1.12D**). From these experiments, the authors concluded that prodigiosin **1** can successfully facilitate anion exchange or antiport mechanism between  $\text{Cl}^-$  and a less hydrophilic anion,  $\text{NO}_3^-$ . In contrast, in the presence of a more hydrophilic anion  $\text{SO}_4^{2-}$ , prodigiosin **1** instead catalyzes the symport of  $\text{H}^+/\text{Cl}^-$  across the liposomal membranes.

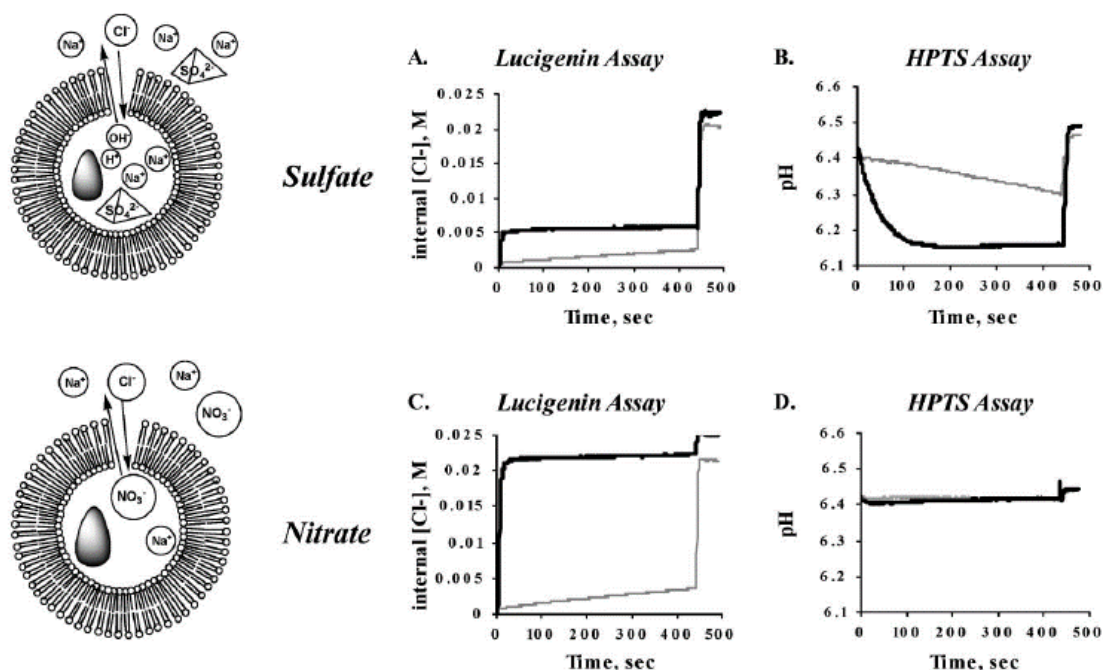


**Figure 1.12.** Chloride gradient assays on 100 nm EYPC liposomes in 10 mM sodium phosphate (pH 6.4) containing either 75 mM  $\text{Na}_2\text{SO}_4$  (**A** and **B**) or 100 mM  $\text{NaNO}_3$  (**C** and **D**). The chloride gradient was initiated by adding NaCl to give an external concentration of 25 mM. Chloride concentration inside the vesicles (panels **A** and **C**) was calculated from the fluorescence of entrapped LG dye. The pH (panels **B** and **D**) is calculated from the fluorescence ratio of HPTS dye emitted at 510 nm when excited at 403 and 460 nm in a dual wavelength assay. The trace shown in grey represents DMSO blanks. Reprinted with permission from *Chem. Commun.* **2005**, (46), 5781-5783. Copyright (2005) Royal Society of Chemistry.<sup>31</sup>

Another experiment using dipalmitoyl-phosphatidylcholine (DPPC) liposomes demonstrated that prodigiosin moves anions across membrane by an ion carrier mechanism and not by forming channels. Thus, the paper was significant for two

reasons: a) it was the first study to show that prodigiosin **1** can facilitate anion exchange across lipid bilayers and b) depending on the environmental conditions, prodigiosin's  $\text{Cl}^-$  transport mechanism can switch between  $\text{H}^+/\text{Cl}^-$  co-transport or  $\text{OH}^-/\text{Cl}^-$  antiport.

### 1.5.3 Prodigiosin Facilitates Transmembrane Movement of $\text{HCO}_3^-$

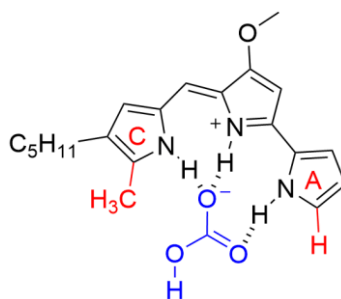


**Figure 1.13.** Proposed structure of a complex between  $\text{HCO}_3^-$  and prodigiosin  $\mathbf{1}\cdot\text{H}^+$ . The H5 proton on ring A and the methyl group on ring C are highlighted in red.

Nitrate and bicarbonate anions have similar shapes and sizes, yet, it is more challenging to transport  $\text{HCO}_3^-$  across lipid bilayers due to its higher hydrophilicity ( $\Delta G_{\text{hyd}} = -388 \text{ kJ/mol}$ ) as compared to the  $\text{NO}_3^-$  ion ( $\Delta G_{\text{hyd}} = -300 \text{ kJ/mol}$ ).<sup>79</sup> This study showed that prodigiosin **1** can transport  $\text{HCO}_3^-$  across lipid membranes.<sup>32</sup> The rationale for selecting prodigiosin as a  $\text{HCO}_3^-$  receptor was the presence of hydrogen bond donors and acceptors that provide a complimentary binding site for the anion. Binding between prodigiosin **1** and  $\text{HCO}_3^-$  anion was demonstrated by using NMR spectroscopy. In the NMR titration between prodigiosin **1** and tetraethylammonium bicarbonate (TEAB), the proton resonances most influenced were for the H5 proton on ring A and the methyl group on ring C (highlighted in red in **Figure 1.13**). Based on

the NMR observations, a structure was proposed where all the rings were in cis conformation, forming a  $\text{HCO}_3^-$  binding cleft.

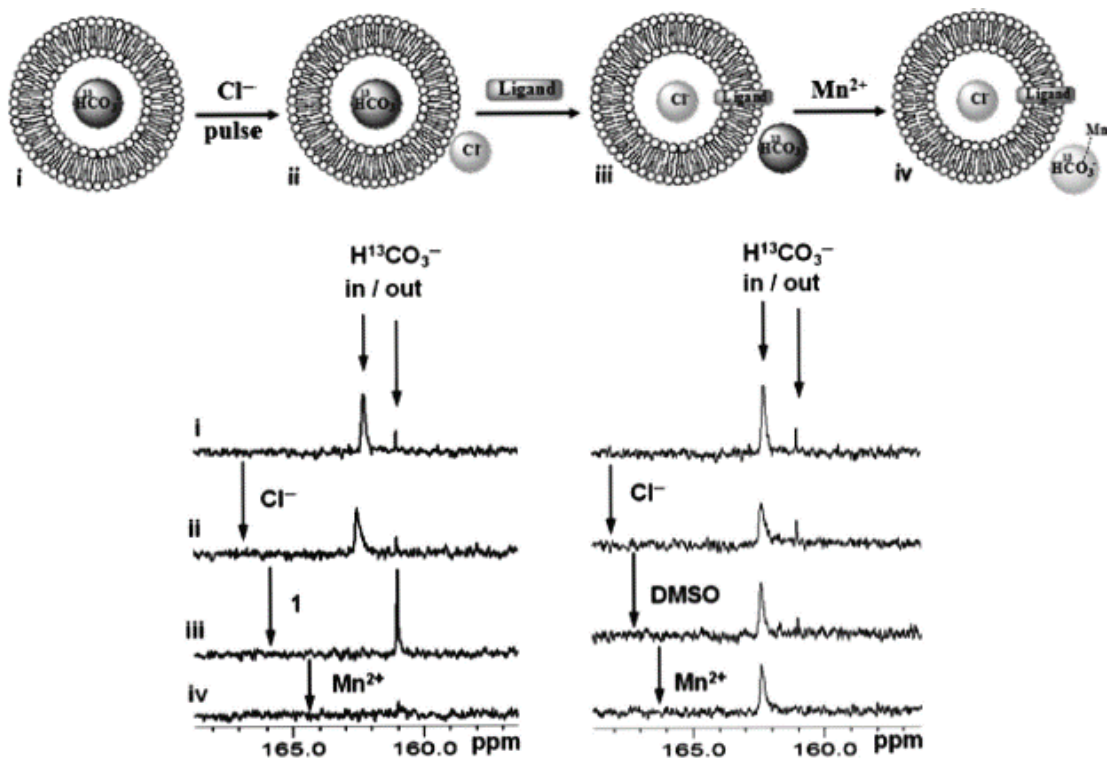


**Figure 1.14.**  $^{13}\text{C}$  NMR experiments demonstrate that prodigiosin **1** is able to facilitate  $\text{Cl}^-/\text{HCO}_3^-$  antiport. Titration sequence for monitoring the transmembrane transport of bicarbonate ions in  $\text{H}^{13}\text{CO}_3^-$  loaded EYPC liposomes by prodigiosin **1** and DMSO.  $^{13}\text{C}$  NMR spectra (i) before and (ii) after the addition of the 50 mM NaCl pulse to EYPC vesicles loaded with 100 mM  $\text{NaH}^{13}\text{CO}_3$ , 20 mM HEPES buffer, and dispersed in 75 mM  $\text{Na}_2\text{SO}_4$ , 20mM HEPES buffer, pH 7.5; (iii) after the addition of prodigiosin **1** or DMSO (**1**, 0.1 mol%; DMSO, 870 mol%); (iv) after the addition of 0.5 mM  $\text{Mn}^{2+}$  (1:100  $\text{Mn}^{2+}/\text{Cl}^-$  ratio). Reprinted with permission from *Nat. Chem.* **2009**, *1* (2), 138-144. Copyright (2009) Nature Publishing Group.<sup>32</sup>

Using a  $^{13}\text{C}$  NMR assay, **Figure 1.14** shows data illustrating prodigiosin-mediated  $\text{HCO}_3^-/\text{Cl}^-$  exchange. EYPC liposomes (5 mM) filled with 100 mM  $\text{NaH}^{13}\text{CO}_3$  were suspended in a sulfate solution and a 50 mM NaCl pulse was added to this solution. A sharp  $^{13}\text{C}$  NMR signal for the intravesicular  $\text{H}^{13}\text{CO}_3^-$  was observed at  $\delta$  162 ppm. After addition of prodigiosin **1**, a sharp  $^{13}\text{C}$  NMR signal for  $\text{H}^{13}\text{CO}_3^-$  appeared due to transport of bicarbonate out of the liposome mediated by **1**. A paramagnetic ion,  $\text{Mn}^{2+}$  was added to broaden any  $^{13}\text{C}$  NMR signal originating from extravesicular  $\text{H}^{13}\text{CO}_3^-$  anion, whereas the  $^{13}\text{C}$  NMR signals for intravesicular  $\text{H}^{13}\text{CO}_3^-$  remained unaffected by the membrane-impermeable  $\text{Mn}^{2+}$ . Thus, these NMR experiments allowed for the discrimination of extravesicular and intravesicular  $\text{H}^{13}\text{CO}_3^-$  and enabled the transmembrane movement of anion to be established.

The natural product prodigiosin **1** facilitated  $\text{Cl}^-/\text{HCO}_3^-$  anion exchange, a process that is typically mediated by membrane proteins. Since then the field of anion recognition and transport has seen the advent of many innovative receptors. The investigations have also paved way for new guest molecules and the study of their transmembrane transport properties. Scientists are become increasingly interested in looking at membrane transport of biologically relevant ions or small molecules other than chloride, nitrate and bicarbonate anions. These new molecules include oligonucleotides, amino acids, and less-common anions.

#### **1.5.4 Prodigiosin 1 can Target Anions Other than $\text{Cl}^-$**

Chloride, nitrate and bicarbonate anions are the most commonly studied anions for the purpose of transmembrane anion transport. More recently, research groups have

looked at anions like sulfate,<sup>80</sup> perrhenate ( $\text{ReO}_4^-$ ),<sup>81</sup> lactate, pyruvate and propionate<sup>82</sup> and the receptors that can selectively assist these anions to diffuse through membranes. Hou and group have been working with pillarenes that can transport chiral amino acids selectively across liposomal membranes.<sup>83</sup> Gokel *et. al.* expanded their chloride transporting dipicolinamide derivatives into receptors that are capable of binding and transporting large DNA plasmids (>20 kb) across cell membranes of *E. Coli*.<sup>82,84</sup> Matile, Riezman and group have developed a library of dynamic amphiphiles that can help in migration of siRNA into HeLa cells and human primary fibroblasts.<sup>85</sup> There are many other examples that illustrate the expansion in the field of anion transport with respect to the targeted anions. Even though prodigiosin **1** is one of the most effective anion transporters in literature,<sup>86</sup> it has not been used for binding any anions other than the commonly found  $\text{Cl}^-$ ,  $\text{NO}_3^-$  and  $\text{HCO}_3^-$  anions. In **Chapter 5**, we have described a study involving investigation of binding interactions between prodigiosin **1** and a polyanionic species, DNA. We found that prodigiosin **1** can end stack with a G-quadruplex DNA. This study is of potential significance, as it could provide another mechanism to explain the anti-cancer properties of prodigiosenes. Additionally, it gives rise to the prospect of developing prodigiosenes as telomerase inhibiting ligands.

Over time, groups have also become interested in developing methodologies that can be used to regulate ion transport across membranes, using external stimuli. The next section deals with the concept of gating the movement of ions in natural and synthetic systems.



## 1.6 Some Examples of Gating Anion Transport

Last decade saw a wealth of receptor molecules that were developed to selectively move anions across a bilayer.<sup>74,75,87,88</sup> In most cases, the process of ion transport was triggered by imbalance in either ion concentration or pH across the lipid membrane. However, scientists have started to think a step beyond these regular ion transport processes. Research groups are now looking for a greater control of ion transport process. In nature, the conduction of ions across membranes is controlled by various mechanisms. One such example of ClC channel is described below.<sup>89</sup> For this reason, methodologies are being developed that would allow for regulation of flow of ions across a membrane using an external stimuli. Some of these examples of gating of anion transport in natural and vesicle-like systems are discussed.

### 1.6.1 Gating Influenced by Conformational Changes in ClC Channel

Naturally-occurring ClC channel is an example of a pre-organized active site in an ion channel for binding chloride selectively.<sup>89</sup> Serine (S107), tyrosine (Y445), and isoleucine (I356) residues form a portal to the channel opening. All these residues undergo hydrogen bond formation with Cl<sup>-</sup> anion by using their NH and OH protons. A glutamate residue (E148) is present at the opening of the selectivity filter (**Figure 1.15**).<sup>89,90</sup> ClC channel makes use of the glutamate residue (E148) to control opening and closing of the channel, which ultimately regulates the flow of Cl<sup>-</sup> ions. A conformational change caused due to protonation of glutamate residue can result in opening of the channel while, deprotonation can cause the channel to close in its resting state.<sup>89</sup> Presently, few synthetic receptors allow for similar control of ion movement

across membranes. Some examples are described next, which allow for an on/off mechanism for transport of ions.

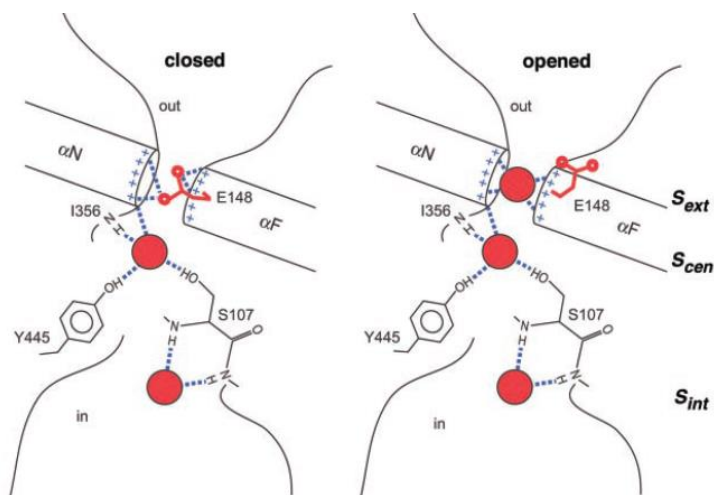


**Figure 1.15.** Schematic drawing of the closed and opened conformation of a ClC chloride channel. In the closed conformation, the ion-binding sites  $S_{int}$  and  $S_{cen}$  are occupied by  $Cl^-$  ions, and the ion-binding site  $S_{ext}$  is occupied by the side chain of Glu (E148). In the opened conformation, the side chain of E148 has moved out of binding site  $S_{ext}$  into the extracellular vestibule.  $S_{ext}$  is occupied by a third  $Cl^-$  ion. Chloride ions are shown as red spheres, the E148 side chain is colored red, and hydrogen bonds are drawn as dashed lines. Reprinted with permission from *Science* **2003**, *300*, 108-112. Copyright (2003) AAAS.<sup>89</sup>

## 1.6.2 Photoresponsive Ion Gating

Zhu and group designed a novel compound **13**, which is a combination of a crown ether and a photo-responsive azobenzene group.<sup>91</sup> Ion conduction by **13** can be regulated by *cis-trans* photoisomerization. The structural design of **13** comprises a crown ether that can stack to form an ion channel while the photoresponsive

azobenzene group acts as a switch to regulate ion flow (**Figure 1.16**). A 12-carbon chain helps in providing enough hydrophobicity to the molecule so that it can partition in and out of the membrane. There is an additional amide NH group, which contributes towards the supramolecular assembly via hydrogen-bonding to the target anion.



**Figure 1.16.** Structure of compound **13**. **a)** Schematic representation of the light-regulated ion channel. The switching between *trans* and *cis* isomer at 365 nm and 450 nm. *Trans* isomer tends to aggregate in solution and shows low transport activity, whereas the *cis* isomer forms a channel inside the membrane resulting in a high transport activity. **b)** Transport activity measured based on fluorescence of safranin O dye for *cis* and *trans* isomer. Adapted with permission from *Chem. Commun.* **2013**, (49), 10311-10313. Copyright (2013) Royal Society of Chemistry.<sup>91</sup>

Patch-clamp technique and HPTS assay in liposomes were employed to monitor transport activity, and confirm channel formation along with *cis-trans* transformation. In the *trans* conformation, compound **13** prefers formation of smaller aggregates rather

than partitioning into the membrane. Due to decreased partitioning ability, *trans*-**13** tends to precipitate out of solution, leading to low ion transport activity (**Figure 1.16**). An increase in transport activity was observed upon irradiation at 365 nm. *Trans* to *cis* conversion takes place at 365 nm so the increased transport activity was attributed to the newly formed *cis* conformation. Another irradiation at 450 nm switched the *cis*-isomer back to *trans*. The photoswitching was followed by a decrease in current flow, which was attributed to the low transport activity exhibited by *trans*-isomer.

### 1.6.3 Voltage-Gated Anion Transport

Anion transport can also be regulated as a function of voltage, as illustrated in the work done by Hou *et. al.*<sup>92</sup> Inspiration for this work came from naturally occurring voltage-gated K<sup>+</sup> channels that contain positively charged Arg units.<sup>93</sup> Hou and group had previously demonstrated that hydrazide-appended pillar[5]enes containing phenylalanine residues can selectively transport certain amino acids such as glycine, alanine, serine, etc.<sup>83</sup> In the same scaffold, Arg units were introduced to give new pillarenes **14**.<sup>92</sup> Arg residues are positively charged and therefore, hydrophilic by nature. Due to the hydrophilic Arg units, peptide **14** is unable partition into the lipid bilayer of KCl encapsulated EYPC vesicles (**Figure 1.17a**), as determined by patch-clamp experiments. In the patch-clamp experiment, negative potential was set to increase from -10 to -100 mV in ten steps, with every pulse lasting 30 s, while the positive potential was kept constantly at +100 mV, with the pulsing time being 90 s (**Figure 1.17c**).

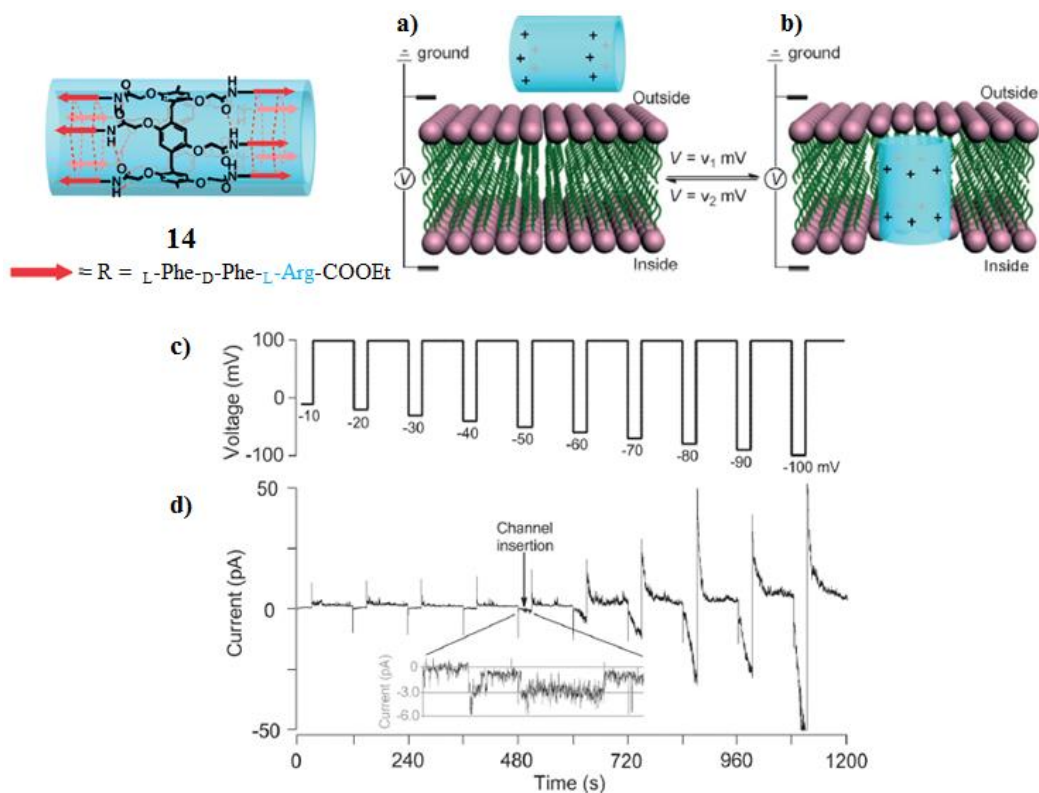


**Figure 1.17.** Structure of pillarenes **14**. Schematic presentation for the voltage-driven channel insertion and exit from the lipid bilayer. **a)** High hydrophilicity of arg units restricts the entry of pillarenes into the lipid membrane. **b)** Application of voltage polarizes the membrane which, facilitates the insertion of pillarene **14** into the membrane. **c)** The alternative negative potential (30 s) and +100 mV (90 s) potential pulse protocol. The negative potential (30 s) increased from -10 to -100 mV in ten steps, while the positive potential was kept constantly at +100 mV. **d)** The macroscopic current trace of **14** by applying the pulse in (c). Inset: The expanded current trace (30 s) at -50 mV showing the single-channel current. Reprinted with permission from *Angew. Chem. Int. Ed.* **2014**, 53 (18), 4578-4581. Copyright © 2014 Wiley-VCH Verlag GmbH & Co. KGaA, Weinheim.<sup>92</sup>

Negative potential facilitated the insertion of channels while a positive potential drove them away from the bilayer. Channel insertions were accompanied by current flow that was measured (**Figure 1.17d**). Thus, the voltage variation influenced the insertion and departure of channels from the bilayer and subsequently, the conduction of ions through the lipid membranes.

#### **1.6.4 Inhibition of Ion Activity by Formation of Inclusion Complexes**

Two examples have been described here that make use of inclusion complexes for inhibiting ion transport activity of ionophores in solution. Imidazolium salts (**15**) are a new and unexplored class of potential anion transporters (**Figure 1.18**).<sup>94</sup> They can self-organize through H-bonds,  $\pi$ -stacking and electrostatic interactions. The resulting assemblies can insert into bilayers and act as ion channels.<sup>94</sup> In this study, the authors explored the possibility of formation of inclusion complexes by imidazolium salt **15** in presence of  $\alpha$ -CD or CB7, which would inhibit the anion transport activity of imidazolium salt **15** in aqueous conditions. The hypothesis was that both  $\alpha$ -CD and CB7 would incorporate the aromatic arms of **15** into their hydrophobic cavity (**Figure 1.18b**). The  $\alpha$ -CD and CB7 are hydrophilic by nature and do not interact with the lipid membrane. In a liposome experiment using the LG assay, vesicles encapsulated with NaCl and LG were used. To initiate Cl<sup>-</sup> transport, compound **15** was added along with 1 or 2 eq of either  $\alpha$ -CD or CB7. It was found that 1 or 2 eq of CB7 partially inhibited the transport ability of **15** (**Figure 1.18c**). An addition of 2 eq of  $\alpha$ -CD completely inhibited Cl<sup>-</sup> transport process.

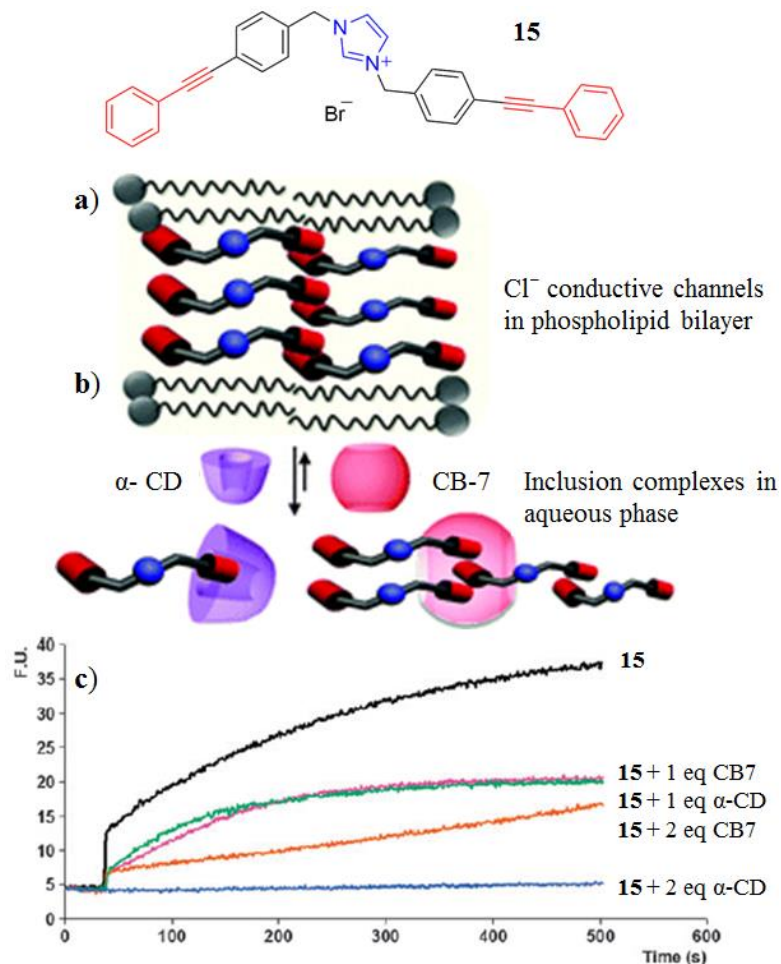


**Figure 1.18.** a) Structure of imidazolium salt **15** b) Schematic representation of the formation of inclusion complexes of **15** with CB7 and  $\alpha$ -CD and displacement of the transporter from the bilayer. c) Relative activity of compound **15** (0.25 mM) in the presence of  $\alpha$ -CD and CB7: intravesicular 100 mM NaCl, 10 mM phosphate buffer, extravesicular 100 mM NaNO<sub>3</sub>, 10 mM phosphate buffer (pH 6.4). Receptor **15** was injected at  $t = 35$  s. Triton-X was injected at  $t = 500$  s. Adapted and reprinted with permission from *Chem. Commun.* **2011**, 47, 1788-1790. Copyright (2011) Royal Society of Chemistry.<sup>94</sup>

The formation of the inclusion complexes between **15** and  $\alpha$ -CD or CB7 was confirmed by  $^1\text{H}$  NMR, UV spectroscopy studies and Jobs' plots. The authors rationalized that the formation of water-soluble inclusion complexes between **15** and  $\alpha$ -CD or CB7 probably reduces the chances of **15** to partition into the lipid bilayer. Since less self-assembled aggregates of **15** are present in the bilayer, transmembrane anion transport is inhibited.

Another example of inhibition of anion transport is of the cholic acid functionalized thread.<sup>95</sup> The anion transport activity of the amphiphilic thread could be inhibited in solution by the assembly of a [2]-pseudorotaxane between compounds **16** and **17** (**Figure 1.19b**), due to interaction between the quaternary ammonium site on **16** and macrocycle **17**, also confirmed by  $^1\text{H}$  NMR studies. Formation of the [2]-pseudorotaxane blocks the ammonium site, which reduces  $\text{Cl}^-$  complexation and transport. **Figure 1.19c** shows the order of addition of **16** and **17** is not important. The anion transport activity of the [2]-pseudorotaxane is identical to that of free **17**, as well as the mechanically blocked [2]-rotaxane. A sudden quenching in fluorescence is observed when **17** is added after **16**, presumably due to formation of the pseudorotaxane. The residual  $\text{Cl}^-$  transport after formation of the [2]-pseudorotaxane is probably due to the complexation of  $\text{Cl}^-$  by the pyridinium moiety of the macrocycle **17**. Upon complexation between the quaternary ammonium site on **16**, macrocycle **17** releases  $\text{Cl}^-$  in the bilayer or inside the liposomes.<sup>95</sup>



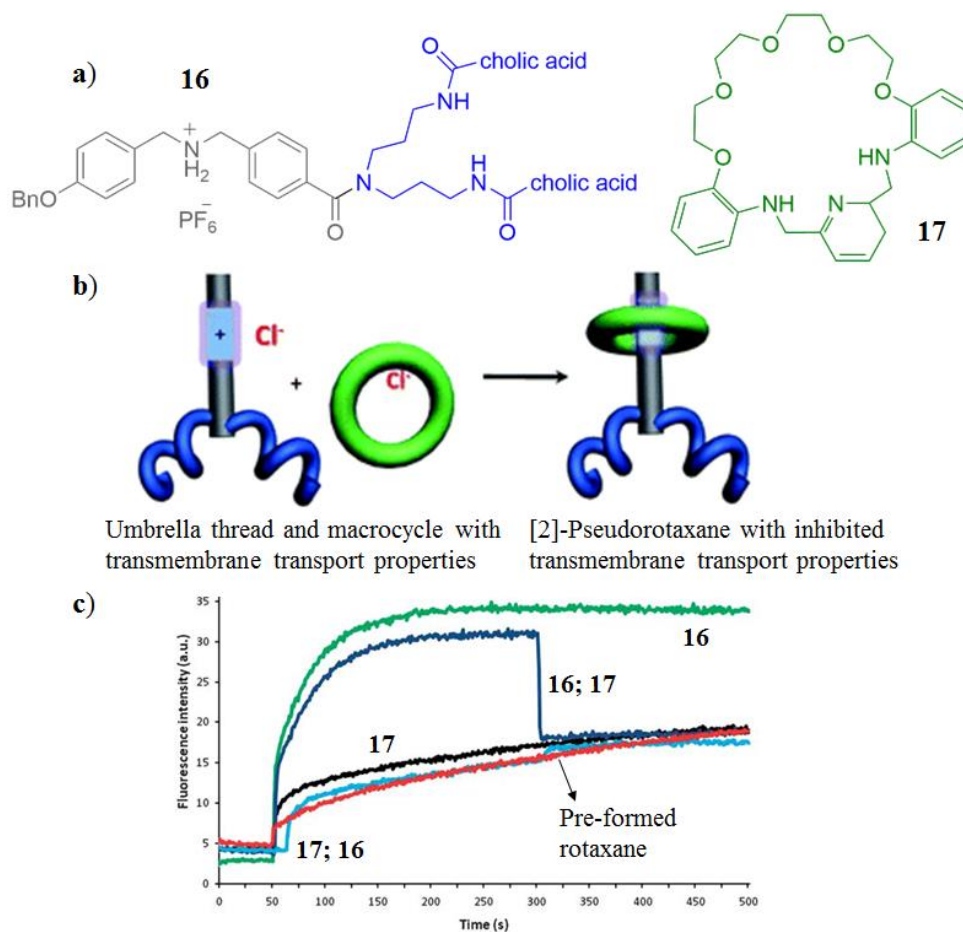


**Figure 1.19.** a) Structure of amphiphilic thread **16** and pyridyl containing macrocycle **17**. b) Schematic representation of the formation of inclusion complexes between **16** and **17**. c) Relative anion transport activity of compounds **16**, **17**, their complex and the pre-formed rotaxane in the LG-based assay. Intravesicular conditions: 100 mM NaCl, 10 mM phosphate buffer, 2 mM LG; extravesicular conditions: 100 mM NaNO<sub>3</sub>, 10 mM phosphate buffer (pH 6.4). Adapted and reprinted with permission from *Med. Chem. Commun.* **2011**, 2, 978-990. Copyright (2011) Royal Society of Chemistry.<sup>95</sup>

The two examples described above successfully demonstrate that the anion transport properties of certain anionophores can be modulated by complexation with other macrocycles in solution.

### 1.6.5 Effect of Intramolecular Hydrogen Bonding on Anion Transport Property

In a series of publications including a QSAR analysis of phenylthiourea receptors, the authors showed that the anion transport ability of thioureas could be modulated by the varying lipophilicity of the receptors, triggered by substituent effects.<sup>96,97</sup> Lipophilicity plays an essential role in drug design as it affects the membrane permeability, absorption and distribution of a drug.<sup>98</sup> Usually, lipophilicity of a molecule can be enhanced by introducing lipophilic functional groups onto the scaffold. In this study, intramolecular hydrogen bonding and substituent effects were utilized to increase the lipophilic character of novel series of anion receptors acylthioureas.<sup>99</sup> However, the description below focuses on a simple unsubstituted acylthiourea **19** and thiourea **18** (**Figure 1.20**). As shown in **Figure 1.20b**, acylthiourea can form six-membered intramolecular hydrogen-bonded rings that reduce the hydrophilicity of the receptor. As a result, acylthiourea **19** was reasoned to be more lipophilic than analogous thiourea **18**. The intramolecular H-bonding in **19** was confirmed by X-ray crystal structure that showed a 6-membered hydrogen-bonded ring with the thiourea binding unit adopting an *anti* conformation.

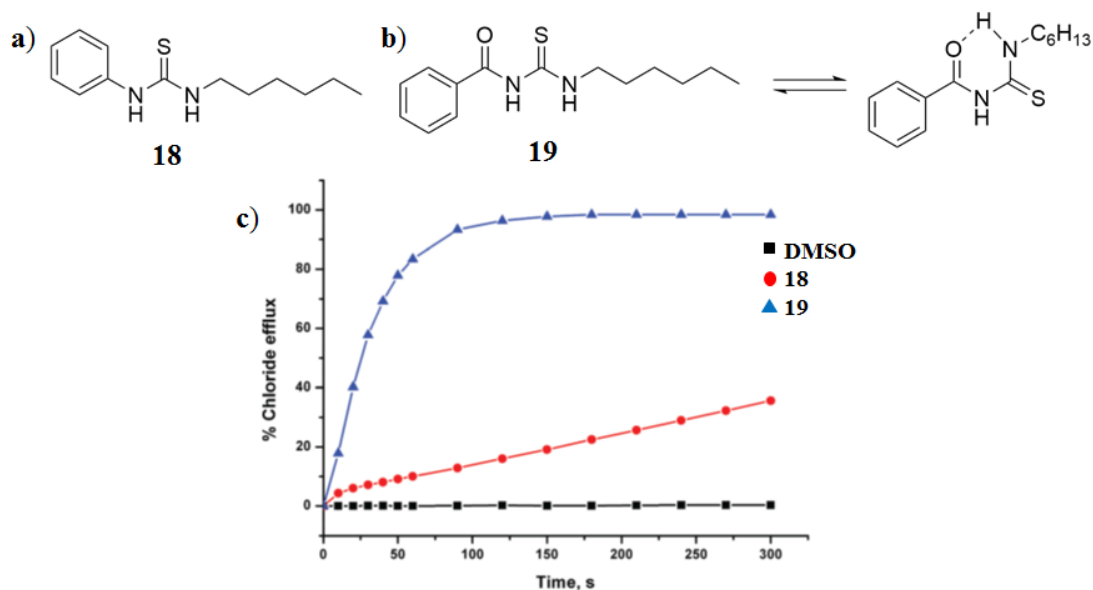


**Figure 1.20.** a) and b) show structures of thiourea **18** and acylthiourea **19**. c) Chloride efflux mediated by receptors **18** and **19** (2 mol% with respect to lipid) from POPC vesicles containing 489 mM NaCl buffered to pH 7.2 with 5 mM sodium phosphate salts. The vesicles were suspended in 489 mM NaNO<sub>3</sub> buffered to pH 7.2 with 5 mM sodium phosphate salts. Receptors were injected into the lipid solution. Adapted from *Org. Biomol. Chem.* **2014**,12, 62-72. Copyright (2014) Royal Society of Chemistry.<sup>99</sup>

Anion transport activities of thiourea and acylthiourea in lipid vesicles were compared using a chloride selective ion electrode assay (**Figure 1.20c**).<sup>99</sup> Compound **19** was found to be more active in exchanging anions across bilayer as compared to **18**. In conclusion, acylthioureas were found to be more efficient anion receptors as compared to thioureas due to higher lipophilicity caused by the formation of an intramolecular hydrogen bond, which shields the binding site from interactions with water. Therefore, anion transport by receptors can be modulated by manipulating the

lipophilicity of the receptor, which can be varied based on different substituents added to the receptor scaffold.

### 1.6.6 Ion-Gating in Nanochannels

In this paper, a non-covalent approach was adopted for regulation of ion transport in nanochannels.<sup>100</sup> Flow of ions through nanochannels depended on the surface charge inside the channels. Using two different approaches, the ion flow could be switched to be selective to cations, anions or ambipolar flow. The first approach made use of charge-transfer (C-T) supramolecular motifs between a dicationic viologen **20** as acceptor and trianionic pyranine **21** as donor (**Figure 1.21**). The second approach depended on pH and has been explained in more detail.

The transport across the nanopores of viologen-modified mesoporous silica films (MF-V) was investigated using cyclic voltammetry with  $[\text{Fe}(\text{CN})_6]_3^-$  and  $[\text{Ru}(\text{NH}_3)_6]^{3+}$  as anionic and cationic electroactive probes, respectively. The viologen-coated positively charged pores of the MF-V elicited a strong and selective electrochemical response for the transport of anionic  $[\text{Fe}(\text{CN})_6]_3^-$  probe. No response to the cationic  $[\text{Ru}(\text{NH}_3)_6]^{3+}$  probe was observed owing to the unipolar environment inside the nanopores. To reverse the surface charge within the pores, MF-V was soaked in pyranine **21** solution for 16 h. This resulting MF-V incorporated non-covalent interactions between the positively charged viologen **20** (with a 2+ charge) and negatively charged pyranine **21** (with a 3- charge), showing a strong electrochemical response to cationic probe,  $[\text{Ru}(\text{NH}_3)_6]^{3+}$  and no response for anionic  $[\text{Fe}(\text{CN})_6]_3^-$  in

the cyclic voltammogram. A complete reversal of ionic transport from anion selective to cation selective indicating charge-reversal inside the nanopores was observed.

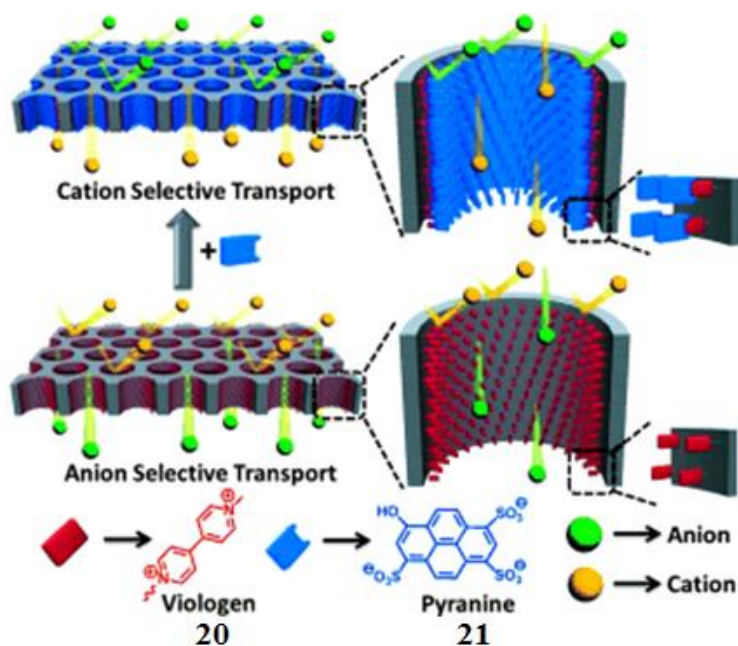


**Figure 1.21.** Non-covalent functionalization of viologen **20** modified nanopores with negatively charged donor, pyranine **21**, to switch the gating properties of the nanopores from anion selective ( $[\text{Fe}(\text{CN})_6]_3^-$ ) to cation selective ( $[\text{Ru}(\text{NH}_3)_6]^{3+}$ ). Reprinted with permission from *Angew. Chem. Int. Ed.* **2014**, 53 (48), 13073-13077. Copyright © 2005 Wiley-VCH Verlag GmbH & Co. KGaA, Weinheim.<sup>100</sup>

The second approach also made use of CT-supramolecular motifs, but depended on pH regulation. In this case, the donor species was replaced by coronene tetracarboxylate (CS) **22** with four carboxylate groups whose protonation can be modulated with pH. The viologen containing MF-V films were soaked in CS solution (1 mm, pH 6) to non-covalently functionalize the nanopores.

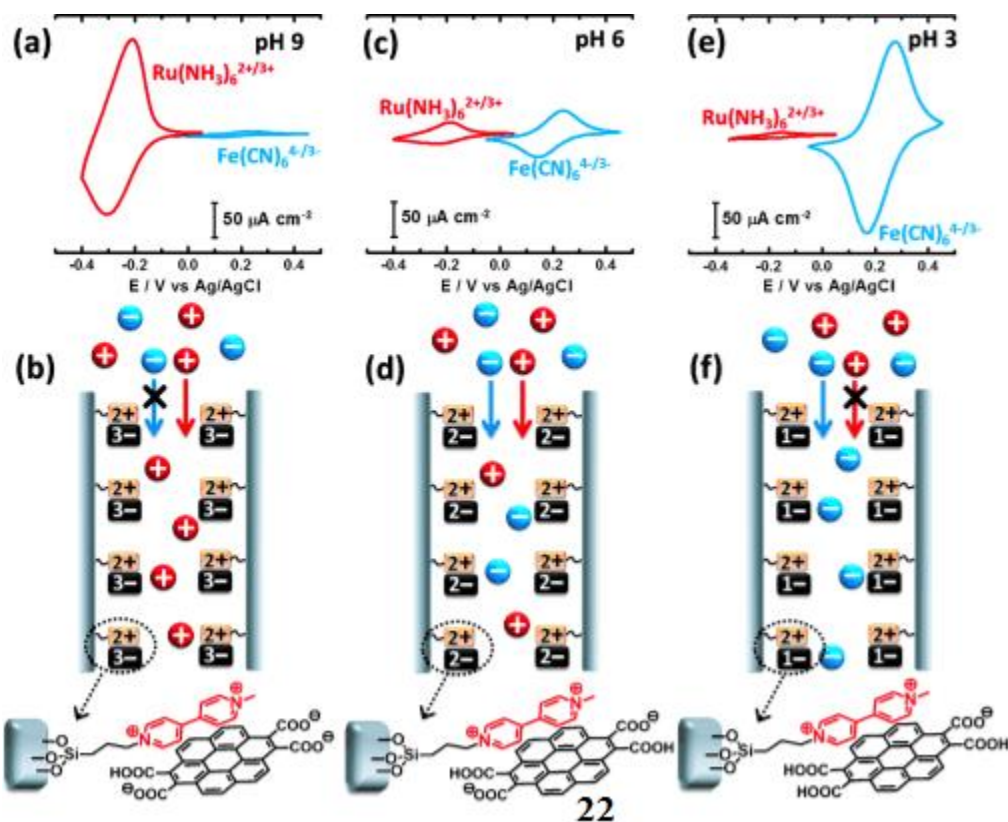


**Figure 1.22.** Cyclic voltammograms corresponding to coronene tetracarboxylate **22** bound MF-V in the presence of 1 mM  $[\text{Ru}(\text{NH}_3)_6]^{3+}$  (red trace) and 1 mM  $[\text{Fe}(\text{CN})_6]^{3-}$  (blue trace) at different pH conditions: **a)** 9, **c)** 6 and **e)** 3. Scan rate:  $200 \text{ mVs}^{-1}$ , supporting electrolyte: 0.1m KCl. The corresponding schematics are given as **(b)**, **(d)** and **(f)**. Reprinted with permission from *Angew. Chem. Int. Ed.* **2014**, 53 (48), 13073-13077. Copyright © 2005 Wiley-VCH Verlag GmbH & Co. KGaA, Weinheim.<sup>100</sup>

To explore pH responsive transport, ion conductance through the nanopores of CS bound MF-V film was investigated at pH 9, 6 and 3. At pH 9, voltammogram showed a high transport for positively charged  $[\text{Ru}(\text{NH}_3)_6]^{3+}$  probe, suggesting negatively charged pore walls (**Figure 1.22a**). This was probably due to the higher

number of deprotonated carboxylate groups of **22** at pH 9 (**Figure 1.22b**). At pH 6, voltammograms were similar for both positive and negative probes indicating ambipolar transport (**Figure 1.22c**), suggesting that probably two of the four CS carboxylate groups are protonated, which neutralized the dicationic viologen inside the pores (**Figure 1.22d**). At pH 3, negatively charged  $[\text{Fe}(\text{CN})_6]_3^-$  was preferentially transported as most of the carboxylate groups were protonated (**Figure 1.22e-f**). Thus, a pH responsive donor facilitated the switching between selectivity towards cation, anion and ambipolar conductance through the nanopores. Voltammograms were reproducible through three cycles of pH switching, thus showing good reversibility. Thus, the supramolecular C-T motif allowed for a unique nanochannel system whose ion transport activity could be regulated by different approaches.

### 1.6.7 pH Tunable Thiosquaramides as Anion Transporters

A series of thiosquaramides were synthesized and tested for their pH-dependent chloride binding and anion transport behavior using  $^1\text{H}$  NMR titrations, single crystal X-ray diffraction and a variety of lipid vesicles-based techniques.<sup>101</sup> Based on UV-vis titrations,  $\text{p}K_a$  values of the thiosquaramides were found to be in the range 4.0–8.0. This would imply that at pH 7.2 or greater, a large proportion of the thiosquaramides will be deprotonated and in a negatively charged form (**Figure 1.23a**). Due to charge repulsion, the anion binding and transporting ability of squaramides will be switched OFF. Inversely, at  $\text{pH} < 7$ , majority of the compound should be present in its neutral form and anion transport should be switched ON (**Figure 1.23a**).

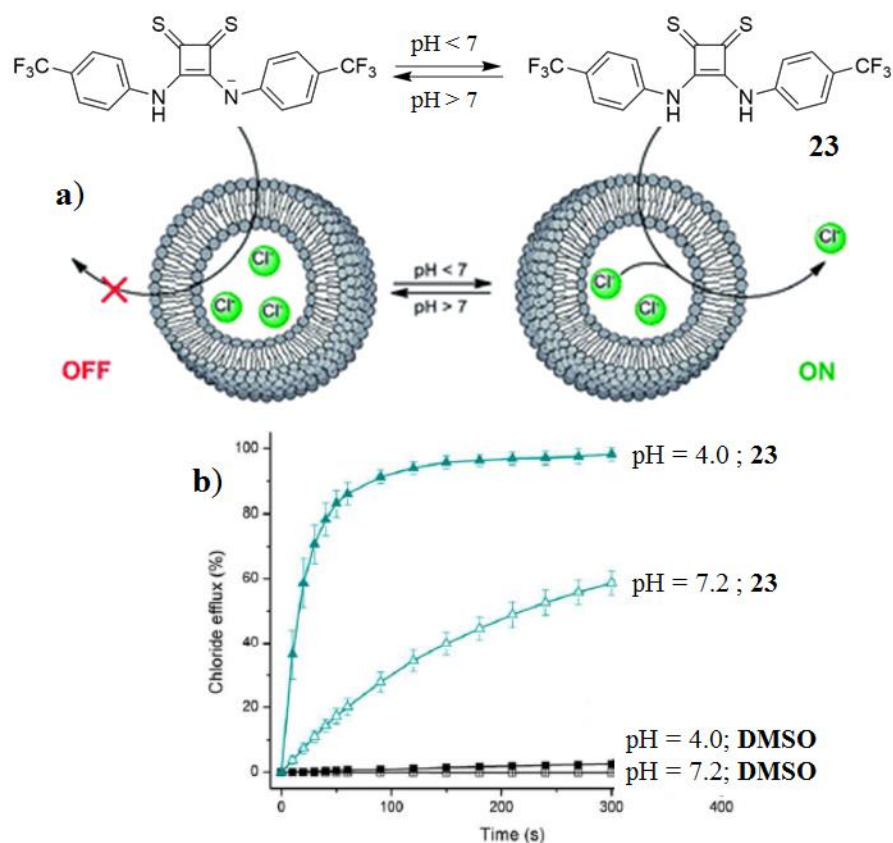


**Figure 1.23.** a) Schematic representation showing ON/OFF switching of anion transport by thiosquaramide **23**. b) Chloride efflux from POPC vesicles at pH 7.2 and pH 4.0. POPC vesicles were loaded with a 489 mM NaCl solution buffered to pH 7.2 with 5 mM phosphate salts or to pH 4.0 with 5 mM citrate salts, and were suspended in a 489 mM NaNO<sub>3</sub> solution buffered to pH 7.2 with 5 mM phosphate salts or to pH 4.0 with 5 mM citrate salts. DMSO was used as a control. Adapted from *Chem. Sci.* **2014**, *5*, 3617-3626. Copyright (2014) Royal Society of Chemistry.<sup>101</sup>

This hypothesis was tested in liposomes loaded with a NaCl solution (489 mM) and suspended in a NaNO<sub>3</sub> solution (489 mM) buffered to pH 7.2. Chloride efflux was initiated by addition of receptors and monitored using an ion selective electrode (ISE).



The anion transport data is shown for thiosquaramide **23** in **Figure 1.23b**. At pH 7.2, low anion transport was reported for **23**. Similar anion transport experiments were repeated at pH 4.0. This time, the anion transport ability of thiosquaramide **23** was significantly enhanced. The transport results at different pH values support the initial hypothesis about pH regulated anion transport ability of thiosquaramides. Similar results were obtained with different vesicle assays. The pH-switchable transport behavior gives the thiosquaramides more potential for biological significance, since the control of ion transport process is of utmost importance in a biological setting.

The examples discussed above involved regulation of ion flow through a phospholipid membrane under the influence of structural changes, voltage, light and pH. As described earlier, many of the naturally occurring chloride transporting proteins or channels exhibit a gating or switching mechanism (**Section 1.6.1**). In **Section 1.4.2.2.**, the correlation between HCl symport and apoptosis was also described. This correlation has encouraged the possibility of using ion transporters for cancer therapy.<sup>10,25,27</sup> The internal and external pH of cancer cells has been shown to be different from that of healthy cells.<sup>63</sup> Therefore, pH switchable chloride transporters have the potential to become promising leads for anti-cancer drugs. For the ion receptors to be biologically relevant, the pH-regulation must occur around the physiological pH of 7.4. Additionally, the range of pH switch should correspond to the  $pK_a$  value of the receptor under the conditions of the anion transport experiments. In **Chapter 2** and **3**, I have described a novel set of prodigiosenes whose anion transport activity can be influenced depending upon the basicity of the receptor and the solution

pH. Most prodigiosenes have  $pK_a$  values in the range of physiological pH (6 to 8), therefore, improving the chances of using these analogs as anti-cancer agents. To our knowledge, this is the first time that a pH-regulated transmembrane anion transport study has been done with prodigiosenes.

## 1.7 Summary

Prodigiosin **1** is a natural product with three pyrrole rings. Compared to naturally occurring ion channels and proteins, it is a small molecule. Yet, based on multiple scientific undertakings, it has been shown to be an excellent transmembrane anion transporter in the field.<sup>86</sup> Prodigiosenes have been identified for their different biological activities such as anti-cancer,<sup>2-4</sup> immunosuppressive,<sup>5,6</sup> anti-malarial,<sup>7</sup> and antimicrobial<sup>8</sup> therapeutic properties. They can also intercalate with dsDNA.<sup>39</sup> Naturally, the biological diversity of prodigiosenes has ensured the development and study of numerous synthetic analogs for ion transport or biological activities.<sup>9,10, 24,77</sup> Despite the large amount of work that has already been done with prodigiosenes in establishing their many roles as potential therapeutics, there's still a lot more to do. For instance, the molecular mechanism of action for the anti-cancer properties of prodigiosenes still needs to be unambiguously established.

This chapter described two major roles of prodigiosenes – a) in the movement of anions across membranes and b) their potential as anti-cancer agents. The proposed mechanisms for anti-cancer properties of prodigiosenes were discussed. Further, some groups have found correlations between the *in vitro* anti-cancer activity of prodigiosenes and their anion transport rates in phospholipid vesicles. Prodigiosenes

have been extensively tested for their anion transport properties with goal of developing these compounds as potential drugs for treatment of diseases like Bartter syndrome and cystic fibrosis. Our contribution to the field of anion transport is the identification of novel prodigiosenes, some of which, have shown excellent transport rates with reduced cytotoxicity (**Chapter 2**). We were also successful in manipulating the transport rates by changing the basicity of prodigiosin derivatives (**Chapter 3**). Specific chemical properties of prodigiosenes are explored in **Chapter 4**. Lastly, **Chapter 5** is a significant study demonstrating that prodigiosin **1** can bind with G-quadruplex DNA.

## 2 Chapter 2: Synthetic Prodigiosenes and the Influence of C-Ring Substitution on Transmembrane Chloride Transport and Basicity

*The majority of this chapter has been published in reference 114:*

- Rastogi, S.; Marchal, E.; Uddin, I.; Groves, B.; Colpitts, J.; McFarland, S. A.; Davis, J. T.; Thompson, A. “Synthetic Prodigiosenes and the Influence of C-Ring Substitution on DNA Cleavage, Transmembrane Chloride Transport and Basicity” *Org. Biomol. Chem.*, **2013**, *11*, 3834-3845.

*Syntheses of all compounds 2a-j and 24 described in this chapter were performed by Dr. Alison Thompson and her group, our collaborators from Dalhousie University, Canada. Compounds 1, 2 and 24 were tested against 60 human cancer cell lines by the Developmental Therapeutic Program at NCI, NIH.*

### Background

#### 2.1 Introduction

Prodigiosin is the parent compound of the tripyrrolic natural products known as the prodigiosenes.<sup>1</sup> Although the prodigiosenes possess various biological activities, they have also displayed high cytotoxicity in early studies.<sup>11</sup> As a result, it becomes imperative to develop new synthetic analogs that share the same level of therapeutic efficacy as the natural products but exhibit reduced cytotoxicity. In this chapter, analogs of the tripyrrolic natural product prodigiosin **1** bearing an additional methyl and a carbonyl group at the C-ring were synthesized by our collaborators and evaluated by us as anion transporters. The *in vitro* anticancer activity screening (NCI) and

transmembrane transport of chloride anions of these synthetic analogs (**2a-j** and **24**) showed that the presence of the extra methyl group is not detrimental to activity. Furthermore, although the presence of an ester conjugated to the prodigiosene C-ring decreases both  $pK_a$  and chloride transport efficiency, as compared to the natural product **1**, these analogs still exhibit a high rate of chloride transport. The effect of C-ring modifications in prodigiosenes **2a-j** and **24** on their basicity, transmembrane anion transport ability and their *in vitro* anticancer activity have been described in this chapter. For background on C-ring modified prodigiosenes, I have given a brief account of the studies previously done, with particular emphasis on their biological activity.

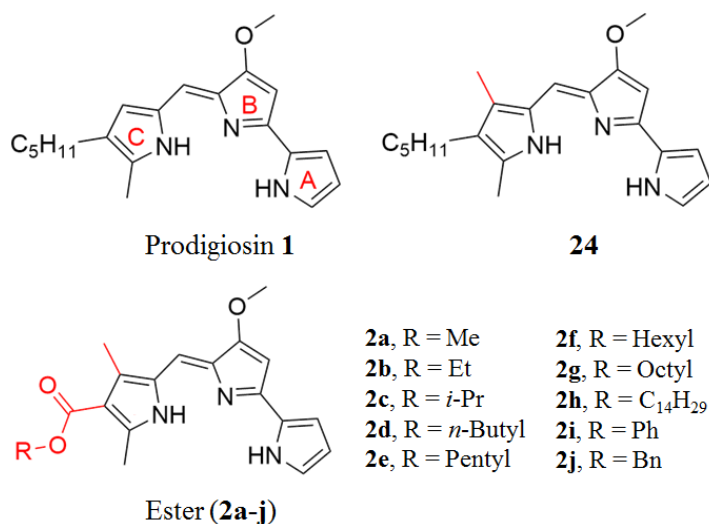


**Figure 2.1.** Natural product prodigiosin (**1**) and C-ring modified synthetic analogs – ester (**2a-j**) and **24**.

## 2.2 Previous Work with C-Ring Modified Prodigiosenes

Prodigiosin **1** is a red tripyrrolic pigment isolated from bacteria of the *Serratia* and *Streptomyces* genus (**Figure 2.1**).<sup>6,9,42,102</sup> This natural product and some of its natural or synthetic analogs possess a wide range of biological properties, one of them

being the ability to induce apoptosis of malignant cells.<sup>21-23,48</sup> Considering these properties, considerable effort has been directed towards the synthesis of prodigiosin and its analogs.<sup>5,12,103-107</sup> In the next section, a few examples of the C-ring functionalized prodigiosin analogs have been described.

### 2.2.1 Earlier Examples of C-Ring Modified Prodigiosenes

For the goal of synthesizing prodigiosenes with enhanced cytotoxicity and improved toxicological profiles, derivatives with various functional groups have been synthesized, such that the newly introduced functional groups might help in attaching cell-targeting moieties.<sup>108</sup> Discussed below are some examples of C-ring modified prodigiosenes and their reported biological activity.

#### 2.2.1.1 Boger's Prodigiosene 25

In order to investigate the effect of peripheral appendages on prodigiosin scaffold, Boger and Patel synthesized analog **25** (**Figure 2.2**).<sup>103</sup> Compound **25** does not contain any functional groups on rings B and C. In an *in vitro* cell proliferation study, comprising of various cancer cell lines for melanoma (B16 mouse), leukemia (L1210 mouse, 9PS (P388) mouse) and human epidermoid carcinoma of the nasopharynx (9KB), compound **25** was found to be ineffective as compared to prodigiosin **1**. For all cancer cell lines, prodigiosin **1** was found to have IC<sub>50</sub> values that were at least 200 times lower than the values for **25**. IC<sub>50</sub> values are defined as the inhibitory concentration for 50% cell growth relative to untreated control. The study by Boger and Patel suggested that the substituents on the prodigiosin scaffold are essential for its anticancer activity.

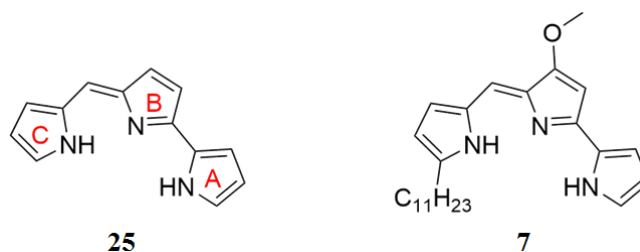


**Figure 2.2.** Structures of prodigiosene **25** and prodigiosin 25-C (**7**).

### 2.2.1.2 Prodigiosin 25-C

Prodigiosin 25-C (undecylprodigiosin) **7** has been extensively studied for its biological activity (**Figure 2.2**).<sup>5,19,57</sup> Compound **7** differs from prodigiosin **1** due to the presence of a 11 carbon aliphatic chain on its C-ring. In 1995, Kataoka and colleagues showed that prodigiosin 25-C could neutralize acidic organelles located within the cytotoxic T cells.<sup>19</sup> By neutralizing the acidic interiors of T cells, prodigiosin C-25 acted as an immunosuppressant and inhibited the cytotoxicity of T cells.

In a separate paper in 1995, Kataoka and group explained that the immunosuppressive properties of **7** were due to its ability to neutralize the proton-translocation activity of V-ATPase enzyme.<sup>57</sup> The neutralization of proton pump does not affect the ATP hydrolysis activity of V-ATPase. This study by Kataoka and colleagues further bolstered the theory about immunosuppressive properties of prodigiosin 25-C.

As described in **Section 1.4.2.1**, compound **7** was also used in experiments done to prove that prodigiosenes uncouple V-ATPase proton translocation activity by facilitating  $H^+Cl^-$  symport or  $OH^-/Cl^-$  antiport across membranes.<sup>25,27,30,109</sup> This was

the first time that prodigiosenes were proposed to bind and transport anions across natural bilayer membranes.

### 2.2.1.3 Indole-Based Prodigiosenes by Wasserman

Wasserman and colleagues synthesized a library of indole-based derivatives, like **26**, called indoloprodigiosins.<sup>110</sup> These compounds were formed by the condensation of a C-10 methoxybipyrrole aldehyde with different indole derivatives. Some of the indoloprodigiosins contained an aromatic benzene group fused with ring C, while others contained a fused aliphatic group like cyclohexane. The indoloprodigiosins were tested and compared with prodigiosin **1** for their cytotoxicity towards different cancer cells (A549, DLD-1, HT29, MDA-MB-231 and NCI-H460).<sup>110</sup> Prodigiosin **1** was found to be most active amongst the compounds tested, with IC<sub>50</sub> values in the range of 0.03 – 0.17 μM for all cancer cell lines. Amongst the tested indoloprodigiosins, compound **26** was found to cause maximum inhibition in cellular proliferation with IC<sub>50</sub> values ranging between 0.2 to 1.3 μM (**Figure 2.3**). The significant activity shown by compound **26** was attributed to the ability of ring C to react as a dialkyl pyrrole, similar to prodigiosin **1**. Based on the cell proliferation studies, Wasserman and his group concluded that the mechanism of action for cytotoxicity exhibited by prodigiosin and indoloprodigiosins might be related. However, more investigations need to be made to identify the common mode of action.



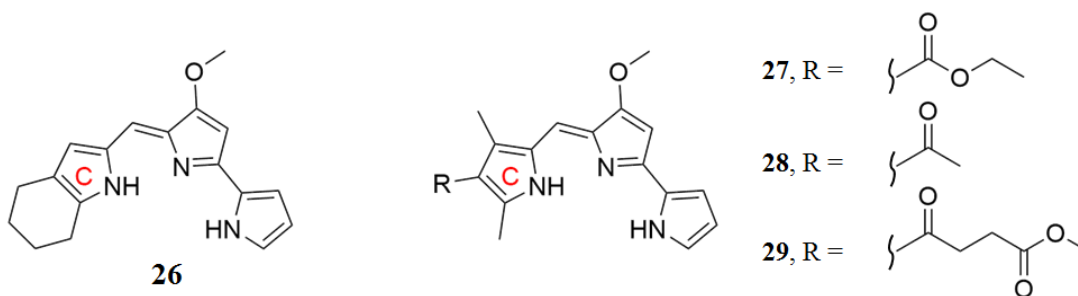


**Figure 2.3.** Structures of indoloprodigiosin **26** and C-ring prodigiosenes **27-29**.

#### 2.2.1.4 C-Ring Functionalized Prodigiosenes by Thompson

In 2007, Thompson and group synthesized a series of prodigiosin derivatives with pendant functional groups such as esters (**27**) and ketones (**28**) on ring C (**Figure 2.3**).<sup>2</sup> Pendant groups like esters can help in further derivatization of the prodigiosin skeleton. Later on in 2013, compound **29** was tested for its antimicrobial activity and found to be reasonably active.<sup>8</sup> New prodigiosene conjugates were synthesized by addition of tamoxifen, estrone and porphyrin moieties to **29** and analogs. These prodigiosene conjugates were tested for their anti-cancer activity.<sup>4,111</sup> Some of the conjugates were found to be active, even at nM concentrations, thereby, paving the way for more investigations into these new class of compounds.

However, when these pendant prodigiosenes were first synthesized in 2007, it was essential to determine the effect of the pendant groups on the biological activity of these new prodigiosenes **27-29**. Therefore, some of the analogs were tested against 60 human cell lines derived from nine cancer cell types by the National Cancer Institute (NCI). The anti-cancer activity of the synthetic derivatives was compared with that of prodigiosin **1**. The *in vitro* activity of prodigiosenes **27-29** was measured in terms of

GI<sub>50</sub>, TGI and LC<sub>50</sub> (**Table 2.1**). Compound **27** was found to have *in vitro* activity comparable to that of prodigiosin **1** (**Table 2.1**). Compound **29** exhibited sufficient activity to indicate potential broad spectrum growth inhibition of a variety of tumors. On the other hand, **28** did not exhibit any relevant anti-cancer activity. From these collective results of *in vitro* cell proliferation studies, a conclusion was made that the conjugated ester (**27**) or the pendant ester (**29**) did not significantly affect the activity of prodigiosenes because derivatives bearing these functional groups exhibited anti-cancer activity very similar to that of prodigiosin **1**.<sup>2</sup>

**Table 2.1.** The *in-vitro* activity of prodigiosenes **27-29** over 60 cancer cell lines.<sup>2</sup>

| Compound             | Log <sub>10</sub> mean<br><sup>a</sup> GI <sub>50</sub> | Log <sub>10</sub> mean<br><sup>b</sup> TGI | Log <sub>10</sub> mean<br><sup>c</sup> LC <sub>50</sub> |
|----------------------|---|--|---|
| Prodigiosin <b>1</b> | -7.85   | -5.68                                      | -6.65   |
| <b>27</b>            | -7.33   | -5.96                                      | -4.91   |
| <b>28</b>            | -6.15   | -4.39                                      | -4.05   |
| <b>29</b>            | -6.10   | -5.49                                      | -4.91   |

<sup>a</sup>GI<sub>50</sub> = half maximal growth inhibition concentration. <sup>b</sup>TGI = total growth inhibition concentration. <sup>c</sup>LC<sub>50</sub> = half maximal lethal concentration

### 2.2.2 Rationale for Studying Influence of C-Ring Substitution on Transmembrane Chloride Transport and Basicity

We have studied prodigiosin derivatives, including those with an extra methyl group on the C-ring (**24**), as well as analogs (**2**) that bear a C-ring conjugated carbonyl.<sup>2,112</sup> These extra groups have been introduced so as to confer increased stability of the synthetic intermediates and facile isolation of this genre of compounds compared to the natural product.<sup>17</sup> The pendant groups like ester functionality also help

in conjugation of other moieties to the prodigiosene scaffold.<sup>4,8,111</sup> In this chapter, we report the influence of these C-ring modifications upon the ability of the prodigiosenes to effect *in vitro* anticancer activity and their ability to catalyze transmembrane anion exchange. Of particular importance are the findings that: (i) the extra methyl group on the C-ring of **24** does not significantly diminish the *in vitro* anticancer activity, or the anion transport activities of the synthetic analogs relative to prodigiosin **1**; (ii) the analogs generally retain the potent *in vitro* anticancer activities of the parent natural product; and (iii) the electron-withdrawing carbonyl functionality on the C-ring makes the synthetic esters **2** less basic than the natural product **1**, which helps to rationalise why the ester analogs are less effective than prodigiosin **1** as transmembrane anion transporters at pH 7.4.

## **Results**

### **2.3 Study of Transmembrane Anion Transport Activity of Prodigiosin **1**, Ester Analog **2** and **24****

To investigate possible mechanisms that might contribute toward the anticancer activities of prodigiosenes, the transmembrane anion transport properties of synthetic prodigiosenes **2** and **24** were evaluated using an EYPC (egg-yolk 1-phosphatidylcholine) liposome model. For this assay the chloride-specific fluorescent dye lucigenin (LG) was used as a probe to track chloride ion export from the liposome, since LG fluorescence is selectively quenched by chloride, but not by nitrate anion.<sup>113</sup> Thus, EYPC liposomes loaded with LG and NaCl were suspended in a buffered solution (pH 7.4) containing NaNO<sub>3</sub>. Upon addition of prodigiosenes to the suspension

of EYPC liposomes, the fluorescence of the intravesicular LG increased, indicating that the added transporter was catalyzing an anion exchange process between the intravesicular chloride anion and the extravesicular nitrate anion (**Figure 2.4**). Based on the results obtained from the liposome experiments, we were able to make some conclusions about the anion transport activity of prodigiosenes **2** and **24**. The observations made from different liposome experiments and their conclusions are described in the following sections.

### **2.3.1 EC<sub>50</sub> Values for Cl<sup>-</sup>/NO<sub>3</sub><sup>-</sup> Exchange Process Demonstrate the Effect of C-Ring Modifications in Prodigiosenes**

**Figure 2.4** shows representative LG fluorescence curves from preliminary screening experiments, plotted as a function of time, after addition of either the natural product prodigiosin **1**, the methylated analog **24** or the pentyl-ester **2e** (in each case the prodigiosene was added as a DMSO solution at a concentration that was 0.04 mol% ligand:lipid ratio). Under these conditions, the synthetic prodigiosene **24** had a qualitatively similar Cl<sup>-</sup>/NO<sub>3</sub><sup>-</sup> anion transport activity as did prodigiosin **1**. This result indicates that addition of the extra methyl group to the C-ring does not diminish the prodigiosenes' anion transport activity. This is a significant result since it is easier to synthesize the methyl analog **24** than the natural product prodigiosin **1**.<sup>114</sup>

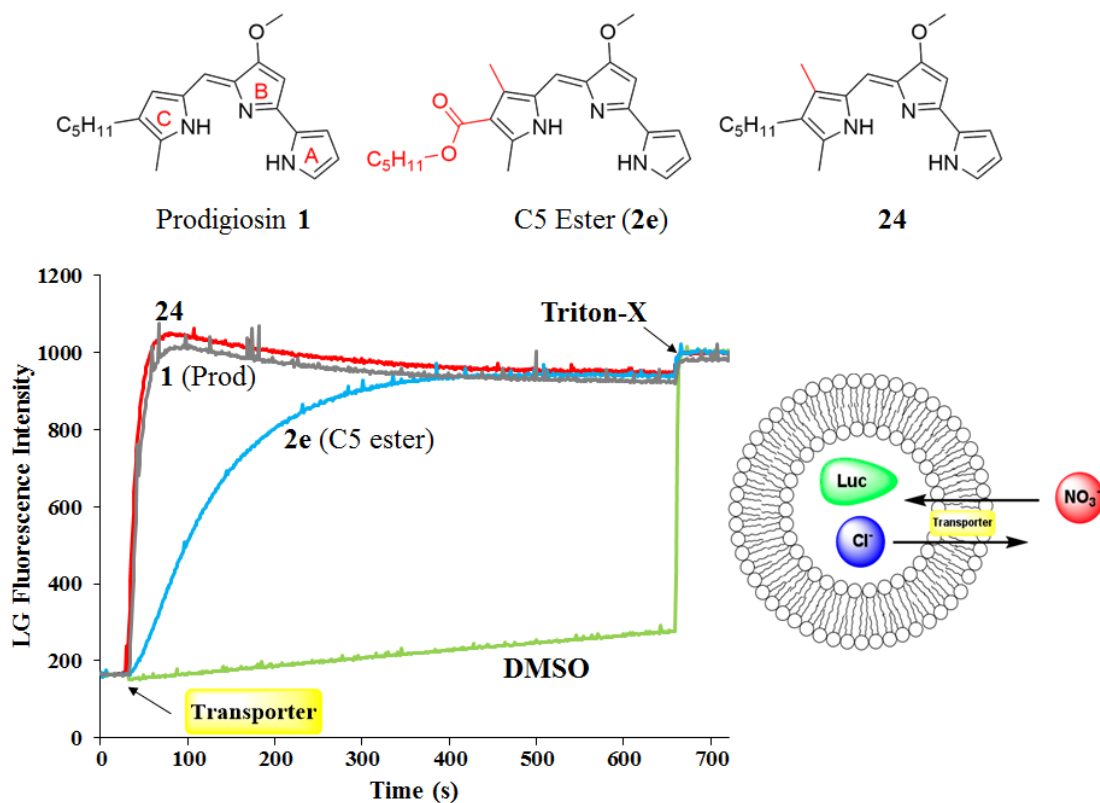


**Figure 2.4.** Structures of compounds **1**, **2e** and **24**. Anion exchange results for the natural product prodigiosin **1** relative to synthetic analogs **2e** and **24**. Anion exchange in EYPC liposomes was monitored by measuring the fluorescence of LG ( $\lambda_{\text{ex}} = 372$  nm,  $\lambda_{\text{em}} = 504$  nm) at 25 °C after addition of 0.04 mol% of prodigiosene transporter relative to EYPC lipid. The EYPC liposomes, containing 1 mM LG, 20 mM HEPES buffer (pH 7.4) and 100 mM NaCl were suspended in a solution of 100 mM NaNO<sub>3</sub> and 20 mM HEPES buffer (pH 7.4). At  $t = 30$  s, the prodigiosene transporter in DMSO was added. At  $t = 660$  s, addition of Triton-X lysed the liposomes. Traces shown are an average of three trials.

In contrast to the methylated analog **24**, the pentyl-ester **2e** is a less efficient anion transporter than the natural product **1** (**Figure 2.4**). To be able to quantitatively

compare the anion transport abilities of **1**, **24** and the ester-containing analog **2e**, the EC<sub>50</sub> values for each receptor were calculated. EC<sub>50</sub> is defined as the concentration of transporter needed to achieve 50 % of maximal chloride efflux at t = 150 s at 25 °C. The EC<sub>50</sub> values are calculated based upon the Hill equation, which considers the degree of saturation (or maximal Cl<sup>-</sup> efflux) as a function of ligand concentration.<sup>115</sup> In the experiment, a series of concentration dependent fluorescence measurements were performed for Cl<sup>-</sup>/NO<sub>3</sub><sup>-</sup> exchange catalyzed by these three analogs. For each receptor concentration, the LG fluorescence measurements were converted into the concentration of Cl<sup>-</sup> ion efflux ([Cl<sup>-</sup>]<sub>eff</sub>) by using Stern-Volmer equation.<sup>115,116</sup> Then, the EC<sub>50</sub> values were determined from a dose-response curve plotted between the concentrations of a receptor and the [Cl<sup>-</sup>]<sub>eff</sub> facilitated by that particular receptor. More details on the procedure for calculating EC<sub>50</sub> values (including dose-response curves) are described in **Chapter 7**. The calculated EC<sub>50</sub> values for transporters **1**, **2e** and **24** are recorded in **Table 2.2**. The increased EC<sub>50</sub> values for ester **2e**, relative to prodigiosin **1** and the methylated analog **24**, indicates that substitution of the prodigiosene C-ring with an electron-withdrawing ester decreases the anion transport efficiency of the compound, since **2e** (EC<sub>50</sub> =18.7 nM) had an EC<sub>50</sub> value that was approximately 10-fold higher than **24** (EC<sub>50</sub> =1.3 nM).

**Table 2.2.** EC<sub>50</sub> values for the transmembrane anion transport abilities of **1**, **2e** and **24**.

| <b>Prodigiosene</b>                | <b>1</b> | <b>2e</b> | <b>24</b> |
|------------------------------------|----------|-----------|-----------|
| <sup>a</sup> EC <sub>50</sub> (nM) | 3.2      | 18.7      | 1.3       |

<sup>a</sup>EC<sub>50</sub> values indicate the concentration of transporter needed to achieve 50% of maximal chloride efflux at t = 150 s and 25 °C in 20 mM HEPES buffer (pH 7.4).

Even though the ester **2e** showed a decreased anion transport ability when compared to prodigiosin **1** and its methyl analog **24**, it should be recognized that this synthetic prodigiosene remains an extremely potent anion transporter. For example, the experiments in **Figure 2.4** were conducted using a relatively low concentration of prodigiosene (0.04 mol% ligand:lipid ratio). For comparison, many synthetic transmembrane chloride transporters described in the literature are typically used at concentrations as high as 1-2 mol% relative to lipid to achieve similar rates of transmembrane chloride transport.<sup>117</sup>

### **2.3.2 Ester Chain Length Affects the Ability to Transport Cl<sup>-</sup> Across Bilayers**

Having demonstrated that ester **2e** was a formidable anion transporter, next, we investigated the influence of the alkoxy group on the transmembrane anion transport with same experimental conditions as before (**Figure 2.4**). The experiment involved testing ester analogs **2** of varying chain lengths as anion transporters. Receptors with shorter chain lengths (**2a-2d**) were found to be better anion transporters than compounds with longer chains (**2g**).

By varying the length of alkoxy chain on ring C, the lipophilicity of the prodigiosenes **2** was manipulated. In their publications, Quesada and Gale showed, based on a series of related compounds, that lipophilicity can play a vital role in the process of ion transport.<sup>118,119</sup> In pharmaceutical industry, lipophilicity is an important parameter in drug development.<sup>98</sup> The effective application of a therapeutic drug involves membrane translocation steps.<sup>120</sup> Quesada and colleagues recently showed that the transport activity of synthetic tambjamines, that are analogous to prodigiosenes,

can be tuned by varying their lipophilicity.<sup>118</sup> Gale and group studied a series of urea and thiourea based anion receptors.<sup>119</sup> They varied the log *P* values and found that the change in lipophilicity had a direct impact on the transport ability of these urea and thiourea based receptors. Log *P*, the logarithm of the octanol/water partition coefficient, is the most widely used measure of lipophilicity.

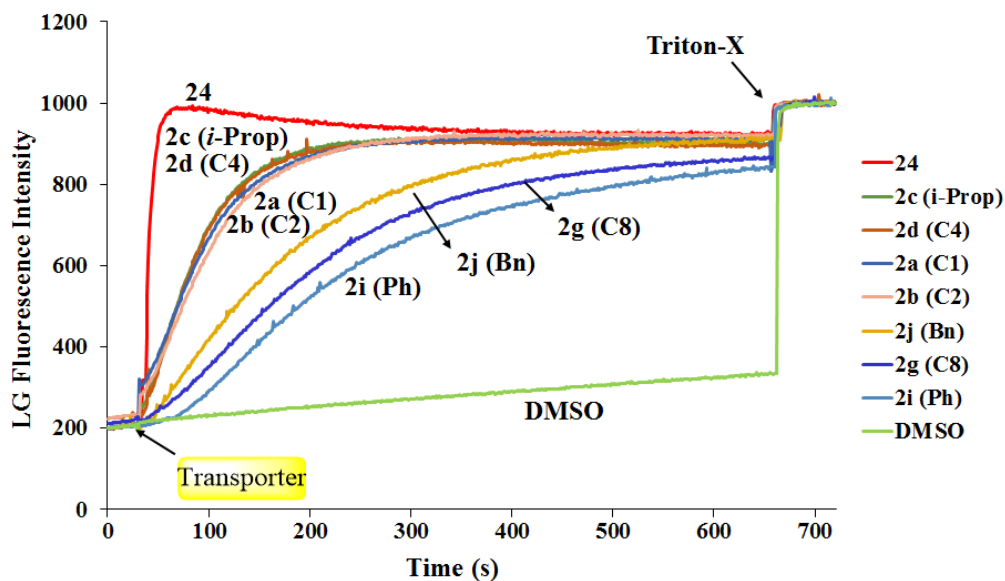


**Figure 2.5.** Anion exchange results for prodigiosenes **2a-d**, **2g** and **2i-j**, relative to **24**.

Anion exchange in EYPC liposomes was monitored by measuring the fluorescence of LG at 25 °C after addition of 0.04 mol% of prodigiosene transporter relative to EYPC lipid. The EYPC liposomes, containing 1 mM LG, 20 mM HEPES buffer (pH 7.4) and 100 mM NaCl were suspended in a solution of 100 mM NaNO<sub>3</sub> and 20 mM HEPES buffer (pH 7.4). At *t* = 30 s, the prodigiosene transporter was added and the change in fluorescence of LG was monitored ( $\lambda_{\text{ex}} = 372$  nm,  $\lambda_{\text{em}} = 504$  nm). At *t* = 660 s, the addition of Triton-X lysed the liposomes. Traces shown are an average of three trials.



**Figure 2.5** shows the increase in LG fluorescence after the addition of various prodigiosene esters at a concentration of 0.04 mol% relative to the EYPC lipid. It is apparent from the results that the length of the alkoxy functionality influences the efficiency of anion transport under these conditions. For example, the best transporters were the “short-chain” prodigiosene esters (methyl **2a**, ethyl **2b**, *i*-propyl **2c** and butyl **2d** esters). Clearly, these short-chain alkyl esters were more effective anion transporters than esters that contained either a longer alkyl chain, such as the octanoate **2g**, or had aromatic substitution like the benzyl ester **2j** and the phenyl ester **2i**.

To more clearly illustrate how the lipophilicity of the alkyl chain plays a significant role in the transport ability of prodigiosene esters, we carried out a set of comparative anion exchange assays using prodigiosenes **2f** (hexanoate), **2g** (octanoate) and **2h** (tetradecanoate) with same experimental conditions as before (**Figure 2.4** and **Figure 2.5**). **Figure 2.6** shows that increasing the chain lengths of the C-ring ester alkoxy functionality results in slower rates of transmembrane anion exchange. A plausible reasoning for the reduced activity with long chain esters could be the more hydrophobic nature of the longer chains. The long alkyl chains would favor the formation of self-assembled aggregates such as micelles in water, thereby limiting the rate at which the compounds could partition into the lipid membrane.

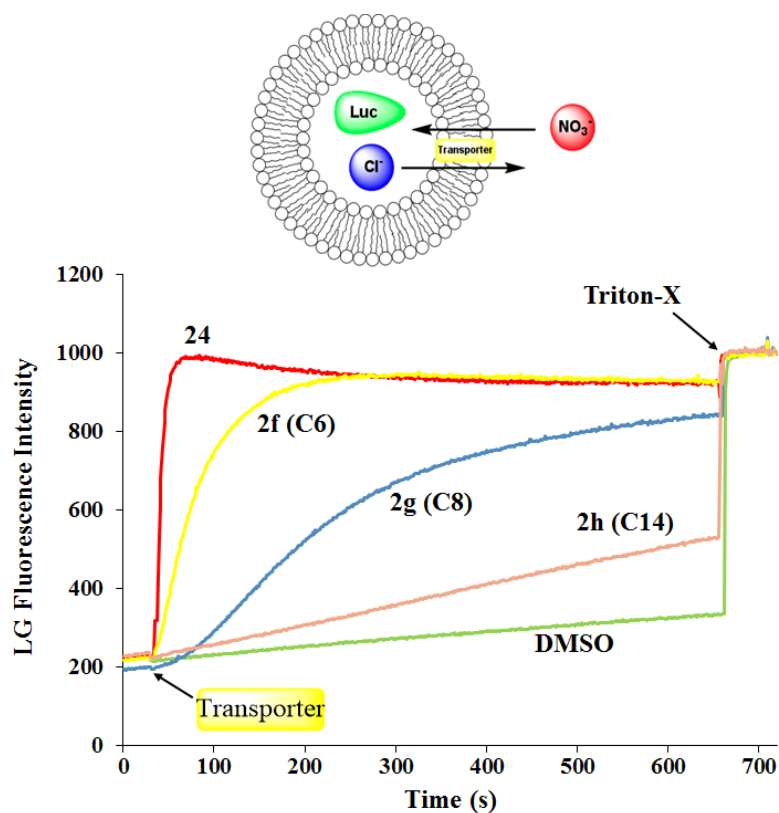


**Figure 2.6.** Anion exchange results for prodigiosenes **2f**, **2g**, **2h**, relative to **24** in EYPC liposomes was monitored by measuring the change in the fluorescence of LG at 25 °C after addition of 0.04 mol% of prodigiosene transporter relative to EYPC lipid. At  $t = 30$  s, the prodigiosene transporter was added and the change in fluorescence of LG was monitored ( $\lambda_{\text{ex}} = 372$  nm,  $\lambda_{\text{em}} = 504$  nm). At  $t = 660$  s, the addition of Triton-X lysed the liposomes. Traces shown are an average of three trials.

Due to the long carbon chain, **2h** ester prodigiosene is comparatively more lipophilic than an ester with a shorter chain length (say compound **2a** with a methyl group). Our hypothesis was that for compound **2h** in an aqueous solution, the hydrophobicity of the long alkyl chain will push the equilibrium in the direction of self-assembled aggregates (**Figure 2.7**). Since prodigiosenes catalyse anion transport by the

ion carrier mechanism,<sup>31</sup> it is essential for the aggregates to break apart so that the individual receptor molecules can bind and move anions across the lipid bilayer.

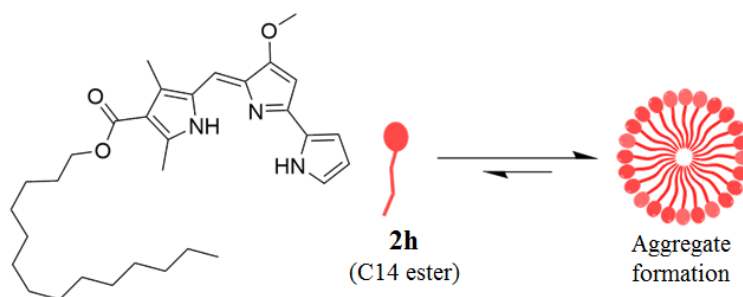


**Figure 2.7.** The long C14 chain on prodigiosene **2h** will tend to promote formation of aggregates in an aqueous solution.

To test our hypothesis about higher tendency of aggregate formation by **2h**, we performed transport experiments where the compound **2h** was incubated with a liposome sample (**Figure 2.8**). For this experiment, two sets of conditions were applied. A sample of EYPC liposomes loaded with LG and NaNO<sub>3</sub>, and suspended in a HEPES, NaNO<sub>3</sub> buffer was taken. For condition I of “**no incubation**”, the transporter **2h** was added at 0.04 mol% ligand:lipid ratio to the liposome sample, a pulse of NaCl was then added immediately, followed by measurement of LG fluorescence. For condition II involving “**incubation**”, **2h** was added to the liposome sample and allowed to incubate for 300 s, followed by addition of NaCl pulse and measurement of LG fluorescence. The change in fluorescence was found to be similar for both set of conditions.

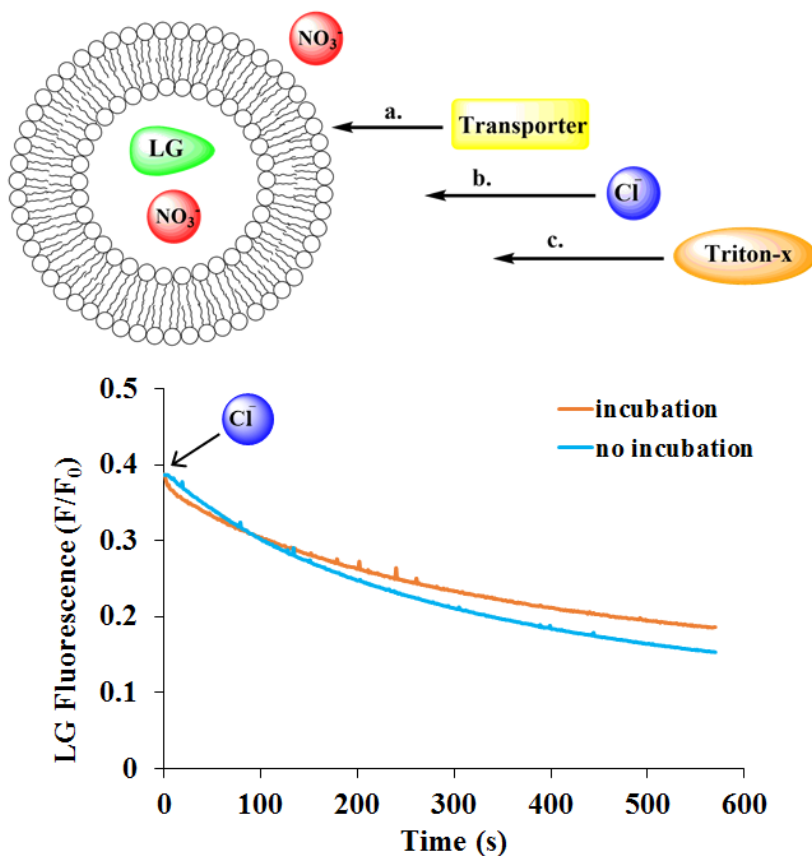


**Figure 2.8.** Anion exchange assay for prodigiosene **2h** in EYPC liposomes was monitored by measuring the change in the fluorescence of LG at 25 °C after addition of **a)** 0.04 mol% of **2h** relative to EYPC lipid. **b)** NaCl pulse was applied immediately (trace labeled no incubation) or after letting compound **2h** incubate for 300s (trace labeled incubation). **c)** Triton-X was added at 570s to lyse the liposomes. Traces shown are an average of three trials.

The change in LG fluorescence was found to be similar for both sets of conditions, despite incubation of C14 ester **2h** with the liposome sample. This result implies that the ester **2h** has a greater tendency to form aggregates in aqueous solution

due to its hydrophobic C14 alkyl chain. Therefore, the higher lipophilicity of **2h** may be restricting its transmembrane anion transport ability.

#### **2.4 <sup>1</sup>H NMR Competition Experiment Proves that Prodigiosin 1 is More Basic than Ester Analog 2e**

As illustrated in **Table 2.2**, the Cl<sup>-</sup>/NO<sub>3</sub><sup>-</sup> anion transport data indicates that compounds featuring a C-ring conjugated ester (**2e**) exhibit transmembrane transport activity that is about an order of magnitude lower than the natural product **1** or the methylated analog **24**. We hypothesized that the C-ring ester derivatives are less basic than **1**, and so the protonated form of the anionophore **2e•H<sup>+</sup>** would be less prevalent in the case of ester **2e**. To investigate the effect of the ester group on the acid-base properties of the prodigiosenes, a simple competition NMR experiment in CD<sub>3</sub>CN was done (**Figure 2.9**). A 1:1 mixture of prodigiosin in free-base form (**1**) and C5 ester analog as an HCl salt (**2e•HCl**) was prepared. When the <sup>1</sup>H NMR of this sample was recorded, it was found that the prodigiosin was in protonated form (**1•HCl**) and ester analog (**2e**) was in the free-base form (Trace **c** in **Figure 2.9**). Since prodigiosin **1** is more basic than the ester **2e**, it is preferentially protonated in the mixture of compounds. Therefore, the final protonation states were reversed as compared to the initial starting material. These changes in protonation states were reflected by the differences in chemical shift for the methoxy peak of prodigiosin and ester compound. **Figure 2.9** illustrates the competition exhibited by prodigiosin **1** and ester **2e** for a proton. **Figure 2.9a** shows the NMR resonances for the methoxy groups of free-bases of **1** and **2e**. **Figure 2.9b** shows the NMR resonances for the methoxy groups of protonated forms

of prodigiosenes  $1\cdot\text{H}^+$  and  $2e\cdot\text{H}^+$ . Traces **a** and **b** in **Figure 2.9** were used to assign the NMR resonances in trace **c**.

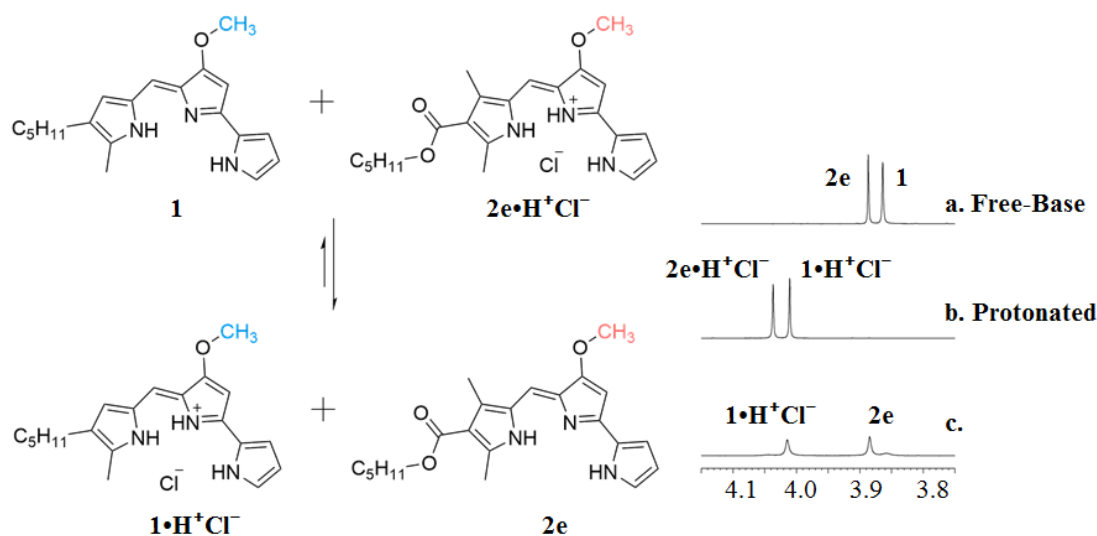


**Figure 2.9.** A 1:1 mixture of the free-base form of prodigiosin **1** and C5 ester analog  $2e\cdot\text{HCl}$  was prepared in  $\text{CD}_3\text{CN}$ . The  $^1\text{H}$  NMR of the 1:1 mixture (top trace) showed that prodigiosin was in the protonated form ( $1\cdot\text{HCl}$ ), while the ester was in the free-base form (**2e**).

Later, a  $^1\text{H}$  NMR titration was done with a mixture of free-bases of prodigiosin **1** and ester analog **2e** with  $\text{MeSO}_3\text{H}$  (**Figure 2.10**). The NMR titration examined the step-by-step protonation process of both prodigiosenes, when treated with acid. Changes in protonation states of **1** and **2e** were reflected by the chemical shifts of the methoxy groups of both compounds. Trace **a** in **Figure 2.10** shows the  $^1\text{H}$  NMR spectra of free-base form of prodigiosin **1** and the pentyl ester prodigiosene (**2e**).<sup>32</sup> The  $^1\text{H}$  NMR chemical shift of the methoxy group of prodigiosin **1** appeared at  $\delta$  3.86 ppm and the methoxy peak of the free-base of ester **2e** at  $\delta$  3.88 ppm (trace **a**).

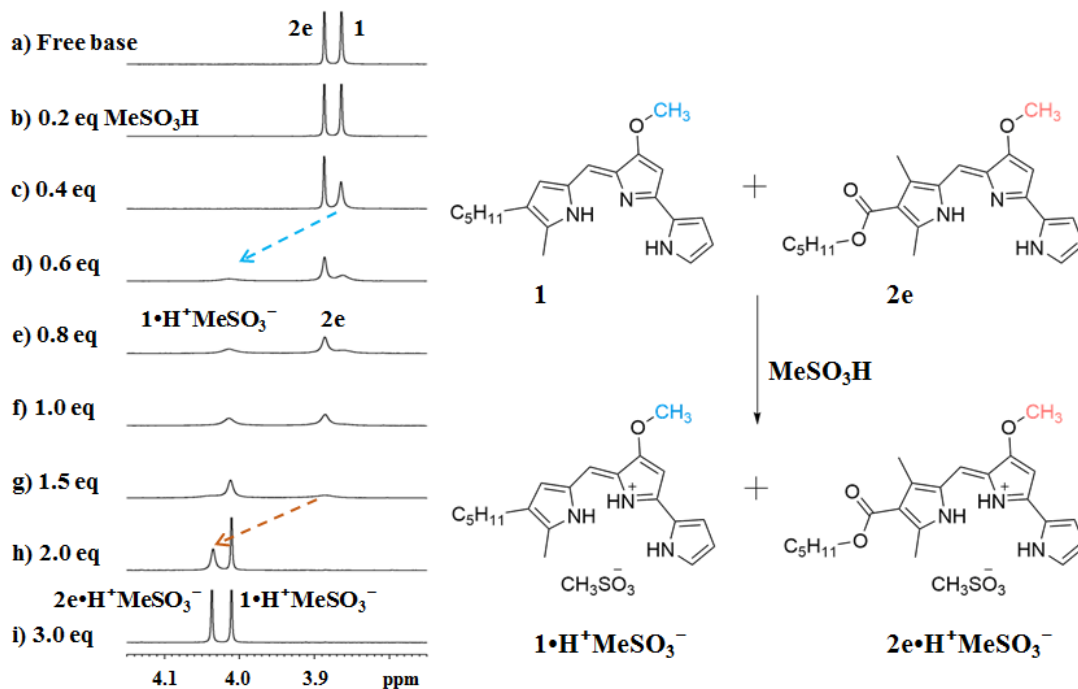


**Figure 2.10.**  $^1\text{H}$  NMR spectra showing the B-ring  $-\text{OCH}_3$  signals during titration of a 1:1 mixture of prodigiosin **1** and ester **2e** (1 mM) with  $\text{MeSO}_3\text{H}$  in  $\text{CD}_3\text{CN}$  at  $25^\circ\text{C}$ . Increments of  $\text{MeSO}_3\text{H}$  were sequentially added to the equimolar mixture of the two prodigiosenes **1** and **2e**.

After the addition of 0.4 eq of  $\text{MeSO}_3\text{H}$ , only the methoxy peak for prodigiosin **1** selectively broadened and decreased in relative intensity (trace **c**). The methoxy peak corresponding to the protonated species  $\mathbf{1}\cdot\text{H}^+$  began to appear at  $\delta$  4.01 ppm after addition of 0.6 eq of  $\text{MeSO}_3\text{H}$  (trace **d**). This peak grew and sharpened until 2 eq of acid had been added to the mixture (trace **h**). Simultaneously, the methoxy peak of ester **2e** at  $\delta$  3.88 ppm started to decrease after addition of 0.6 eq of  $\text{MeSO}_3\text{H}$  (trace **d**), and a new signal ultimately appeared for  $\mathbf{2e}\cdot\text{H}^+\text{Cl}^-$  at  $\delta$  4.03 ppm. After the addition of 3 eq of  $\text{MeSO}_3\text{H}$  (trace **i**), both compounds were fully protonated. The results from this

NMR competition experiment clearly indicate that prodigiosin **1** is more basic than the prodigiosene ester **2e**.

## 2.5 Determination of $pK_a$ of Ester Analog **2f** and Prodigiosin **1**

Having obtained qualitative  $^1\text{H}$  NMR evidence that the electron-withdrawing C-ring ester in **2** influences the proton affinity of the tripyrrolic unit, we next determined the apparent  $pK_a$  values of prodigiosin  $\mathbf{1\cdot H^+}$  and a C-ring hexyl ester analog  $\mathbf{2f\cdot H^+}$ . The apparent  $pK_a$  values correspond to the equilibrium mixture of  $\alpha$  and  $\beta$  isomers of the B-ring prodigiosenes (**Figure 2.11**). As an example, the  $\alpha$  and  $\beta$  isomers of compound **2f** are shown in the free-base form and the protonated form in **Figure 2.11**. As the UV-vis titration progresses, prodigiosene **2f** goes from protonated form ( $\mathbf{2f\cdot H^+}$ ) to the free-base form (**2f**). For the mixture of  $\alpha$  and  $\beta$  isomers in free-base form ( $\alpha\mathbf{2f}$  and  $\beta\mathbf{2f}$ ),  $\lambda_{\text{max}}$  was at 450 nm. For the mixture of  $\alpha$  and  $\beta$  isomers in protonated form ( $\alpha\mathbf{2f\cdot H^+}$  and  $\beta\mathbf{2f\cdot H^+}$ ),  $\lambda_{\text{max}}$  was at 517 nm. To measure the apparent  $pK_a$  values, we used a spectrophotometric procedure described by Manderville and colleagues.<sup>33</sup> In the method used to determine apparent  $pK_a$  value of prodigiosenes, a solution of the specific prodigiosene was prepared in a 1:1 mixture of  $\text{CH}_3\text{CN-H}_2\text{O}$  (v/v) at 25 °C (0.1 M NaCl) at a slightly acidic pH. This solution of prodigiosene ( $\mathbf{1\cdot H^+}$  and  $\mathbf{2f\cdot H^+}$ ) was titrated with aliquots of NaOH. After each addition of NaOH, the absorbance of the solution containing prodigiosene was measured (**Figure 2.12**). The apparent  $pK_a$  values were determined from plots of the log (ionization ratio) vs. pH.



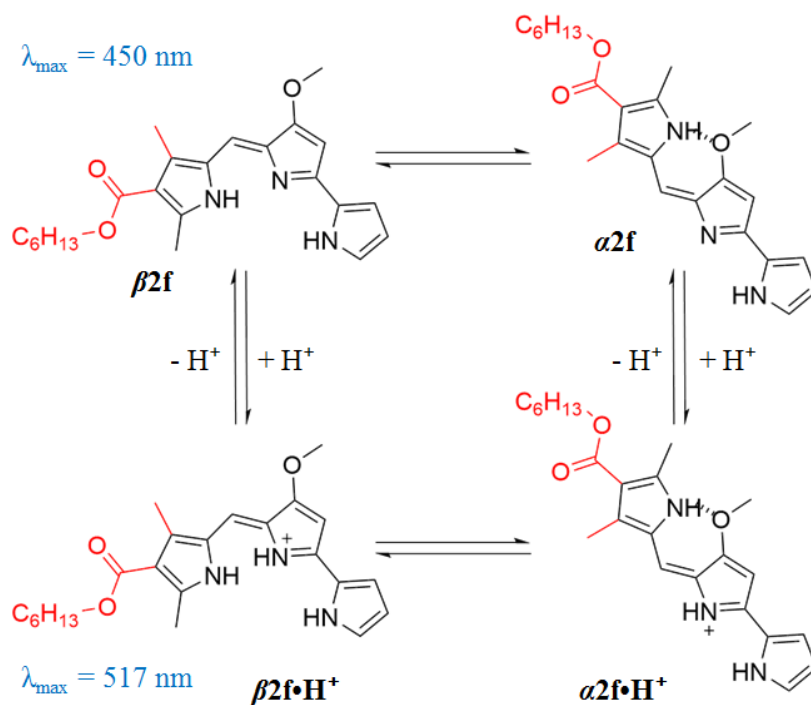


**Figure 2.11.** The  $\alpha$  and  $\beta$  isomers of prodigiosene **2f** in free-base and protonated form are in equilibrium with each other in solution. The apparent  $pK_a$  values were calculated for an equilibrium mixture of  $\alpha$  and  $\beta$  isomers of protonated prodigiosene  $\mathbf{2f}\cdot\mathbf{H}^+$ .

**Figure 2.12** shows UV-vis titrations for the natural prodigiosin **1** (**Figure 2.12a**) and the synthetic ester **2f** (**Figure 2.12b**) in 1:1  $\text{CH}_3\text{CN}/\text{H}_2\text{O}$ . As can be seen in **Figure 2.12a**, the  $\lambda_{\max}$  for the protonated form of prodigiosin  $\mathbf{1}\cdot\mathbf{H}^+$  at 533 nm and the  $\lambda_{\max}$  for the free-base **1** at 460 nm are well separated. From this titration data, we determined that the natural product  $\mathbf{1}\cdot\mathbf{H}^+$  has an apparent  $pK_a$  of 8.2. An apparent  $pK_a$  value of 7.98 for  $\mathbf{1}\cdot\mathbf{H}^+$  in aqueous acetonitrile was previously reported.<sup>22</sup> For the hexyl ester derivative **2f**, the  $\lambda_{\max}$  for the protonated form  $\mathbf{2f}\cdot\mathbf{H}^+$  was at 517 nm and  $\lambda_{\max}$  for the free-base **2f** was at 450 nm (**Figure 2.12b**). Based on the UV-vis spectra for the corresponding titration, we determined that the synthetic ester  $\mathbf{2f}\cdot\mathbf{H}^+$  has an apparent

$pK_a$  of 6.5. These UV-vis titrations demonstrate that the electron-withdrawing carbonyl group on the C-ring of **2f** makes the ester significantly less basic than the natural product **1**. Relative to prodigiosin **1**, the reduced basicity of ester **2f** would make it more difficult to protonate this analog near neutral pH, which would then decrease the ability of the protonated esters (**2f**•H<sup>+</sup>) to bind and transport anions. This hypothesis was demonstrated experimentally by a pH variation study, as described in the next section.

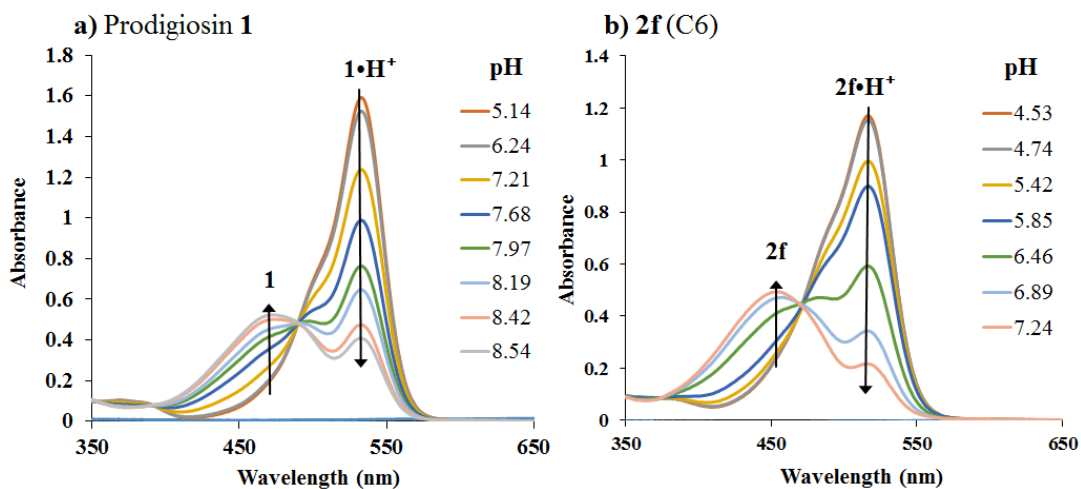


**Figure 2.12.** UV-vis absorbance spectra for **a)** prodigiosin **1** and **b)** ester **2f** as a function of pH in 1:1 CH<sub>3</sub>CN/H<sub>2</sub>O (v/v) at 25 °C (0.1 M NaCl).

## 2.6 Transmembrane Anion Transport as a Function of pH

Having shown that the differing basicities of the natural product **1** and an ester-bearing analog **2** influence the transmembrane anion transport activity, we next investigated the pH dependence of Cl<sup>-</sup>/NO<sub>3</sub><sup>-</sup> exchange as catalyzed by these prodigiosenes. For these experiments, we prepared EYPC liposomes encapsulating NaNO<sub>3</sub> (100 mM, pH 7.5 with 10 mM phosphate) and 1 mM of LG, the chloride-selective dye.

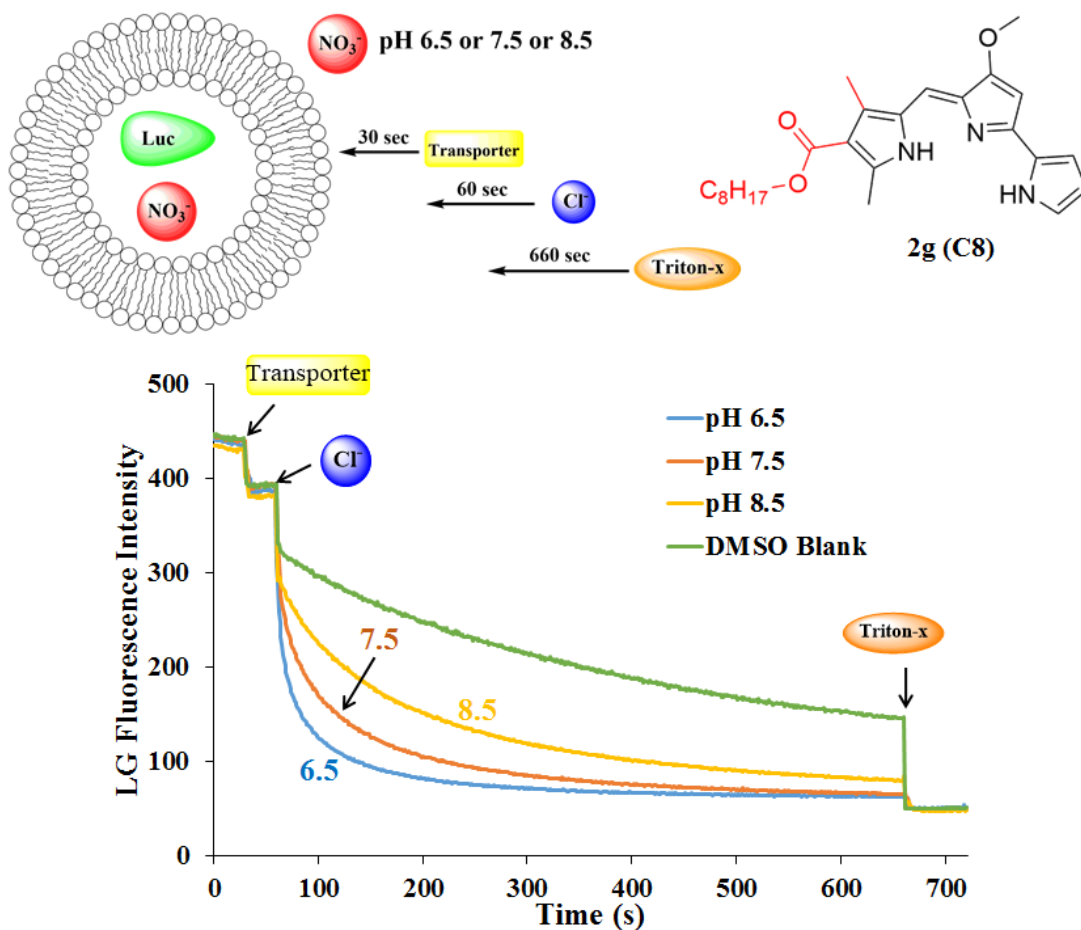


**Figure 2.13.** Experimental procedure for the pH variation experiments performed with octyl ester analog **2g**. Chloride influx promoted by 0.05 mol % of ester **2g** as a function of extravesicular pH. At  $t = 30$  s, a solution of **2g** was added to a solution of EYPC vesicles, loaded with 1 mM LG and 100 mM NaNO<sub>3</sub>. The liposome sample was suspended in 10 mM phosphate buffer (pH 6.5, 7.5 or 8.5). At  $t = 60$  s, NaCl solution was added to give a final extravesicular Cl<sup>-</sup> concentration of 100 mM. At the end of the experiment, Triton-X detergent was added to lyse the vesicles. The faster fluorescence decay at pH 6.5 indicates faster anion exchange, as mediated by ester **2g**•H<sup>+</sup>. Traces shown are an average of three trials.

The experimental procedure is depicted in **Figure 2.13**. At  $t = 30$  s, the octyl-ester prodigiosene **2g** (0.05 mol % relative to EYPC lipid) was added to the liposome solution. Then, at  $t = 60$  s, a pulse of 10 mM phosphate buffer (at pH 6.5, 7.5 or 8.5) containing 1 M NaCl and 100 mM NaNO<sub>3</sub> was added to give an extravesicular Cl<sup>-</sup> concentration of 100 mM (**Figure 2.13**). **Figure 2.13** shows this transporter-mediated anion exchange as a function of extravesicular pH. The observed decrease in the LG fluorescence is due to influx of Cl<sup>-</sup>, as catalyzed by the prodigiosene ester **2g•H<sup>+</sup>**, and so faster decay indicates faster anion exchange. Chloride transport by **2g•H<sup>+</sup>** increased as the pH was decreased from 8.5 to 6.5. This systematic increase in transport activity with decreasing pH is consistent with increased ion pairing between the target anions and the protonated tripyrrolic head-group of the prodigiosene **2g•H<sup>+</sup>**, whose pK<sub>a</sub> we determined to be 6.5. These experiments show that transmembrane transport of anions by the prodigiosene ester **2g** can be modulated by controlling the external pH.

### **2.7 *In vitro* Anticancer Activity of C-Ring Functionalized Prodigiosenes**

The *in vitro* anticancer activity of some C-ring synthetic prodigiosenes was evaluated at the National Cancer Institute (NCI) against a standard panel of 59 human cell lines, derived from nine cancer cell types.<sup>121</sup> **Table 2.3** shows averaged concentrations for activity across all lines for prodigiosenes **1**, **2** and **24**. Compared to the natural prodigiosin **1** (Entry **1**), prodigiosene **24** exhibited a slightly improved anticancer activity, in terms of TGI values, and a reduced toxicity (Entry **2**). Some of the prodigiosene esters (Entries **2**, **6** and **7**) exhibited anticancer activities that were similar in magnitude to those of the natural compound **1**, demonstrating that

introduction of a C-ring carbonyl moiety is not detrimental to the anticancer activity of this series of compounds.

**Table 2.3.** Mean *in vitro* activity of prodigiosenes over 59 cancer cell lines.<sup>121</sup>

| Entry    | C-ring variation           | <sup>b</sup> GI <sub>50</sub><br>nM mean | <sup>c</sup> TGI<br>μM mean | <sup>d</sup> LC <sub>50</sub><br>μM mean |
|----------|----------------------------|--|-----------------------------|--|
| <b>1</b> | Prodigiosin <b>1</b>       | 14                                       | 2.1                         | 0.3                                      |
| <b>2</b> | <b>24</b>                  | 15                                       | 0.1                         | 1.0                                      |
| <b>3</b> | methyl <b>2a</b>           | 347                                      | 6.0                         | 49.0                                     |
| <b>4</b> | <i>i</i> -propyl <b>2c</b> | 59                                       | 1.0                         | 7.9                                      |
| <b>5</b> | butyl <b>2d</b>            | 117                                      | 2.0                         | 14.5                                     |
| <b>6</b> | pentyl <b>2e</b>           | 36                                       | 0.6                         | 4.6                                      |
| <b>7</b> | octyl <b>2g</b>            | 28                                       | 1.9                         | 18.6                                     |
| <b>8</b> | phenyl <b>2i</b>           | 214                                      | 2.0                         | 14.5                                     |
| <b>9</b> | benzyl <b>2j</b>           | 129                                      | 2.0                         | 14.5                                     |

<sup>a</sup> <http://dtp.cancer.gov>. <sup>b</sup> GI<sub>50</sub> = half maximal growth inhibition concentration. <sup>c</sup>TGI = total growth inhibition concentration. <sup>d</sup>LC<sub>50</sub> = half maximal lethal concentration.

An analysis of the data shown in **Table 2.3** allows an appreciation for the concentrations at which *in vitro* activity was observed. For example, the prodigiosenes **24** and **2e** effect growth inhibition for most strains at nM concentrations, similar to the natural product **1**. Unlike Sessler's synthetic analogs (**Section 1.5.1**),<sup>10</sup> no clear correlations could be made between anion transport results and the *in vitro* anticancer activity of the prodigiosenes **1**, **2** and **24**. Some compounds such as **2e** (C5) and **24**, with alkoxy chain lengths similar to prodigiosin **1** showed good anion transport activity, and also inhibited cell growth at low nM concentrations with low cytotoxicities (GI<sub>50</sub> and LC<sub>50</sub> values, respectively in entries **1**, **2**, **6** and **7** in **Table 2.3**). Other compounds such as **2a** (Me), **2c** (*i*-Pr) and **2d** (C4) also displayed good anion transport activity but exhibited high cytotoxicity combined with low cell growth inhibition (entries **3-5** in

**Table 2.3**). In particular, compound **24** with no ester group was the most effective at cell growth inhibition and as an anion transporter as well. These screening activity results across a range of cancer cell types demonstrate that inclusion of the extra methyl group on ring C is not detrimental for *in vitro* anticancer activity. However, the same cannot be said unambiguously for the ester group. Along with the ester functionality, the alkoxy chain length seems to play a vital role in defining the anticancer activity as well as the ability of prodigiosenes **2** as anion transporters. These findings are important given that the incorporation of the additional C-ring methyl group facilitated synthesis of the prodigiosene core.<sup>114</sup> Additionally, the incorporation of the ester moiety enabled variation in chain lengths and a probe into the electronic effects in prodigiosenes.

## 2.8 Conclusions

A series of C-ring modified prodigiosenes were studied for their ability to transport anions across lipid bilayers and their *in vitro* anti-cancer activities using the NCI panel of 60 cancer cell lines. The methylated analog **24** exhibited very good anticancer activity, as compared to the natural product **1**, with a decreased TGI value and lower toxicity. Some of the synthetic esters (**2c** and **2g**) had similar anti-cancer potency as the natural product prodigiosin **1**.

Additionally, these results based on anticancer activity of the synthetic prodigiosenes show that the extra methyl group added to the C-ring is not detrimental to the *in vitro* anticancer activity of these new prodigiosenes (**2** and **24**). Although the presence of an ester on the C ring decreases the p*K*<sub>a</sub> and the anion transport rate of prodigiosene ester **2•H<sup>+</sup>**, these compounds are still effective transporters, even at low

concentrations.<sup>117</sup> The possibility to regulate anion transport activity of prodigiosenes as a function of their basicity and extravesicular pH intrigued us. By manipulating the basicity of these synthetic prodigiosenes and variation in solution pH (**2g** in **Figure 2.13**), the extent of protonation for the receptors (**2g•H<sup>+</sup>**) could be modulated. Since it is the protonated receptor that catalyzes anion transport, the process of anion binding and subsequently, anion transport across bilayers was also affected. With this information, we proceeded to study the correlation between the basicity of prodigiosenes and their rate of anion transport through lipid bilayers in greater detail in **Chapter 3**.

### 3 Chapter 3: Influence of B-Ring Modifications on Proton Affinity, Transmembrane Anion Transport and Anti-Cancer Properties of Synthetic Prodigiosenes

*The majority of this chapter has been published in reference 131:*

- Marchal, E.; Rastogi, S.; Thompson, A.; Davis, J. T. “Influence of B-Ring Modifications on Proton Affinity, Transmembrane Anion Transport and Anti-Cancer Properties of Synthetic Prodigiosenes” *Org. Biomol. Chem.*, **2014**, *12*, 7515-7522.

*Syntheses of all compounds 3a-h described in this chapter were performed by Dr. Estelle Marchal and Dr. Alison Thompson, our collaborators from the Dalhousie University, Canada. Compounds 3a, 3b, 3d and 3h were tested against 60 human cancer cell lines by the Developmental Therapeutic Program at NCI, NIH.*

#### **Background**

##### **3.1 Introduction**

One mechanism put forth to explain the biological activities of the prodigiosenes is that since prodigiosenes are typically protonated at physiological pH, they can alter intracellular pH *via* H<sup>+</sup>Cl<sup>-</sup> co-transport (or Cl<sup>-</sup>/OH<sup>-</sup> exchange) across cell membranes.<sup>27,48</sup> In this chapter, we studied a series of prodigiosene analogs **3** with different -O-aryl substituents attached to the B-ring of the tripyrrolic skeleton (**Figure 3.1**). We found that the electronic nature of the O-aryl substituent on the B-ring influences the rate at which these prodigiosenes catalyze transmembrane anion



transport, i.e. the prodigiosenes with the higher  $pK_a$  had greater  $Cl^-/NO_3^-$  exchange rates. Four of the synthetic prodigiosenes were tested for their *in vitro* anti-cancer activities in the NCI60 human tumor panel. Before describing the studies done to correlate basicity of prodigiosenes **3** with their transmembrane anion transport efficiency, I first provide a brief background on work previously done with other B-ring modified prodigiosenes. Then, I present my experimental results that show that anion transport ability of B-ring modified aryl prodigiosenes **3** is dependent on the basicity of these analogs.

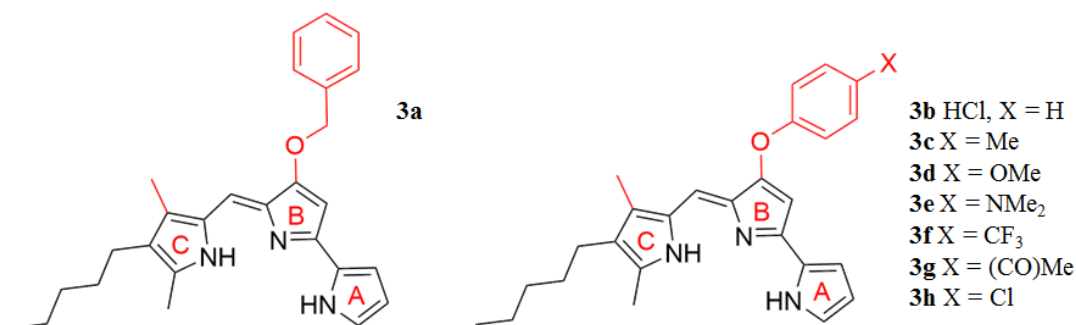


**Figure 3.1.** Structures of B-ring modified prodigiosenes **3a-h**.

### 3.2 Earlier Work with B-Ring Modified Prodigiosenes

In the last decade various compounds that catalyze transmembrane transport of anions have been identified.<sup>75,79</sup> Much of this activity has been driven by supramolecular chemists interested in systems that work at the water-lipid interface.<sup>74,122</sup> An important factor promoting this research is the possibility that anion transporters might be developed into therapeutics for diseases, like cystic fibrosis, that are caused by defective transport of  $Cl^-$ .<sup>76,123</sup>

Some synthetic transporters have been developed after considering how nature catalyzes the process. For example, peptides that contain domains of the  $\text{Cl}^-$  channel can transport anions across lipid membranes,<sup>124,125</sup> while modification of natural amphiphiles like cholic acid has provided potent anion carriers.<sup>126,127</sup> The tripyrrolic prodigiosenes are known to catalyze transmembrane anion transport.<sup>31,32,77,114,128</sup> The parent compound, prodigiosin (**1**) has much biological potential,<sup>6,129</sup> as it is able to permeabilize cell membranes, alter intracellular pH and trigger apoptosis.<sup>48,27</sup> Early studies indicated that prodigiosin is too cytotoxic for healthy cells and, for this reason, it was not initially pursued as a drug candidate.<sup>130</sup> There has been a renewed interest in prodigiosenes since some synthetic analogs have promising anti-cancer,<sup>2-4</sup> immunosuppressive,<sup>5, 6</sup> anti-malarial,<sup>7</sup> and antimicrobial<sup>8</sup> activities at concentrations below where they are cytotoxic to healthy cells.

### **3.2.1 Rationale for Studying the Anion Transport Activity by B-Ring Modified Aryl Prodigiosenes**

As depicted in **Figure 3.2** protonated prodigiosin **1•H<sup>+</sup>** has a binding pocket for anions, using hydrogen bonds and electrostatic interactions for anion coordination. The resulting amphiphilic neutral salt **1•HCl** can then readily diffuse through the cell membrane. It has been previously shown that prodigiosin **1•HCl** catalyzes the transmembrane exchange of anions such as  $\text{Cl}^-$ ,  $\text{NO}_3^-$  and  $\text{HCO}_3^-$ .<sup>31, 32, 114</sup>

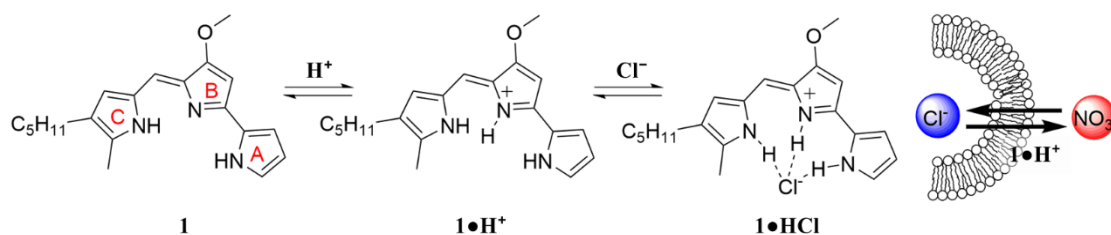


**Figure 3.2.** Protonation of prodigiosin **1** and subsequent binding of chloride anion by **1•H<sup>+</sup>**. The schematic at the right depicts the protonated prodigiosin **1•H<sup>+</sup>** catalyzing the exchange of anions across a lipid bilayer.

In **Chapter 2**, I showed that ester **2f** (**Figure 3.3**), with an electron-withdrawing carbonyl group appended to the C-ring, was less basic by two orders of magnitude than the parent prodigiosin **1** (prodigiosin **1•H<sup>+</sup>**,  $pK_a = 8.2$ ; **2f•H<sup>+</sup>**,  $pK_a = 6.5$ ) and also a much less effective anion transporter than **1**.<sup>114</sup> We suggested that the ease of protonation of the carrier and, thus, its consequent anion transport activity was modulated by changing the electronic properties of the C-ring substituents. Herein, I describe a systematic study on B-ring analogs **3** that confirms transmembrane anion transport rates can be modulated by tuning the  $pK_a$  of the prodigiosene skeleton. I describe the anion transport and *in vitro* anti-cancer properties of prodigiosenes **3** with different  $-OAr$  substituents attached to the tripyrrolic B-ring. The synthetic prodigiosenes **3** used in this study have an A-ring pyrrole, a B-ring pyrrole substituted with various aryl groups (**Figure 3.3**) to modulate  $pK_a$ , and a C-ring pyrrole that differs from the natural compound **1** by an extra methyl group on the heterocyclic unit.

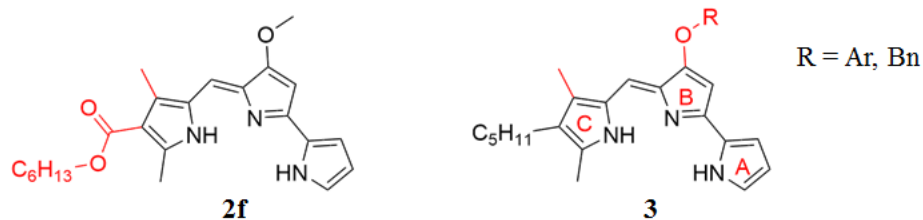


**Figure 3.3.** Structures of prodigiosene ester analog **2f** and phenyl analog **3**.

### 3.2.2 Examples of Previous B-Ring Modified Prodigiosenes

There are a few reports regarding synthetic modification of the prodigiosene B-ring, such as the compounds developed by Boger, Sessler and D'Alessio (**Figure 3.4**).<sup>5,10,103</sup> Described below are selective examples of the B-ring modified prodigiosenes that have shown significant biological activity.

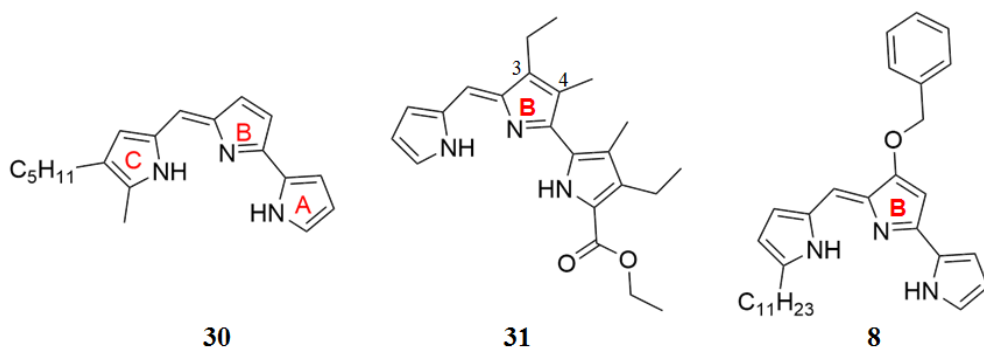


**Figure 3.4.** Structures of prodigiosenes **30**, **31** and PNU-156804 (**8**).

#### 3.2.2.1 Desmethoxyprodigiosin by Boger

Desmethoxyprodigiosin **30** was synthesized by Boger and his group (**Figure 3.4**).<sup>103</sup> There were no functional groups present on the pyrrole ring B of **30**. The analog **30** was evaluated for its *in vitro* cytotoxicity. The *in vitro* cytotoxic studies were comprised of assays with various cancer cell lines for melanoma (B16 mouse), leukemia (L1210 mouse, 9PS (P388) mouse) and human epidermoid carcinoma of the

nasopharynx (9KB) using established protocols. The IC<sub>50</sub> values (defined as the inhibitory concentration for 50% cell growth relative to untreated control) of prodigiosin **1** and desmethoxyprodigiosin **30** were compared for the 4 cell lines mentioned above. For each cancer cell line, prodigiosin displayed substantial cytotoxic activity as compared to the analog **30** (**Table 3.1**). Prodigiosin was found to be exceptionally potent against the P388 leukemia cell line (IC<sub>50</sub> = 0.00037 µg/ mL) in comparison to the desmethoxyprodigiosin **30** (IC<sub>50</sub> = 0.03 µg/ mL).

**Table 3.1.** The *in vitro* cytotoxic activity (IC<sub>50</sub>) of prodigiosin **1** and desmethoxyprodigiosin **30** against four cancer cell lines - leukemia (L1210 mouse), melanoma (B16 mouse), 9PS (P388 mouse) and human epidermoid carcinoma of the nasopharynx (9KB).<sup>103</sup>

|           | IC <sub>50</sub> (µg/mL) |      |            |      |
|-----------|--------------------------|------|------------|------|
|           | L1210                    | B16  | 9PS (P388) | 9KB  |
| <b>1</b>  | 0.02                     | 0.03 | 0.00037    | 0.04 |
| <b>30</b> | 12                       | 24   | 0.03       | 0.7  |

The relative inactivity of desmethoxyprodigiosin **30** as an anti-cancer agent, as compared to the parent prodigiosin **1**, was attributed to the absence of the –OMe group on ring B. Molecular modeling studies were done to ascertain the impact of the methoxy group on conformation and chemical reactivity of prodigiosenes by comparing structural and electronic aspects of prodigiosin **1** and **30**. However, the theoretical studies revealed no substantial structural or electronic differences that might correlate the relative cytotoxicity of the two compounds with the role of the methoxy

substituent. Boger *et al.* concluded from this study that the presence of an –OMe group on the B-ring is essential for prodigiosin’s biological activity.<sup>103</sup>

### 3.2.2.2 Sessler’s B-Ring Modified Prodigiosene

Unlike Boger’s compound **30**, compound **31** (**Figure 3.4**) synthesized by Sessler and his group demonstrated reasonable anti-cancer activity, despite the missing methoxy group on ring B.<sup>10</sup> Prodigiosene **31** has an ethyl group in place of the methoxy group on 3-position and a methyl group on 4-position on ring B. Anti-cancer activity was assessed using a cell proliferation assay with two different cancer cell lines – A549 human lung cancer and PC3 human prostate cell lines. For both cell lines, compound **31** completely inhibited cell proliferation at 40  $\mu\text{M}$  concentration. Additionally, Sessler *et al.* reported that the anti-cancer activity of **31** correlated well with its efficiency to catalyze  $\text{Cl}^-$  anion transport across liposomal membranes.

### 3.2.2.3 PNU-156804 by D’Alessio

PNU-156804 (**8**) was designed and synthesized by D’Alessio and his group (**Figure 3.4**).<sup>5</sup> Compound **8** has a –OBn group on ring B instead of the –OMe group. Due to its immunosuppressive properties,<sup>5</sup> PNU-156804 has been used as an anti-rejection compound in organ transplants.<sup>15</sup> For compound **8**, installation of a larger –OBn group on ring B led to a reduction in its immunosuppressive activity as compared to compounds with a methoxy group. However, the decrease in immunosuppressive activity was balanced by a significant decrease in cytotoxicity. As a result, compound **8** exhibited nM  $\text{IC}_{50}$  values against leukemia and melanoma cells, thus, making it an attractive immunosuppressant.<sup>5</sup>

In the study presented here, our collaborators Dr. Estelle Marchal and Dr. Alison Thompson prepared novel derivatives **3** substituted with different –OAr groups on the B-ring, alongside common features at the A and C-ring. These novel compounds **3** were used to probe the influence of electronic effects upon  $pK_a$  values, transmembrane anion exchange rates and anti-cancer activity. This is, to our knowledge, the first report of prodigiosenes substituted with –OAr groups on the B-ring.

## Results

### 3.3 Novel Phenyl Analogs **3** and a Comparison of their Basicity

A series of 8 prodigiosenes with electron withdrawing or electron donating groups on ring B were synthesized by Dr. Estelle Marchal and Dr. Alison Thompson from Dalhousie University, Canada.<sup>131</sup> These compounds are listed in **Figure 3.5**.

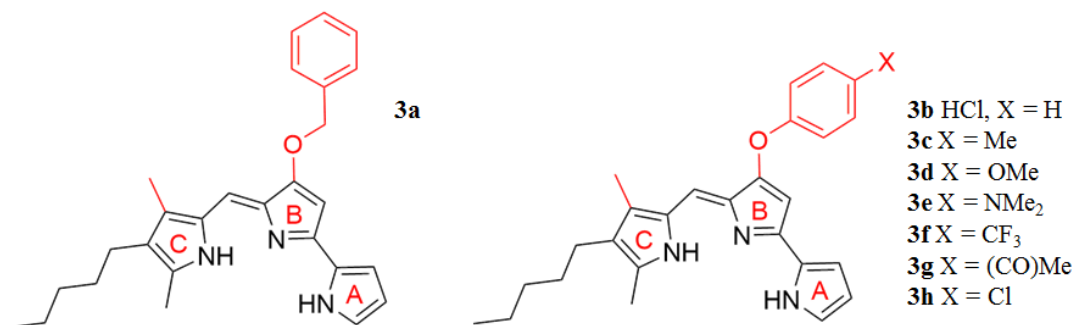


**Figure 3.5.** Structures of B-ring modified prodigiosenes **3a-h**.

As described below, we next conducted mechanistic studies to investigate the proton affinities, transmembrane anion transport activities and anti-cancer properties for this class of B-ring compounds.

### 3.3.1 Determination of Apparent $pK_a$ Values for Synthetic Prodigiosenes

We hypothesized that prodigiosene basicity would correlate with its efficiency as an anion transporter, since the protonated prodigiosene  $\mathbf{3}\cdot\mathbf{H}^+$  is the likely transporter. The concept that transporter efficiency can be tuned by modulating the acidity of hydrogen bond donors has been demonstrated with other systems. Gale and colleagues demonstrated that anion binding abilities of some mono-thioureas can be modulated by the (hydrogen bond) acidity of the thiourea NH function.<sup>96</sup> In a separate paper, Gale *et. al.* showed that the anion transport activity of a series of easy-to-make fluorinated tripodal urea-based transporters could be enhanced significantly by the introduction of fluorinated groups. The fluorinated groups helped in increasing the acidity of anion binding protons as well as increasing lipophilicity of the receptor.<sup>119</sup>

To learn how B-ring substitution influences the acid-base properties of these synthetic prodigiosenes, I used a spectrophotometric method described by Manderville,<sup>33</sup> to measure the apparent  $pK_a$  values for five B-ring analogs: the  $-\text{OPh}$  derivative ( $\mathbf{3b}\cdot\mathbf{H}^+$ ), two analogs with electron-donating groups on the  $-\text{OAr}$  ring ( $\mathbf{3d}\cdot\mathbf{H}^+$  X = OMe,  $\mathbf{3e}\cdot\mathbf{H}^+$  X = NMe<sub>2</sub>), and two analogs with electron-withdrawing groups on the B-ring ( $\mathbf{3f}\cdot\mathbf{H}^+$  X = CF<sub>3</sub>,  $\mathbf{3h}\cdot\mathbf{H}^+$  X = Cl). The apparent  $pK_a$  values correspond to the equilibrium mixture of  $\alpha$  and  $\beta$  isomers of the prodigiosenes (**Figure 3.6**). As an example, the  $\alpha$  and  $\beta$  isomers of compound  $\mathbf{3d}$  are shown in the free-base form and the protonated form in **Figure 3.6**. As the UV-vis titration progresses, prodigiosene  $\mathbf{3d}$  goes from protonated form ( $\mathbf{3d}\cdot\mathbf{H}^+$ ) to the free-base form ( $\mathbf{3d}$ ). For the



mixture of  $\alpha$  and  $\beta$  isomers in free-base form ( $\alpha\mathbf{3d}$  and  $\beta\mathbf{3d}$ ),  $\lambda_{\max}$  was at 484 nm. For the mixture of isomers in protonated form ( $\alpha\mathbf{3d}\cdot\mathbf{H}^+$  and  $\beta\mathbf{3d}\cdot\mathbf{H}^+$ ),  $\lambda_{\max}$  was at 541 nm.

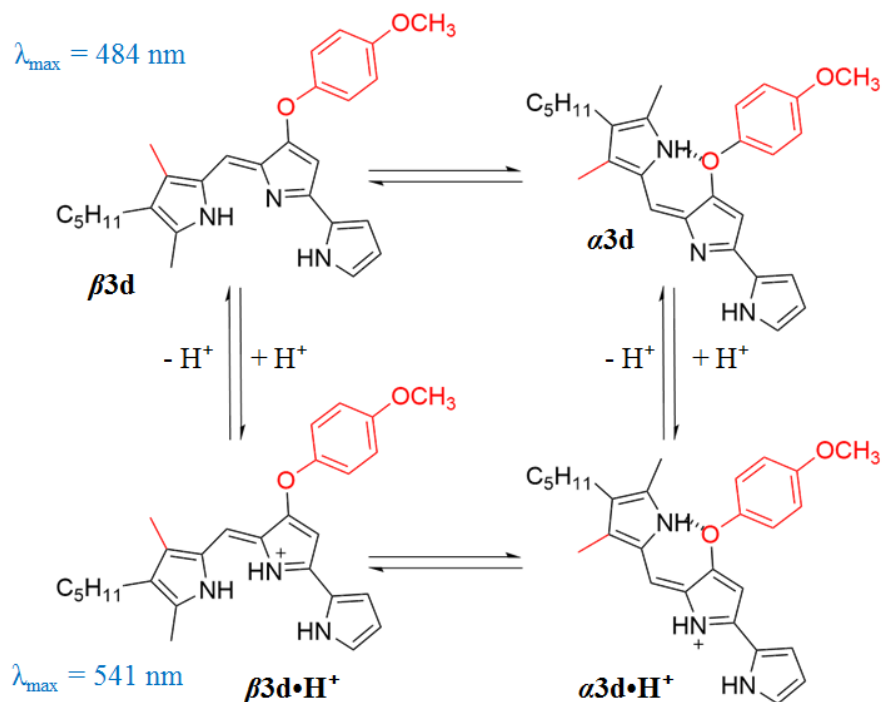


**Figure 3.6.** The  $\alpha$  and  $\beta$  isomers of prodigiosene **3d** in free-base and protonated form are in equilibrium with each other in solution. The apparent  $pK_a$  values were calculated for an equilibrium mixture of  $\alpha$  and  $\beta$  isomers of protonated prodigiosene  $\mathbf{3d}\cdot\mathbf{H}^+$ .

In the method used to determine apparent  $pK_a$  value of a prodigiosene **3**, a solution of the specific prodigiosene was prepared in a 1:1 mixture of  $\text{CH}_3\text{CN}-\text{H}_2\text{O}$  (v/v) at 25 °C (0.1 M NaCl) at a slightly acidic pH. The solution of prodigiosene was titrated against NaOH. After each addition of NaOH, the absorbance of the solution containing prodigiosene **3** was measured (**Figure 3.7**). The apparent  $pK_a$  values, which correspond to values for the equilibrium mixture of  $\alpha$  and  $\beta$  isomers, for these B-ring prodigiosenes were determined from plots of the log (ionization ratio) vs. pH.<sup>33</sup>

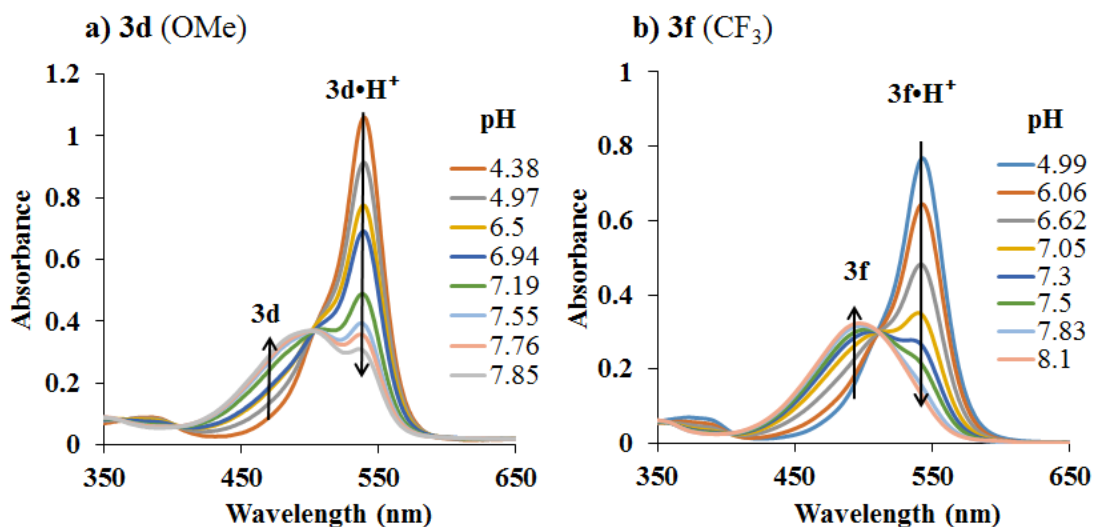


**Figure 3.7.** UV-vis absorbance spectra for **a) 3d** (OMe) and **b) 3f** (CF<sub>3</sub>) as a function of pH in 1:1 CH<sub>3</sub>CN–H<sub>2</sub>O (v/v) at 25 °C (0.1 M NaCl).

In solution, protonated prodigiosenes are pink with absorbance maxima above 500 nm.<sup>132</sup> The free-base absorbs below 500 nm. **Figure 3.7** shows representative pH-dependent spectra for **3d** and **3f** in 1:1 acetonitrile-water at 25 °C. Absorption maxima for the free-base of the OMe analog **3d** ( $\lambda_{\text{max}} = 484$  nm) and its protonated form **3d•H<sup>+</sup>** ( $\lambda_{\text{max}} = 541$  nm) are well separated (**Figure 3.7a**). The CF<sub>3</sub> derivative showed similar properties, with  $\lambda_{\text{max}} = 490$  nm for the free-base **3f** and  $\lambda_{\text{max}} = 545$  nm for **3f•H<sup>+</sup>** (**Figure 3.7b**). Furthermore, the ionization states of **3d/3d•H<sup>+</sup>** and **3f/3f•H<sup>+</sup>** change smoothly as a function of pH, both revealing isosbestic points. As seen in **Table 3.2**, analogs with electron-donating groups on the B-ring, namely **3d•H<sup>+</sup>** (X = OMe, p*K*<sub>a</sub> = 7.3) and **3e•H<sup>+</sup>** (X = NMe<sub>2</sub>, p*K*<sub>a</sub> = 7.4) are weaker acids than are analogs with electron-withdrawing groups, **3f•H<sup>+</sup>** (X = CF<sub>3</sub>, p*K*<sub>a</sub> = 6.7) and **3h•H<sup>+</sup>** (X = Cl, p*K*<sub>a</sub> = 6.8). This means that the free-bases of **3d** (X = OMe) and **3e** (X = NMe<sub>2</sub>) are more basic than **3f** (X = CF<sub>3</sub>) and

**3h** (X = Cl). The increased basicity of **3d** and **3e** means that a greater percentage of these analogs would be protonated at pH 7.4, which should enhance their ability to extract anions from water and transport these bound anions as neutral complexes **3•HA** across lipid membrane.

**Table 3.2.** The  $pK_a$  values for synthetic prodigiosenes **3b**, **3d-f** and **3h** with different –OAr groups on the B-ring.

| <b>3•H<sup>+</sup></b> | <b>3d</b><br>(OMe) | <b>3e</b><br>(NMe <sub>2</sub> ) | <b>3b</b><br>(H) | <b>3h</b><br>(Cl) | <b>3f</b><br>(CF <sub>3</sub> ) |
|------------------------|--------------------|----------------------------------|------------------|-------------------|---------------------------------|
| <b>pK<sub>a</sub></b>  | 7.3 ± 0.1          | 7.4 ± 0.1                        | 7.2 ± 0.1        | 6.8 ± 0.1         | 6.7 ± 0.1                       |

### 3.4 Correlation Between Anion Transport Rates and Transporter Basicity

Having established that B-ring substitution influences the acid-base properties of –OAr analogs **3b**, **3d-f** and **3h**, I next compared the ability of these synthetic prodigiosenes to catalyze the exchange of anions across phospholipid vesicles. Transmembrane transport was evaluated with a liposome model that uses the chloride-sensitive dye LG, to monitor anion exchange.<sup>113</sup> This assay works because LG fluorescence is quenched by Cl<sup>-</sup> but not by NO<sub>3</sub><sup>-</sup>. Thus, egg-yolk phosphatidylcholine (EYPC) liposomes loaded with 1.0 mM LG and NaCl were suspended in a solution (pH 7.4) containing extravesicular NaNO<sub>3</sub>. Upon the addition of the synthetic prodigiosenes **3** the fluorescence of the intravesicular LG increases, indicating Cl<sup>-</sup> efflux and NO<sub>3</sub><sup>-</sup> influx from the vesicles.

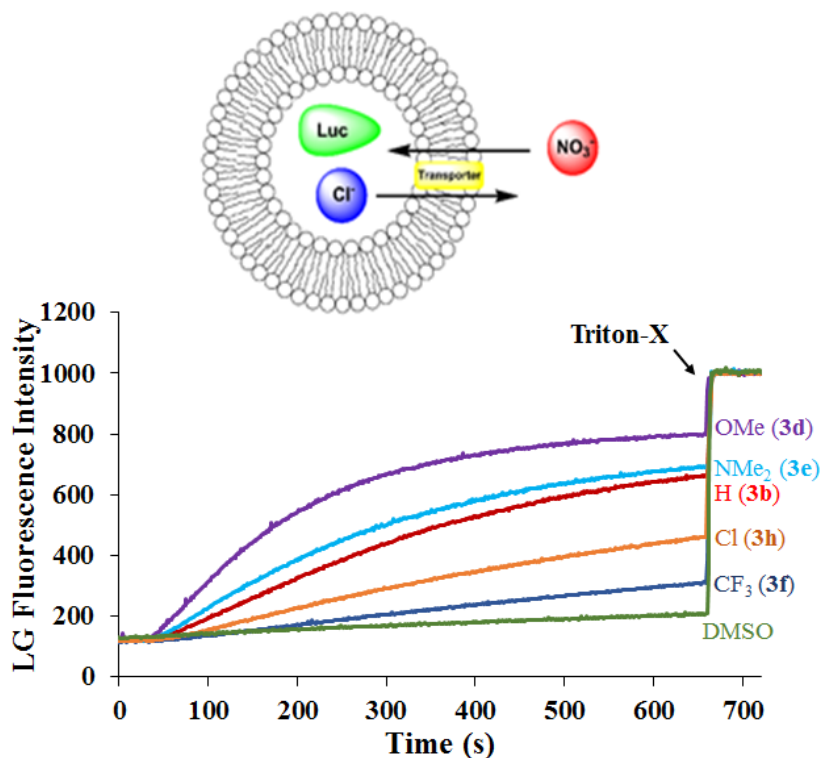


**Figure 3.8.** Anion exchange assay for analogs **3b**, **3d-f** and **3h**. Change in fluorescence of LG observed in EYPC liposomes at 25°C. The data was collected using 0.0008 mol% of transporter compounds relative to EYPC lipid. Liposomes containing 1 mM LG, 20 mM HEPES buffer and 100 mM NaCl (pH 7.4) were suspended in 20 mM HEPES and 100 mM NaNO<sub>3</sub> solution (pH 7.4); at  $t = 30$  s, prodigiosene transporter was added and the LG fluorescence monitored ( $\lambda_{\text{ex}} = 372$  nm,  $\lambda_{\text{em}} = 504$  nm); at  $t = 660$  s, addition of Triton-X; traces shown are an average of three trials.

**Figure 3.8** shows representative LG fluorescence curves, plotted as a function of time, after addition of analogs **3b**, **3d-f** and **3h**. I quantified transport rates by a) determining the initial rate of change of the relative fluorescence of the intravesicular LG and b) estimating the half-life of the exchange reaction (**Table 3.3**).

**Table 3.3.** The  $pK_a$  values, transmembrane anion exchange rates and half-life of the anion transport process for prodigiosenes **3b**, **3d-f** and **3h** with different –OAr groups on the B-ring.

| <b>3•H<sup>+</sup></b>        | <b>pK<sub>a</sub></b> | <b>Initial rate for Cl<sup>-</sup>/NO<sub>3</sub><sup>-</sup> exchange (s<sup>-1</sup>)</b> | <b>t<sub>1/2</sub> for Cl<sup>-</sup> efflux (s)</b> |
|-------------------------------|-----------------------|---|--|
| <b>3d</b> (OMe)               | 7.3 ± 0.1             | 15.1 ± 0.2  | 65 ± 2   |
| <b>3e</b> (NMe <sub>2</sub> ) | 7.4 ± 0.1             | 10.8 ± 0.3  | 87 ± 3   |
| <b>3b</b> (H)                 | 7.2 ± 0.1             | 10.8 ± 0.3  | 90 ± 5   |
| <b>3h</b> (Cl)                | 6.8 ± 0.1             | 3.4 ± 0.1   | 168 ± 3  |
| <b>3f</b> (CF <sub>3</sub> )  | 6.7 ± 0.1             | 1.0 ± 0.1   | 287 ± 2  |

The data in **Figure 3.8** and **Table 3.3** contain important findings. First, these synthetic prodigiosenes, especially **3d** and **3e**, are potent anion transporters and relatively low transporter loadings are needed to observe significant Cl<sup>-</sup> efflux from the liposomes. For example, only 0.0008 mol% of transporter relative to EYPC lipid (1 transporter for 125,000 lipid molecules or about 2.5 transporters per liposome) was used to generate the data in **Figure 3.8**. This is one of the lowest transporter loadings reported to date.<sup>86</sup> Second, substitution of the B-ring with an –OAr group does not perturb the ability of these analogs to catalyze anion exchange. Indeed, the electron-rich **3d•H<sup>+</sup>** (X = OMe) is qualitatively similar to the natural product prodigiosin **1•H<sup>+</sup>** in terms of the efficiency at which it exchanges Cl<sup>-</sup> and NO<sub>3</sub><sup>-</sup> anions across the EYPC bilayer (**Figure 3.9**) Most importantly, compounds substituted with electron-donating groups (**3d** and **3e**) are better anion transporters than analogs containing electron-withdrawing groups (**3f** and **3h**). These results indicate that the catalytic efficiency of

transmembrane anion exchange correlates with how much of the prodigiosene is in its protonated form  $3\cdot\text{H}^+$ .

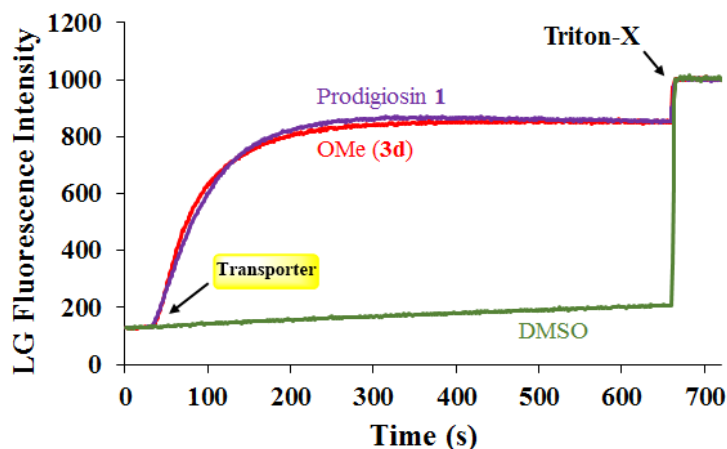


**Figure 3.9.** Anion exchange assay for prodigiosin **1** and analog **3d**. Change in fluorescence of LG observed in EYPC liposomes at 25°C. The data was collected using 0.004 mol% of each prodigiosene transporter relative to EYPC lipid. Liposomes containing 1 mM LG, 20 mM HEPES buffer, 100 mM NaCl (pH 7.4) were suspended in 20 mM HEPES and 100 mM NaNO<sub>3</sub> solution (pH 7.4); at  $t = 30$  s, prodigiosene transporter was added and the LG fluorescence monitored ( $\lambda_{\text{ex}} = 372$  nm,  $\lambda_{\text{em}} = 504$  nm); at  $t = 660$  s, addition of Triton-X; traces shown are an average of three trials.

### 3.5 *In Vitro* Anti-Cancer Properties

The *in vitro* activity of some of the B-ring analogs was evaluated at the National Cancer Institute (NCI, <http://dtp.cancer.gov>) against the standard NCI60 panel of 60 human cell lines.<sup>133</sup> Prodigiosenes selected for testing were the benzyl (**3a**) and phenyl (**3b**) analogs and derivatives with an electron-donating (**3d** X = OMe) and an electron-withdrawing group (**3h** X = Cl). Activities against the NCI60 panel are reported in

**Table 3.4** as mean values averaged over all 60 cell lines; these activities are 1) the half maximal growth inhibition concentration, GI<sub>50</sub>, 2) the total growth inhibition concentration, TGI, and 3) the half maximal lethal concentration, LC<sub>50</sub>. All four synthetic prodigiosenes exhibited GI<sub>50</sub> values in the nM range, indicating that replacement of the B-ring OMe by an O-aryl group is not universally detrimental to anti-cancer activity. These synthetic analogs also show LC<sub>50</sub> values in the μM range that could indicate a lower toxicity compared to the natural compound **1** (LC<sub>50</sub> = 300 nM). The phenyl analog **3b** was the most active of the derivatives with a mean GI<sub>50</sub> value of 18 nM. A more detailed analysis in **Figure 3.10** shows that **3b** was also typically the most active of the four synthetic prodigiosenes against all 60 cell lines.

**Table 3.4.** *In vitro* activity of prodigiosenes **1**, **3a-3b**, **3d** and **3h** over the NCI60 cancer cell lines. Values are a mean of two experiments. (<http://dtp.cancer.gov>)

|                                    | <b>1</b> | <b>3a</b><br>(Bn) | <b>3b</b><br>(X = H) | <b>3d</b><br>(X = OCH <sub>3</sub> ) | <b>3h</b><br>(X = Cl) |
|------------------------------------|----------|-------------------|----------------------|--------------------------------------|-----------------------|
| GI <sub>50</sub> (nM) <sup>a</sup> | 14       | 44                | 18                   | 74                                   | 62                    |
| TGI (μM) <sup>b</sup>              | 2.1      | 0.6               | 0.2                  | 0.8                                  | 1.9                   |
| LC <sub>50</sub> (μM) <sup>c</sup> | 0.3      | 4.8               | 2.5                  | 7.2                                  | 14.4                  |

<sup>a</sup>GI<sub>50</sub> = half maximal growth inhibition concentration. <sup>b</sup>TGI = total growth inhibition concentration. <sup>c</sup>LC<sub>50</sub> = half maximal lethal concentration

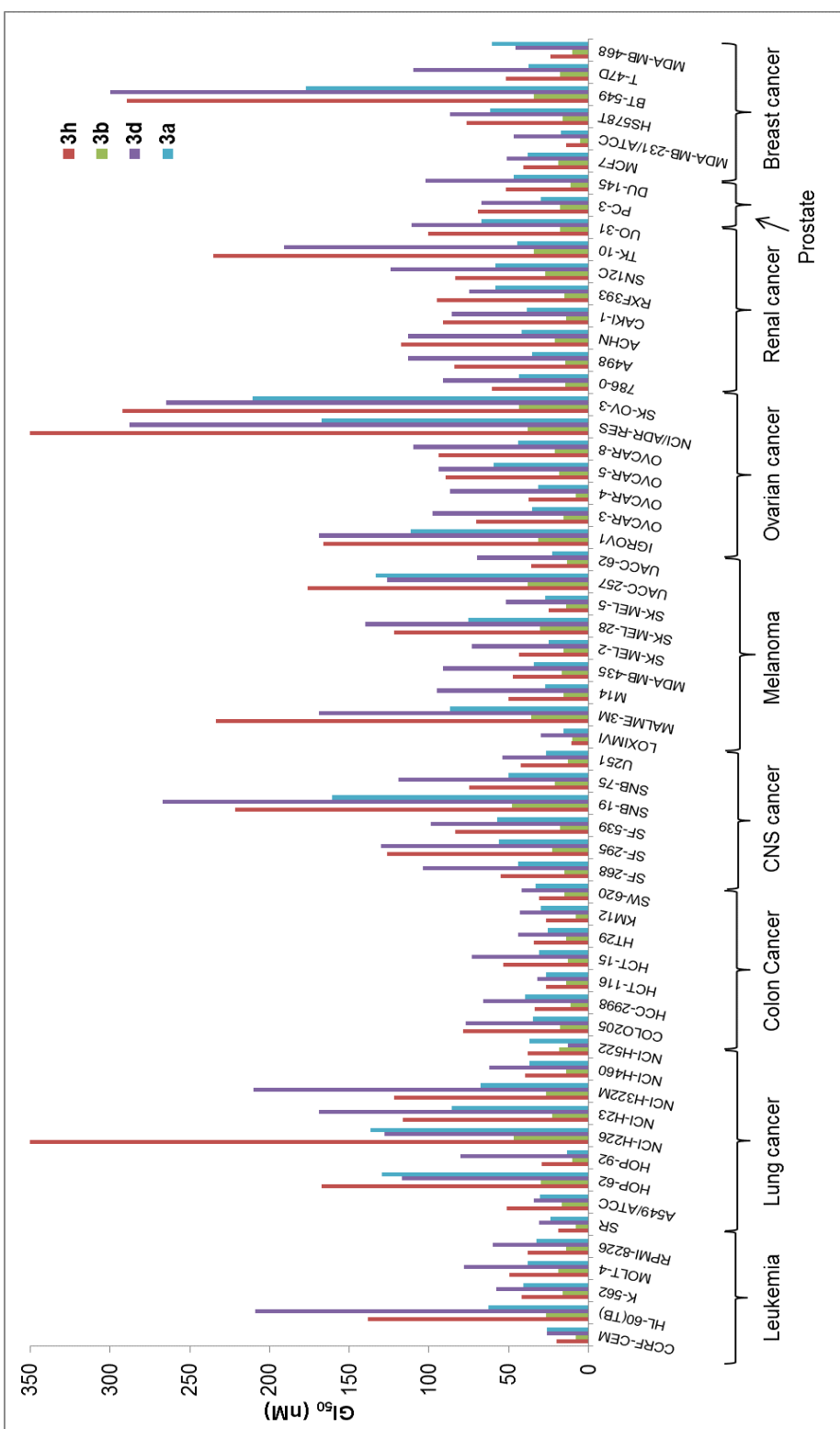


**Figure 3.10.** GI<sub>50</sub> concentrations (half maximal growth inhibition concentrations) of some synthetic prodigiosenes **3a**, **3b**, **3d** and **3h** against 60 human cancer cell lines representing 9 different cancer types; see <http://dtp.cancer.gov>



Two questions that we sought to answer were: would the prodigiosene basicity 1) correlate with its ability to catalyze transmembrane anion exchange and 2) correlate with its anti-cancer activity. The data presented herein suggest that the ease of protonation controls the transmembrane anion exchange. However, despite their significant *in vitro* anti-cancer activity, there is no evidence that those anti-cancer properties universally correlate with, or are caused by, the acid-base properties of the prodigiosene. Thus, the most basic prodigiosene **3d** and the least basic prodigiosene **3h** had similar mean GI<sub>50</sub> values, 74 and 62 nM respectively, and both analogs were less potent than the phenyl analog **3b** (GI<sub>50</sub> = 18 nM).

### 3.6 Conclusions

Prodigiosenes, both naturally occurring and synthetic analogs, are outstanding catalysts for transport of anions across lipid membranes. Being able to control the efficiency of this transmembrane transport of anions would be valuable for various reasons, such as the potential development of therapeutics or anion sensors. In this chapter, I studied some unique prodigiosene analogs with different –OAr substituents attached to the B-ring of the tripyrrolic skeleton. I measured the apparent p*K*<sub>a</sub> values of five B-ring analogs, namely the O-phenyl derivative (**3b•H<sup>+</sup>**), two O-aryl analogs with electron-donating groups and two O-aryl analogs with electron-withdrawing groups. These five derivatives were then tested for their ability to catalyze transmembrane exchange of Cl<sup>-</sup> and NO<sub>3</sub><sup>-</sup> anions in EYPC liposomes. The data indicated that the efficiency of anion transport can indeed be modulated by the electronic nature of the O-aryl substituent on the B-ring. Thus, more basic analogs **3d** (X = OMe, p*K*<sub>a</sub> = 7.3)

and **3e** ( $X = \text{NMe}_2$ ,  $\text{p}K_a = 7.2$ ) showed significantly greater  $\text{Cl}^-/\text{NO}_3^-$  exchange rates than the less basic analogs **3h** ( $X = \text{Cl}$ ,  $\text{p}K_a = 6.8$ ) and **3f** ( $X = \text{CF}_3$ ,  $\text{p}K_a = 6.7$ ). This suggests that the key factor controlling anion transport for this family of synthetic analogs, and presumably for the natural product prodigiosin, is the protonation of the prodigiosene to give an amphiphilic cation **3•H<sup>+</sup>**. This cation extracts anions from water to give a neutral complex **3•HA** that then diffuses rapidly across the lipid membranes. In addition to the synthetic and mechanistic work, the anti-cancer activity of four synthetic prodigiosenes were tested at the NCI (NCI60 human tumor panel). All four analogs showed potent anti-cancer activities, with mean  $\text{GI}_{50}$  values in the nM range, indicating that substitution of the B-ring with OAr groups can give potent anti-cancer agents. Despite their promising *in vitro* anti-cancer activity and their excellent anion transport properties, there was no evidence that the anti-cancer activity is due to the ease of protonation of these synthetic prodigiosenes. The lack of substantive evidence gives rise to the issue that mechanisms other than transport of  $\text{H}^+\text{Cl}^-$  across membranes may be responsible for the anti-cancer activities of the prodigiosenes. In **Chapter 5**, one such possible mechanism will be discussed. Based on my studies, I found that prodigiosin can end stack with G-quadruplex DNA. This is the first time that binding interactions between G-quadruplex and prodigiosin have been established. The relevance of G-quadruplex DNA and its binding ligands has been discussed in more detail in **Chapter 5**.

## 4 Chapter 4: Conformations and Anion Binding Properties of Prodigiosenes

*Some sections of this chapter have been published in reference 131:*

- Marchal, E.; Rastogi, S.; Thompson, A.; Davis, J., “Influence of B-ring modifications on proton affinity, transmembrane anion transport and anti-cancer properties of synthetic prodigiosenes.” *Org. Biomol. Chem.* **2014**, *12*, 7515-7522.

*The computational modelling and calculations for ester analog 2e, described in this chapter were performed by Ms. Maria Garcia Valverde and Dr. Roberto Quesada, collaborators from the University of Burgos, Spain.*

### **Background**

#### **4.1 Introduction**

The goal of this chapter is to explore conformational aspects of prodigiosin **1** and its synthetic derivatives. A study of the conformations of prodigiosin and its analogs is important to gather in-depth knowledge about how the ligands orient themselves in different solvents. This information could provide an essential bridge between the observed biological activities of prodigiosenes and their preferred conformational states. Based on the research described in this chapter, I found that 1) both  $\alpha$  and  $\beta$  isomers of prodigiosenes bind anions with distinct binding patterns 2) the  $\alpha$  isomer uses a CH hydrogen to bind bidentate anions such as  $\text{MeSO}_3^-$  3) anions can influence the  $\alpha/\beta$  conformational ratio for prodigiosin, but not for the ester analog **2e**, and 4) presence of water affects the population of  $\alpha$  isomer of prodigiosin **1** in solution.

Before describing my research, a brief background has been provided for the previous conformational analysis on prodigiosenes done by other groups.

#### 4.2 Previous Work on Conformations of Prodigiosenes

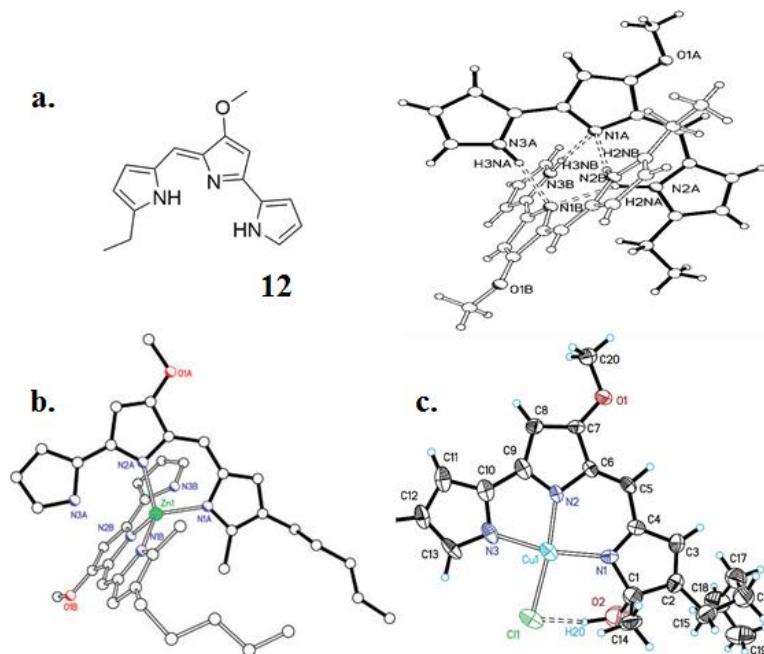


**Figure 4.1.** a) Structure of prodigiosene **12**. Two molecules of **12** bind non-covalently to form a dimer. Reprinted with permission from *Chem. Res. Toxicol.* **2002**, *15* (5), 734-741. Copyright (2002) American Chemical Society.<sup>33</sup> b) Perspective drawing of solid state structure of Zn•(**1**)<sub>2</sub>. Zinc atom is represented by the green sphere. c) Proposed ORTEP plot of solid state structure from reaction of **1** with CuCl<sub>2</sub>. Cu(II) is represented by the blue sphere. Reprinted with permission from *Org. Lett.* **2002**, *5* (2), 113-116. Copyright (2002) American Chemical Society.<sup>34</sup>

Structurally, prodigiosin **1** appears to be a simple compound at first glance. It has a 4-methoxy bipyrrole moiety linked to another functionalized pyrrole ring. Yet,

the compound can exist in multiple conformations as tautomers and rotamers. Owing to the versatility of possible structures and conformations, prodigiosin **1** can behave differently depending on solvent and other surrounding factors. Prodigiosenes can exist in either protonated or non-protonated states. When in its free-base form, prodigiosene **12** can form non-covalent dimers (**Figure 4.1a**).<sup>33</sup> Two molecules of prodigiosin **1**, in its deprotonated form, can form a dimer with Zn(II) in the center (**Figure 4.1b**).<sup>34</sup> Prodigiosin **1** can also bind with Cu(II) (**Figure 4.1c**).<sup>34</sup>

In both its protonated and deprotonated form, prodigiosin **1** can bind and transport anions (such as  $\text{Cl}^-$ ,  $\text{NO}_3^-$  and  $\text{HCO}_3^-$ ) across liposomal and cell organelle membranes.<sup>10,25,27</sup> Protonation also affects the preferable conformation adopted by prodigiosenes. Despite the versatility of conformations and its possible impact on the biological properties of prodigiosenes, few in-depth studies have been done on prodigiosene conformations. The work done by Quesada and group in 2012 is an extensive NMR and computational study undertaken to learn more about the different conformations, their relative energies and anion binding strengths.<sup>36</sup> Before this, Rizzo *et. al.* briefly described their work on the  $\alpha$  and  $\beta$  forms of another prodigiosene analog.<sup>37</sup> McNab was the first one to identify the structure of the  $\alpha$  conformation of prodigiosenes.<sup>134</sup>

#### 4.2.1 Work with $\alpha$ -Conformation by McNab

In 1990, McNab described a convenient synthetic route to synthesize three-ring systems related to prodigiosin.<sup>134</sup> He synthesized compound **32** with rings B and C similar to prodigiosin **1**. Ring A was a thiophene, while ring C contained an extra

methyl group at the 4-position. In the process, he obtained the crystal structure of **32** in a conformation that was later assigned as the  $\alpha$ -conformation (**Figure 4.2**). He reported that the three rings in the  $\alpha$  conformer were almost coplanar. The methoxy group was oriented such that it formed an intramolecular H-bond with the NH proton of ring C (**Figure 4.2a**). The  $\alpha$  conformation owes its existence to the methoxy group on ring B. It has been proposed that this resulting configuration of rings could be instrumental for the biological activities observed for prodigiosin.<sup>134</sup>

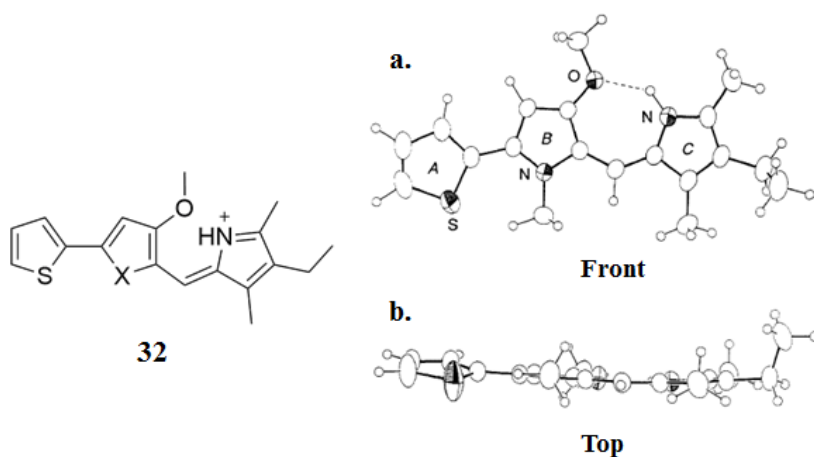


**Figure 4.2.** Structure of compound **32**. Crystal structure of compound **32** from **a**) front and **b**) top. Reprinted with permission from *J. Chem. Soc., Chem. Commun.* **1990**, (10), 734-736. Copyright (1990) Royal Society of Chemistry.<sup>134</sup>

#### 4.2.2 Kinetics of $\alpha,\beta$ -Rotamer Interconversion by Rizzo

Almost a decade later, Rizzo and his group published their work on kinetics of  $\alpha/\beta$  interconversion of a prodigiosin derivative PNU-156804 **8**.<sup>37</sup> Using HPLC, they showed a pH-dependent separation of  $\alpha$  and  $\beta$  isomers. At pH 9, the neutral form of compound **8** dominated, while at pH 5, the protonated form of the analog dominated.

At pH 2.2, two separate peaks were observed, with the minor peak assigned to the  $\beta$  conformation (**Figure 4.3**).

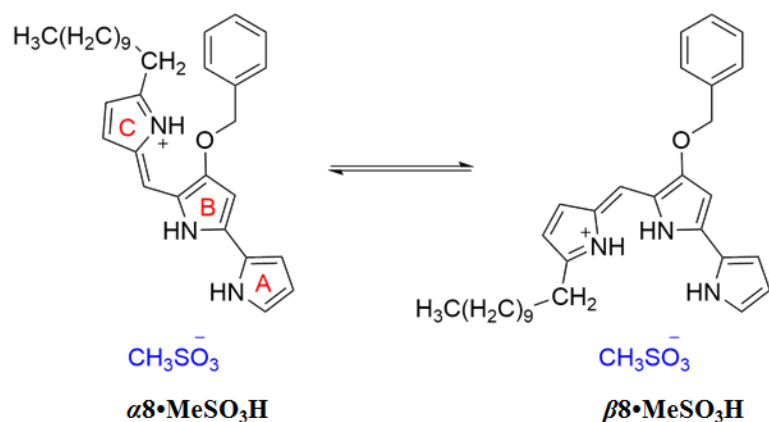


**Figure 4.3.** The  $\alpha$  and  $\beta$  conformations of (**8**•MeSO<sub>3</sub>H).

The rate of interconversion between the two isomers was slow enough to allow calculation of  $\text{p}K_a$  for the  $\alpha$  ( $8.23 \pm 0.03$ ) and  $\beta$  ( $5.4 \pm 0.2$ ) forms. The protonated compound formed a seven-member ring stabilized by intramolecular H-bonding in the  $\alpha$  conformation. The HPLC data was corroborated by UV-visible spectrophotometric data. In a spectrophotometric study, Rizzo and group used the absorption bands of free-base ( $\lambda_{\text{max}} = 460 \text{ nm}$ ) and protonated ( $\lambda_{\text{max}} = 525 \text{ nm}$ ) forms to plot a titration curve that gave an apparent  $\text{p}K_a$  value of 7.20 for an equilibrium mixture of the two isomers.<sup>37</sup>

In order to get more structural information about  $\alpha$  and  $\beta$  isomers of compound **8**, the authors performed NMR experiments using different counter-anions. The <sup>1</sup>H NMR spectra of **8**•HCl in CDCl<sub>3</sub> gave a single set of resonances, consistent with the  $\beta$ -isomer, demonstrating that the Cl<sup>-</sup> anion could influence ligand conformation in a non-polar solvent. The Cl<sup>-</sup> anion can H-bond with the NH protons on the three pyrrole rings arranged in  $\beta$  conformation. However, it was reported that in a solvent mixture

containing CD<sub>3</sub>CN/D<sub>2</sub>O (1/1, pH 1.1), NMR signals of the two conformers ( $\alpha/\beta$ ) were observed at about 2/1 ratio. The conformer ratio obtained from NMR was slightly different from the HPLC data where a 3/1 ratio was reported for  $\alpha/\beta$  conformers.

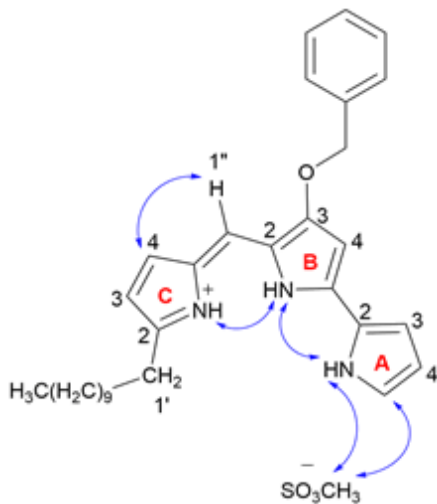


**Figure 4.4.** Structure of the methanesulfonate salt of PNU-156804 (**8•MeSO<sub>3</sub>H**) in its  $\beta$  conformation. Selective NOESY cross-peaks are indicated with blue colored double-headed arrows. Adapted with permission from *J. Pharm. Sci.* **1999**, 88 (1), 73-78. Copyright (1999) Wiley-Liss, Inc. and the American Pharmaceutical Association.<sup>37</sup>

On the other hand, the MeSO<sub>3</sub><sup>-</sup> salt of PNU-156804 gave a different conformational ratio for the mixture of conformers ( $\alpha/\beta= 1/2$ ) in CDCl<sub>3</sub>. According to NOESY data, the two geometrical isomers of **8** have different torsion angles about the C<sub>B2</sub>-C<sub>1''</sub> bonds. In a Newman projection for 4 atoms in a chain, A-B-C-D, torsion angle is defined at the angle between A-B-C plane and the B-C-D plane.<sup>115</sup> The torsion angle was close to 0° for  $\beta$  while the  $\alpha$  conformer has an angle of 180°. An angle of 180° is stabilized by hydrogen bonding between the NH proton on ring C and the exocyclic oxygen on ring B. The observations made from the <sup>1</sup>H NMR spectrum were further



supported by NOE experiments. NOE interactions between the three NH-exchangeable protons ( $\text{NH}_A$  to  $\text{NH}_B$  and  $\text{NH}_B$  to  $\text{NH}_C$ ) and the  $\text{H}_{C4}$  to  $\text{H}_1$  confirmed the arrangement for  $\beta$ -isomer in  $\text{CDCl}_3$  (**Figure 4.4**). Further, an NOE cross-peak between the methyl group on  $\text{MeSO}_3^-$  anion and NH and CH hydrogens on  $\mathbf{8}\cdot\text{H}^+$  scaffold indicated ion-pair formation and hydrogen bonding between the receptor and  $\text{MeSO}_3^-$  ion. Thus, Rizzo and group were able to show specific evidence for the existence of  $\alpha$  and  $\beta$  isomers in solution.

#### 4.2.3 Conformational Analysis of Prodigiosene-Anion Complexes by Quesada

Quesada and colleagues published their study of the conformational analysis of a synthetic prodigiosene **33**.<sup>36</sup> Their work was important as it explored the conformations of analog **33**, and its associated anion binding affinities, in detail using NMR, X-ray diffraction and computational modelling along with DFT calculations.

Compound **33** in its neutral form, depending on the location of the unprotonated azafulvene nitrogen atom, can exist in three tautomeric forms: **I** (ring B), **II** (ring C) and **III** (ring A). Further, each tautomer can exist in four conformations –  $\alpha$ ,  $\beta$ ,  $\gamma$  and  $\delta$ . Three pyrrole rings are oriented cis to each other, with the nitrogen atoms forming a cleft at the center in the  $\beta$  isomer. A *cis-trans* isomerization around the double bond between rings B and C gives rise to the  $\alpha$  isomer. The  $\alpha$  conformation is stabilized by intramolecular hydrogen bonding between the NH proton on ring C and the exocyclic oxygen on ring B. The  $\gamma$  and  $\delta$  isomers arise due to rotation around the single bond between rings A and B in the  $\alpha$  and  $\beta$  isomers, respectively. Therefore, the neutral form

of compound **33** can exist in any of the twelve structures. The four isomers ( $\alpha$ ,  $\beta$ ,  $\gamma$  and  $\delta$ ) of tautomer **I** are depicted in **Figure 4.5**.

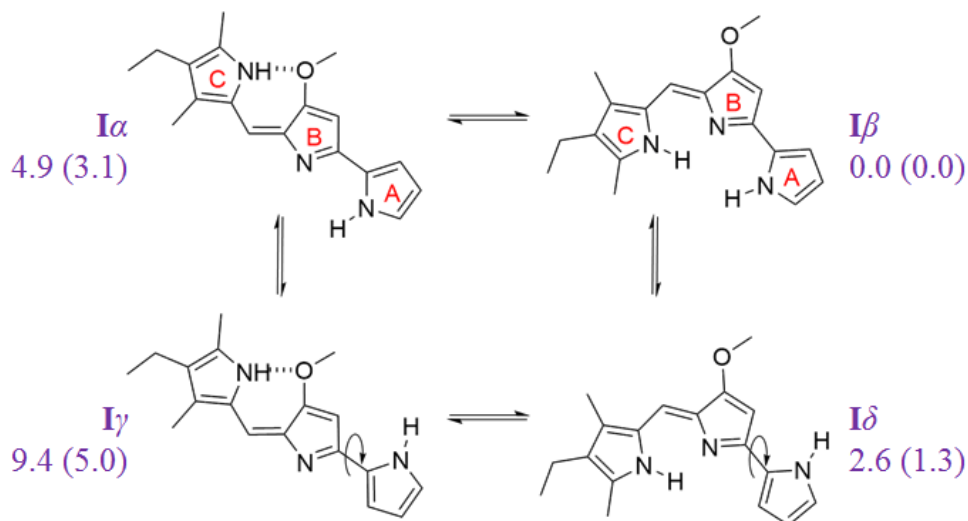


**Figure 4.5.** Structure of prodigiosene derivative **33**. Tautomer **I** is shown as  $\alpha$ ,  $\beta$ ,  $\gamma$  and  $\delta$  isomers for the computational study of a neutral prodigiosene **33**. Relative energies are in kcal/mol for both the gas phase and in solution (in parentheses).<sup>36</sup>

Quesada and colleagues performed a detailed computational study of the equilibria in both the gas phase and in solution for the neutral form of compound **33** (**Figure 4.5**). Based on DFT calculations, they found that the lowest energy isomer in both phases was **I $\beta$** , which was taken as an energetic reference. In general, tautomer **I** was found to have relatively low energies in comparison to the other two tautomers (**II** and **III**), which means that deprotonation is most preferred on ring B. As a result, tautomer **I** was chosen for further conformational analysis of a protonated prodigiosene. When different isomers ( $\alpha$ ,  $\beta$ ,  $\gamma$  and  $\delta$ ) of protonated form of tautomer **I** were analyzed, the  $\gamma$  isomer was found to be energetically most stable (shown as **IV $\gamma$**

in **Figure 4.5**). In order to study the anion binding affinity for different isomers, chloride ( $\text{Cl}^-$ ) and mesylate ( $\text{MeSO}_3^-$ ) complexes of **IV $\gamma$**  were studied in more detail. Four structures were proposed for each of the anion complexes as shown in **Figure 4.6**.

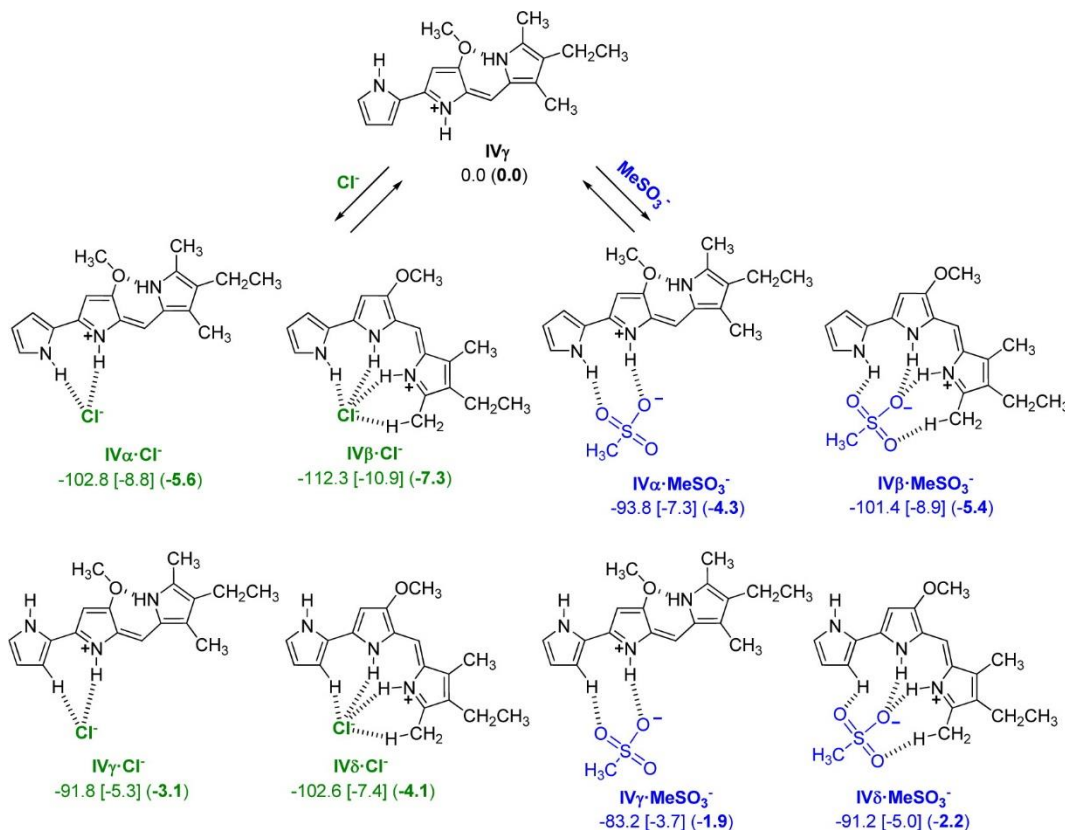


**Figure 4.6.** Isomer **IV $\gamma$**  can bind  $\text{Cl}^-$  and  $\text{MeSO}_3^-$  anions to give four possible complexes each. Binding energies were calculated in kcal/mol for each mesylate ( $\text{MeSO}_3^-$ ) and chloride ( $\text{Cl}^-$ ) complex in gas phase, DMSO (in brackets), and water (in parentheses). Reprinted with permission from *J. Org. Chem.* **2012**, *77*, 6538-6544. Copyright (2012) American Chemical Society.<sup>36</sup>

DFT calculations indicated that for all the isomers in all three phases, interaction energy for the **33·HCl** complexes was larger than that of **33·MeSO $_3$ H**

complexes. This data was in agreement with a  $^1\text{H}$  NMR titration study, where  $\text{Cl}^-$  displaced  $\text{MeSO}_3^-$  anion in a solution containing **33•MeSO<sub>3</sub>H**. Moreover, in both gas and solution phase, the  $\beta$  isomer of **IV** was found to be the most favored for binding anions, with lowest energies for either ions –  $\text{Cl}^-$  (-7.3 kcal/mol) and  $\text{MeSO}_3^-$  (-5.4 kcal/mol). This theoretical calculation agreed with NOESY experimental data. NOESY spectra of both the **33•HCl** and **33•MeSO<sub>3</sub>H** complexes in  $\text{CDCl}_3$  gave the  $\beta$  form as the predominant isomer. These NMR results and DFT calculations were supported by solid state structures, obtained from X-ray diffraction studies. For both anion complexes, receptor **33•H<sup>+</sup>** was found to be in  $\beta$  conformation. The tripyrrolic structure was planar, showing high conjugation within the molecule.

The results were even more interesting for a polar solvent like DMSO. The anion binding energy for the  $\beta$  form of **33•HCl** complex in DMSO was -10.9 kcal/mol. The binding energy for the  $\alpha$  isomer of **33•HCl** complex was 2.1 kcal/mol. For the **33•MeSO<sub>3</sub>H** complex, the  $\beta$  isomer was calculated to have anion binding energy of -8.9 kcal/mol, whereas the  $\alpha$  isomer had a binding energy of -7.3 kcal/mol. Consistent with small energy difference between  $\alpha$  and  $\beta$  isomers for the **33•MeSO<sub>3</sub>H** complex (1.6 kcal/mol), both species were observed in the  $^1\text{H}$  NMR spectrum. In the NMR spectrum, the  $\beta$  conformer was identified as the major isomer while  $\alpha$  was the minor isomer. Conversely, the energy difference was quite large for the  $\alpha$  and  $\beta$  isomers of **33•HCl**, which was consistent with the appearance of only  $\beta$  form in the  $^1\text{H}$  NMR spectrum.

Thus, the protonation of the prodigiosene **33** greatly affected its conformational equilibrium and its rate of interconversion between the  $\alpha$  and  $\beta$  conformations. DFT calculations supported the results observed in solution and solid state. The results from different techniques such as NMR, X-ray crystallography and molecular modeling showed that prodigiosene conformation in solution is influenced by the nature of the solvent, the counterion as well as the compound's protonation state.

## Results

### **4.3 Using NH Protons to Analyze Anion Binding Patterns in $\alpha$ and $\beta$ Isomers**

Transmembrane exchange of  $\text{Cl}^-$  and  $\text{NO}_3^-$  anions by prodigiosin (**1**) involves anion binding by the protonated transporter (**1**• $\text{H}^+$ ). This is followed by diffusion of the neutral complex **1**• $\text{HCl}$  across the lipid membrane, and  $\text{Cl}^-/\text{NO}_3^-$  anion exchange at the lipid–water interface.<sup>31</sup> The anion binding and transport processes are potentially complicated by the fact that protonated prodigiosenes often exist as two isomers in solution – the  $\alpha$  and  $\beta$  conformations. This  $\alpha/\beta$  conformational equilibrium can vary as a function of ligand structure and environmental conditions.<sup>36,37</sup> Both  $\alpha$  and  $\beta$  prodigiosene conformations should be able to bind anions.

Despite the importance of prodigiosin and its biological properties, little conformational work has been done on this compound and its analogs. In this chapter, I have worked with prodigiosin (**1**) and its synthetic analogs (**2** and **3**), to investigate some qualitative aspects of the solution-state conformation of these tripyrrole derivatives.

### 4.3.1 NMR Titrations Reveal $\alpha,\beta$ Conformations of Phenyl Analog **3b**

Anion exchange by prodigiosin (**1**), ester (**2e**) and phenyl (**3b**) analogs was studied in detail by using NMR. These experiments also allowed us to analyze the anion binding pattern for the two isomers –  $\alpha$  and  $\beta$ . In particular, the phenyl analog helped us in confirming  $\alpha$  and  $\beta$  conformations in solution. The complex **3b**•HCl (1 mM) showed one set of signals, consistent with the  $\beta$  conformation, when initially dissolved in CDCl<sub>3</sub> (**Figure 4.7**).

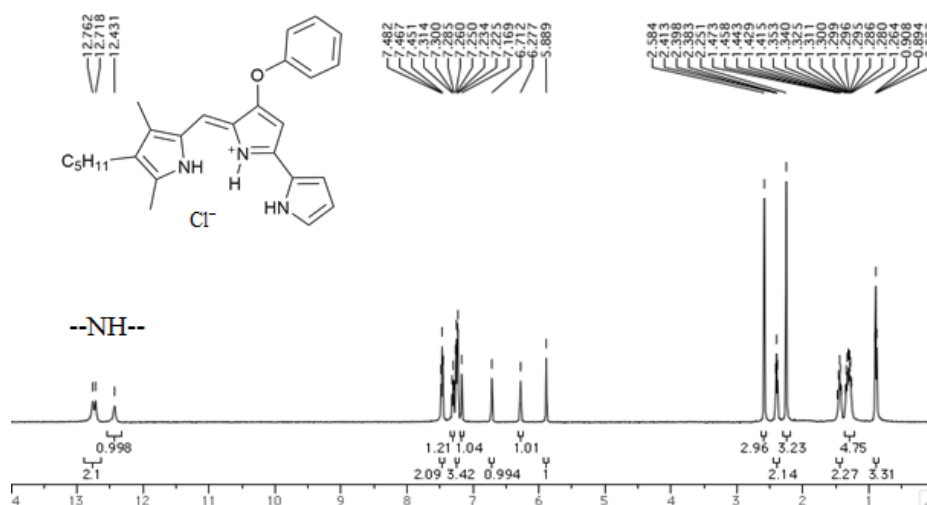


**Figure 4.7.** <sup>1</sup>H NMR for the phenyl analog **3b**•HCl in CDCl<sub>3</sub> shows a single set of peaks belonging to the  $\beta$  isomer.

However, over time, the sample in CDCl<sub>3</sub> showed two sets of <sup>1</sup>H NMR signals in an approximate 3:1 ratio. Based on analogy with previous NMR studies of other prodigiosenes in CDCl<sub>3</sub>,<sup>36,37</sup> the major set of NMR signals was assigned to the  $\beta$  isomer of **3b**•HCl and the minor set of signals to the  $\alpha$  isomer.

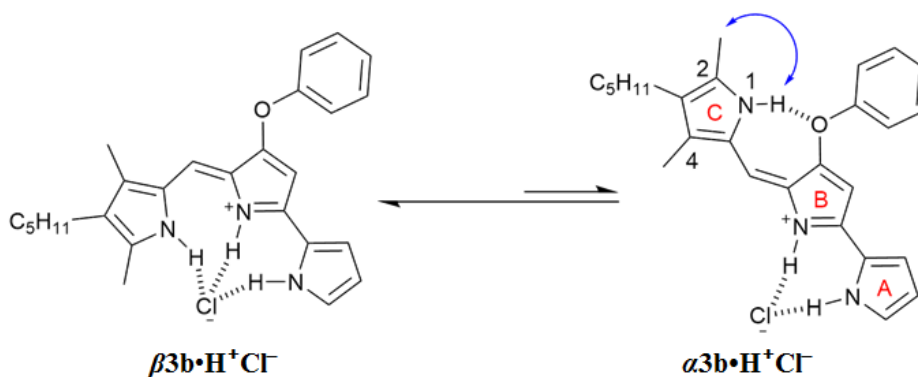


**Figure 4.8.**  $\beta$  and  $\alpha$  conformational isomers of prodigiosene  $3b \cdot H^+$ . Both the major  $\beta$  and minor  $\alpha$  isomers should be able to bind anions as indicated by H-bonds.

Next, both conformers of  $3b \cdot H^+$  were investigated for anion binding and exchange in the  $CDCl_3$  solution. Thus, methanesulfonic acid ( $MeSO_3H$ ) was titrated into a solution of  $3b \cdot HCl$  in  $CDCl_3$  and changes in  $^1H$  NMR signals for the pyrrolic NH protons ( $\delta$  12–13 ppm) were followed. The changes in this region of the spectrum would reflect anion binding and exchange between  $Cl^-$  and  $MeSO_3^-$  anions, since it is the pyrrole NH atoms that should hydrogen bond with the anions. **Figure 4.9** shows representative spectra from the titration.

The NH region of the  $^1H$  NMR spectrum for the  $3b \cdot HCl$  complex (**Figure 4.9a**) indicates a mixture of isomers, but the NMR signals were poorly resolved. However, this overlap for the pyrrolic NH protons was removed upon the addition of  $MeSO_3H$  to a solution of  $3b \cdot H^+ Cl^-$  (**Figure 4.9b**). As shown in **Figure 4.9b**, I observed two resolved sets of three pyrrolic NH signals for the  $3b \cdot H^+ MeSO_3^-$  complex. There were two important findings here. First, the NH chemical shifts change upon addition of the  $MeSO_3H$ , suggesting that both the  $\alpha$  and  $\beta$  isomers bind this anion. Thus, chemical

shifts for the six NH protons moved upfield when MeSO<sub>3</sub>H was added to a solution of **3b•HCl** (Figure 4.9b). The NH chemical shifts moved upfield as Cl<sup>-</sup> is replaced by the softer MeSO<sub>3</sub><sup>-</sup> anion in the binding site of the prodigiosene. Second, the  $\alpha/\beta$  isomer ratio for **3b•HCl** and **3b•MeSO<sub>3</sub>H** did not change significantly with the change in bound anion (Figure 4.9c).

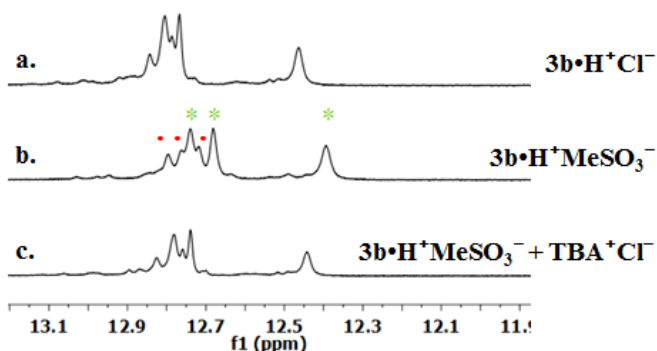


**Figure 4.9.** <sup>1</sup>H NMR spectra in CDCl<sub>3</sub> for the pyrrolic NH region of: (a) **3b•HCl**; (b) after addition of 6 eq of MeSO<sub>3</sub>H to sample **a**; two sets of NH signals were resolved for each  $\alpha$  (●) and  $\beta$  (\*) conformer; (c) after addition of 1 eq of tetrabutylammonium chloride (TBACl) to sample **b**.

#### 4.3.2 NOESY Data Shows Presence of $\alpha$ Conformation in CDCl<sub>3</sub> Solution

Before proceeding to study anion binding patterns of different conformations, it was essential to establish the existence of  $\alpha$  and  $\beta$  conformations in solution. Figure 4.8 illustrates the two main conformations of the phenyl analog **3b•H<sup>+</sup>**. Generally, the  $\beta$  isomer can be easily observed in solution. It is often difficult, however, to identify and confirm the presence of the minor  $\alpha$  isomer.



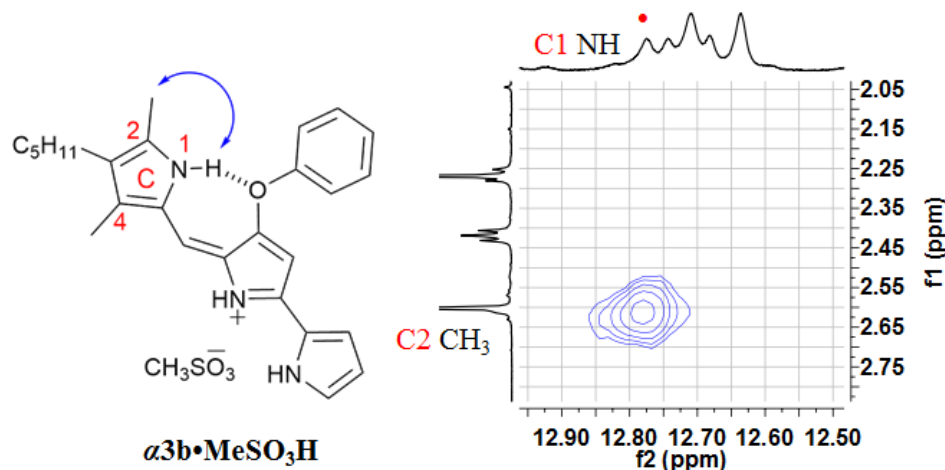


**Figure 4.10.** A region of the NOESY spectrum of **3b•MeSO<sub>3</sub>H** in CDCl<sub>3</sub> shows a NOE between one of the “minor” pyrrole NH protons and C2 methyl hydrogens. This correlation is consistent with the pyrrolic NH of the C-ring being involved in a solvent-shielded intramolecular H-bond with the –OPh group of the B-ring.

A 2D NOESY NMR experiment of the **3b•MeSO<sub>3</sub>H** complex in CDCl<sub>3</sub> allowed us to assign signals for the three NH protons in the major  $\beta$  isomer, and for the three NH protons in the  $\alpha$  isomer. The NOE correlation that best supports my assignments can be observed between one of the minor pyrrole NH signals and the signal corresponding to the C2 methyl group. For the  $\alpha$  isomer, the C-ring NH proton forms an intramolecular hydrogen bond with the –OPh group on the B-ring ( $\alpha$  isomer in **Figure 4.10**). Presumably, this hydrogen-bonded NH proton exchanges much more slowly with residual water in the CDCl<sub>3</sub> and, therefore, shows a NOE correlation with its neighboring C2-methyl group. Diagnostic NOE interactions were also observed for the  $\beta$  isomer. These NOEs have been previously reported by Quesada and Rizzo in their publications.<sup>36,37</sup>

After some success in examining anion exchange with phenyl analog, my focus shifted to the study of anion binding patterns for  $\alpha$  and  $\beta$  conformations of prodigiosenes. However, the NMR signals for anion binding NH protons of **3b•HCl** were not resolved enough to provide us with information about the anion binding patterns (**Figure 4.9b-c**). Upon carrying out similar experiments, both prodigiosin **1•H<sup>+</sup>** (**Figure 4.11a**) and ester **2e•H<sup>+</sup>** (**Figure 4.11b**) showed presence of  $\alpha$  and  $\beta$  conformations in CD<sub>3</sub>CN, which were consistent with the NMR signals observed for **3b•H<sup>+</sup>A<sup>-</sup>**. The well-resolved signals for NH pyrrole protons of  $\alpha$  and  $\beta$  isomers in compounds **1•H<sup>+</sup>** and **2e•H<sup>+</sup>** allowed us to clearly follow the anion binding patterns for the two isomers.

### 4.3.3 NH Protons of Prodigiosin 1 and Ester 2e Reveal Anion Binding Patterns

Although other groups have proposed the anion binding patterns for prodigiosenes, no direct supporting proof has been published that both  $\alpha$  and  $\beta$  conformers bind anions. As described below, I found that the two conformers -  $\alpha$  and  $\beta$ , do exhibit distinct binding patterns with Cl<sup>-</sup> and MeSO<sub>3</sub><sup>-</sup> anions. In the  $\beta$  conformation, all 3 NH protons bind with the anion, whereas in  $\alpha$  conformation, only two NH's are available for binding. The third NH proton in the  $\alpha$  conformer is involved in intramolecular hydrogen bond with the OMe group on ring B (**Figure 4.11**), and thus is not involved in anion binding.

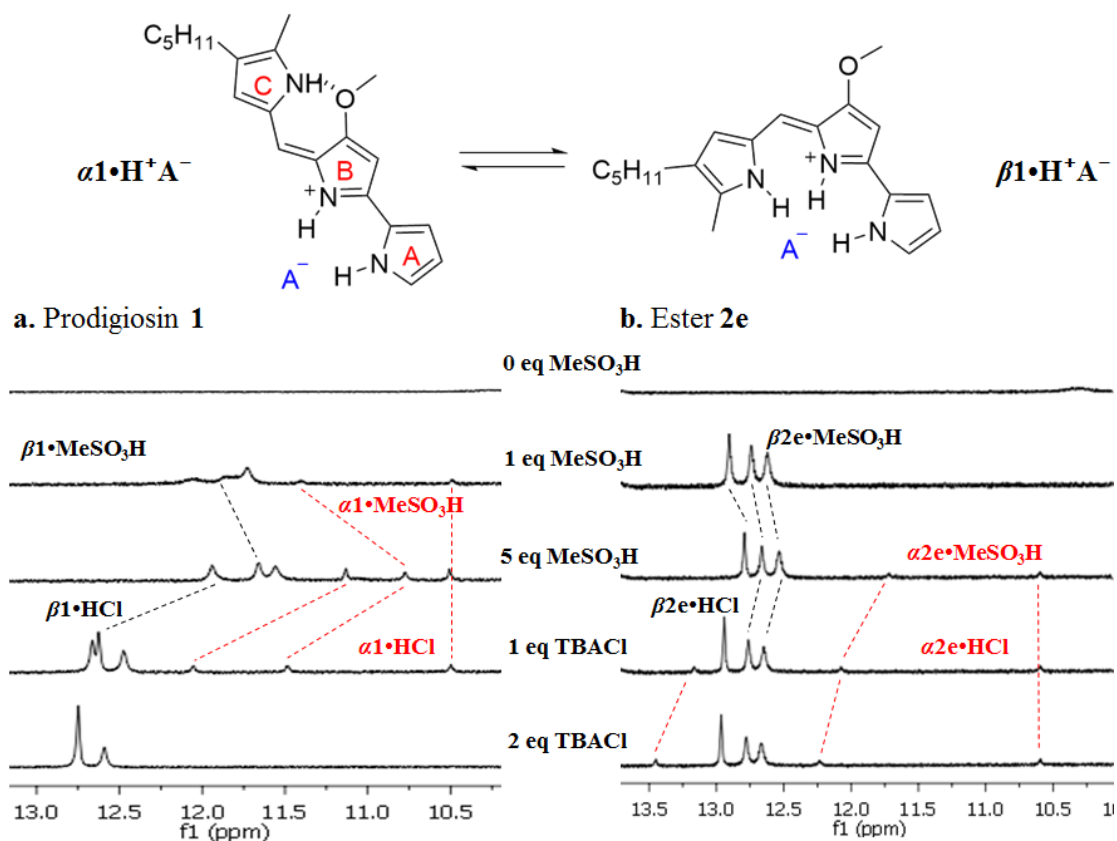


**Figure 4.11.** Structures of  $\alpha$  and  $\beta$  isomers of  $\mathbf{1}\cdot\text{H}^+\text{A}^-$  are illustrated at the top to show the interaction between NH protons and anion  $\text{A}^-$ .  $^1\text{H}$  NMR spectra shows the changes in conformations for (a) prodigiosin  $\mathbf{1}\cdot\text{H}^+$  and (b) ester  $\mathbf{2e}\cdot\text{H}^+$  based on the chemical shifts of the NH protons as MeSO<sub>3</sub>H and TBACl are added to the sample in CD<sub>3</sub>CN at  $-10^\circ\text{C}$ . Shifting of signals has been highlighted by red dashed lines for  $\alpha$  isomer and black dashed lines for  $\beta$  isomer.

Each sample containing prodigiosin **1** or ester **2e** was titrated with MeSO<sub>3</sub>H. In both cases, the compounds underwent binding with the MeSO<sub>3</sub><sup>-</sup> anion (spectrum labeled **1 eq MeSO<sub>3</sub>H** in **Figure 4.11**). Movement of signals has been highlighted by red and black dashed lines for  $\alpha$  and  $\beta$  isomer, respectively in **Figure 4.11**. Resonances

for  $\alpha$  and  $\beta$  conformations are visible for **1•MeSO<sub>3</sub>H** complex whereas only signals for the  $\beta$  isomer were observed for ester **2e•MeSO<sub>3</sub>H**. Addition of increasing equivalents of MeSO<sub>3</sub>H led to an upfield movement in chemical shifts (**5 eq MeSO<sub>3</sub>H** in **Figure 4.11**), due to weak binding interactions between MeSO<sub>3</sub><sup>-</sup> anion and **1•H<sup>+</sup>** and **2e•H<sup>+</sup>** cations. Moreover at **5 eq MeSO<sub>3</sub>H**, both compounds clearly show distinguishable  $\alpha$  and  $\beta$  conformations in solution. When TBACl was added to the samples, any protons involved in anion binding underwent changes in chemical shifts, due to displacement of bound MeSO<sub>3</sub><sup>-</sup> by Cl<sup>-</sup> anion. For **1•HCl** and **2e•HCl**, all three NH protons belonging to the  $\beta$  isomer underwent a downfield shift upon addition of **1 eq** of **TBACl**. This result follows the hypothesis that  **$\beta$ 1•H<sup>+</sup>** and  **$\beta$ 2e•H<sup>+</sup>** bind chloride anion using all three of their pyrrole NH protons. For the minor set of peaks belonging to  **$\alpha$ 1•H<sup>+</sup>** and  **$\alpha$ 2e•H<sup>+</sup>**, only 2 NH signals experienced downfield shift upon addition of Cl<sup>-</sup>. The third NH signal (at approx.  $\delta$  10.5 ppm in **1 eq TBACl** in **Figure 4.11**) remained stationary after addition of Cl<sup>-</sup>. The NH proton at  $\sim\delta$  10.5 ppm was identified as the NH proton on ring C, which is involved in hydrogen bonding with the OMe group on ring B. Thus, because this NH proton is involved in an intramolecular hydrogen bond, it does not experience any change in chemical shift as a function of Cl<sup>-</sup> addition. Upon addition of **2 eq TBACl**, the  $\alpha$  isomer of prodigiosin **1•HCl** was completely converted to its  $\beta$  form (spectrum labeled **2 eq TBACl** in **Figure 4.11a**). In the case of the ester **2e•H<sup>+</sup>**, addition of 2 eq of TBACl did not lead to the complete conversion of  $\alpha$  to  $\beta$  isomer (spectrum labeled **2 eq TBACl** in **Figure 4.11b**). Because of weak binding between  $\alpha$  isomer and

$\text{Cl}^-$ , these 2 NH protons keep moving downfield as more equivalents of  $\text{Cl}^-$  are added to the solution (10 eq TBACl in Figure 4.12).

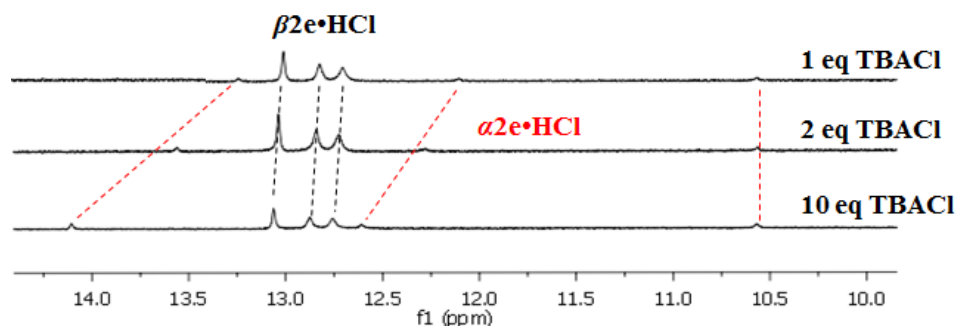


**Figure 4.12.**  $^1\text{H}$  NMR spectra of  $\alpha$  and  $\beta$  conformations of  $2\mathbf{e}\cdot\text{HCl}$  shows the changes in chemical shifts of NH protons as TBACl is added to the sample in  $\text{CD}_3\text{CN}$  at  $-10^\circ\text{C}$ . Shifting of signals has been highlighted by red dashed lines for  $\alpha$  isomer and black dashed lines for  $\beta$  isomer. Note that the NH proton at 10.5 ppm does not move with addition of TBACl.

The study of the chemical shifts of NH protons of the  $\alpha$  and  $\beta$  isomers of ester analog  $2\mathbf{e}\cdot\text{H}^+$  enabled us to assemble an equilibrium diagram for the different processes taking place in solution for compound  $2\mathbf{e}$  (Figure 4.13). The equilibrium diagram depicts the slow rate of interconversion between the  $\alpha$  and  $\beta$  isomers of  $2\mathbf{e}\cdot\text{MeSO}_3\text{H}$  and  $2\mathbf{e}\cdot\text{HCl}$  complexes. Conversely, the NMR results for prodigiosin  $1$  in Figure 4.11 are indicative of a faster rate of interconversion between the  $\alpha$  and  $\beta$  conformers of  $1\cdot\text{HCl}$  complex.

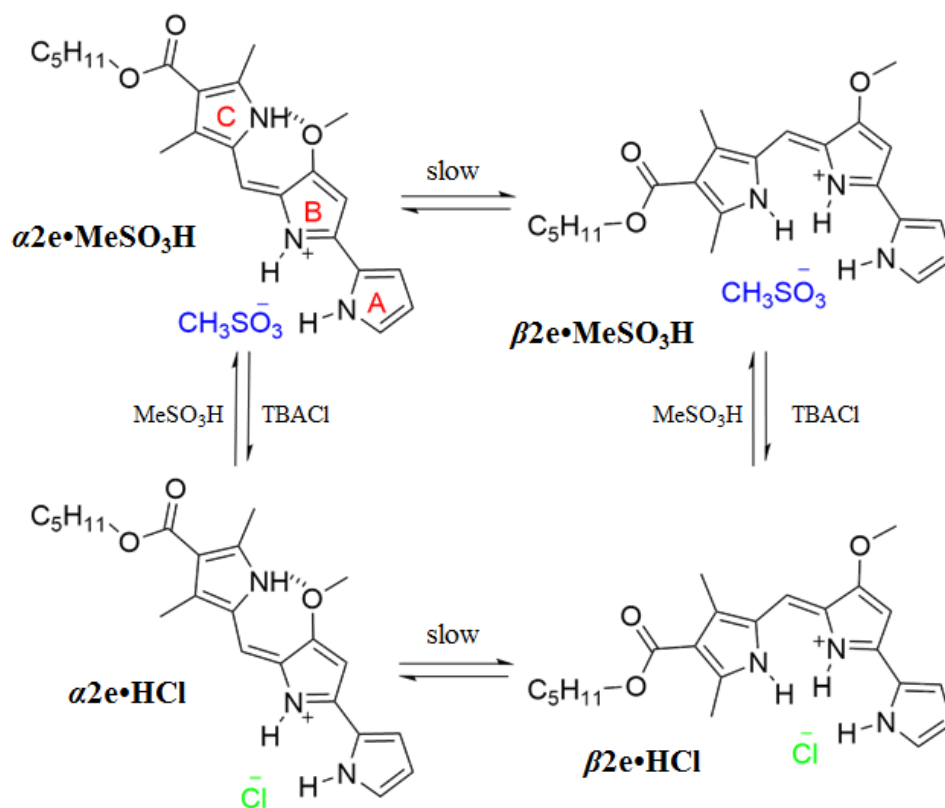


**Figure 4.13.** Structures of  $\alpha$  and  $\beta$  conformations of  $2e \cdot \text{MeSO}_3\text{H}$  and  $2e \cdot \text{HCl}$  complexes. The  $\alpha$  and  $\beta$  isomers are in slow equilibrium with each other for both anion complexes of the ester compound ( $2e \cdot \text{MeSO}_3\text{H}$  and  $2e \cdot \text{HCl}$ ).

In conclusion, the assumption of assigning  $\alpha$  and  $\beta$  conformations for prodigiosin  $1 \cdot \text{H}^+$  and ester  $2e \cdot \text{H}^+$  in **Figure 4.11** was confirmed by the observed changes in NMR chemical shifts for the pyrrole NH protons. Chemical shift patterns for the pyrrole NH's of  $\alpha$  and  $\beta$  conformations of prodigiosin  $1 \cdot \text{H}^+$  and ester  $2e \cdot \text{H}^+$  were clear and distinct based on their binding with anion. These NMR titrations allowed us to conclude that (1) both the major  $\beta$  and minor  $\alpha$  isomers bind and exchange anions; (2) the  $\alpha$  conformer

uses only two NH protons to bind anions and (3)  $\text{Cl}^-$  interacts more strongly than  $\text{MeSO}_3^-$  with the receptor cations ( $\mathbf{1}\cdot\text{H}^+$ ,  $\mathbf{2e}\cdot\text{H}^+$  and  $\mathbf{3b}\cdot\text{H}^+$ ).

#### 4.4 Evidence for $\text{CH}\cdots\text{Anion}$ Hydrogen-Bonding by $\alpha$ -Isomer of Prodigiosenes

In the last decade, explorations into receptors that are capable of binding anions using CH hydrogens have been made. The unconventional  $\text{C-H}\cdots\text{A}^-$  interactions are a specific type of hydrogen-bond interactions and have found some significance in anion transport.<sup>135</sup> In 2005, Hay and colleagues showed by using theoretical calculations, examination of crystallographic data and experimental binding energies that even in the absence of electron-withdrawing substituents, simple arenes like benzene can form hydrogen bonds with anions (such as  $\text{Cl}^-$ ,  $\text{NO}_3^-$  and  $\text{ClO}_4^-$ ). Therefore, these moieties can be included in receptors to enhance their anion binding affinity and could provide additional binding sites within the host cavity.<sup>136</sup>

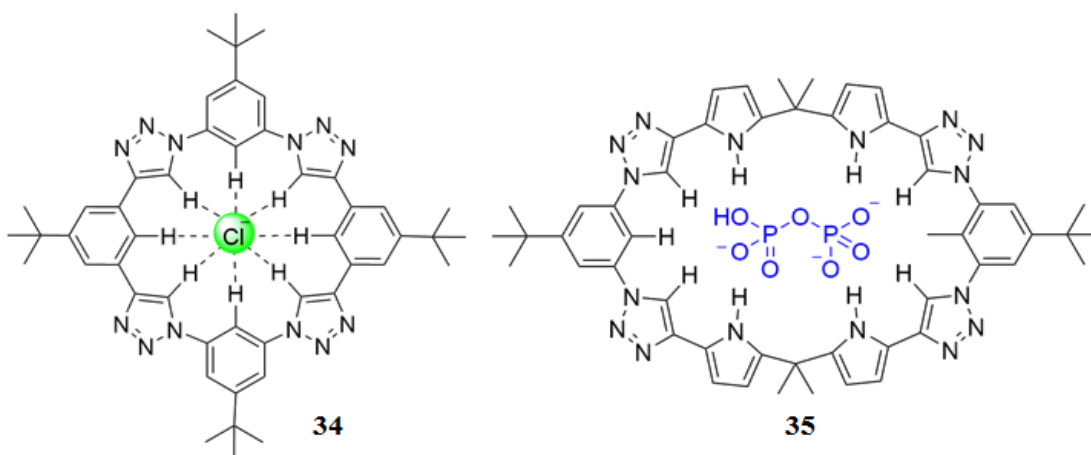


**Figure 4.14.** Examples of receptors that can bind anions using CH and NH hydrogens.

In 2008, Flood group introduced the macrocyclic receptor **34** (Figure 4.14).<sup>137</sup> The macrocycle **34** consisted of triazole rings substituted with phenyl groups at 1,4

positions and displayed a high affinity for anion binding using C-H...Cl<sup>-</sup> interactions. While macrocycle **34** based receptors were specific for binding Cl<sup>-</sup>, there have been other anionophores that have been investigated for binding different anions. For example, Sessler and group worked with a pyrrole based triazolophane **35** that selectively binds pyrophosphate anion using NH and CH hydrogens in organic solvents (**Figure 4.14**).<sup>138</sup>

#### 4.4.1 CH Hydrogen Assisted Anion Binding by Tambjamines

Although there are no known examples of prodigiosenes employing CH hydrogens to bind anions, the closest reference can be made to tambjamines. In 2014, Quesada and colleagues demonstrated tambjamine analog **36** utilizes CH hydrogens for binding anions.<sup>139</sup> Direct proof was obtained when analog **36** was titrated with increasing amounts of tetrabutylammonium chloride (TBACl). Binding between **36** and Cl<sup>-</sup> ions was followed by <sup>1</sup>H NMR spectroscopy. When TBACl was titrated into a solution of **36** in *d*<sub>6</sub>-DMSO-0.5H<sub>2</sub>O, one would expect the acidic NH pyrrole protons to undergo changes in chemical shifts due to binding with Cl<sup>-</sup>. Instead in this case, the chemical shift of one of the NH protons (NH<sub>1'</sub>) remained unaltered whereas that of a CH hydrogen (H<sub>3'</sub>) on the same ring shifted downfield as varying equivalents of chloride anion were added to the NMR sample (**Figure 4.15**). The downfield movement of H<sub>3'</sub> hydrogen on ring A is evidence of its involvement in chloride binding and complex formation.



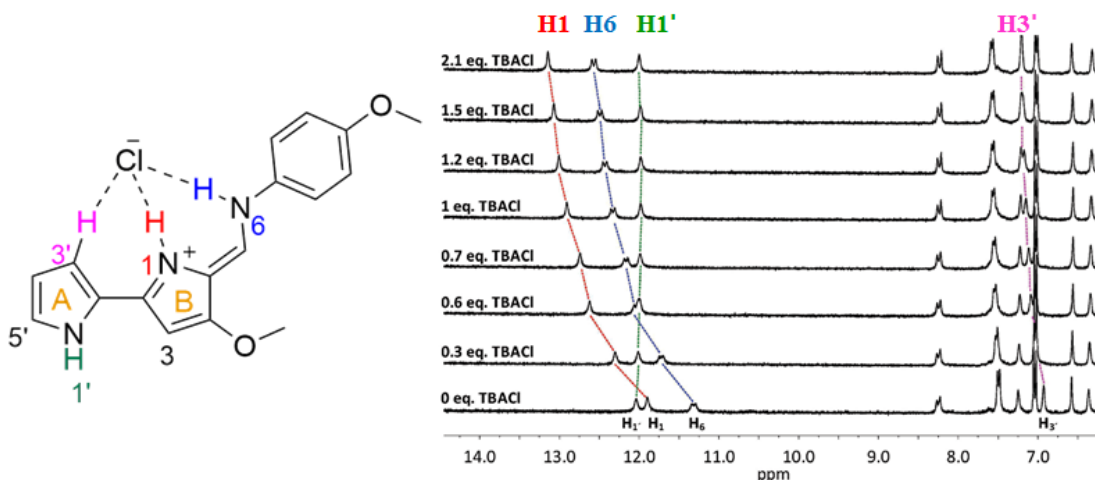


**Figure 4.15.** Stack plot of  $^1\text{H}$  NMR titration of **36** with TBACl in  $d_6$ -DMSO- $0.5\text{H}_2\text{O}$ .

#### 4.4.2 The $\alpha$ -H1'' Hydrogen on Prodigiosenes **1** and **2e** Binds Anions

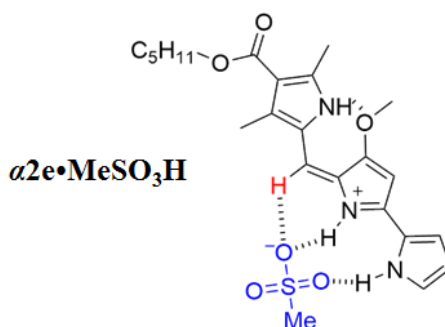


**Figure 4.16.** The H1'' (highlighted in red) in  $\alpha 2e \cdot \text{MeSO}_3\text{H}$  complex is involved in binding  $\text{MeSO}_3^-$  anion in addition to the two NH protons on rings A and B.

Until now, it has been widely accepted that the NH protons of prodigiosenes are involved in anion binding. However, for the first time, we have shown that a CH hydrogen belonging to the  $\alpha$  isomer is involved in binding anion. While studying the CH hydrogens on pyrrole rings, I noticed a significant change in chemical shift of the  $\alpha$ -H1'' hydrogen upon addition of anions. **Figure 4.16** illustrates the involvement of

H1" hydrogen of  $\alpha$  isomer of **2e**•MeSO<sub>3</sub>H complex in binding with the MeSO<sub>3</sub><sup>-</sup> anion along with the pyrrolic NH protons on rings A and B. Due to the bidentate nature of the MeSO<sub>3</sub><sup>-</sup> anion, the  $\alpha$ -H1" hydrogen of **2e**•H<sup>+</sup> is able to interact with the anion. A monodentate anion such as Cl<sup>-</sup> does not interact with the H1" hydrogen of  $\alpha$  isomer. In fact, Nager has reported that a polydentate anion such as the gluconate anion can help solubilize prodigiosin in aqueous solutions.<sup>140</sup> The structure in **Figure 4.16** is based on computational modelling and calculations performed by Ms. Maria Garcia Valverda and Dr. Roberto Quesada, collaborators from the University of Burgos, Spain.

As increasing equivalents of MeSO<sub>3</sub>H were added to a NMR sample of prodigiosin **1**, the chemical shift for the H1" hydrogen on the  $\alpha$  isomer shifted upfield indicating binding with the MeSO<sub>3</sub><sup>-</sup> anion (**Figure 4.17a-c**). Based on my NMR results with prodigiosin **1**•H<sup>+</sup> and the computational modeling done with ester analog **2e**, a structure has been proposed to depict the binding of MeSO<sub>3</sub><sup>-</sup> anion using the H1" and NH protons on rings A and B of  $\alpha$ **1**•MeSO<sub>3</sub>H (**Figure 4.17**). Addition of MeSO<sub>3</sub>H was followed by TBACl addition to displace MeSO<sub>3</sub><sup>-</sup> with Cl<sup>-</sup> anion in the binding pocket. Addition of Cl<sup>-</sup> anion caused complete conversion of  $\alpha$  to  $\beta$  isomer overtime. However, at **1 eq TBACl** in **Figure 4.17d**, a small signal is visible for the  $\alpha$ -H1" that has shifted downfield. The downfield shift is presumably due to the displacement of a weakly binding MeSO<sub>3</sub><sup>-</sup>•H<sup>+</sup> by a strongly binding Cl<sup>-</sup> anion (**Figure 4.17**). At 2 eq of TBACl, the conversion between isomers was complete and therefore, no peak for  $\alpha$  isomer was observed (**2 eq TBACl** in **Figure 4.19a**). Importantly, no change in chemical shift of the H1" signal for the  $\beta$ -isomer was observed.

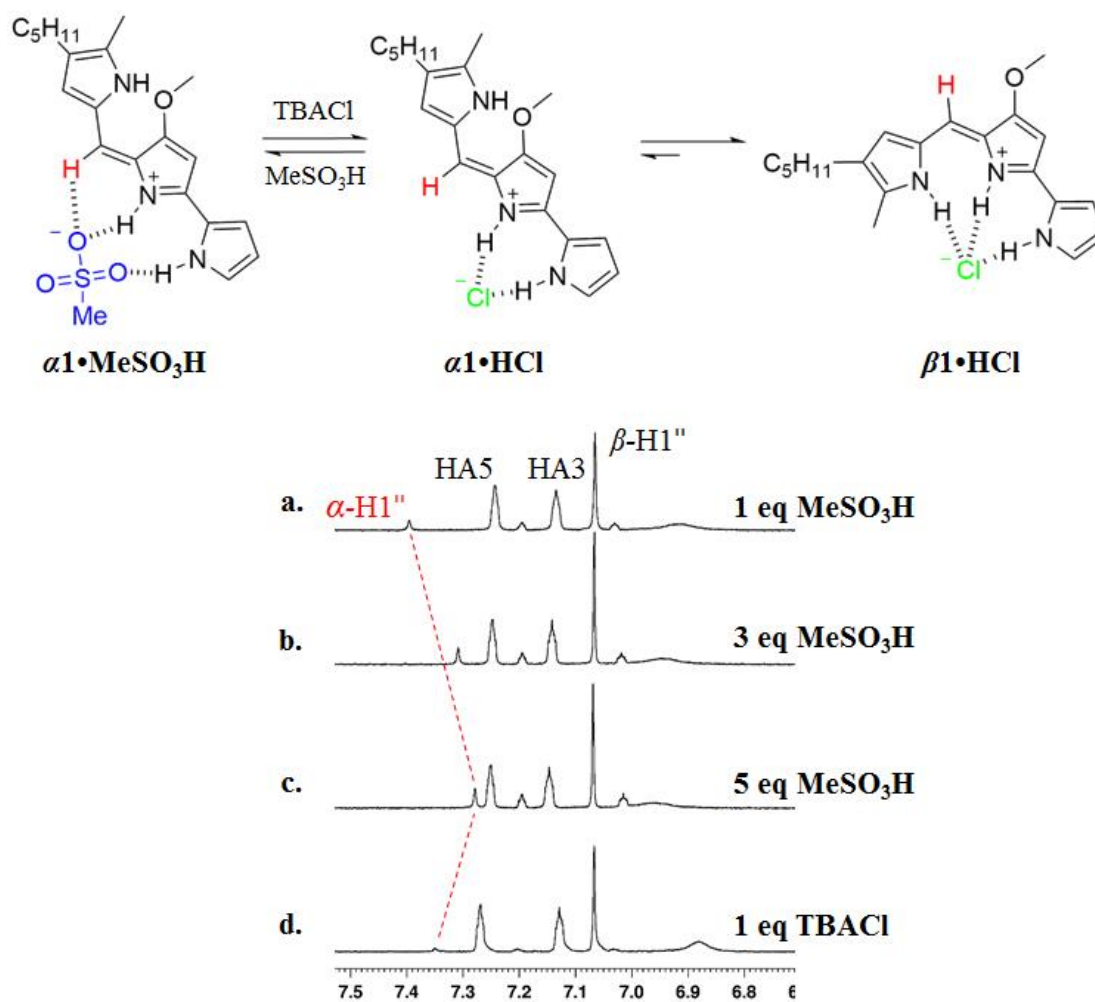


**Figure 4.17.** Proposed structure depicts the involvement of  $\alpha$ -H1'' (highlighted in red) hydrogen in  $1 \cdot \text{MeSO}_3\text{H}$  complex for binding  $\text{MeSO}_3^-$  anion, in addition to the two NH protons on rings A and B.  $^1\text{H}$  NMR spectra shows the changes in chemical shift for H1'' on  $\alpha$  isomer of prodigiosin  $1 \cdot \text{H}^+$  as  $\text{MeSO}_3\text{H}$  and TBACl are titrated into the NMR sample in  $\text{CD}_3\text{CN}$  at  $25^\circ\text{C}$ . When 1 eq of TBACl is added,  $\text{MeSO}_3^-$  is displaced by the strongly binding  $\text{Cl}^-$  anion to give  $\alpha 1 \cdot \text{HCl}$  complex. The exchange of anions is also accompanied by complete conversion of  $\alpha$  to  $\beta$  isomer over time. Note that the H1'' on the  $\beta$ -isomer does not move.

For the ester compound **2e**, as equivalents of MeSO<sub>3</sub>H were added to the solution, the signal for  $\alpha$ -H1" proton grew in intensity (**Figure 4.18b-c**). Also, the signal shifted downfield with each addition of MeSO<sub>3</sub>H. Using computational modeling, a structure was generated to depict the binding of MeSO<sub>3</sub><sup>-</sup> anion by the H1" hydrogen of the  $\alpha$  isomer of **2e**•MeSO<sub>3</sub>H (**Figure 4.18**). As shown in **Figure 4.18**, the bidentate MeSO<sub>3</sub><sup>-</sup> anion is bound using two pyrrolic NH protons on rings A and B along with the H1" hydrogen of **2e**•H<sup>+</sup> cation. When TBACl was added to the sample, displacement of bound MeSO<sub>3</sub><sup>-</sup> by Cl<sup>-</sup> anion took place. Addition of equivalents of TBACl led to an upfield movement of the  $\alpha$ -H1" resonance (**1 eq TBACl** NMR spectrum in **Figure 4.18d**). Moreover, no interconversion between the  $\alpha$  and  $\beta$  isomers was observed. The resonance for  $\alpha$ -H1" hydrogen continued to shift upfield as more equivalents of chloride were added (**2-10 eq TBACl** in **Figure 4.18e-f**). According to the computational model of **2e**•HCl in **Figure 4.18**, the H1" is not involved in binding monodentate Cl<sup>-</sup> anion. Upon addition of multiple equivalents of TBACl, the weakly bound MeSO<sub>3</sub><sup>-</sup> anion gets slowly displaced from the binding pocket by Cl<sup>-</sup>, resulting in an upfield movement of the  $\alpha$ -H1" resonance (**1-10 eq TBACl** in **Figure 4.18d-f**). This behavior was in contrast to the pattern observed for  $\alpha$ -H1" of prodigiosin (**Figure 4.17d**). No change in chemical shift for  $\beta$ -H1" of **2e**•H<sup>+</sup> was observed.

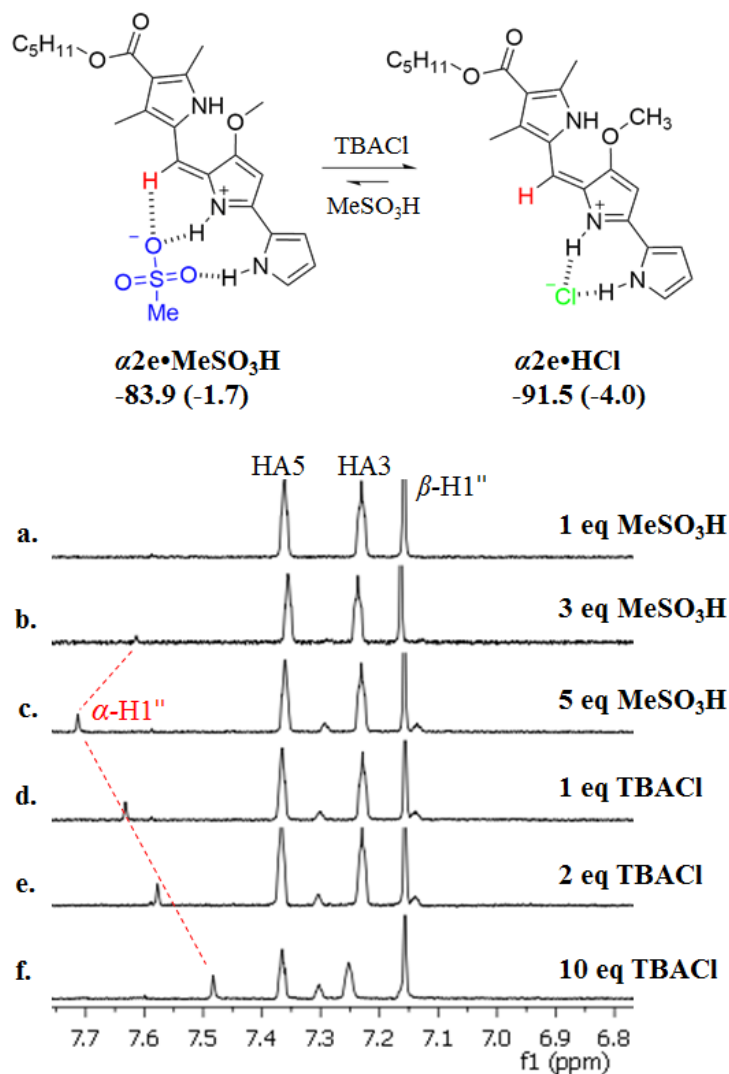


**Figure 4.18.** Structures showing the H1'' (highlighted in red) in  $\alpha$  isomer of  $2e \cdot \text{MeSO}_3\text{H}$  complex, involved in binding  $\text{MeSO}_3^-$  in addition to the two NH protons on rings A and B. For the  $\alpha$  isomer of  $2e \cdot \text{HCl}$  complex, the H1'' is no longer involved in binding  $\text{Cl}^-$ . Calculated Gibbs' free energies for each complex are in kcal/mol, in gas phase and acetonitrile (in parenthesis). <sup>1</sup>H NMR spectra shows the changes in chemical shift for H1'' on  $\alpha$  isomer of ester analog  $2e \cdot \text{H}^+$  as  $\text{MeSO}_3\text{H}$  and TBACl are titrated into the NMR sample in CD<sub>3</sub>CN at 25°C.

Thus, the NMR experiments described in this section provided us with substantial evidence for the involvement of a CH hydrogen of  $\alpha$  isomer of prodigiosenes in binding anions. This data is especially exciting due to the proposed involvement of the  $\alpha$  conformation in the biological activities observed for prodigiosin **1**.<sup>134</sup> The importance of the  $\alpha$  conformation is further elevated by the finding that population of  $\alpha$  isomer of **1**•H<sup>+</sup> increases in solution in presence of water, as described in the next section.

#### 4.5 Factors Affecting $\alpha/\beta$ Conformational Ratio

After confirming the presence of  $\alpha$  and  $\beta$  conformations in solution for prodigiosin **1** and its analogs (**2e** and **3b**), the next step was to investigate the conditions under which the ratio of  $\alpha/\beta$  isomers could be varied. Quesada and his group, in their work with synthetic prodigiosene **33**, had concluded that the  $\alpha/\beta$  isomer ratio could be manipulated by changing the counterion or solvent.<sup>36</sup> Rizzo briefly mentioned that solvents such as water can drastically change the  $\alpha/\beta$  ratio.<sup>37</sup> However, none of the groups have studied the original natural product prodigiosin **1**. We made an attempt to study the factors that affect conformations of **1** and a few of its synthetic analogs.

##### 4.5.1 Anions Affect the $\alpha/\beta$ Conformational Ratio

By looking closely at the NH pyrrole protons, I was able to ascertain the binding patterns adopted by  $\alpha$  and  $\beta$  conformations of prodigiosenes. Similarly, by observing CH pyrrole protons, the role of anion in influencing  $\alpha/\beta$  conformer ratio in different compounds was determined. In the <sup>1</sup>H NMR experiments described below, samples of **1** and **2e** were titrated with MeSO<sub>3</sub>H in CD<sub>3</sub>CN at 25 °C.

**Figure 4.19a** shows a series of NMR spectra, highlighting aromatic CH hydrogens of prodigiosin **1**. Only one set of signals was observed for CH hydrogens initially (**0 eq MeSO<sub>3</sub>H** in **Figure 4.19a**). An addition of 1 eq of MeSO<sub>3</sub>H led to downfield movement of peaks (H3, H5 on ring A and the bridging proton H1") due to formation of **1•MeSO<sub>3</sub>H** complex (**1 eq MeSO<sub>3</sub>H** in **Figure 4.19a**). Addition of excess acid gave rise to a second set of peaks of lower intensity (**5 eq MeSO<sub>3</sub>H** in **Figure 4.19a**). The major set of peaks was assigned to  $\beta$  isomer of **1•MeSO<sub>3</sub>H** while the minor set of peaks were assigned to  $\alpha$  isomer. The  $\alpha$ : $\beta$  ratio was roughly 1:3 after addition of 5 eq of MeSO<sub>3</sub>H. When 1 eq of TBACl was added to the sample, all of  $\alpha$  isomer immediately converted into  $\beta$  form (**2 eq TBACl** in **Figure 4.19a**). Addition of excess equivalents of TBACl caused no other changes to the conformer ratio. The shift in equilibrium presumably took place because the  $\beta$ -isomer of **1•H<sup>+</sup>Cl<sup>-</sup>** is favored over the  $\alpha$  isomer. This extra stability of  $\beta$  form is a result of the contribution of all 3 pyrrole NH protons being able to bind Cl<sup>-</sup> ion. A change in binding strength owing to stronger association between **1•H<sup>+</sup>** cation and Cl<sup>-</sup> anion is apparently enough to influence the conformer ratios for the natural product prodigiosin **1**.

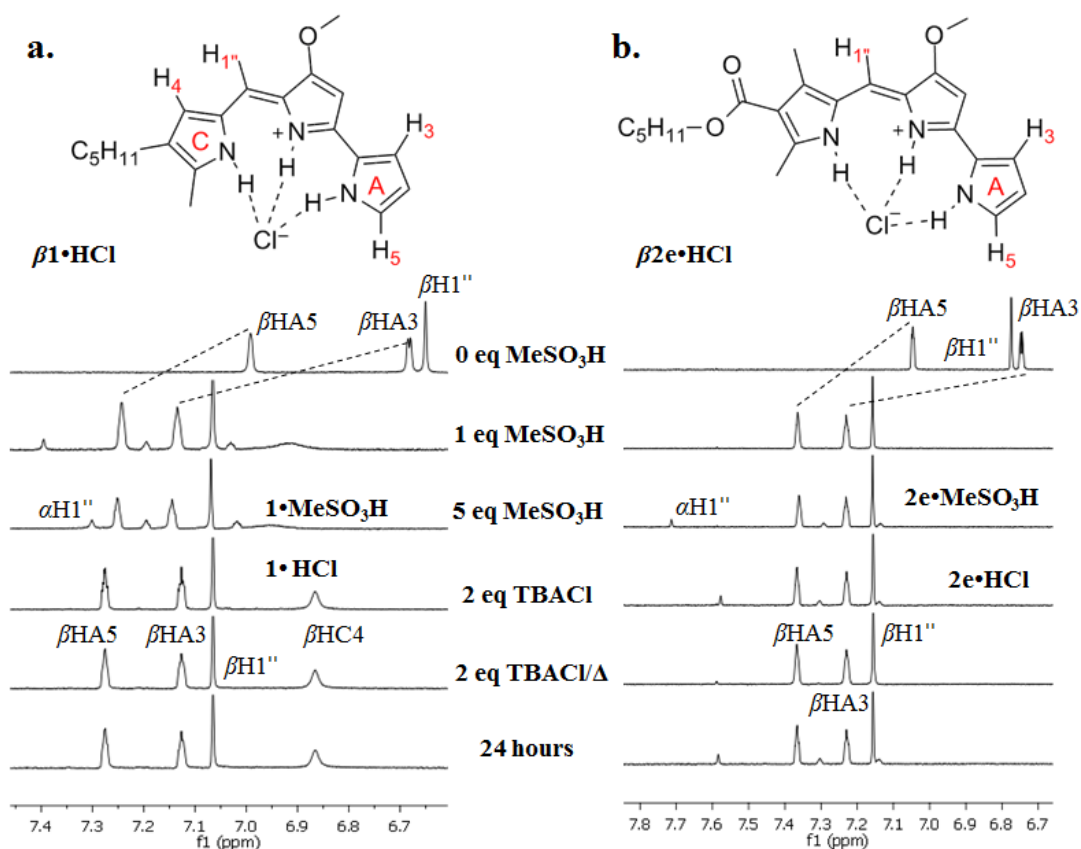


**Figure 4.19.**  $^1\text{H}$  NMR spectra shows the changes in conformer ratios for (a) prodigiosin  $1 \cdot \text{H}^+$  with respect to aromatic CH hydrogens as  $\text{MeSO}_3\text{H}$  and TBACl are titrated into the NMR sample in  $\text{CD}_3\text{CN}$  at  $25^\circ\text{C}$ . The results for prodigiosin have been contrasted with results obtained from ester  $2e \cdot \text{H}^+$  (b).

Similar to prodigiosin **1**, ester **2e** shows a single set of peaks for CH hydrogens H3, H5 on ring A and bridging hydrogen H1". When 1 eq of  $\text{MeSO}_3\text{H}$  was added to the sample, peaks for  $\beta$  conformer were observed predominantly (1 eq  $\text{MeSO}_3\text{H}$  in Figure 4.18b). As increasing increments of acid were added to the solution, a second set of minor peaks appeared (5 eq  $\text{MeSO}_3\text{H}$  in Figure 4.18b). The ratio of  $\alpha$  and  $\beta$  conformers was found to be 1:4. When TBACl was added to the solution,  $\alpha$ : $\beta$  equilibrium ratio was



maintained and no detectable interconversion between conformations took place (**2 eq TBACl** in **Figure 4.19b**). When the sample was heated up to 75°C, it was found that the equilibrium could be pushed more toward the  $\beta$  conformation (**2 eq TBACl**,  $\Delta$  in **Figure 4.19b**; NMR spectrum was recorded after cooling the sample to room temperature for 1 hour). However, signals for  $\alpha$  isomer reappeared after a day, bringing the  $\alpha$ : $\beta$  conformation ratio back to the original ratio of 1:4 (**24 hours** in **Figure 4.19b**). This property shown by the ester analog was in contrast to prodigiosin **1•HCl**. In order to understand why ester **2e•HCl** maintained a  $\alpha$ / $\beta$  conformation ratio of 1:4 despite the addition of excess  $\text{Cl}^-$  and a thermal push, we asked our collaborators to perform DFT calculations to compare and contrast the  $\text{Cl}^-$  binding affinities of the  $\alpha$  and  $\beta$  conformations of **2e•HCl** in  $\text{CH}_3\text{CN}$ . These calculations, along with molecular modeling, were performed by Ms. Maria Garcia Valverde and Dr. Roberto Quesada at the University of Burgos, Spain.

#### 4.5.1.1 Binding Energies of $\alpha$ and $\beta$ Conformations of **2e•HCl**

Since we were interested in studying the conformations of the HCl complex of ester **2e**, we wanted to know about the relative energies of protonated species **2e•H<sup>+</sup>**. Our collaborators calculated energies for both gas and solution (acetonitrile) phases. Based on DFT calculations, the  $\gamma$  isomer was found to have the minimum energy (**Figure 4.20**). Therefore, it was used as a starting point for  $\text{Cl}^-$  binding studies. In order to study the  $\text{Cl}^-$  binding affinity for different isomers, chloride ( $\text{Cl}^-$ ) complexes of  **$\gamma$ 2e•H<sup>+</sup>** were studied in more detail. Four structures were proposed for  $\text{Cl}^-$  complexes as shown in **Figure 4.20**.

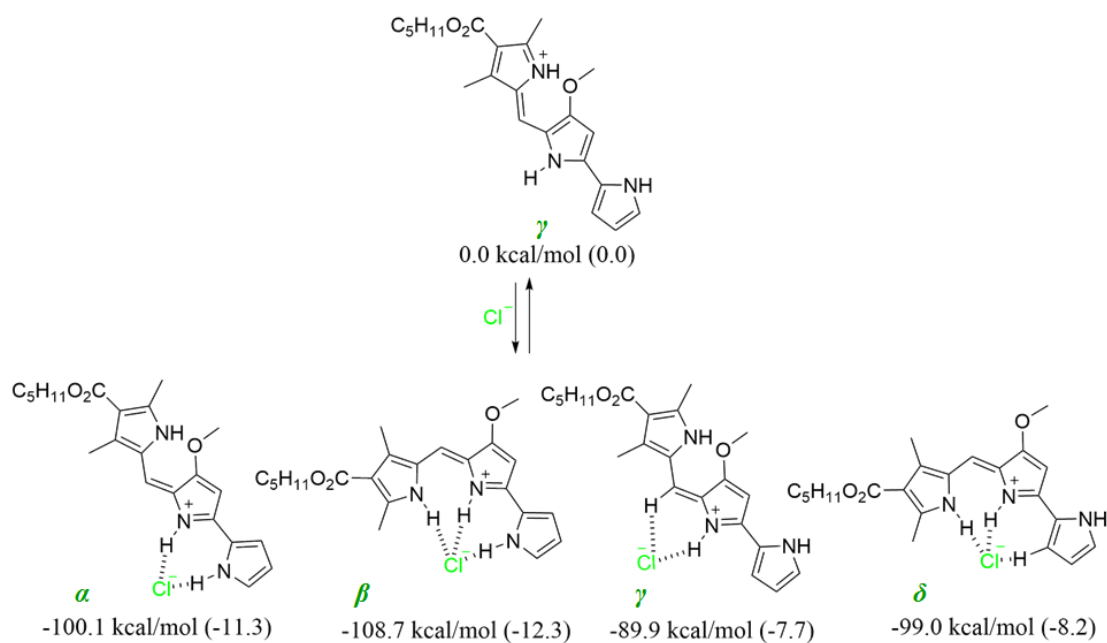


**Figure 4.20.** The  $\gamma 2\mathbf{e}\cdot\mathbf{H}^+$  cation can bind  $\text{Cl}^-$  to give four possible isomers. Binding energies were calculated in kcal/mol for each chloride ( $\text{Cl}^-$ ) complex in gas phase and acetonitrile (in parentheses).

The DFT calculations indicated that in both gas and solution phases, interaction energy for the  $\beta$  isomer was lowest (-12.3 kcal/mol). This theoretical calculation is in agreement with the solution NMR data, where  $2\mathbf{e}\cdot\mathbf{HCl}$  gave  $\beta$  form as the dominant isomer. Further, the anion binding energy for the  $\beta$  form of  $2\mathbf{e}\cdot\mathbf{HCl}$  complex in  $\text{CH}_3\text{CN}$  was -12.3 kcal/mol, whereas the binding energy for the  $\alpha$  isomer of  $2\mathbf{e}\cdot\mathbf{HCl}$  complex was -11.3 kcal/mol. The small energy difference between  $\alpha$  and  $\beta$  conformers (1.0 kcal/mol) might explain the presence of both species in the  $^1\text{H}$  NMR spectrum. Despite addition of excess  $\text{Cl}^-$  anion and heating of the sample, the equilibrium ratio was maintained at 1:4 for the  $\alpha$  and  $\beta$  isomers at room temperature (**Figure 4.19b**).

Thus, some of the DFT calculations supported the results observed in NMR experiments. With the aid of NMR experiments, I was able to show that in presence of  $\text{Cl}^-$  anion, the  $\beta$ -conformation of prodigiosin  $\mathbf{1}\cdot\text{H}^+$  is favored over the  $\alpha$ -conformation. But the same is not true for the ester analog  $\mathbf{2e}\cdot\text{H}^+$ .

#### 4.5.2 Water Influences Population of $\alpha$ Isomer in Solution

In their 1999 publication, Rizzo *et al.* briefly mentioned that conformer  $\alpha$  and  $\beta$  coexisted at about 2/1 ratio in a 1:1  $\text{CD}_3\text{CN}/\text{D}_2\text{O}$  (pH 1.1) solvent system.<sup>37</sup> They provided no data, however, for this assertion. Quesada *et al.* acknowledged this finding when they affirmed in their publication that conformation ratio was influenced by solvents.<sup>36</sup> They were able to confirm solvent influence based on the studies performed with compound **33** in DMSO and  $\text{CDCl}_3$ . However, none of the groups have looked at the natural product prodigiosin **1** and the influence of solvent on its conformations.

In an aprotic solvent such as  $\text{CD}_3\text{CN}$ , protonated prodigiosin  $\mathbf{1}\cdot\text{H}^+\text{MeSO}_3^-$  exists in the  $\alpha:\beta$  conformation ratio of 1:3 (**Figure 4.21**). The next goal was to evaluate the conformation ratio of prodigiosin in aqueous solution, a more biologically relevant system. However, prodigiosin has a low solubility (18  $\mu\text{M}$ ) in water at pH 7.0 at 25  $^\circ\text{C}$ .<sup>141</sup> Therefore, a 1:1 mixture of  $\text{CD}_3\text{CN}$  and  $\text{D}_2\text{O}$  was used for NMR studies. A  $^1\text{H}$  NMR spectrum of prodigiosin  $\mathbf{1}\cdot\text{H}^+\text{MeSO}_3^-$  (2 mM) in presence of 3 eq of methanesulfonic acid was recorded in  $\text{CD}_3\text{CN}:\text{D}_2\text{O}$  (1:1) at 25  $^\circ\text{C}$  (**Figure 4.21**). This aqueous solvent system gave a higher population of  $\alpha$  conformer (1:2), in contrast to the 1:3 ratio observed for  $\alpha/\beta$  isomers of  $\mathbf{1}\cdot\text{H}^+\text{MeSO}_3^-$  in  $\text{CD}_3\text{CN}$ .

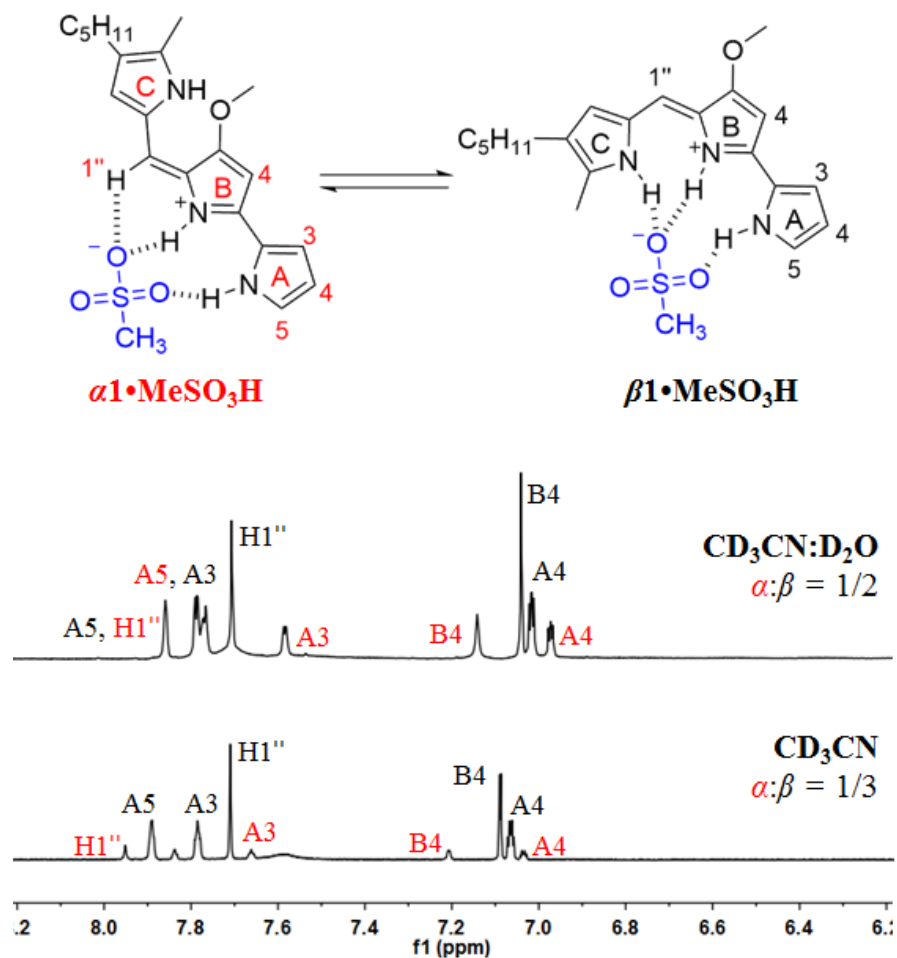


**Figure 4.21.** Structures of the  $\alpha$  and  $\beta$  conformations of  $1 \cdot \text{MeSO}_3\text{H}$ .  $^1\text{H}$  NMR spectra of prodigiosin  $1 \cdot \text{MeSO}_3\text{H}$  in presence of 3 equivalents of  $\text{MeSO}_3\text{H}$  in  $\text{CD}_3\text{CN}$  (bottom) and 1:1 mixture of  $\text{CD}_3\text{CN}:\text{D}_2\text{O}$  (top) at 25 °C.

The higher ratio of  $\alpha$  was evident based on the aromatic protons between 6-8 ppm (**Figure 4.21**). The higher population of  $\alpha$  isomer indicates the extra stabilization of the structure in water. The  $\alpha$  isomer is characterized by intramolecular hydrogen bonding between the NH proton on ring C and the exocyclic oxygen on ring B (**Figure 4.21**). As a solvent, water may provide a network of H-bonds to stabilize the flipping of ring C, which increases the population of  $\alpha$  isomer in the equilibrium mixture.

In **Section 4.2**, I described the ability of analog **12** to form non-covalent dimers in absence or presence of metal ions.<sup>33, 34</sup> The change in  $^1\text{H}$  NMR spectrum of **1•MeSO<sub>3</sub>H** in presence of water could be due to the formation of dimeric and monomeric species.<sup>142</sup> The possibility of dimer formation by **1•MeSO<sub>3</sub>H** in  $\text{CD}_3\text{CN}:\text{D}_2\text{O}$  was examined by performing a dilution experiment and DOSY NMR. No changes in chemical shifts were observed throughout the dilution experiment.

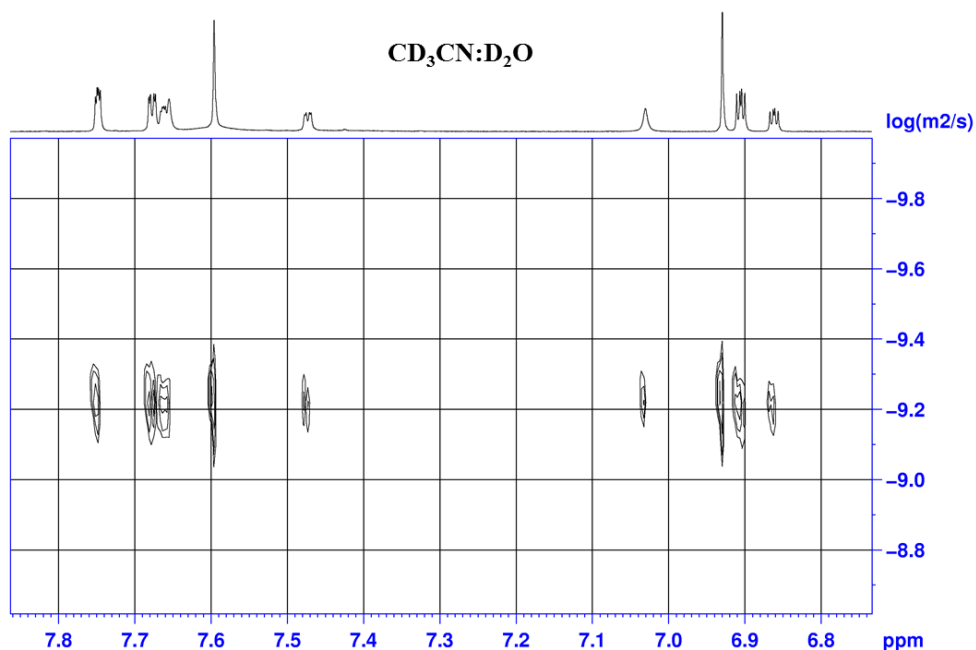


**Figure 4.22.** DOSY NMR of prodigiosin **1•MeSO<sub>3</sub>H** with 3 equivalents of MeSO<sub>3</sub>H in a 1:1 mixture of  $\text{CD}_3\text{CN}:\text{D}_2\text{O}$  at 25 °C. Only one set of DOSY signals were observed for all aromatic protons.

DOSY NMR of **1•MeSO<sub>3</sub>H** in  $\text{CD}_3\text{CN}:\text{D}_2\text{O}$  showed a single set of peaks for all aromatic protons in the two isomers (**Figure 4.22**), which indicates that the sample contains different species of similar molecular weight. Thus, diffusion NMR data eliminated the possibility of dimer formation by **1•MeSO<sub>3</sub>H** in the 1:1 solvent mixture.

Other 2D NMR experiments such as NOESY and ROESY were attempted to assign the various peaks to  $\alpha$  or  $\beta$  isomer in the 1:1 CD<sub>3</sub>CN:D<sub>2</sub>O solution. NOESY and ROESY experiments were ineffective in gathering any details about the isomers. Based on COSY NMR, the resonances were separated into two sets (**Figure 4.23**). This separation was based on the knowledge that three protons from ring A (H3, H4 and H5) and H4 proton from ring B will show COSY correlation. As expected, three signals in each set showed correlation that allowed us to segregate the signals for two isomers.

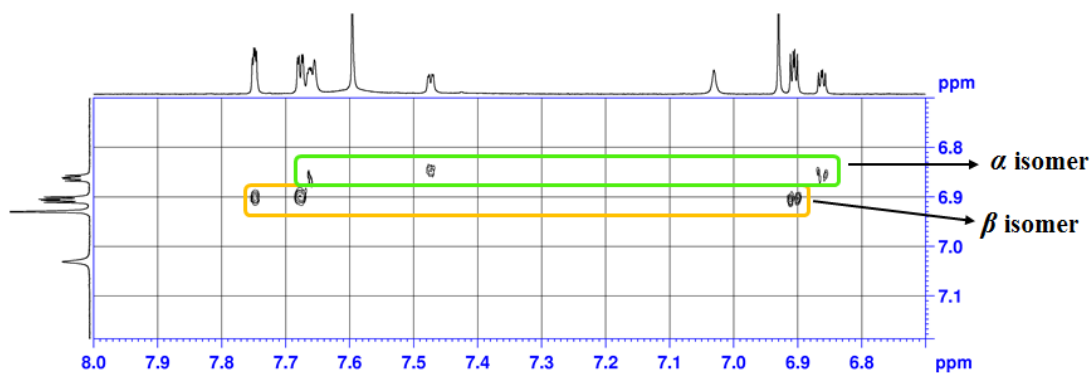


**Figure 4.23.** 2D COSY NMR of prodigiosin **1•MeSO<sub>3</sub>H** with 3 equivalents of MeSO<sub>3</sub>H in a 1:1 mixture of CD<sub>3</sub>CN:D<sub>2</sub>O at 25 °C. The signals for aromatic protons could be segregated for the two isomers.

The results obtained in this section are quite interesting, when combined with Rizzo's findings.<sup>37</sup> According to my results, **1•MeSO<sub>3</sub>H** exists in an  $\alpha/\beta$  conformational ratio of 1:2 in a 1:1 mixture of CD<sub>3</sub>CN:D<sub>2</sub>O. The population of  $\alpha$  isomer of **1•MeSO<sub>3</sub>H** increases by 17% in presence of D<sub>2</sub>O. Although similar experiments were not attempted with **1•HCl** complex, Rizzo's findings with **8•HCl** salt give insight into different possibilities. Rizzo and colleagues found that the **8•HCl** salt in

CD<sub>3</sub>CN:D<sub>2</sub>O (1/1, pH 1.1) gave a ratio of 2:1 for the  $\alpha/\beta$  isomers in an NMR experiment (Section 4.2.2). One common observation in both set of results is the increase in population of  $\alpha$  isomer in presence of water, possibly due to the stabilizing effect of water on the structure of the  $\alpha$  form. Therefore, leading us to questions, regarding the relevance of  $\alpha$  conformation in biological systems where water is the major solvent.

Chapter 2 and 3 explored the ability of prodigiosin **1** and its analogs (**2**, **3**) to bind and transport anions in aqueous buffers. Multiple research groups have suggested that the  $\beta$ -isomer exhibits stronger anion binding due to the tridentate binding motif and therefore, must be the major conformer responsible for anion transport.<sup>33, 36-38</sup> But these observations were mostly based on binding studies done in organic solvents. Moreover, the experiments with **1**•MeSO<sub>3</sub>H have shown that depending on the counter-anion, the CH hydrogen in  $\alpha$ -isomer can also be involved in anion binding, thus, giving rise to a tridentate motif (Section 4.5.1). Based on the above arguments, it is possible that the  $\alpha$ -isomer also plays an important role, like the  $\beta$ -isomer in the process of anion transport.

Prodigiosin **1** can intercalate with dsDNA, as illustrated by Manderville, Perez-Tomas and Zhou.<sup>39-41</sup> Prodigiosin's ability to interact with DNA has been suggested as possible mechanism for explaining its anticancer activity. However, the existing studies do not explore the conformation adopted by prodigiosin while binding with DNA. In 1990, McNab made an interesting correlation.<sup>134</sup> In his paper, he wrote "*...the configuration of the methoxy group is particularly noteworthy, allowing a seven-membered ring hydrogen bond with the pyrrole NH of ring C. It is possible that the*

*configuration of the rings defined by hydrogen bonding in this way may be associated with the biological activity of prodigiosins, which is known to be dependent on the presence of the ring B methoxy group*". The last sentence highlights the dependence of biological activity of prodigiosenes on the methoxy group on ring B. At the same time, the arrangement of rings in  $\alpha$  conformer is also a result of the methoxy group. Therefore, the arguments put forth suggest a larger role for the  $\alpha$  conformation in biological systems. More in-depth studies need to be pursued to realize the complete contribution of  $\alpha$ -isomer in the observed biological activities of prodigiosenes. The NMR results described in this chapter are a stepping stone in realizing this goal.

#### 4.6 Conclusions

The work presented in this chapter was inspired by the transport mechanism proposed by Davis and colleagues.<sup>31,32</sup> Davis and group proposed that prodigiosin  $\mathbf{1}\cdot\mathbf{H}^+$  is protonated at physiological pH of 7.4. In its protonated state, prodigiosin  $\mathbf{1}\cdot\mathbf{H}^+$  binds chloride and transports it as  $\mathbf{1}\cdot\mathbf{H}^+\mathbf{Cl}^-$  across liposomal membrane. In this chapter, binding of anions by prodigiosin  $\mathbf{1}\cdot\mathbf{H}^+$  and its analogs ( $\mathbf{2e}\cdot\mathbf{H}^+$ ,  $\mathbf{3b}\cdot\mathbf{H}^+$ ) was studied. Binding studies were initiated by confirming existence of  $\alpha$  and  $\beta$  isomers for analog  $\mathbf{3b}\cdot\mathbf{H}^+$  in organic solvents. From NMR results, the distinct anion binding patterns of  $\alpha$  and  $\beta$  isomers were recognized. The involvement of a CH hydrogen of  $\alpha$  isomer in binding anions was a significant finding. This is the first time that prodigiosenes have been shown to employ a CH hydrogen for anion binding. The  $\text{CH}\cdots\text{A}^-$  interaction is an important contribution to the study of diverse non-covalent interactions in the ever-expanding field of supramolecular chemistry. There is another observation to be made



from the data in **Figure 4.18**. The  $\text{Cl}^-$  anion is smaller in size as compared to the  $\text{MeSO}_3^-$  anion. Based on computer modeling and NMR data (upfield movement of  $\alpha\text{-H1}''$  when TBACl is added; trace **d-f** in **Figure 4.18**), the  $\alpha\text{-H1}''$  hydrogen is not involved in binding  $\text{Cl}^-$ . However, due to the bidentate nature of the  $\text{MeSO}_3^-$  anion, the  $\alpha\text{-H1}''$  hydrogen is able to interact with it. Similarly, it will be interesting to explore other polydentate anions such as some of the biologically relevant carboxylate anions (for *eg.* acetate, oxalate, citrate, *etc.*) and their binding interactions with prodigiosenes. In fact, Nager has reported that the gluconate anion can help solubilize prodigiosin in aqueous solutions.<sup>140</sup> Prodigiosin completely dissolved in a 3% gluconic acid solution by forming a gluconate salt. When the solution was freeze-dried under vacuum, prodigiosin gluconate was obtained in amorphous form which was readily soluble in water. This finding can be applied in biological studies of prodigiosin as it is poorly soluble in aqueous medium.<sup>141</sup> An investigation of similar anions can be insightful in learning more about the involvement of  $\alpha\text{-H1}''$  hydrogen in anion binding. Further, it might contribute towards understanding of prodigiosenes solution properties.

Additionally, it was shown that counter-anions can influence the  $\alpha/\beta$  conformer ratio for protonated prodigiosenes in different ways. Solvents can also influence the  $\alpha/\beta$  conformer ratio. An  $\alpha/\beta$  ratio of 1:3 is observed in  $\text{CD}_3\text{CN}$ , whereas a mixed solvent system like  $\text{CD}_3\text{CN}:\text{D}_2\text{O}$  (1:1) changes the conformer ratio. Apparently, the presence of water provides additional stability to the  $\alpha$  isomer, leading to an increase in its population in solution.

In conclusion, conformations of prodigiosenes were studied in greater detail in this chapter. Computer modeling results coincided with the NMR observations. We were able to predict anion binding patterns of prodigiosenes and the factors influencing them. This study will lead to a better understanding of the biological activity shown by prodigiosenes.

## 5 Chapter 5: Prodigiosin as a G-Quadruplex DNA Binding Ligand

*The 2D NMR experiments were performed in collaboration with Dr. Daoning Zhang at the Biomolecular NMR Facility at the University of Maryland, College Park.*

### 5.1 Introduction

The goal of the research described in this chapter was to confirm and establish binding between G-quadruplex DNA and prodigiosin **1**. A hexameric DNA sequence (5'-TGGGGT-3') was used to form a G-quadruplex d[TGGGGT]<sub>4</sub> in the presence of K<sup>+</sup> or Na<sup>+</sup> cations. By <sup>1</sup>H NMR spectroscopy, it was found that prodigiosin binds at the 3' end of the quadruplex DNA. Before describing the studies done to establish interactions between G-quadruplex DNA and prodigiosin **1**, I first provide a brief background on G-quadruplexes, significance of drug-G-quadruplex DNA interactions, some selective examples of G-quadruplex binding ligands and previous studies done to investigate interactions between prodigiosin **1** and duplex DNA.

### 5.2 A background on G-Quadruplex DNA

In 1960, Gellert *et al.* first described the G-quartet arrangement adopted in gels formed by 5'-guanylic acid.<sup>143</sup> By using crystallographic methods, they demonstrated the square planar arrangement of four guanosine bases within a G-quartet. Each guanosine uses its N1 and N2 amide NH protons as hydrogen bond donors and N7 and O6 as hydrogen bond acceptors. A total of eight hydrogen bonds are found in a G-quartet (**Figure 5.1a**).

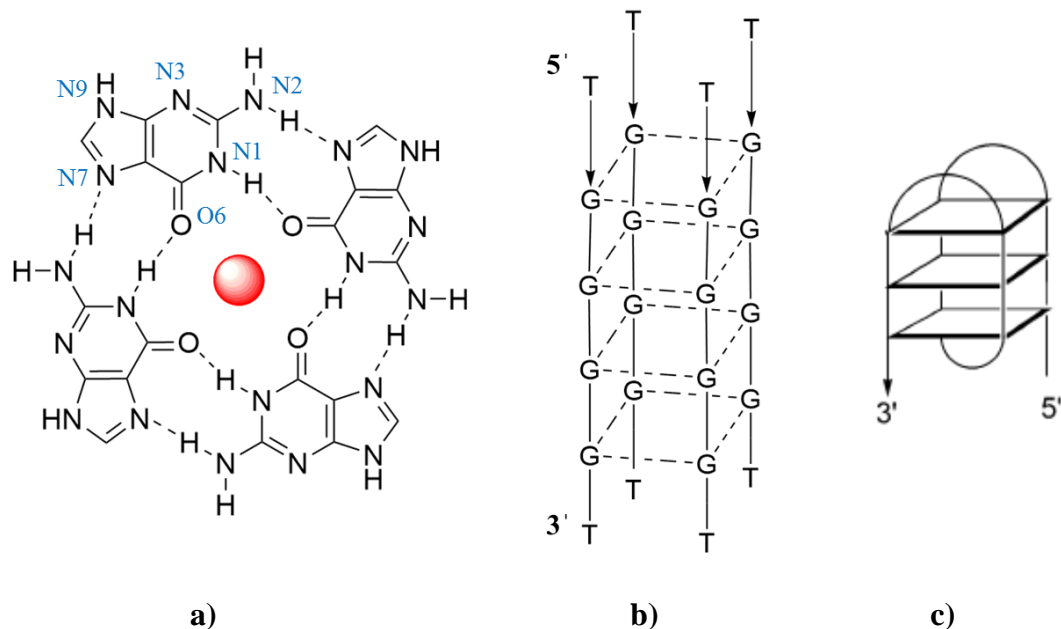


**Figure 5.1.** a) A G-quartet showing hydrogen bonds between the Hoogsteen and Watson-Crick faces of guanosine bases. b) Depiction of an intermolecular G-quadruplex 5'-d[TG<sub>4</sub>T]<sub>4</sub> formed by assembly of four strands aligned parallel to each other. c) Depiction of an anti-parallel intramolecular G-quadruplex formed by the folding of a single-strand of DNA.

Later, it was found that G-rich sequences are located at the end of eukaryotic chromosomes, so-called telomeres. These G-rich telomeric DNA sequences can fold to form compact, well-defined and stable intramolecular G-quadruplexes that are involved in multiple processes.<sup>144, 145</sup> G-quadruplexes are formed due to stacking of G-quartets on top of each other. The G-quadruplex structure can vary extensively depending on the folding, strand stoichiometry, nature and location of loops that link the stretches of guanine bases.<sup>146</sup> For example, four DNA strands can align in a parallel manner to form the intermolecular quadruplex 5'-d[TG<sub>4</sub>T]<sub>4</sub>-3' (**Figure 5.1b**).

Alternatively, a single-strand with repeating G-rich units can fold to form an anti-parallel intramolecular quadruplex such as d[GGTTGGTGTGGTTGG] (**Figure 5.1c**). The solution environment, such as metal ions, ligands, molecular crowding conditions can affect the stability and topology of quadruplexes.<sup>147,148</sup> The stability of G-quadruplexes depends on non-covalent interactions such as base stacking, hydrogen-bonding, hydration and metal ion coordination.<sup>146,149</sup>

The higher order structures formed by G-quartets protect the ends of chromosomes from damage or attachment to other chromosomes or unwanted species. Shortening of G-rich sequences has been shown to trigger cell senescence whereas lengthening of the G-rich sequence can lead to cell proliferation as seen in cancerous growth.<sup>150</sup> Telomerase is an enzyme involved in the synthesis of G-rich fragments of DNA. In most cancerous cells, telomerase is highly active. Telomerase requires a single-stranded telomeric primer to carry out the replication process. If small molecules that stabilize the G-quadruplex are present, the G-quadruplex structure may be stopped from unfolding, which subsequently inhibits the telomerase activity.<sup>151</sup> Therefore, drugs that target G-quadruplexes are seen as a promising way to interfere with telomerase functioning and act as potential anti-cancer agents.<sup>144,145</sup>

### 5.2.1 Examples of G-Quadruplex Binding Ligands

Although there are hundreds of examples of drugs and dyes that bind G-quadruplexes,<sup>152,153</sup> a few selective examples are discussed here. Thioflavin T **37** (**Figure 5.2**) acts as a fluorescent probe that binds with G-quadruplexes, including G-quadruplex d[TG<sub>4</sub>T]<sub>4</sub>.<sup>154,155</sup> Thioflavin T can induce G-quadruplex folding in human

telomeric DNA sequences. Under certain conditions, ThT **37** can cooperatively stabilize a G-quadruplex in presence of  $K^+$  ions. Interaction of **37** with the G-quadruplex results in an increase in the dye's fluorescence emission of up to 2100 fold. Depending on the folding topology of the particular G-quadruplex, ThT can bind at the grooves, stack at the top or bottom G-quartet or intercalate between different G-quartet planes.<sup>154</sup>

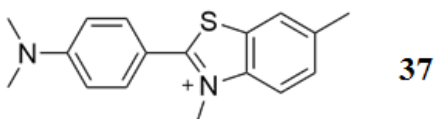


**Figure 5.2.** Structure of G-quadruplex binding Thioflavin T **37**.

Most telomerase inhibitors are aromatic compounds with electron-deficient heterocyclic rings. Due to their electron-deficiency, these compounds can stack or intercalate with the G-quartets. Telomestatin **38**, a natural product isolated from *Streptomyces anulatus* (**Figure 5.3**), is a potent telomerase inhibitor that selectively interacts with intramolecular G-quadruplexes.<sup>156</sup> In fact, telomestatin can induce G-quadruplex folding in the absence of monovalent cations.<sup>157</sup> Depending on the buffer conditions, telomestatin can influence the folding of G-quadruplex into either parallel to anti-parallel orientation. This particular ability of telomestatin **38** to modulate G-quadruplex morphologies extends beyond the usual consequences of ligand binding, such as G-quadruplex stabilization and telomerase inhibition.<sup>156</sup>

Distamycin A **39** is another drug that has been extensively studied for its ability to bind with G-quadruplexes in a 4:1 ligand:G-quadruplex stoichiometry (**Figure 5.3**).

Two anti-parallel distamycin dimers bind in two opposite grooves of G-quadruplex formed by d[TGGGGT]<sub>4</sub>.<sup>158, 159</sup>

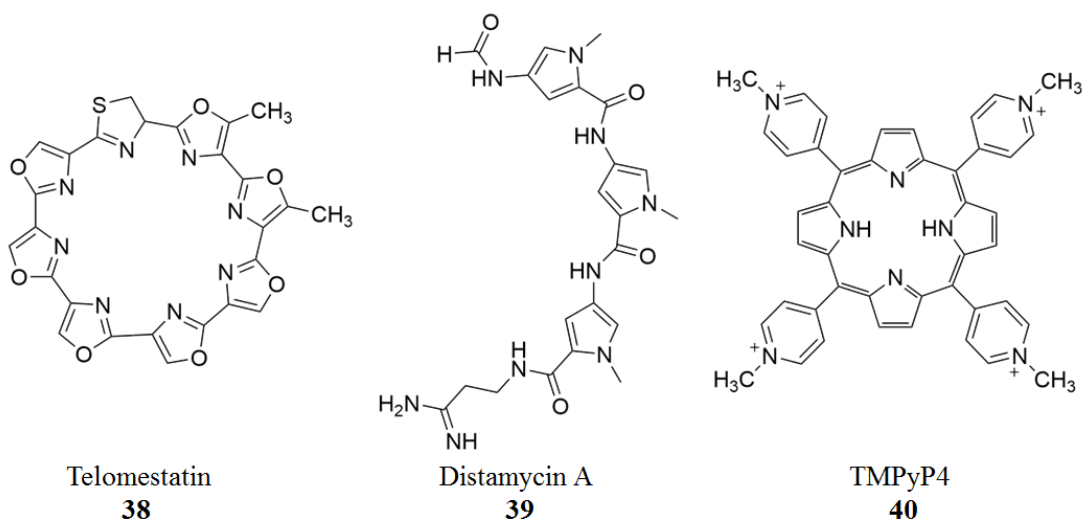


**Figure 5.3.** Structures of quadruplex binding drugs – Telomestatin **38**, Distamycin A **39** and TMPyP4 **40**.

Lastly, the porphyrin TMPyP4 **40** is another example of a telomerase inhibitor. TMPyP4 binding with G-quadruplexes has been tested using different DNA sequences that can form intermolecular quadruplexes, including d[TG<sub>4</sub>T]<sub>4</sub>, or intramolecular quadruplexes (d(G<sub>4</sub>T<sub>4</sub>G<sub>4</sub>)<sub>2</sub> and AG<sub>3</sub>(T<sub>2</sub>AG<sub>3</sub>)<sub>3</sub>). Porphyrin **40** was found to end stack in a 2:1 binding mode with d[TG<sub>4</sub>T]<sub>4</sub>, whereas it intercalates between two G-tetrads and diagonal loop regions of d(G<sub>4</sub>T<sub>4</sub>G<sub>4</sub>)<sub>2</sub> and lateral loop regions of AG<sub>3</sub>(T<sub>2</sub>AG<sub>3</sub>)<sub>3</sub>.<sup>160</sup>

These, and many other compounds, are being engineered for structure specific G-quadruplex binding and stabilization. These G-quadruplex binding ligands are being studied for therapeutic and diagnostic applications. As shown later in this chapter, we have found that the natural product prodigiosin **1** is able to bind to the intermolecular

G-quadruplex d[TG<sub>4</sub>T]<sub>4</sub>. This finding can lead to the study of prodigiosene analogs as potential G-quadruplex ligands and telomerase inhibitors.

### 5.3 Characterizing Ligand-Quadruplex Interactions

A G-quadruplex:ligand complex can be characterized by multiple techniques. In many studies, there may be a limited availability of the ligand or of the DNA. Therefore, the techniques most often used require low quantities of material. Additionally, these techniques show sensitivity to changes induced in the G-quadruplex structure due to ligand binding. In this chapter, some of the techniques that were used include UV-vis spectroscopy, circular dichroism spectroscopy (CD), fluorescence spectroscopy and nuclear magnetic resonance spectroscopy (NMR). These methods are discussed briefly in the following section. To learn more about other methods used to study G-quadruplex:ligand interactions, such as X-ray crystallography, fluorescence resonance energy transfer (FRET) assays, isothermal titration calorimetry (ITC) and more, the reader is directed to an excellent review written by Gu. *et. al.*<sup>145</sup>

#### 5.3.1 UV-vis Spectroscopy

UV-vis spectroscopy is a frequently used method for characterizing G-quadruplexes and ligand binding. Upon binding with G-quadruplex, the UV-vis spectrum of the ligand undergoes a hypochromic shift in its solet band (wavelength of maximum absorption) upon binding. The hypochromic effect is due to electronic interactions between the DNA bases and a chromophore on the ligand. **Figure 5.4** illustrates the hypochromic effect observed for TMPyP4 **40** (structure shown in **Figure 5.3**) in the presence and absence of an intermolecular parallel-stranded quadruplex



formed by 5'-T<sub>4</sub>G<sub>4</sub>-3'. A shift of 12 nm was observed in the porphyrin's solet band as it bound with the G-quadruplex DNA.<sup>161</sup>

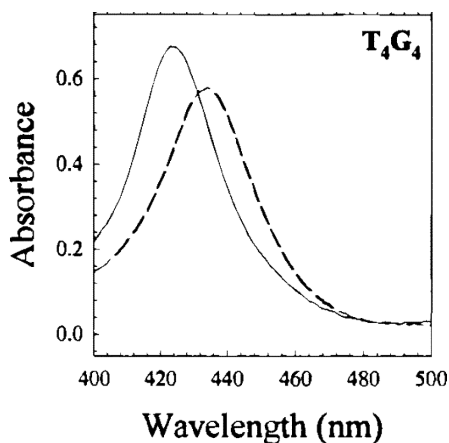


**Figure 5.4.** UV-vis spectra of TMPyP4 **40** in absence (solid line) and presence (dashed line) of d[T<sub>4</sub>G<sub>4</sub>]<sub>4</sub> at a [porphyrin]/[DNA quadruplex] ratio of 8.33. The solet band for the porphyrin undergoes a red shift from 422 nm in its unbound state to 434 nm in its bound state. Reprinted with permission from *Biochemistry* **1998**, 37 (9), 2709-2714. Copyright (1998) American Chemical Society.<sup>161</sup>

In order to quantify the impact of binding of a ligand to G-quadruplex structures, UV-vis spectroscopy can be used to compare the melting temperature of G-quadruplex and quadruplex-ligand complex. Nucleic acids give a strong absorbance around 260 nm. In quadruplex like structures, the absorbance at 260 nm is reduced due to quenching caused by the  $\pi$ -stacking of nucleobases. Upon heating, unstacking of these bases leads to a hypochromic effect that can be monitored by UV-vis spectroscopy. The melting temperature is determined from a plot of absorbance of the G-quadruplex at a fixed wavelength ( $\lambda_{\text{max}}$  of a quadruplex) and temperature. Similar experiments are performed on the quadruplex-ligand complex. An increase in the

melting temperature of G-quadruplex:ligand complex is indicative of binding of that ligand and stabilization of the G-quadruplex structure.<sup>145, 146</sup>

### 5.3.2 Circular Dichroism

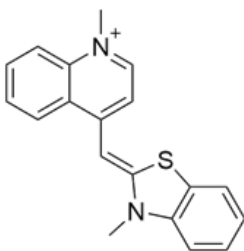
G-quadruplexes form helical structures. CD spectroscopy can provide information about the conformation and topology of such chiral structures. The CD spectrum of a G-quadruplex is dependent on the stacking interactions between adjacent G-quartets. Parallel and anti-parallel folded quadruplex structures can be differentiated by CD spectroscopy. Parallel intermolecular quadruplex are characterized by a positive maximum at 260 nm and a negative minimum at 240 nm. Anti-parallel intramolecular quadruplexes exhibit a positive band at 295 nm and a negative band at 260 nm.<sup>145, 146</sup>

Many small ligands are achiral and therefore, are CD inactive themselves. However, sometimes due to binding interactions, the chiral environment of G-quadruplex can give rise to an induced circular dichroism in the ligand at its maximum wavelength of absorbance.<sup>153</sup>

### 5.3.3 Fluorescence Spectroscopy

It has been shown that energy absorbed by a donor DNA base pair can be transferred to an intercalated or an end-stacked ligand that serves as an electron acceptor. Groove binders, on the other hand, do not exhibit similar energy transfer from donor to acceptor.<sup>39</sup> Fluorescence spectroscopy is commonly used for screening and comparing potential G-quadruplex binding ligands. Certain dyes such as thiazole orange **41** (TO; **Figure 5.5**) bind G-quadruplexes with high affinity. The fluorescence of unbound TO is quenched in solution, but upon binding with G-quadruplex DNA, the

fluorescence of **41** increases by many fold.<sup>162</sup> Due to this property of TO, it is used in ligand displacement assays to screen for G-quadruplex binding ligands.<sup>163</sup>



Thiazole orange (TO)  
**41**

**Figure 5.5.** Structure of thiazole orange (TO) **41**.

When a ligand is titrated into a quadruplex DNA solution, the change in fluorescence intensity of ligand is indicative of its binding to the DNA. In cases where the ligand is non-fluorogenic, fluorescence resonance energy transfer (FRET) assay can be used to detect binding and conformational changes in the DNA assembly. DNA strands are tagged with fluorescent dyes at both their 5' and 3' ends. When the DNA strand folds to form a G-quadruplex, the two dyes come in close vicinity to each other, leading to energy transfer. Thus, the fluorescence is typically quenched when the DNA is in its G-quadruplex state. Upon heating, the G-quadruplex unfolds resulting in increased distance between the fluorescent dyes, which then increases the fluorescence intensity. This technique is applied to many ligand-quadruplex complexes so as to determine their melting temperature and learn about the stabilizing effect of ligand binding on quadruplex.<sup>39, 146, 164</sup>

### 5.3.4 NMR Spectroscopy

NMR is a versatile technique that gives a wealth of atomic-level information about the G-quadruplex structure. NMR can be readily used to differentiate between single-stranded oligonucleotides and higher order structures such as G-quadruplexes. It can also be used to study the solution structure of complexes formed by oligonucleotides. In a study conducted by Lilley *et. al.*, the quadruplex formed by the d[TG<sub>4</sub>T] hexanucleotide in the presence of 100 mM NaCl, 1mM EDTA, 10 mM phosphate buffer (pH 7.1; D<sub>2</sub>O) was studied by <sup>1</sup>H NMR at variable temperature.<sup>165</sup> At lower temperatures (30 °C), 6 distinct peaks were observed around 7-8 ppm. Using 2D NMR techniques, four peaks were assigned to the H8 proton of four guanosine bases and two peaks assigned to the H6 of the two terminal thymine bases (**Figure 5.6**). As the temperature was increased, another set of 6 peaks started appearing. These peaks belonged to the aromatic protons on bases in the single-stranded DNA d[TG<sub>4</sub>T]. At 50 °C, the two sets of peaks were present at 1:1 ratio. When the sample was further heated to 70 °C, only the second set of peaks corresponding to the single-stranded form was visible. This transition between the two sets of peaks was attributed to a slow exchange between the two forms of DNA, namely d[TG<sub>4</sub>T] and its self-assembled G-quadruplex d[TG<sub>4</sub>T]<sub>4</sub>. (**Figure 5.6**). Thus, NMR spectroscopy helped in conducting a real-time study of self-association of the d[TG<sub>4</sub>T] nucleotide. Further, 2D COSY and NOESY experiments helped in ascertaining that d[TG<sub>4</sub>T] forms a parallel stranded tetraplex structure in the presence of Na<sup>+</sup> cations.

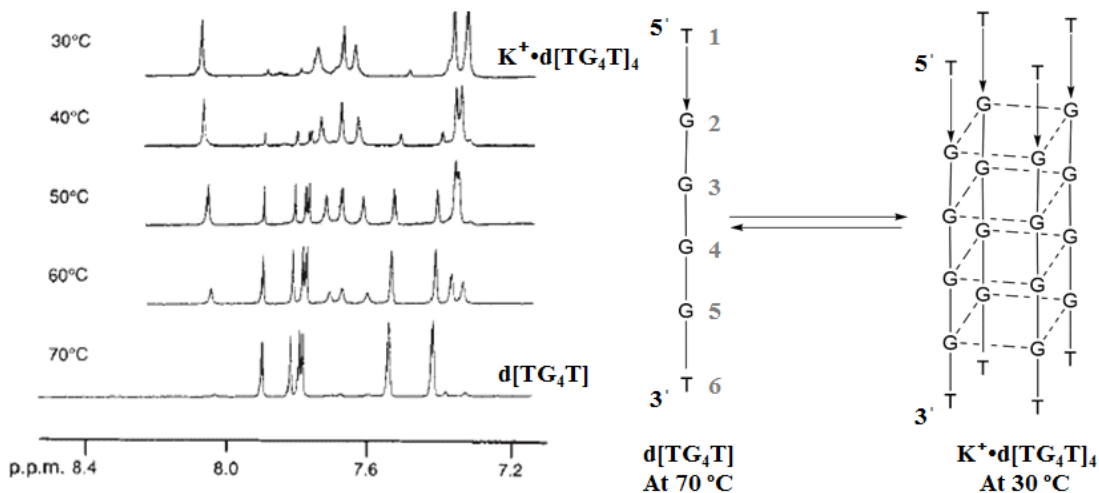


**Figure 5.6.**  $^1\text{H}$  NMR stack plot illustrating the slow exchange for single-stranded and G-quadruplex forms of  $\text{d}[\text{TG}_4\text{T}]$ . At  $30^\circ\text{C}$ ,  $\text{d}[\text{TG}_4\text{T}]$  nucleotide exists exclusively in the G-quadruplex form. As temperature is increased to  $50^\circ\text{C}$ , the tetraplex starts dissociating into single-strands as indicated by the second set of peaks growing in. At  $70^\circ\text{C}$ , only the distinct set of peaks due to the single-stranded DNA  $\text{d}[\text{TG}_4\text{T}]$  are visible. Reprinted by permission from *Nature* **1992**, 360 (6401), 280-282. Copyright (1992) Macmillan Publishers Ltd.<sup>165</sup>

More structural information can be obtained by performing 2D NMR heteronuclear correlation experiments. Use of sophisticated NMR cryoprobes has drastically cut down the amount of sample needed to carry out experiments, thereby making NMR an attractive technique for working with relatively large oligonucleotides.<sup>146</sup> In the studies described below, I have used multidimensional and multinuclear NMR to show that prodigiosin interacts with G-quadruplex DNA  $\text{K}^+\cdot\text{d}[\text{TG}_4\text{T}]_4$ .

## 5.4 Rationale for Studying the Binding Interactions Between Prodigiosin **1** and G-Quadruplex DNA

As described in **Section 1.4**, there are two proposed mechanisms currently used to explain the ability of prodigiosin **1** to induce apoptosis in cells. The first mechanism involves acidification of cell organelles caused by prodigiosin's ability to catalyze  $\text{H}^+/\text{Cl}^-$  symport or  $\text{OH}^-/\text{Cl}^-$  exchange across cell membranes.<sup>30</sup> The second mechanism suggests that the oxidative cleavage of DNA can be triggered by prodigiosene• $\text{Cu}^{2+}$  complexes.<sup>51</sup> There are additional examples that show that prodigiosin **1** intercalates preferably at AT sites of poly d[A-T]<sub>2</sub> and calf thymus DNA (ct-DNA).<sup>39,40</sup> With this collective evidence, I wanted to explore the possibility that prodigiosin **1** might act as a G-quadruplex binding ligand.

To first study potential interactions between prodigiosin **1** and a lipophilic G-quadruplex,<sup>147,166,167</sup> I performed a <sup>1</sup>H NMR titration with compound **1** and the lipophilic G-quadruplex (**42**)<sub>16</sub>•3K<sup>+</sup>•4DNP (**Figure 5.7**) in a 1:1 mixture of CD<sub>2</sub>Cl<sub>2</sub>:CD<sub>3</sub>CN. No changes in chemical shifts for the receptor (G-quadruplex (**42**)<sub>16</sub>•3K<sup>+</sup>•4DNP) or the ligand (prodigiosin **1**) protons were observed in the <sup>1</sup>H NMR spectra during the titration (**Figure 5.8c**). The absence of interactions between the G-quadruplex (**42**)<sub>16</sub>•3K<sup>+</sup>•4DNP and prodigiosin **1** were attributed to the lipophilic nature of both receptor and ligand species.

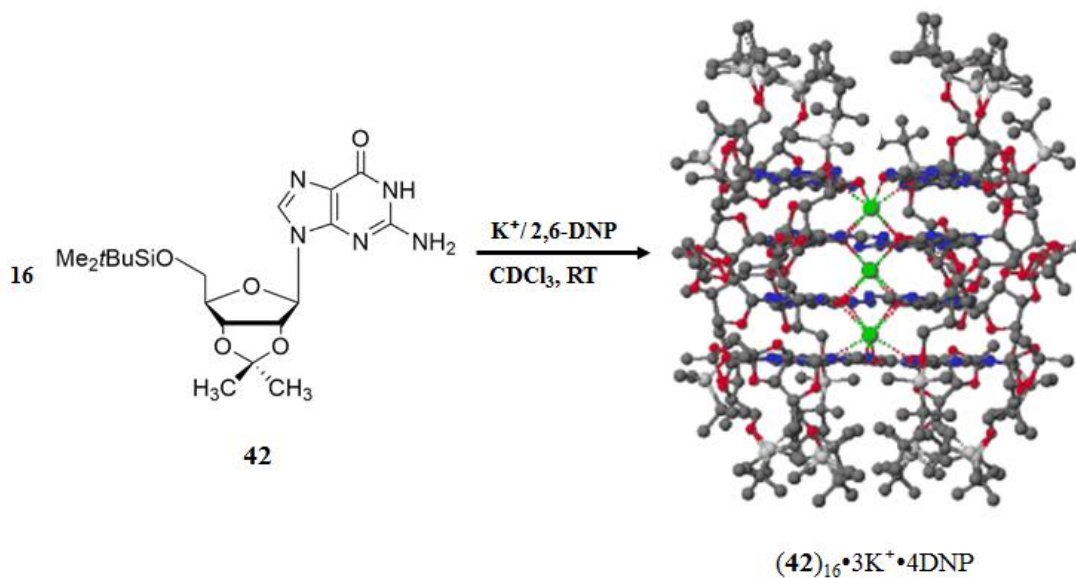


**Figure 5.7.** The cation-templated self-assembly of 16 equivalents of 5'-silyl-2',3'-O-isopropylidene guanosine (**42**) gives a lipophilic G-quadruplex  $(\mathbf{42})_{16} \cdot 3\text{K}^+ \cdot 4\text{DNP}$  in the solid state and in solution (green K, blue N, red O). Modified and reprinted with permission from *Angew. Chem. Int. Ed.* **2004**, *43* (6), 668-698. Copyright (2004) Wiley-VCH Verlag GmbH & Co. KGaA, Weinheim.<sup>147</sup>

Our hypothesis was that replacing the organic solvent with water might enhance the affinity of prodigiosin **1** for G-quartets. For this reason, a known G-quadruplex  $\text{K}^+ \cdot \text{d}[\text{TG}_4\text{T}]_4$  DNA assembly was selected for the studies in aqueous conditions.<sup>165</sup> By using a G-quadruplex DNA assembly ( $\text{K}^+ \cdot \text{d}[\text{TG}_4\text{T}]_4$ ), I was also able to work more closely with the biological conditions. Additionally, at the experimental condition of pH 7.0, prodigiosin is in its protonated cation form  $\mathbf{1} \cdot \text{H}^+$ , while DNA is anionic. We hypothesized that prodigiosin  $\mathbf{1} \cdot \text{H}^+$  might interact with the anionic phosphate backbone

of G-quadruplex DNA assembly, and potentially intercalate with the G-quartets due to prodigiosin's  $\pi$ -conjugation, as well as lipophilicity.

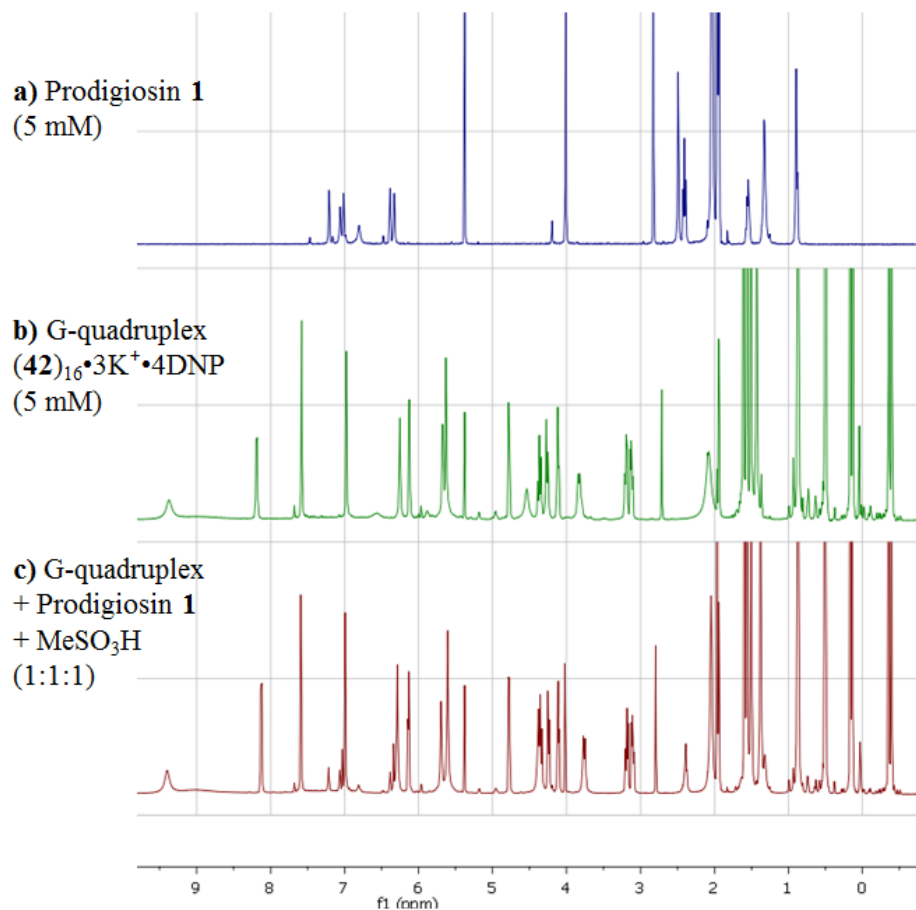


**Figure 5.8.** A <sup>1</sup>H NMR stack plot of **a)** Prodigiosin **1** (5 mM), **b)** G-quadruplex (42)<sub>16</sub>•3K<sup>+</sup>•4DNP (5 mM) and **c)** Prodigiosin **1**: (42)<sub>16</sub>•3K<sup>+</sup>•4DNP:MeSO<sub>3</sub>H in 1:1:1 ratio in a 1:1 mixture of CD<sub>2</sub>Cl<sub>2</sub>:CD<sub>3</sub>CN. No changes in chemical shifts of NMR resonances for prodigiosin **1** or G-quadruplex (42)<sub>16</sub>•3K<sup>+</sup>•4DNP were observed in NMR spectrum **c)**.

The ability of prodigiosin **1** to bind G-quadruplexes could lead to another possible mechanism to explain the anti-cancer properties of this natural product. Before



describing the work done to establish binding between prodigiosin and d[ $\text{TG}_4\text{T}$ ] $_4$  tetraplex, three previous examples of prodigiosin-duplex DNA binding are discussed.

#### 5.4.1 Prodigiosin Intercalates Preferably at AT-Rich Sites in Duplex DNA

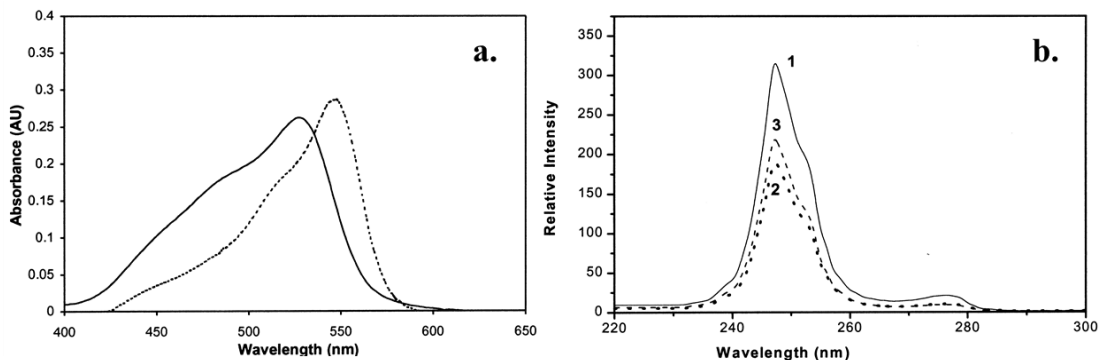


**Figure 5.9.** **a)** UV-Vis spectra of prodigiosin **1** (4 μM) in absence (solid line) and presence (dashed line) of 10 bp equivalents of poly d[A-T] $_2$  in 10 mM NaCl-50 mM MES buffer at pH 6.5. A bathochromic shift of 20 nm was observed. **b)** Fluorescence intensity of prodigiosin **1** (4 μM) in the presence of 10 bp equivalent of poly d[A-T] $_2$  (**1**), ct-DNA (**2**) and poly d[G-C] $_2$  (**3**) 10 mM NaCl-50 mM MES buffer at pH 6.5. The maximum increase in prodigiosin's fluorescence intensity was observed with poly d[A-T] $_2$ . Reprinted with permission from *The Journal of Organic Chemistry* **1999**, *64* (18), 6861-6869. Copyright (1999) American Chemical Society.<sup>39</sup>

Manderville and his group conducted a study to determine the binding properties of prodigiosin for three types of DNA – calf thymus-DNA (ct-DNA), poly d[A-T] $_2$  and poly d[G-C] $_2$ .<sup>39</sup> ct-DNA is extracted from the thymus gland of calf and is used in various biophysical and biochemical studies. It has a variable molecular weight of 120-140 KDa.<sup>168</sup> Poly d[A-T] $_2$  is a DNA polymer sequence rich in A and T bases,

while poly d[G-C]<sub>2</sub> is rich in G and C bases. Manderville *et. al.* showed that prodigiosin binds DNA by intercalating preferably at A-T sites. This finding was based on a series of comparative UV-vis absorbance (**Figure 5.9a**) and fluorescence studies (**Figure 5.9b**). The absorbance for prodigiosin underwent a 6 nm bathochromic shift in the presence of 10 base pair equivalents of ct-DNA, whereas an even smaller shift was observed in presence of poly d[G-C]<sub>2</sub>. Poly d[A-T]<sub>2</sub> induced the highest bathochromic shift of 20 nm for prodigiosin, suggesting that **1** prefers to intercalate at A-T base pairs.

The relative fluorescence intensity of prodigiosin **1** was also compared in the presence of the three varieties of DNA. It was proposed that an intercalated fluorophore, such as prodigiosin **1** will undergo efficient energy transfer from donor DNA base pairs. Indeed, a maximum change in fluorescence intensity of prodigiosin was observed in the presence of the A-T DNA polymer. This was another evidence that prodigiosin intercalates preferably into A-T sites in duplex DNA.

#### **5.4.2 Prodigiosin Inhibits Topoisomerases I and II**

Montaner and colleagues examined the mechanism of action of prodigiosin **1**, focusing on its interaction with DNA and its ability to inhibit both topoisomerase I and topoisomerase II.<sup>41</sup> A single mammalian genome can be approximately 2 meters long, but must be squeezed into a cell nuclear volume of approximately  $10^{-17}$  m<sup>3</sup>.<sup>169</sup> Therefore, cellular DNA is highly compact and generates many curved DNA domains (loops). However, a single-stranded DNA is required for the purpose of replication and other biological processes. Topoisomerases are enzymes involved in relaxing DNA superhelicity.<sup>169</sup> These enzymes can introduce single (type I) or double (type II) DNA

breaks and are involved in DNA repair, replication, transcription, and chromosome segregation during mitosis. Cells that are undergoing rapid proliferation, including cancerous cells, have high levels of topoisomerases I and II. As a result, topoisomerases have been targeted for chemotherapeutic action.

Using a supercoiled plasmid Blue Script cloning vector (pBS) sample and gel electrophoresis, it was shown that prodigiosin intercalates with the DNA helix. In contrast to Manderville's observations,<sup>39</sup> Montaner *et. al.* found that prodigiosin exhibits some preference for the alternating base pairs, but does not discriminate between A-T and G-C sequences. Topoisomerase I and II inhibition was studied by a DNA cleavage assay (TopoGEN) *in vitro* and in cultured cells. The topoisomerases form a catalytic tyrosyl–DNA cleavage intermediate, referred to as the cleavage complex, by covalently binding with DNA. The assay results showed that prodigiosin stabilizes the topoisomerase I and II-DNA cleavage complexes, thereby stimulating enzyme-linked DNA breaks. **Figure 5.10b** shows prodigiosin-treated MCF-7 cells where numerous foci appear in nuclei, indicating high level of ds DNA.

The authors also studied the ability of prodigiosin **1** to induce copper-mediated DNA damage at different pH using a DNA cleavage assay. Their results demonstrated that copper-mediated cleavage activity is enhanced at pH 6.8 rather than pH 7.4. The cleavage activity is also dependent on Cu<sup>2+</sup> ion concentration. The authors pointed out the therapeutic value of prodigiosin due to its effects on several cellular targets. The results from cell assays confirmed the ability of prodigiosin to interact with double-stranded DNA.

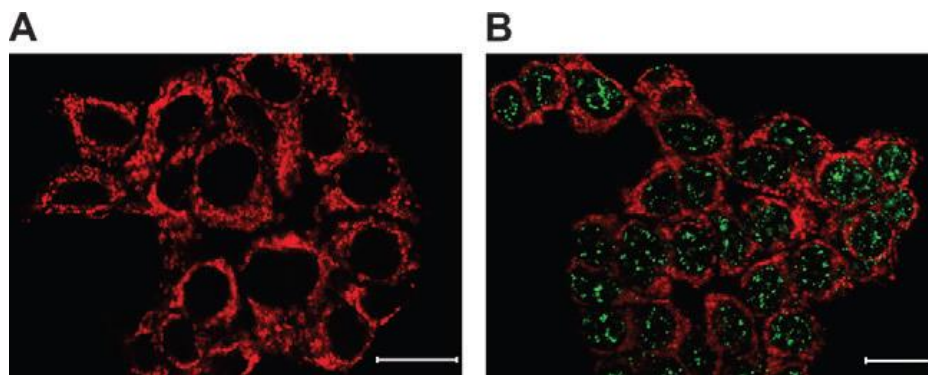


**Figure 5.10.** Prodigiosin-induced ds breakage of genomic DNA independent of the apoptotic process. MCF7 cells untreated (A), or treated with 2  $\mu$ M prodigiosin for 3h (B) were dual stained with primary antibodies directed against apoptosis inducing factor (AIF) and p-H2AX (bar = 20  $\mu$ m). Reprinted with permission from *Toxicological Sciences* **2005**, 85 (2), 870-879. Copyright (2005) Oxford University Press.<sup>41</sup>

### 5.4.3 Prodigiosin Partially Intercalates into ct-DNA

This recent study was a multi-spectroscopic approach to investigate the potential interactions between prodigiosin and ct-DNA.<sup>40</sup> Different techniques like UV-vis absorbance (including thermal denaturation monitoring), fluorescence, circular dichroism and infra-red spectroscopy were used to study the interaction between **1** and ct-DNA. It was found that the melting temperature of ct-DNA increased from 58 to 64  $^{\circ}$ C in the presence of prodigiosin **1**. All these results led towards the assessment that prodigiosin partially intercalates into the DNA helix, something that Manderville had also previously shown.<sup>39</sup>

In the following sections, I report that prodigiosin **1** binds at the 3' end of the G-quadruplex generated by intermolecular assembly of d[ $TG_4T$ ] in the presence of  $K^+$  ions. This conclusion was attained by performing a series of  $^1H$ ,  $^{31}P$  and 2D NMR

experiments, UV-visible spectroscopic and fluorescence titrations. The experiments, observations and inferences made from each experiment are discussed in detail in the following sections.

## Results

### 5.5 G-Quadruplex $K^+ \cdot d[TG_4T]_4$ Increases Solubility of Prodigiosin 1 in Water

A solution of  $d[TG_4T]$  was annealed in the presence of 100 mM KCl in a 10 mM Tris-HCl buffer (pH 7.0) containing 1 mM EDTA in a 90%  $H_2O$ -10%  $D_2O$  solvent system. This oligonucleotide  $d[TG_4T]$  has been previously shown to form a parallel-stranded intermolecular quadruplex with four equivalent grooves in the presence of  $K^+$  ions (**Figure 5.11**).<sup>165, 170</sup>

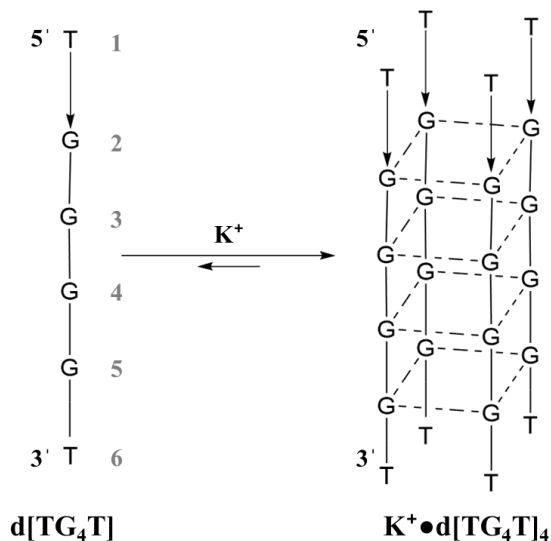


**Figure 5.11.** An illustration showing formation of G-quadruplex  $d[TG_4T]_4$  from hexanucleotide  $5'$ - $d[TG_4T]$ - $3'$  in presence of  $K^+$  cations.

Formation of the  $K^+ \cdot d[TG_4T]_4$  G-quadruplex was confirmed by CD spectroscopy (**Figure 5.12**) and  $^1H$  NMR (**Figure 5.15**). When the sample was annealed in the presence of KCl, the CD spectrum showed a strong peak maxima at around 264 nm with a trough around 240 nm. The peak at 264 nm is a characteristic peak for G-quadruplexes formed by  $d[TG_4T]$ .<sup>171</sup>

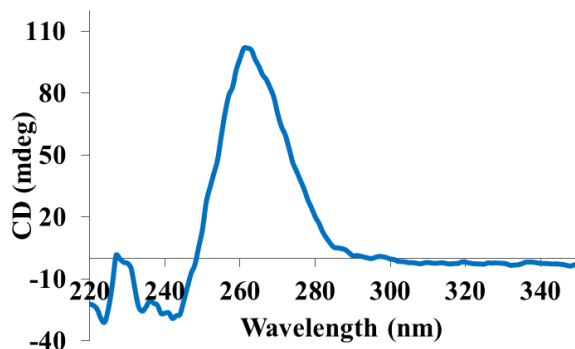


**Figure 5.12.** A CD spectrum showing the characteristic peak for  $d[TG_4T]_4$  in presence of  $K^+$  at 45 °C. A peak maxima was observed at 264 nm and a trough was observed at 240 nm. These two peaks are characteristic for  $K^+ \cdot d[TG_4T]_4$  tetraplex.

Due to the presence of  $\pi$ -conjugation, prodigiosenes have strong absorption bands in the visible regions, which makes it convenient to study their DNA binding properties by UV-vis spectroscopy. Moreover, prodigiosin **1** has a low solubility in water (18  $\mu\text{mol/L}$  at pH 7.0 at 25 °C).<sup>141</sup> UV-vis experiments allowed us to study the interaction between G-quadruplex DNA and prodigiosin, even at micromolar concentrations of compound **1**. To investigate this, a UV-vis titration was performed between **1** and  $K^+ \cdot d[TG_4T]_4$  quadruplex. For this titration, a suspension containing prodigiosin **1** (presumably 50  $\mu\text{M}$ ) was taken in a cuvette. Initially, prodigiosin was

insoluble in water and little absorbance was recorded. Then, increasing equivalents of  $K^+ \cdot d[TG_4T]_4$  were added to the sample. The absorbance was recorded after each addition of G-quadruplex DNA. As increasing amounts of G-quadruplex DNA were added to the cuvette sample containing prodigiosin **1**, a distinct increase in absorbance of **1** was noticed (**Figure 5.13a**). This increase in absorbance is presumably due to a greater amount of **1** getting dissolved in solution aided by the G-quadruplex DNA. The color of the solution also changed from orange to pink, which is a visual indicator for the protonated form of prodigiosin ( $1 \cdot H^+$ ).<sup>132</sup>

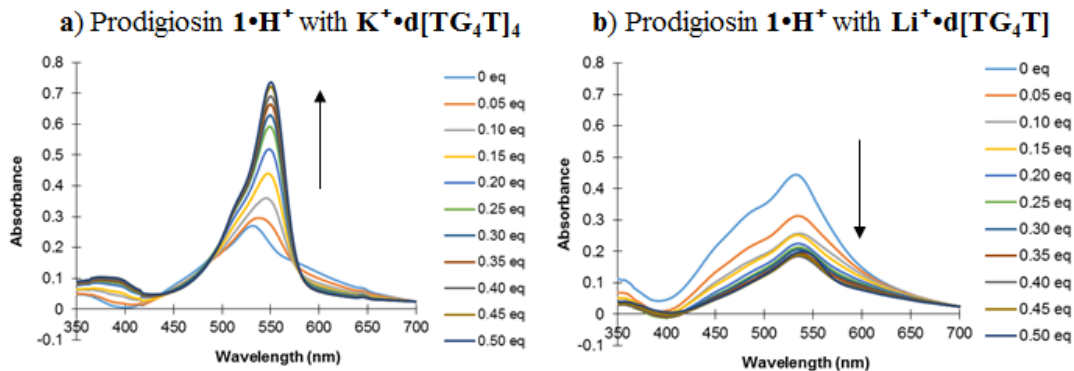


**Figure 5.13.** A UV-Vis titration plot between prodigiosin  $1 \cdot H^+$  ( $\sim 50 \mu M$ ) and variable equivalents of a)  $K^+ \cdot d[TG_4T]_4$  or b)  $Li^+ \cdot d[TG_4T]$  at  $37^\circ C$ . Solutions were made in 10 mM Tris - 1 mM EDTA buffer solutions containing 100 mM KCl or LiCl in 90%  $H_2O$ -10%  $D_2O$  at pH 7. Addition of G-quadruplex DNA causes increase in absorbance of prodigiosin. Soret band of prodigiosin also undergoes a red shift of 20 nm. Addition of single-stranded DNA in LiCl buffer decreased the absorbance of prodigiosin.

Additionally, changes in the Soret band (at 531 nm) of  $1 \cdot H^+$  were observed in presence of G-quadruplex  $K^+ \cdot d[TG_4T]_4$ . This Soret band underwent a red shift of

almost 20 nm during the titration. A red shift for the ligand in presence of DNA is characteristic of DNA-ligand binding.<sup>161, 171</sup> As a control, single-stranded d[TG<sub>4</sub>T] in LiCl buffer was titrated into a solution of **1**. In this case, the absorbance for **1**•H<sup>+</sup> decreased initially and became constant later (**Figure 5.13b**). Addition of single-stranded Li<sup>+</sup>•d[TG<sub>4</sub>T] DNA did not assist in dissolving prodigiosin in aqueous buffer solution, unlike for the case of the G-quadruplex K<sup>+</sup>•d[TG<sub>4</sub>T]<sub>4</sub>.

## **5.6 Fluorescence Studies Indicate Interactions Between G-Quadruplex and Prodigiosin**

Fluorescence spectroscopy is a sensitive and an excellent tool to gain information about interactions between a G-quadruplex and a binding ligand. Prodigiosin **1**•H<sup>+</sup> exhibits a weak emission spectrum by itself in an aqueous solution. However, the fluorescence emission intensity of prodigiosin increased in the presence of G-quadruplex DNA, presumably due to its interaction with the bases in G-quartets. Manderville *et. al.* have also shown that fluorescence of prodigiosin was enhanced in presence of polymeric AT-rich DNA.<sup>39</sup>

To study the changes in fluorescence emission intensity of prodigiosin **1**•H<sup>+</sup> in presence of G-quadruplex, a fluorescence titration experiment was performed between **1**•H<sup>+</sup> and K<sup>+</sup>•d[TG<sub>4</sub>T]<sub>4</sub>. In a solution containing prodigiosin, varying equivalents of tetraplex DNA were added. Fluorescence intensity of prodigiosin was measured after each addition of quadruplex DNA. Addition of K<sup>+</sup>•d[TG<sub>4</sub>T]<sub>4</sub> led to a significant increase in fluorescence of prodigiosin (**Figure 5.14a**). When the same titration experiment was performed with Tris-KCl-EDTA buffer (no DNA) as a control, no



change in fluorescence of prodigiosin was observed. (Figure 5.14b). Thus, fluorescence of prodigiosin is only affected in presence of the G-quadruplex DNA.

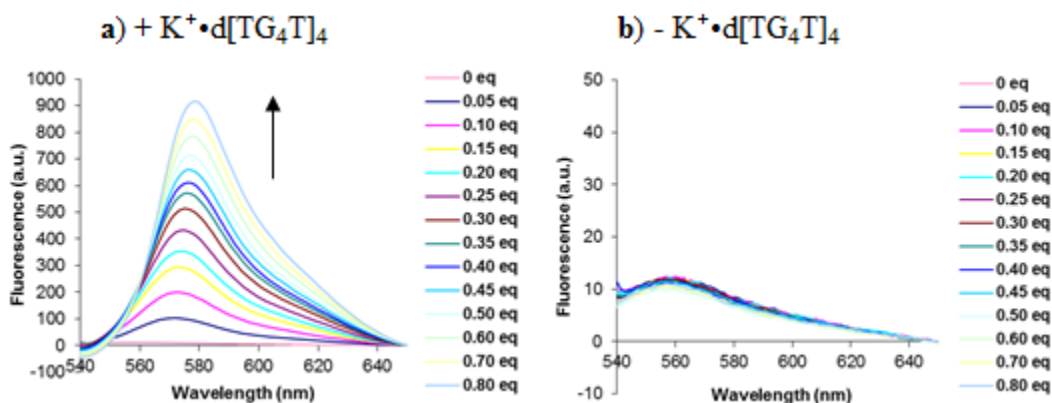


**Figure 5.14.** A fluorescence titration plot between 50  $\mu\text{M}$  prodigiosin  $1\cdot\text{H}^+$  and variable equivalents of a)  $\text{K}^+\cdot\text{d}[\text{TG}_4\text{T}]_4$  b) KCl buffer at 37  $^\circ\text{C}$ . Solutions were made in 10 mM Tris-100 mM KCl-1 mM EDTA buffer solutions in 90%  $\text{H}_2\text{O}$ -10%  $\text{D}_2\text{O}$  at pH 7. Addition of G-quadruplex DNA causes the fluorescence intensity of prodigiosin  $1\cdot\text{H}^+$  to increase. Addition of KCl buffer, without DNA, caused no change to prodigiosin's fluorescence intensity.

In his work, Manderville had pointed out that enhancement in fluorescence of a ligand upon addition of DNA is diagnostic of binding between the two species. In particular, he wrote that the increase in fluorescence is “...ascribed to decreases in degrees of freedom of molecular motion, prevention of collisional deactivation, restricted conformations, favorable microenvironmental polarity effect, and shielding of the excited state from water molecules or other species present in the bulk aqueous solution”. Further, energy from a donor base-pairs (DNA) to the acceptor ligand molecule (prodigiosin) can take place only when the ligand intercalates or stacks with

the base pairs, which can be monitored by fluorescence measurements.<sup>39</sup> This explanation and the results from our fluorescence experiments is again consistent with the proposal that prodigiosin is interacting with the G-quadruplex, probably by intercalation or end-stacking with the G-quartet.

## **5.7 NMR Experiments Reveal that Prodigiosin 1 Binds the G-Quadruplex $K^+ \cdot d[TG_4T]_4$ at its 3' End**

The NMR experiments were initiated by first confirming the formation of G-quadruplex by the sequence  $d[TG_4T]$ . Having confirmed that, I next set out to undertake certain NMR experiments that might probe binding between the G-tetraplex  $K^+ \cdot d[TG_4T]_4$  and prodigiosin 1.

### **5.7.1 Characterization of the $d[TG_4T]_4$ Quadruplex in Solution by $^1H$ NMR**

A solution of  $d[TG_4T]$  was annealed in the presence of 100 mM KCl in a 10 mM Tris-HCl buffer (pH 7.0) containing 1 mM EDTA in a 90%  $H_2O$ -10%  $D_2O$  solvent system. A set of six distinct peaks around the region 7-8 ppm were visible in the  $^1H$  NMR spectrum at 45 °C (**Figure 5.15**). This diagnostic pattern of peaks has been previously identified for a G-quadruplex structure.<sup>165</sup> Four of these peaks belonged to the four H8 protons on the guanosine bases and the remaining two peaks belonged to the H6 protons on the terminal thymine bases. Since the 5'- $d[TG_4T]_4$ -3' tetraplex is a symmetric tetramolecular assembly, all four guanines from a single tetrad are equivalent by NMR. As a result, they resonate at the same frequency, which gives rise to only one peak per G-tetrad. Therefore, only six peaks are visible in the aromatic region, one for each residue in the sequence. Further, four sharp peaks were observed

for the NH imino proton at N1 position of each of the guanosine bases. These NH imino protons are visible in the NMR spectrum because they are involved in G-quartet formation and, therefore, they are in a relatively slow exchange with the solvent.

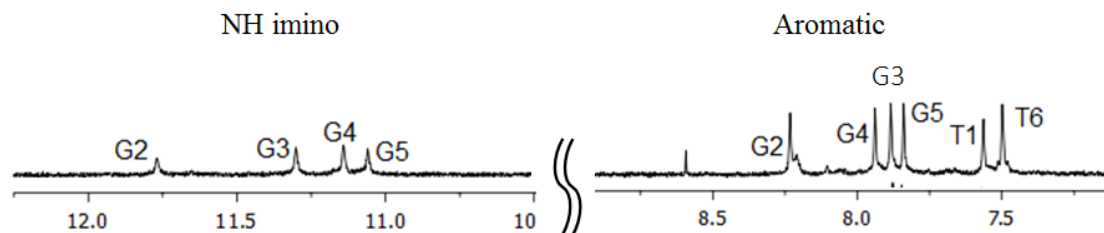


**Figure 5.15.** A portion of the  $^1\text{H}$  NMR of  $\text{K}^+\cdot\text{d}[\text{TG}_4\text{T}]_4$  quadruplex in 90%  $\text{H}_2\text{O}$ -10%  $\text{D}_2\text{O}$  at  $45^\circ\text{C}$  showing six peaks in the aromatic region ( $\delta$  9.0-7.0 ppm), corresponding to the H8 proton on four guanosines and H6 proton on two thymine bases. Another four distinct peaks ( $\delta$  12.0-11.0 ppm) are visible for the imino NH protons on guanosine bases that are involved in G-quartet formation. Assignments were made from 2D NMR and from literature.

The peak assignments for aromatic protons were confirmed by 2D-NOESY experiment (**Figure 5.16**) by applying the “sequential walk” technique. Sequential walking is used to solve 2D NMR spectra of oligonucleotides. In a DNA sequence, the H6 or H8 proton in the aromatic region of each nucleotide is in close proximity to its own H1' sugar proton and a 3' neighbor H1' proton, and would therefore, show a NOESY correlation. For sequential assignments, terminal nucleotides are identified first, depending on different criteria. Sometimes, terminal deoxyriboses are not phosphorylated, so they can be identified by the high field shifts of their 5'  $\text{CH}_2$  or 3' H, or absence of  $^{31}\text{P}$  couplings with these protons. Additionally, the terminal

deoxyribose exhibit only intranucleotide NOEs, which can be used to identify them.<sup>172</sup> Once the cross-peak for T1 base was determined (**Figure 5.16**), the next base was identified by "walking" across the spectrum (to H8 of G2 base). This process was then repeated sequentially until all nucleotides had been assigned.

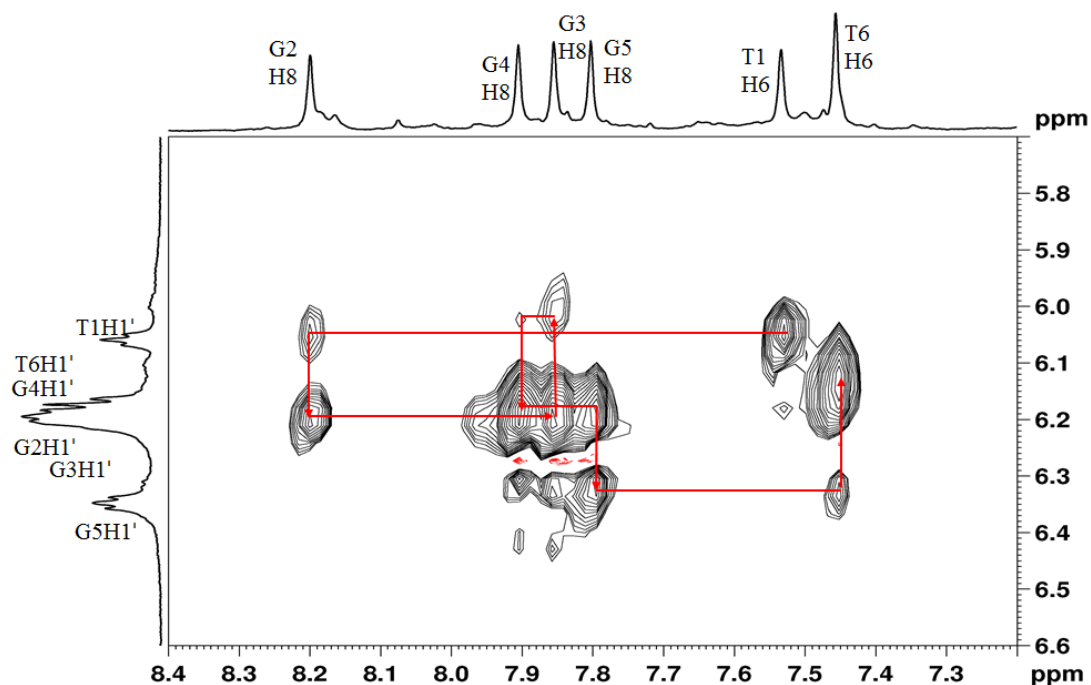


**Figure 5.16.** A 2D NOESY spectrum of  $K^+\cdot d[ TG_4T ]_4$  correlating the aromatic protons on the bases (top) with the H1' protons on sugars (left) in 90%  $H_2O$ -10%  $D_2O$  at 45 °C.

### 5.7.2 NMR Experiments Probing Binding of Prodigiosin 1 to $K^+\cdot d[ TG_4T ]_4$

To study the binding properties of prodigiosin, NMR titrations were performed between the host ( $K^+\cdot d[ TG_4T ]_4$ ) and guest (prodigiosin) molecules. These titrations were performed using 90%  $H_2O$ -10%  $D_2O$  as solvent. Prodigiosin **1** was dissolved in  $d_6$ -DMSO and added in increments to the NMR sample of  $K^+\cdot d[ TG_4T ]_4$ . Both  $^1H$  and

$^{31}\text{P}$  NMR experiments were performed on the sample to study the interaction of prodigiosin with the DNA bases as well as with the phosphate groups.

#### 5.7.2.1 Titration with Prodigiosin 1 in 90% H<sub>2</sub>O-10% D<sub>2</sub>O

To carry out this experiment, a sample of  $\text{K}^+\cdot\text{d}[\text{TG}_4\text{T}]_4$  (0.5 mM tetraplex) was used. Aliquots of prodigiosin **1** dissolved in  $d_6$ -DMSO were titrated into this aqueous NMR sample. In analyzing the  $^1\text{H}$  NMR titration, the chemical shifts for the aromatic protons of the G5 and T6 bases moved downfield most significantly as increasing amounts of prodigiosin was added to the sample (**Figure 5.17**). The bottom spectrum in **Figure 5.17** shows that the H6 proton of T6 base had shifted downfield by almost 0.2 ppm from its original position after the addition of a presumed “3.75” eq of **1**. Peak for H8 proton of G5 residue moved downfield as well. The change in chemical shift of T6 proton was accompanied by the broadening and eventually, disappearance of the signal. However, the signal reappeared at around “6 eq” of prodigiosin **1**• $\text{H}^+$ . By the end of the titration (bottom spectrum in **Figure 5.17**), a broad but significant peak for T6 aromatic proton was observed. A 2D NOESY spectrum was also carried out with a NMR sample containing  $\text{K}^+\cdot\text{d}[\text{TG}_4\text{T}]_4$  and an apparent “4.5 eq” of **1**• $\text{H}^+$  to assign and confirm the movement of these signals (**Figure 5.18**). The two peaks corresponding to G5 and T6 aromatic protons were confirmed to have moved farthest downfield as compared to the original G-quadruplex sample with no added prodigiosin **1**. In contrast, the titration indicated that the NMR signals for the aromatic protons for the first four residues 5'-T1-G2-G3-G4-3' did not change nearly as much as the G5 and T6 signals at the DNA's 3' end.

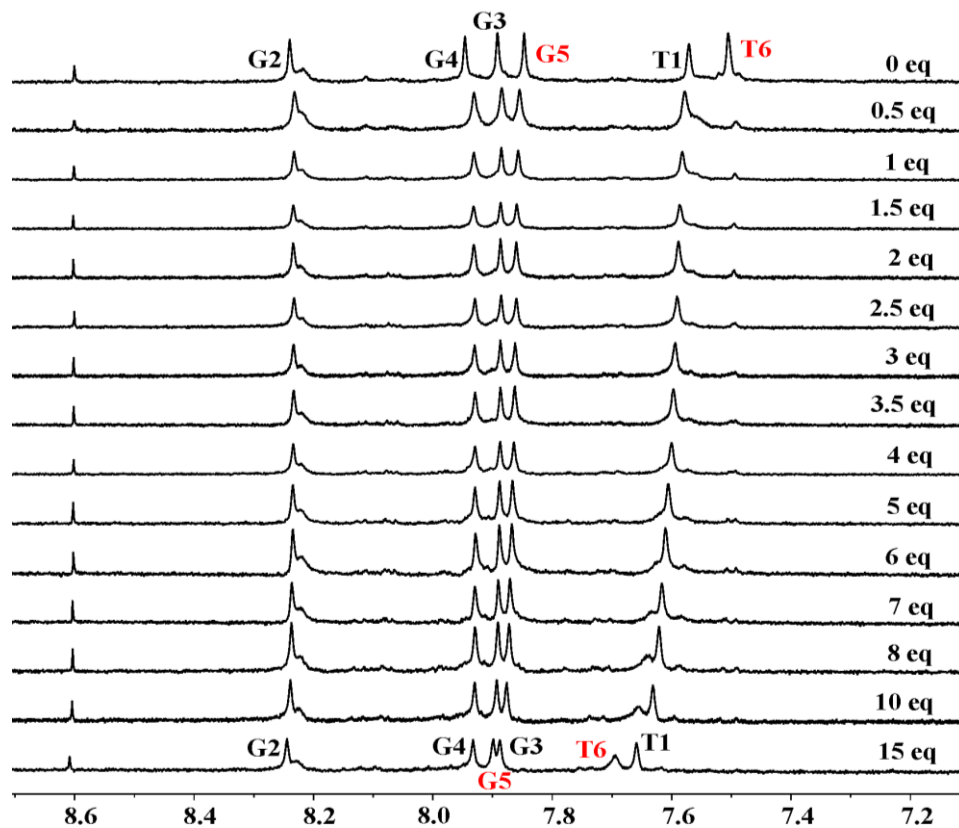


**Figure 5.17.** <sup>1</sup>H NMR stack plot showing titration of  $K^+ \cdot d[ TG_4T ]_4$  with varying “apparent” equivalents of prodigiosin  $1 \cdot H^+$  in 90%  $H_2O$ -10%  $D_2O$  at 45 °C. The G5 and T6 resonances are highlighted in red to show the change in the position of H6 proton of T6, and H8 proton of G5 base at the start and end of titration.

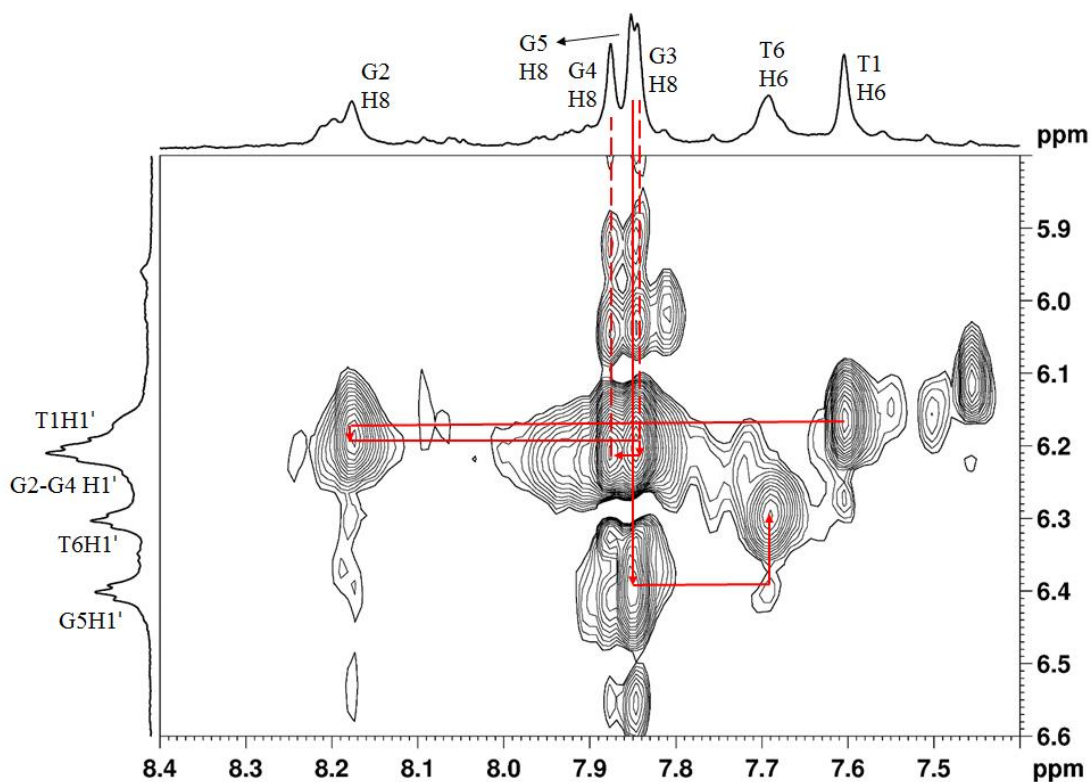


**Figure 5.18.** A 2D NOESY spectrum of  $K^+\cdot d[ TG_4T ]_4$  with “4.5 eq” of prodigiosin  $1\cdot H^+$  in 90%  $H_2O$ -10%  $D_2O$  at 45  $^{\circ}C$ . This spectrum correlates the aromatic protons on bases (top) with the  $H1'$  proton on sugars (left). The experiment confirmed that T6 H6 and G5 H8 had undergone largest changes in  $^1H$  chemical shifts.

Since the most significant change in chemical shift was observed for the aromatic protons on the G5 and T6 bases upon addition of prodigiosin **1**, we proposed that prodigiosin preferably binds at the 3' end of the G-quadruplex  $K^+\cdot d[ TG_4T ]_4$ , probably by end-stacking on the terminal G-quartet (**Figure 5.19**).

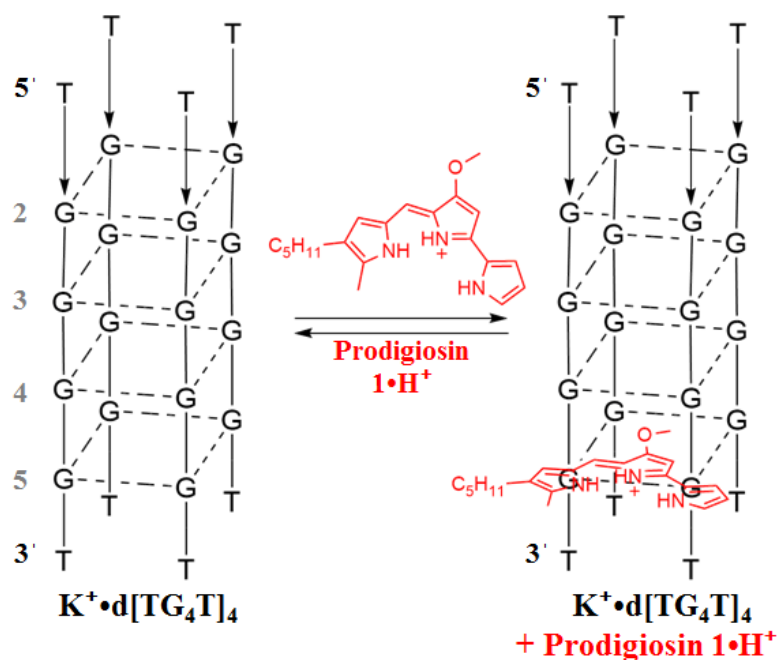


**Figure 5.19.** An illustration showing interaction between protonated form of prodigiosin  $1 \cdot H^+$  and G-quadruplex  $K^+ \cdot d[TG_4T]_4$ . Prodigiosin binds at the 3' end.

### 5.7.2.2 NMR Control Experiments with $d_6$ -DMSO and $K^+ \cdot d[TG_4T]_4$

In a recent publication, Gokel *et al.* addressed the DMSO-aqueous solution conundrum in biological assays.<sup>173</sup> While testing a series of pyrogallol[4]arenes and antibiotic kanamycin for their toxicity to *E. coli*, the authors realized that what seemed like an enhancement of potency of kanamycin against *E. coli* was actually due to the presence of DMSO in the growth media. There are other instances as well where DMSO has interfered in the biological activity with drug testing.<sup>174</sup> Therefore, it was essential to investigate the effect of  $d_6$ -DMSO on the G-quadruplex  $K^+ \cdot d[TG_4T]_4$  since we were adding prodigiosin dissolved in DMSO to the G-quadruplex. The control titration experiment using  $d_6$ -DMSO was performed following the same procedure as described in the last section. Incremental volumes of  $d_6$ -DMSO was added to a solution



of  $K^+ \cdot d[TG_4T]_4$  (0.5 mM tetraplex) followed by recording of  $^1H$  and  $^{31}P$  NMR spectra (Figure 5.20).

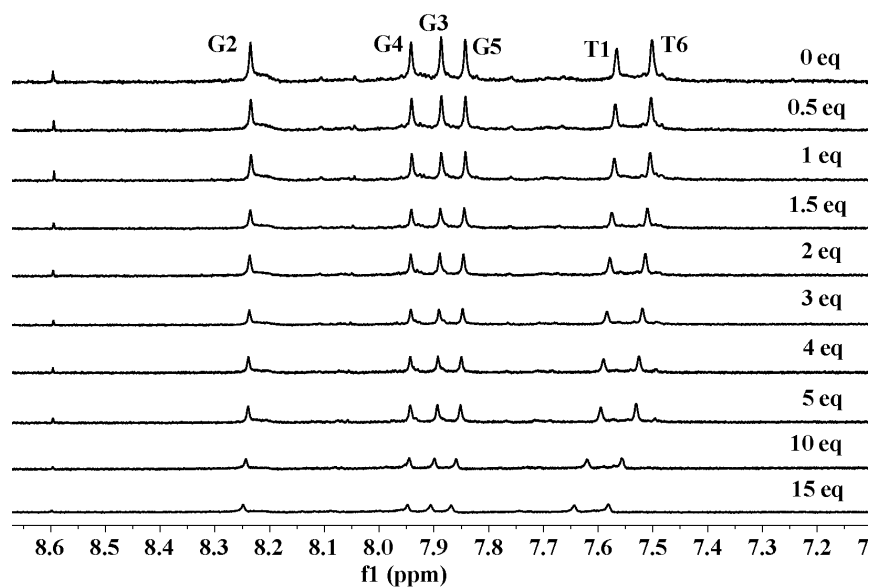


**Figure 5.20.**  $^1H$  NMR stack plot showing titration of  $K^+ \cdot d[TG_4T]_4$  with  $d_6$ -DMSO in 90%  $H_2O$ -10%  $D_2O$  at 45  $^{\circ}C$ . The only changes in chemical shifts observed were for H6 protons of thymines.

**Figure 5.20** shows that DMSO has little effect on chemical shift of DNA. The observed changes in chemical shifts are different from the changes seen in **Figure 5.17** ( $^1H$  NMR stack plot showing titration of  $K^+ \cdot d[TG_4T]_4$  with prodigiosin  $1 \cdot H^+$ ). In the  $^1H$  NMR stack plot, the peaks that underwent the most change in chemical shifts were of the terminal thymine bases T1 and T6 (**Figure 5.20**). Due to the quadruplex structure, terminal groups tend to be most exposed to the solvent. As a result, addition of DMSO caused the peaks for thymine to shift more in comparison to the internal guanosine bases. Thus, the conclusion was that in the titration between  $K^+ \cdot d[TG_4T]_4$

and prodigiosin  $\mathbf{1\cdot H^+}$  (**Figure 5.17**), the significant changes in the G5 and T6 residues are caused by prodigiosin and not added DMSO.

### 5.7.2.3 $^{31}\text{P}$ NMR to Investigate Groove Binding by Prodigiosin

All these NMR experiments were done at pH 7. As described in **Section 2.5**, prodigiosin has a  $\text{pK}_a$  of 8.2,<sup>114</sup> which means that at pH 7, **1** exists mostly in its protonated form ( $\mathbf{1\cdot H^+}$ ). I wanted to determine if protonated  $\mathbf{1\cdot H^+}$  might interact with the negatively-charged phosphate groups located in the grooves of the G-quadruplex. To explore this possibility, separate  $^{31}\text{P}$  NMR titrations were carried out with  $\text{K}^+\cdot\text{d}[\text{TG}_4\text{T}]_4$  and prodigiosin **1** (**Figure 5.21a**) and blank  $d_6$ -DMSO (**Figure 5.21b**). The titration with DMSO was done to address our concern that the DMSO solvent, added along with prodigiosin  $\mathbf{1\cdot H^+}$  (15% relative to total NMR sample volume by the end of the titration), could be causing conformational changes to the G-quadruplex due to molecular crowding and water depletion.<sup>175</sup> In both the titrations involving  $\text{K}^+\cdot\text{d}[\text{TG}_4\text{T}]_4$  with either prodigiosin (**Figure 5.21a**) or  $d_6$ -DMSO (**Figure 5.21b**), peaks for phosphate groups at 1 and 5 positions came close to each other. This effect was more pronounced in the case of prodigiosin  $\mathbf{1\cdot H^+}$  (“15 eq” in **Figure 5.21a**). Conversely, peaks for phosphate groups at 2 and 4 positions behaved differently in presence of prodigiosin  $\mathbf{1\cdot H^+}$  and  $d_6$ -DMSO. For prodigiosin  $\mathbf{1\cdot H^+}$ , the peaks interchanged positions between 0.5 and 4 eq of  $\mathbf{1\cdot H^+}$ . But in the case of  $d_6$ -DMSO, the peaks for P2 and P4 phosphate groups didn’t interchange position until the addition of 5 eq of DMSO. The final order of NMR resonances for phosphate groups at “15 eq” in both  $^{31}\text{P}$  NMR stack plots was the same (5'-P1-P5-P3-P2-P4-3'). The similarity in final

effects on phosphate groups of  $K^+ \cdot d[TG_4T]_4$  G-quadruplex by both prodigiosin  $1 \cdot H^+$  and  $d_6$ -DMSO suggests that a) DMSO is not causing any conformational changes to the G-quadruplex  $K^+ \cdot d[TG_4T]_4$  (based on  $^1H$  and  $^{31}P$  NMR data); b) prodigiosin  $1 \cdot H^+$  interacts with phosphate groups in the grooves of the DNA assembly. Therefore, the ligand binding possibly takes place at two positions in the quadruplex – end-stacking at the terminal 3'-G-quartet and/or interactions in the G-quadruplex grooves.

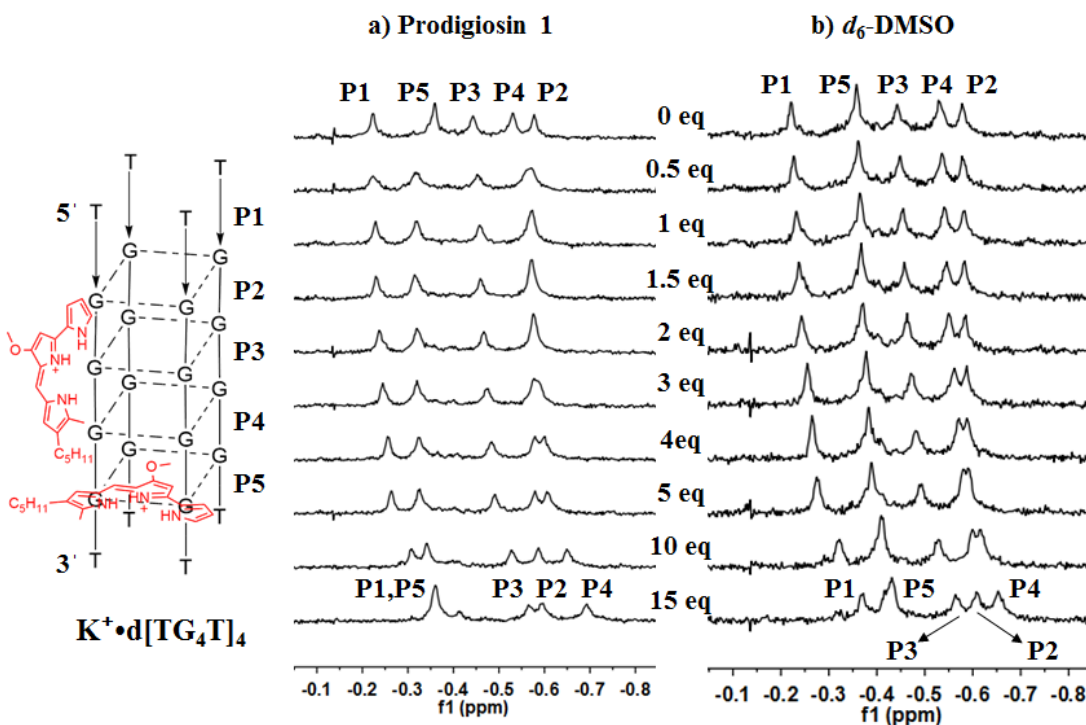


**Figure 5.21.**  $^{31}P$  NMR stack plot showing titration of  $K^+ \cdot d[TG_4T]_4$  with a) prodigiosin  $1 \cdot H^+$  and b)  $d_6$ -DMSO in 90%  $H_2O$ -10%  $D_2O$  at 45  $^{\circ}C$ .

The peaks in the  $^{31}P$  NMR spectrum were assigned by carrying out a  $^1H$ - $^{31}P$  HSQC experiments at 0 eq and “4.5 eq” of prodigiosin  $1 \cdot H^+$  (Figure 5.22). This is the first time that the  $^{31}P$  NMR for the  $d[TG_4T]_4$  nucleotide sequence has been characterized. Phosphate groups are located in between two sugars. By correlating the

sugar  $^1\text{H}$  signals with  $^{31}\text{P}$  NMR signals, the chemical shift assignment and location of each phosphate group in the oligonucleotide can be determined. A  $^1\text{H}$ - $^{31}\text{P}$  HSQC experiment was also performed with the sample containing  $\text{K}^+\cdot\text{d}[\text{TG}_4\text{T}]_4$  G-quadruplex and  $d_6$ -DMSO (from **Figure 5.21b**).

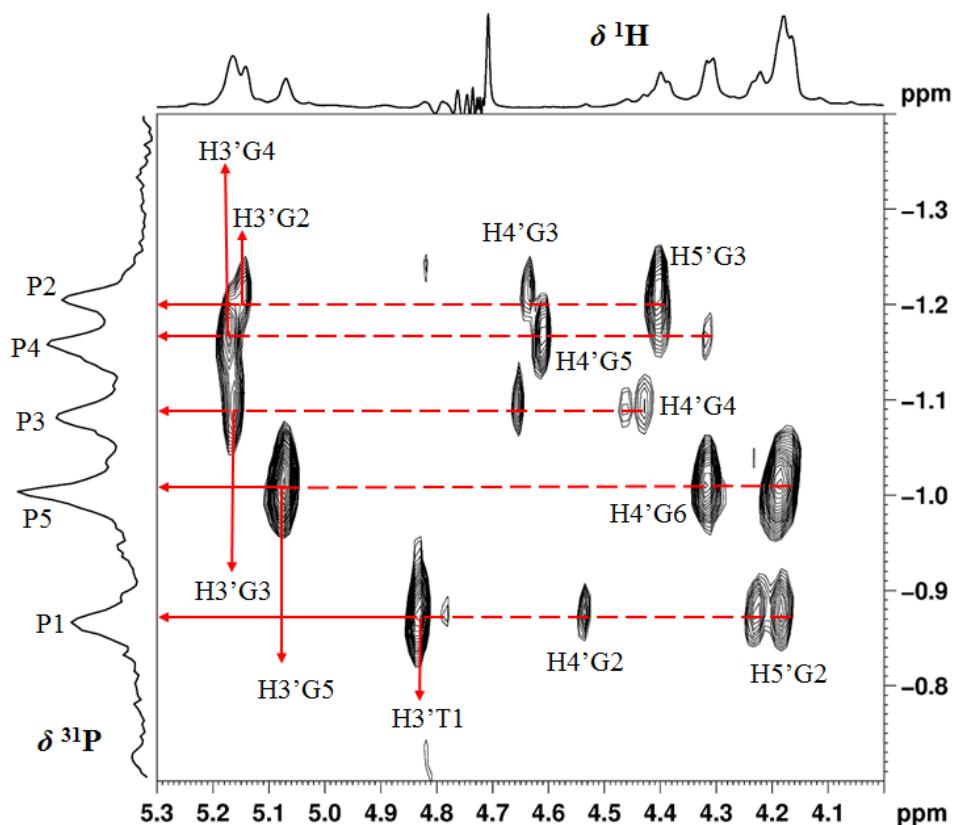


**Figure 5.22.** A 2D  $^1\text{H}$ - $^{31}\text{P}$  HSQC spectrum of  $\text{K}^+\cdot\text{d}[\text{TG}_4\text{T}]_4$  in 90%  $\text{H}_2\text{O}$ -10%  $\text{D}_2\text{O}$  at 45  $^\circ\text{C}$ . This spectrum correlates the sugar protons ( $\text{H}3'$ ,  $\text{H}4'$ ,  $\text{H}5'$  and  $\text{H}5''$  on top) with the phosphate groups (left).

### 5.7.3 Prodigiosin Does Not Bind to Single-Stranded DNA

Although prodigiosin is known to bind dsDNA,<sup>39-41</sup> we were concerned whether prodigiosin  $1\cdot\text{H}^+$  selectively binds with a G-quadruplex in comparison to a DNA

single-strand. To address this concern, I performed a  $^1\text{H}$  NMR titration experiment with single-stranded DNA. For this purpose,  $\text{d}[\text{TG}_4\text{T}]$  was annealed in the presence of 100 mM LiCl (1 mM EDTA-10 mM Tris-HCl buffer; 90%  $\text{H}_2\text{O}$ -10%  $\text{D}_2\text{O}$  at pH 7.0). As  $\text{Li}^+$  does not stabilize a G-quadruplex structure,  $\text{d}[\text{TG}_4\text{T}]$  exists in the single-strand conformation in LiCl solution.<sup>165,176</sup> The  $^1\text{H}$  NMR spectrum for  $\text{Li}^+\cdot\text{d}[\text{TG}_4\text{T}]$  is shown in the top trace of **Figure 5.23**. Six peaks for aromatic protons from each base were visible in the region of 7.5-8.5 ppm. The chemical shifts for each of these peaks have been previously assigned and are different for the single-strand as compared to the G-quadruplex  $\text{K}^+\cdot\text{d}[\text{TG}_4\text{T}]_4$ .<sup>164</sup> Moreover, unlike  $\text{K}^+\cdot\text{d}[\text{TG}_4\text{T}]_4$ , no peaks were observed for the NH imino protons in the region of  $\delta$  10-12 ppm for  $\text{d}[\text{TG}_4\text{T}]$ . This is because as a single-stranded conformation of  $\text{d}[\text{TG}_4\text{T}]$ , the imino NH protons are free to undergo exchange with the solvent ( $\text{H}_2\text{O}$ ).

A  $^1\text{H}$  NMR titration was performed between  $\text{Li}^+\cdot\text{d}[\text{TG}_4\text{T}]$  solution and prodigiosin  $\mathbf{1}\cdot\text{H}^+$  (**Figure 5.23**). Upon adding  $\mathbf{1}\cdot\text{H}^+$  to the NMR sample of DNA, very small changes in chemical shifts were observed for all protons in the  $\text{d}[\text{TG}_4\text{T}]$  single strand. Since no major changes in NMR peaks were observed, the conclusion was that  $\mathbf{1}$  does not interact with the single-stranded DNA  $\text{d}[\text{TG}_4\text{T}]$ .

From these NMR experiments, two conclusions can be made: a) prodigiosin selectively binds quadruplex in comparison to the single-stranded DNA and, b) prodigiosin end-stacks at the 3' end of the  $\text{d}[\text{TG}_4\text{T}]_4$  quadruplex and interacts with the phosphate groups in the G-quadruplex backbone.

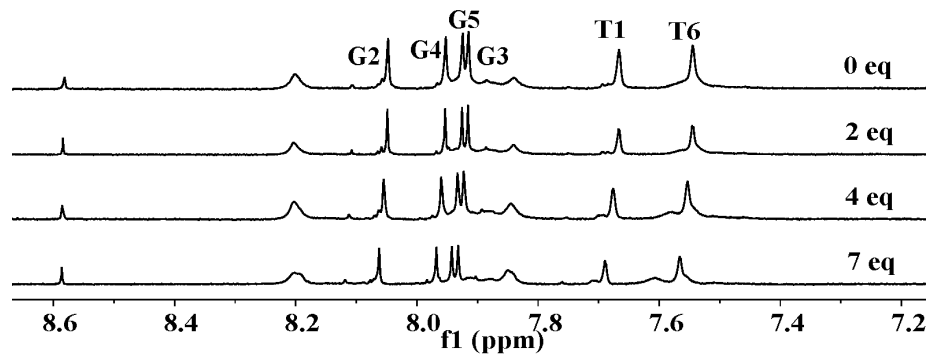


**Figure 5.23.**  $^1\text{H}$  NMR stack plot showing titration of  $\text{Li}^+\cdot\text{d}[\text{TG}_4\text{T}]$  with prodigiosin  $\mathbf{1}\cdot\text{H}^+$  in 90%  $\text{H}_2\text{O}$ -10%  $\text{D}_2\text{O}$  at 45  $^\circ\text{C}$ .

## 5.8 NMR Experiments in Mixed Solvent Systems

Even though binding between prodigiosin and G-quadruplex DNA was established by NMR studies in 90%  $\text{H}_2\text{O}$ -10%  $\text{D}_2\text{O}$ , we were concerned about the poor solubility of prodigiosin **1** in aqueous buffer. Additionally, no signals were detected for prodigiosin in NMR experiments using 90%  $\text{H}_2\text{O}$ -10%  $\text{D}_2\text{O}$  as solvent, even when excess of **1** was added to the solution. For this reason, a mixed solvent system was used, where both DNA and ligand were soluble, to study the binding of prodigiosin **1** and  $\text{K}^+\cdot\text{d}[\text{TG}_4\text{T}]_4$  in solution. A 1:1 mixture of  $d_6$ -DMSO and 90%  $\text{H}_2\text{O}$ -10%  $\text{D}_2\text{O}$  was used for the experiments described in this section. DMSO was chosen as the co-solvent because a) it solubilizes prodigiosin **1** and b) it is miscible with water.

### 5.8.1 NMR Titration in $d_6$ -DMSO: 90% $\text{H}_2\text{O}$ -10% $\text{D}_2\text{O}$ (1:1) Mixture

Before starting binding studies with the DNA-prodigiosin system, peaks assignments were made for prodigiosin in this mixed solvent system. 1D-Selective Total correlation spectroscopy (TOCSY) was used for assigning peaks belonging to

prodigiosin.<sup>177</sup> TOCSY is similar to COSY as it allows detection of cross-peaks for any nuclei that are directly coupled to each other. Additionally, data from a TOCSY experiment also allows one to detect cross-peaks for nuclei that are connected by a chain of couplings. Therefore, it is highly useful for identifying large interconnected networks of spin couplings.

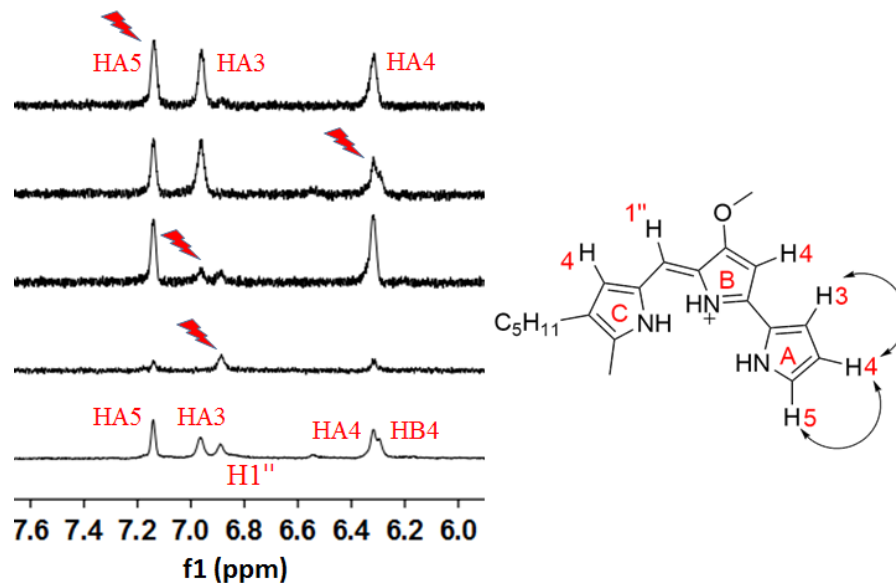


**Figure 5.24.** TOCSY NMR showing correlations between ring A resonances (H3, H4 and H5) in prodigiosin (1 mM) in a 1:1 mixture of  $d_6$ -DMSO and 90%  $H_2O$ -10%  $D_2O$  at 45 °C. Strong correlations were observed between all three protons on ring A.

As shown in **Figure 5.24**, peaks for protons belonging to the rings A and B in  $1\cdot H^+$  were identified from these experiments. First, specific peaks for protons in ring A were irradiated one by one. The protons that coupled with the irradiated peak showed up in the 1D-selective TOCSY spectrum. For example, when the H5 resonance in Ring

A was irradiated, the peaks for H3 and H4 protons on the ring A gave a positive correlation (top spectrum in **Figure 5.24**

). Similarly, protons H3 and H4 on ring A and H1'' were irradiated. All three protons from ring A showed correlations with each other.

Peaks for the G-quadruplex DNA were assigned using NOESY and HSQC experiments as described in **Section 5.7**. Phan *et al.* have previously shown by NMR that certain G-quadruplex DNA fragments can undergo conformational changes under conditions of molecular crowding.<sup>148,175</sup> We found that the G-quadruplex  $K^+ \cdot d[ TG_4 T ]_4$  remained intact in this mixed solvent system. Next, the interactions between G-quadruplex DNA and prodigiosin were explored in the mixed solvent using a NMR titration. A 1 mM solution of prodigiosin  $1 \cdot H^+$  was taken in the mixed solvent system. Variable equivalents of G-quadruplex  $K^+ \cdot d[ TG_4 T ]_4$  were added to the prodigiosin samples (**Figure 5.25**). Concentrations and stoichiometries of G-quadruplex DNA and prodigiosin were determined based on UV-vis absorbance spectra. As a reference, a  $^1H$  NMR spectrum of a G-quadruplex  $K^+ \cdot d[ TG_4 T ]_4$  DNA sample by itself in the mixed solvent system is shown in the lower trace (**Figure 5.25a**). The NMR spectrum is similar to the peak pattern observed in aqueous buffer (**Figure 5.17****Figure 5**). In the presence of 50%  $d_6$ -DMSO, the peaks for H6 protons of T1 and T6 bases move close to each other. To a sample of prodigiosin  $1 \cdot H^+$ , equivalents of tetraplex DNA were added (**Figure 5.25b-d**). Unlike previous titration in aqueous buffer (**Figure 5.17**), the  $^1H$  NMR signals for prodigiosin could be easily identified in the mixed solvent sample. Resonances arising from ring A (H3, H4 and H5) were identified along with H4 on ring



B (Figure 5.25b). As equivalents of tetraplex DNA were added, the peaks corresponding to the A and B ring protons of prodigiosin  $1\cdot\text{H}^+$  shifted upfield (Figure 5.25b-d). For the  $^1\text{H}$  NMR resonances belonging to G-quadruplex  $\text{K}^+\cdot\text{d}[\text{TG}_4\text{T}]_4$ , the observed changes in chemical shifts were similar to previous titration in aqueous buffer (Figure 5.17). NMR signals belonging to H8 proton of G5 and H6 proton of T6 shifted downfield indicating binding between the 3' end of the G-quadruplex and prodigiosin.

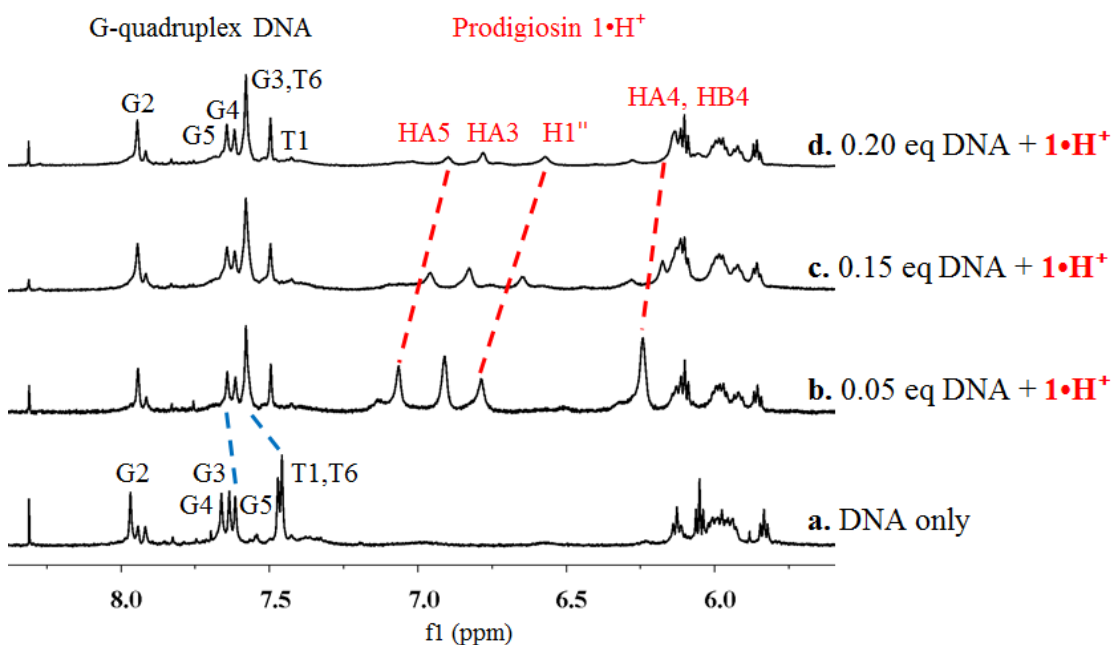


**Figure 5.25.**  $^1\text{H}$  NMR stack plot showing titration of prodigiosin  $1\cdot\text{H}^+$  (1 mM) with different eq of  $\text{K}^+\cdot\text{d}[\text{TG}_4\text{T}]_4$  in 1:1 mixture of  $d_6$ -DMSO and 90%  $\text{H}_2\text{O}$ -10%  $\text{D}_2\text{O}$  at 45 °C. Bottom trace (a) is of G-quadruplex  $\text{K}^+\cdot\text{d}[\text{TG}_4\text{T}]_4$  DNA sample. The changes in chemical shifts for prodigiosin  $1\cdot\text{H}^+$  protons has been marked by red dashed lines. The changes in chemical shifts of G5 and T6 protons of  $\text{K}^+\cdot\text{d}[\text{TG}_4\text{T}]_4$  G-quadruplex have been marked by blue dashed lines.

The  $^1\text{H}$  NMR titration using  $d_6$ -DMSO and water as a mixed solvent not only allowed the detection of prodigiosin in solution, but also helped in monitoring the changes in chemical shifts of some of the aromatic protons on prodigiosin  $\mathbf{1}\cdot\text{H}^+$  upon addition of G-quadruplex DNA. These chemical shift changes for prodigiosin  $\mathbf{1}\cdot\text{H}^+$  indicate that this ligand can bind to G-quadruplex DNA.

### **5.8.2 Saturation Transfer Difference Experiments Confirm Interaction Between Prodigiosin and G-Quadruplex DNA**

Differential frequency-saturation transfer difference (FD-STD) NMR spectroscopy was first introduced in 1999.<sup>178</sup> The goal of STD NMR is to screen libraries of compounds for their binding activity to proteins. STD NMR spectrum shows signals from ligand molecules that have high binding affinity for the protein.<sup>179</sup> Detection of weak binding interactions between ligands and large proteins can possess serious experimental challenges, especially at low physiological concentrations. Saturation transfer difference experiments can be used for a mixture of potential ligands with as little as 1 nmol of protein.<sup>178</sup> As the name suggests, magnetization transferred from the receptor to the bound ligand is measured by directly observing NMR signals from the ligand itself. Low-power irradiation is applied to specific protein signals. The magnetization spreads throughout the protein due to spin diffusion and saturates all protein NMR signals. Signals belonging to a weakly bound ligand become saturated. When the ligand dissociates, intensity of signals decreases as compared to the signals of free ligand in solution. Another experiment is performed where the irradiation pulse hits the spectral region excluding protein and ligand signals. Since no signals are

irradiated, the experiment does not lead to saturation transfer to the ligand signals. A difference spectrum is obtained by subtracting the two resulting spectra. In the final difference spectrum, only signals for the bound ligands are observed.<sup>178</sup>

In 2007, Randazzo *et. al.* used STD NMR to study the binding interactions between distamycin A and d[TG<sub>4</sub>T] quadruplex.<sup>158</sup> These NMR experiments, combined with mechanics and dynamics calculations, helped in establishing that distamycin interacts with d[TG<sub>4</sub>T]<sub>4</sub> in a 4:1 binding mode, with two anti-parallel distamycin dimers binding simultaneously two opposite grooves of the quadruplex.

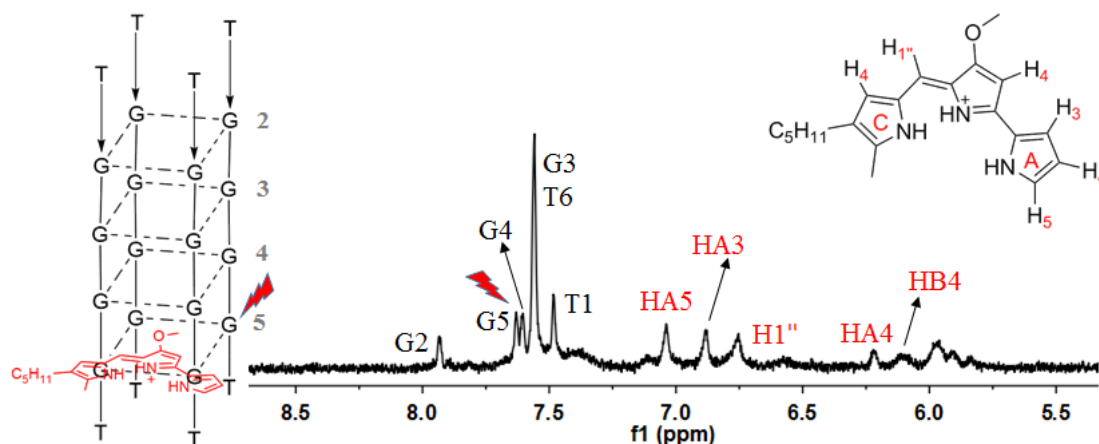


**Figure 5.26.** A STD NMR of 1:20 sample of G-quadruplex K<sup>+</sup>•d[TG<sub>4</sub>T]<sub>4</sub> DNA and prodigiosin 1•H<sup>+</sup> in a 1:1 mixture of *d*<sub>6</sub>-DMSO and 90% H<sub>2</sub>O-10% D<sub>2</sub>O. When <sup>1</sup>H NMR resonance of H8 proton of G5 base on K<sup>+</sup>•d[TG<sub>4</sub>T]<sub>4</sub> G-quadruplex was irradiated, signals for H1'', ring A and B protons of prodigiosin 1•H<sup>+</sup> were observed.

Based on previous studies with K<sup>+</sup>•d[TG<sub>4</sub>T]<sub>4</sub> quadruplex and distamycin A, STD experiments using a 1:20 sample of G-quadruplex DNA:prodigiosin in a 1:1 mixture of *d*<sub>6</sub>-DMSO and 90% H<sub>2</sub>O-10% D<sub>2</sub>O were performed (**Figure 5.26**). When

the  $^1\text{H}$  NMR resonance of H8 proton of G5 residue on  $\text{K}^+\cdot\text{d}[\text{TG}_4\text{T}]_4$  G-quadruplex was irradiated, the resulting spectrum showed distinct signals for the H3, H4, H5 protons on ring A, H4 on ring B and H1'' proton of prodigiosin  $\mathbf{1}\cdot\text{H}^+$ . No signals for ring C proton or for the C5 alkyl chain were observed. In conclusion, we propose that rings A and B of prodigiosin  $\mathbf{1}\cdot\text{H}^+$  are involved in binding to the G-quadruplex  $\text{K}^+\cdot\text{d}[\text{TG}_4\text{T}]_4$  DNA. Ring C of prodigiosin  $\mathbf{1}\cdot\text{H}^+$  is probably projected away from the quadruplex assembly with no involvement in binding.

### 5.9 Molecular Model Showing End-Stacking by Prodigiosin

A molecular model can be an excellent way to visualize the ligand-receptor interactions. In order to study the molecular model of  $\text{K}^+\cdot\text{d}[\text{TG}_4\text{T}]_4$  DNA-prodigiosin complex, an online portal was used that allows the docking of ligands onto selective DNA G-quadruplexes at specific binding sites. The G-quadruplex ligands database (G4LDB) comprises a collection of reported G-quadruplex ligands.<sup>180</sup> The goal of building the G4LDB was to facilitate the discovery and development of new therapeutic and diagnostic G-quadruplex targeting compounds by accumulating existing data, including their physical properties and 3D structure of known G-quadruplex ligands. This accumulated data was combined with web-based tools for design of new G-quadruplex ligands.

We wanted to study the end-stacking of prodigiosin  $\mathbf{1}\cdot\text{H}^+$  at the 3' end of  $\text{K}^+\cdot\text{d}[\text{TG}_4\text{T}]_4$ . But due to the unavailability of the  $\text{d}[\text{TG}_4\text{T}]_4$  G-quadruplex with the 3' end as a ligand docking site in the database, a different G-quadruplex forming sequence was selected. The G-quadruplex formed by 5'- $\text{d}[\text{TTAGGGT}]$ -3' is an intermolecular

parallel-stranded assembly similar to that of 5'-d[TG<sub>4</sub>T]-3'. Prodigiosin was docked at the 3' end of the G-quadruplex d[TTAGGGT]<sub>4</sub>. The 3' ends of G-quadruplexes formed by both sequences - 5'-d[TTAGGGT]-3' and 5'-d[TG<sub>4</sub>T]-3' are similar. Based on the model generated by G4LDB, it was found that rings A and B are stacked parallel to the G-quartet at 3' end (**Figure 5.27**). Ring C is orthogonal to the plane containing rings A and B, thereby, not interacting with the G-quartet. This preliminary model coincides with the results from saturation transfer experiments from **Section 5.8.2**.

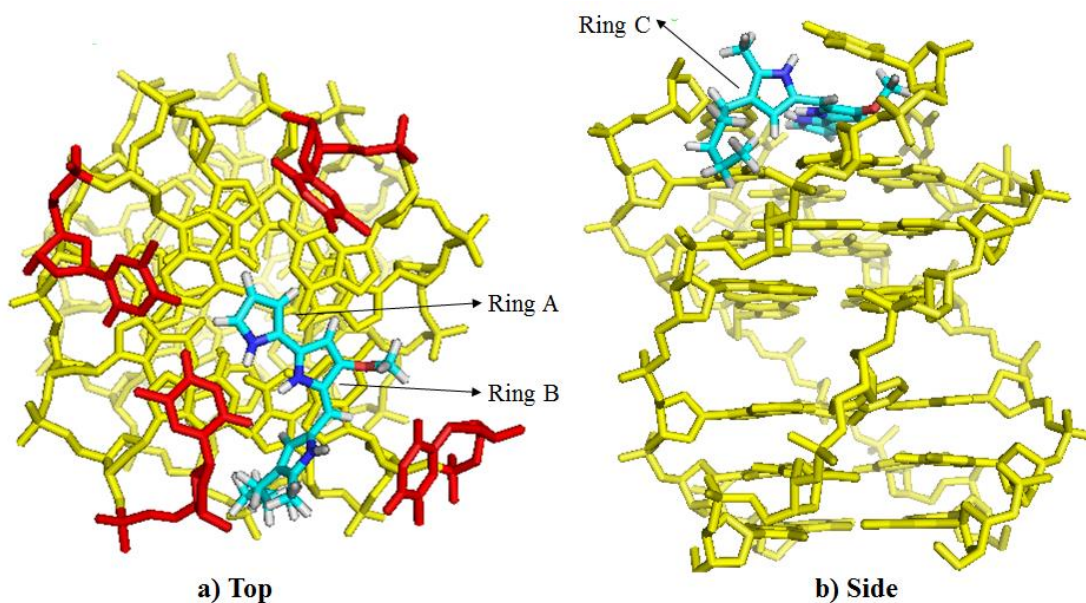


**Figure 5.27.** Molecular models generated for G-quadruplex d[TTAGGGT]<sub>4</sub> and prodigiosin 1•H<sup>+</sup> complex from G-quadruplex ligands database (G4LDB).<sup>180</sup> The model can be seen from **a)** top and **b)** side. Rings A and B in prodigiosin 1•H<sup>+</sup> are stacked parallel to the G-quartet formed by G6 at the 3' end of the DNA. Ring C in prodigiosin 1•H<sup>+</sup> is orthogonal to the plane containing rings A and B. For clarity, the terminal thymine groups (T7) at 3' end are highlighted in red in **a)**.

The model described above is an initial attempt to study the G-quadruplex d[TTAGGGT]<sub>4</sub> and prodigiosin **1•H<sup>+</sup>** complex. More relevant computational modeling studies will be performed for d[TG<sub>4</sub>T]<sub>4</sub> G-quadruplex and prodigiosin **1•H<sup>+</sup>** complex in the near future.

## **5.10 Conclusions**

The study of binding interactions between natural product prodigiosin **1•H<sup>+</sup>** and G-quadruplex DNA has shown significant results. Based on NMR, UV-visible and fluorescence spectroscopy, substantial data has been collected indicating that prodigiosin **1•H<sup>+</sup>** can bind to G-quadruplex assembly K<sup>+</sup>•d[TG<sub>4</sub>T]<sub>4</sub> in solution. In exchange, a hydrophilic and anionic DNA structure helps in solubilizing the lipophilic and cationic prodigiosin **1•H<sup>+</sup>** in aqueous systems. The binding results hold significance in two ways: 1) for the first time, interactions between prodigiosin and G-quadruplex DNA have been established. This finding may lead to a potential mechanism to explain the potent anti-cancer activity of prodigiosin; 2) these findings can serve as a starting point for development of G-quadruplex targeting drugs, based on the prodigiosene structure.

## 6 Chapter 6: Conclusions and Future Directions

The number of studies done to explore the biological activity of prodigiosenes<sup>6,42,181</sup> far exceeds the number of studies done to determine the chemistry behind prodigiosenes biological activity.<sup>36</sup> In order to develop prodigiosenes as effective pharmaceutical drugs, it is essential to learn about the mode of action of prodigiosenes on its cellular targets. One mode of action is dependent on the ability of prodigiosenes to catalyze Cl<sup>-</sup> transport across membranes,<sup>27</sup> which can affect the intracellular pH,<sup>22</sup> a phenomenon known to trigger apoptosis in cells.<sup>29</sup>

In **Chapter 2**, I described research done to investigate some of the C-ring modified prodigiosenes for their ability to transport anions across lipid bilayers and their *in vitro* anti-cancer activities. An important finding was that the presence of an ester on the C ring decreases the pK<sub>a</sub> and the anion transport rate of prodigiosene ester **2**, even though these compounds are still effective transporters at low concentrations.<sup>117</sup> This finding led to the possibility of regulating anion transport activity of prodigiosenes as a function of their basicity and extravesicular pH. The data described in **Chapter 3** indicated that the efficiency of anion transport can indeed be modulated based on the electronic nature of the O-aryl substituent on the B-ring. Further, the key factor controlling anion transport for this family of synthetic analogs, and presumably for the natural product prodigiosin, is the protonation of the prodigiosene. The internal and external pH of cancer cells has been shown to be different from that of healthy cells.<sup>63</sup> Therefore, pH switchable chloride transporters have the potential to become promising leads for anti-cancer drugs. Prodigiosenes such as B-ring modified analogs are an

example of such pH switchable transporters whose transport activity can be switched depending on the solution pH. The biological relevance of these analogs is further enhanced by the knowledge that most prodigiosenes have  $pK_a$  values in the range of physiological pH (6 to 8), therefore, improving the chances of using these analogs as anti-cancer agents.

Previously, multiple groups have shown that prodigiosenes can transport anions across membranes,<sup>31, 32</sup> but no experimental proof had been presented so far, to demonstrate  $Cl^-$  binding by prodigiosenes. The studies done in **Chapter 4** described the distinct anion binding patterns of  $\alpha$  and  $\beta$  isomers of prodigiosenes. The involvement of a CH hydrogen of  $\alpha$  isomer in binding  $MeSO_3^-$  anion was a significant finding. It will be interesting to explore other biologically relevant polydentate anions such as carboxylate anions (for *eg.* acetate, oxalate, citrate, *etc.*) and their binding interactions with prodigiosenes. In fact, Nager has reported that the gluconate anion can help solubilize prodigiosin in aqueous solutions.<sup>140</sup> Another interesting finding was the effect of water on population of  $\alpha$  isomer in solution. This study supported McNab's theory about a great biological significance of  $\alpha$  isomer of prodigiosenes.<sup>134</sup>

**Chapter 5** described the study of binding interactions between natural product prodigiosin  $1 \cdot H^+$  and G-quadruplex DNA. The binding results can be potentially useful for establishing a possible mechanism to explain the potent anti-cancer activity of prodigiosin. Further, the studies can be a starting point for development of prodigiosene-based G-quadruplex targeting drugs.



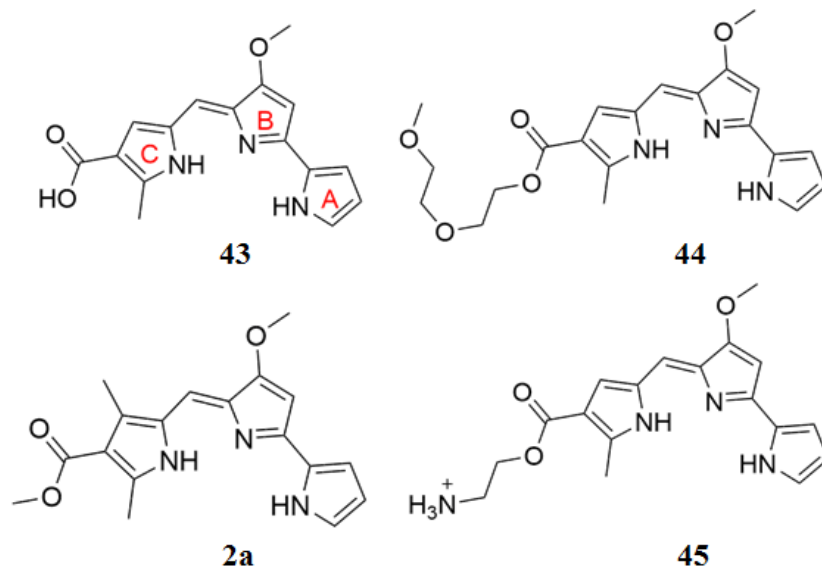


**Figure 6.1.** Structures of proposed prodigiosene analogs **43-45** and ester **2a**.

To confirm the possibility of G-quadruplex as a cellular target for prodigiosin **1**, the ligand-quadruplex assembly interactions will have to be tested in cultured cells. Future studies can also explore structural diversity of the prodigiosin scaffold. One major problem encountered throughout the course of our studies was the low solubility of prodigiosin in water. One way to counter this problem is by generating new analogs **43** with improved water-solubility. Introduction of functionalities such as carboxylic acid on ring C should help improve the water solubility of prodigiosenes **43** (**Figure 6.1**). The carboxylic acid derivatives are an initial intermediate in the synthesis of ester analog **2**. The ester analog **2** can also be explored for its ability to interact with G-quadruplexes. In analog **2a** (**Figure 6.1**), the ester functional group enhances its hydrophilic character which, may help with the DNA:ligand interactions. Other structural changes can also include replacement of alkyl chain on ring C by a

polyethylene glycol chain (**44**). An ammonium group at the terminal end of the alkyl chain could help in binding with the anionic phosphate groups (**45**).

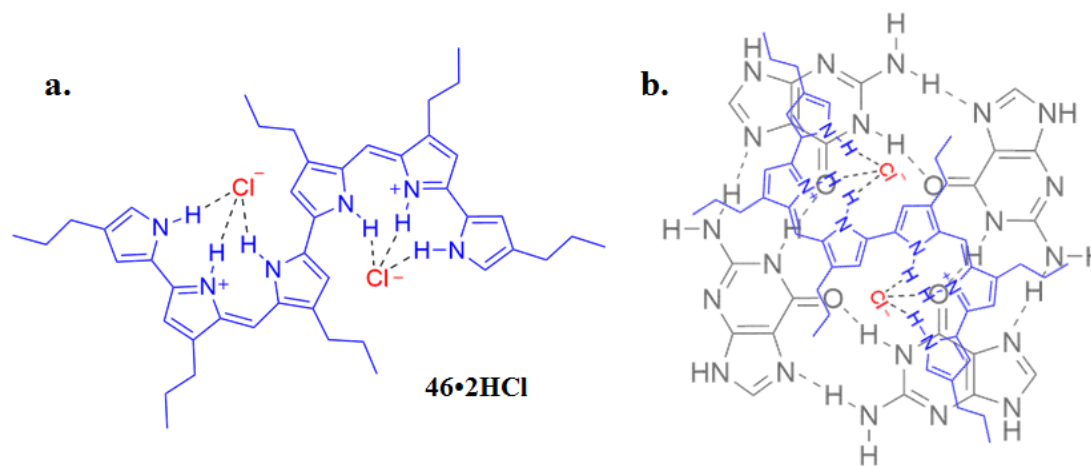


**Figure 6.2.** Structure of the hexapyrrole **46•2HCl** shows two  $\text{Cl}^-$  anions bound to a planar S-shaped conformation. Reprinted with permission from *J. Chem. Soc., Chem. Commun.* **1994**, (11), 1289-1290. Copyright (1994) Royal Society of Chemistry.<sup>182</sup> **b)** Schematic representation of a S-shaped **46•2HCl** stacking over a G-quartet.

Another possible direction can be exploration of compounds similar to **46** (**Figure 6.2a**). Compound **46** is a ‘linear’ hexapyrrole with two prodigiosene units connected together in a S-shaped conformation.<sup>182</sup> Compound **46** was synthesized by Sessler and colleagues to understand the process of anion binding by prodigiosenes. Based on X-ray structure, the authors indicated that both prodigiosene units in the compound **46** were protonated and each unit was bound to a  $\text{Cl}^-$  anion (**Figure 6.2a**). Having two planar prodigiosene units may give rise to better  $\pi$ -stacking between the G-quartet and ligand (as illustrated by a cartoon in **Figure 6.2b**), leading to a higher stabilization of the quadruplex DNA structure.

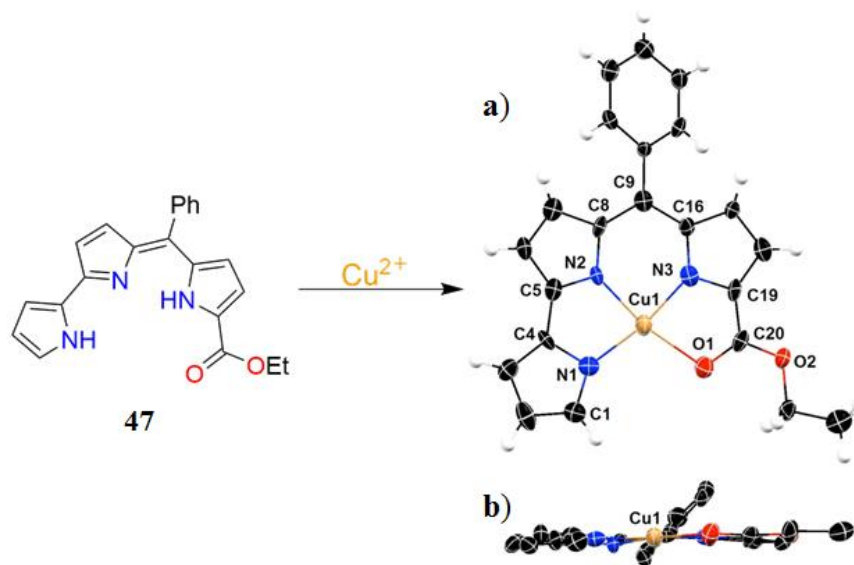


**Figure 6.3.** Compound **47** reacts with  $\text{Cu}^{2+}$  to give prodigiosene-metal complex  $\mathbf{47}\cdot\text{Cu}^{2+}$ . **a)** Top and **b)** side views of the crystal structure of copper(II) complex showing a partial labeling scheme. Adapted with permission from *Inorg. Chem.* **2014**, 53 (14), 7518–7526. Copyright (2014) American Chemical Society.<sup>183</sup> The  $\mathbf{47}\cdot\text{Cu}^{2+}$  complex may make a good ligand for stacking on a G-quartet.

Prodigiosene **47** was shown to form metal complexes in presence of Cu(II) (**Figure 6.3**).<sup>183</sup> G-quadruplexes also require cations (such as  $\text{Na}^+$ ,  $\text{K}^+$ ) in order to stabilize their structure assembly.<sup>146</sup> If the G-quadruplex assemblies are mixed with the prodigiosene metal complexes similar to that of  $\mathbf{47}\cdot\text{Cu}^{2+}$  complex, one might expect some DNA-ligand interactions.

Further, it will be interesting to perform detailed computational modelling for prodigiosin-quadruplex complexes to learn more about the preferred binding conformation of prodigiosin **1**. Our present knowledge about the conformation adopted by compound **1** while binding G-quadruplex DNA is based on the preliminary

molecular model (**Figure 5.27**) and saturation transfer diffusion experiments (**Section 5.8.2**). According to the model, prodigiosin adopts an unusual conformation that has not been assigned previously. Further, we learned in **Section 4.5.2** that water can also effect the  $\alpha/\beta$  conformation ratio of prodigiosin in solution (**Figure 6.4**). It will be fascinating to learn the combined effects of water and quadruplex DNA binding on the conformation of prodigiosenes in solution. Eventually, the information gained can be applied to synthesize new analogs with specific conformations such that the ligands are pre-organized to bind with the quadruplex DNA. The experiments described in this chapter are only the tip of an iceberg in the development of prodigiosene based G-quadruplex targeted drugs.

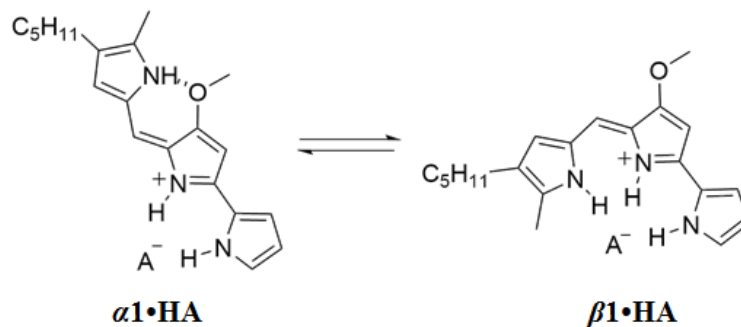


**Figure 6.4.** The  $\alpha$  and  $\beta$  conformations of prodigiosin  $1 \cdot HA$  are shown. Different factors such as water and counter-anion can affect the  $\alpha/\beta$  conformational ratio.

Finally, our studies have been done using a very simple G-quadruplex  $K^+ \cdot d[TG_4T]_4$  DNA. It will be interesting to learn about other G-quadruplex DNAs and their interaction with prodigiosenes, especially the human telomeric quadruplex DNA.

## 7 Chapter 7: Experimental Procedures and Supporting Information

### 7.1 General Experimental

**Materials.** Prodigiosin **1** was provided by the Drug Synthesis and Chemistry Branch, Developmental Therapeutics Program, Division of Cancer Treatment and Diagnosis, NCI. The series of compounds **2** and **3** were synthesized by our collaborators Dr. Estelle Marchal and Dr. Alison Thompson at the Dalhousie University, Canada.

Egg-yolk phosphatidylcholine (EYPC) lipid was purchased from Avanti Polar Lipids. Polycarbonate membranes and the extrusion apparatus used for making the liposomes was also from Avanti Polar Lipids. Salts (> 99% purity) were purchased from Sigma-Aldrich and used as received. The fluorescent dye LG was purchased from Sigma-Aldrich. Buffer solutions were made using ultra-pure water (distilled and then passed through a Millipore filtering system). All pH measurements and adjustments were made using an Accumet AR25A pH/ion meter equipped with a Accumet pH microelectrode. Calibration was achieved using commercial buffers (Thermo Scientific, pH 4.00, 7.00 and 10.00, all  $\pm 0.01$ ). All fluorescence experiments were performed using a Hitachi F-4500 fluorescence spectrophotometer.

**Preparation of EYPC Liposomes.** EYPC lipid solution (~60 mg of lipid) was evaporated under reduced pressure to produce a thin film that was then dried *in vacuo* overnight. The resulting lipid film was hydrated with 1 mL of a LG containing buffer to be encapsulated inside the liposomes.<sup>78,113</sup> After 9 freeze/thaw cycles (thawing and then warming to 45°C), the liposome solution was extruded through a 200 nm polycarbonate membrane 31 times at room temperature to obtain small unilamellar

vesicles (SUVs). The liposome solution was then passed through a Sephadex (G-25) column to remove any excess LG dye. The isolated liposomes were diluted in extravesicular buffer to give a final concentration of 13 mM in EYPC lipid, assuming complete retention of lipid during the gel filtration process. The size of the liposomes was confirmed using dynamic light scattering experiments.

**Determination of pK<sub>a</sub> Values.** A spectrophotometric procedure described by Manderville and colleagues was used to determine the apparent pK<sub>a</sub> values for prodigiosenes.<sup>33</sup> The UV-vis spectra were recorded on a Cary 100 UV-visible spectrophotometer in **Chapter 2** and Shimadzu UV-1800 UV-visible spectrophotometer in **Chapter 3**. Standard 10 mm quartz glass cells from Starna Cells Inc. were used. All UV-Vis spectra were recorded at 25 °C with baseline correction. Stock solutions (2 mM) of prodigiosenes were prepared in CH<sub>3</sub>CN. Then, 15 μL of the stock solution was added to a quartz cuvette containing 2 mL total volume of 1:1 CH<sub>3</sub>CN/H<sub>2</sub>O (v/v). The ionic strength was kept constant by using 0.1 M NaCl. Acidity constants were determined spectrophotometrically by monitoring absorbance changes in the UV-vis spectra after additions of dilute HCl or NaOH solutions under constant temperature conditions. The pK<sub>a</sub> values were determined from a plot of ionization ratio and pH. Ionization ratio is given by the expression in equation 1; where A is the absorbance of the solution containing a certain total concentration of the acid–base mixture, A<sub>base</sub> is the absorbance of the base form at the same concentration, and A<sub>acid</sub> is the absorbance of the protonated form at the same concentration.

$$\log_{10} \frac{A - A_{base}}{A_{acid} - A} \quad (\text{equation 1})$$

## 7.2 Experimental Procedures for Chapter 2

### 7.2.1 Anion Exchange Transport Assays

#### **Chloride-Nitrate Anion Exchange Transport Assay in EYPC Liposomes.**

Liposomes containing 1 mM LG, 20 mM HEPES and 100 mM NaCl buffer (pH 7.4) were prepared. In a typical experiment, 0.04 mL of the stock EYPC liposome solution was diluted into 2 mL of a solution of 20 mM HEPES (pH 7.4, 100 mM NaNO<sub>3</sub>) to give a solution that was 0.2 mM in lipid. The LG's fluorescence was monitored for 720 s with a  $\lambda_{\text{ex}} = 372$  nm and  $\lambda_{\text{em}} = 504$  nm. At  $t = 30$  s, 1  $\mu\text{L}$  of a 0.2 mM DMSO solution of the prodigiosene transporter was added to the cuvette containing the EYPC solution, giving a 1:2,500 ligand to lipid ratio (or 0.04 mol %). The efflux of Cl<sup>-</sup>, facilitated by the transporter was characterized by an increase in the LG's fluorescence. At  $t = 660$  s, 0.05 mL of a solution of 10 % Triton-X detergent was added in order to lyse the liposomes and maximal fluorescence quenching of LG by Cl<sup>-</sup> was measured. Experiments were repeated in triplicate.

#### **Determination of EC<sub>50</sub> Values for Anion Exchange by Prodigiosenes 1, 2e and 24.**

The Hill equation describes the relationship between the concentration of a substrate and an observed effect.<sup>184</sup> It is often used in pharmacodynamics to describe the relationship between drug concentration (X) and observed effect (Y). A form of the Hill equation that is useful in the context of the supramolecular function of ion transport is shown in equation 2, where K (EC<sub>50</sub>) is the transporter's concentration for which 50% of maximum transport is obtained, and n is the Hill coefficient of sigmoidality.

$$Y = V_{\text{max}} \cdot X_n / (K_n + X_n) \quad (\text{equation 2})$$

The Hill equation can be applied to ion transport by examining the effect of varying the concentration of transporter [X] on ion flux (Y). In this way, a value of K (EC<sub>50</sub>) can be calculated and used to quantify transport activity; the lower the value of EC<sub>50</sub>, the more potent the transporter. To calculate the values of K and n for each compound, the transport assay was repeated for different concentrations of transporters with the same batch of EYPC liposomes. The transport experiment was initiated by addition of an aliquot of transporter solution at 25 °C. The fluorescence of intravesicular LG was at  $\lambda_{\text{ex}} = 372$  nm and  $\lambda_{\text{em}} = 504$  nm with a 10 nm slit width. At the end of the experiment, 10 % aqueous Triton-X was injected to lyse the liposomes. LG fluorescence was converted to chloride concentration using the Stern-Volmer constant determined under the assay conditions.<sup>78, 116</sup> To measure the Stern-Volmer constant, liposomes were prepared as above, and then were lysed with Triton-X at t = 30s. 10  $\mu$ L of 2.0 M NaCl was titrated every 30 s via the injection port. The titration was repeated three times. A plot of  $f_0/f$  vs. Cl<sup>-</sup> concentration was generated (**Figure 7.1**), the slope of which is taken to be the Stern-Volmer constant (' $k_q \tau_0$ ' from equation 3). The kinetics of LG fluorescence quenching process is given by the Stern-Volmer relationship (equation 3), where  $f_0$  is the intensity of LG fluorescence without Cl<sup>-</sup>,  $f$  is the intensity with Cl<sup>-</sup>,  $k_q$  is the quencher rate coefficient,  $\tau_0$  is the lifetime of the emissive excited state of LG without Cl<sup>-</sup> present and [Q] is the concentration of the Cl<sup>-</sup>.<sup>185</sup>

$$\frac{f_0}{f} = 1 + k_q \tau_0 \cdot [Q] \quad (\text{equation 3})$$

Using the Stern-Volmer relationship (equation 3), the LG fluorescence intensity was converted into concentration of Cl<sup>-</sup> for each concentration of a compound. The



percentage of  $\text{Cl}^-$  efflux from the vesicles for each transporter concentration at  $t = 150$  s was calculated. The percentage of chloride efflux vs. log of transporter's concentration was fitted into Hill equation (1) to obtain value for  $K$  ( $\text{EC}_{50}$ ) at 150s (Figure 7.2-Figure 7.4).

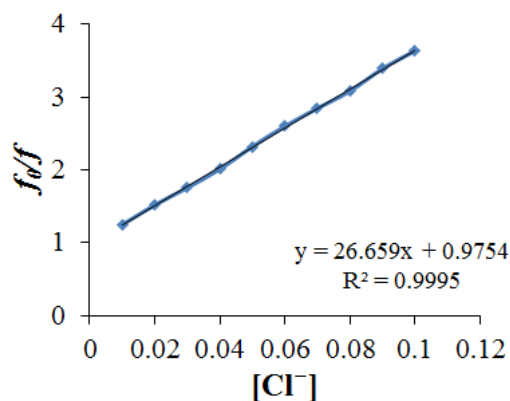


**Figure 7.1.** Determination of the Stern-Volmer constant.

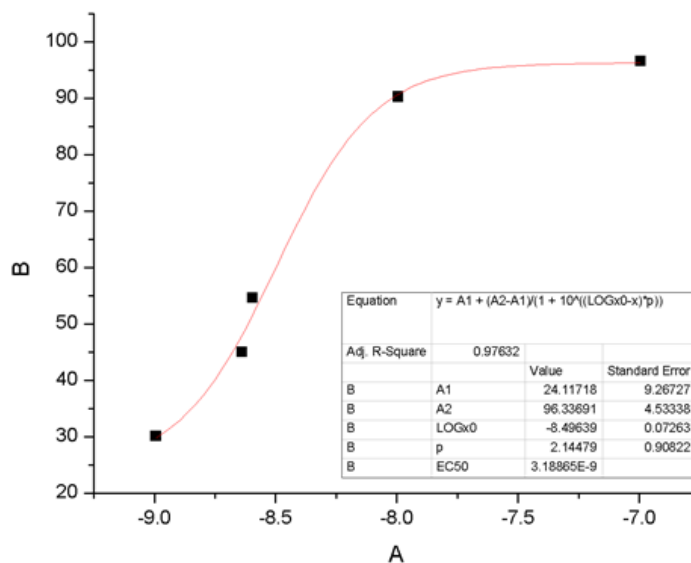


**Figure 7.2.**  $\text{EC}_{50}$  dose response curve for prodigiosin **1** at 150 s.  $\text{EC}_{50}$  value was calculated by plotting the percentage of chloride efflux at 150 s vs. the natural log of concentration of prodigiosin **1** and then fitting to Hill equation.

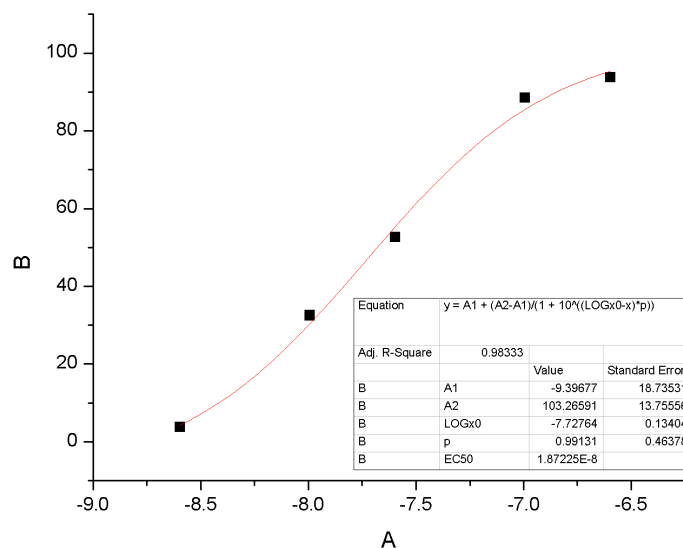


**Figure 7.3.** EC<sub>50</sub> dose response curve for ester **2e** at 150 s. EC<sub>50</sub> value was calculated by plotting the percentage of chloride efflux at 150 s vs. the natural log of concentration of prodigiosin **2e** and then fitting to Hill equation.

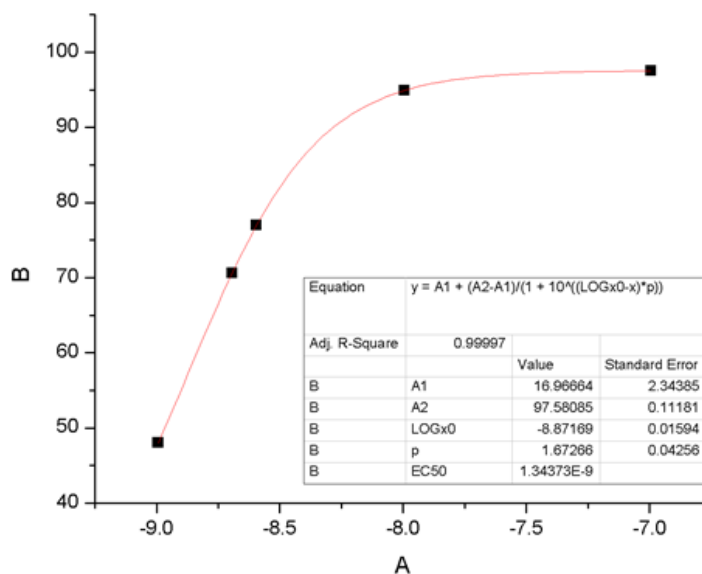


**Figure 7.4.** EC<sub>50</sub> dose response curve for ester **24** at 150 s. EC<sub>50</sub> value was calculated by plotting the percentage of chloride efflux at 150 s vs. the natural log of concentration of prodigiosin **24** and then fitting to Hill equation.

**Receptor Incubation Assay in EYPC Liposomes.** Liposomes containing 1 mM LG, 10 mM phosphate and 100 mM NaNO<sub>3</sub> buffer (pH 7.4) were prepared. In a typical experiment, 0.04 mL of the stock EYPC liposome solution was diluted into 2 mL of a solution of 10 mM phosphate (pH 7.4, 100 mM NaNO<sub>3</sub>) to give a solution that was 0.2 mM in lipid. The LG's fluorescence was monitored for 620 s with a  $\lambda_{\text{ex}} = 372$  nm and  $\lambda_{\text{em}} = 504$  nm. For this experiment, two sets of conditions were applied. For condition I of “**no incubation**”, the transporter **2h** was added at 0.04 mol% ligand:lipid ratio to the liposome sample, immediately followed by addition of a 200  $\mu$ L pulse of 1M NaCl, 10 mM phosphate, 100 mM NaNO<sub>3</sub> buffer. LG fluorescence was measured. For condition II involving “**incubation**”, **2h** was added to the liposome sample and allowed to incubate for 300 s, followed by addition of NaCl pulse and measurement of fluorescence. The influx of Cl<sup>-</sup>, facilitated by the transporter was characterized by a decrease in the LG's fluorescence. At t = 560 s, 0.05 mL of a solution of 10 % Triton-X detergent was added in order to lyse the liposomes and maximal fluorescence quenching of LG by Cl<sup>-</sup> was measured. Experiments were repeated in triplicate.

**pH Variation Assay in EYPC Liposomes.** Liposomes containing 1 mM LG, 10 mM phosphate and 100 mM NaNO<sub>3</sub> buffer were prepared. In a typical experiment, 0.04 mL of the stock EYPC liposome solution was diluted into 2 mL of a solution of 10 mM phosphate (pH 6.5, 7.5 or 8.5) containing 100 mM NaNO<sub>3</sub> to give a solution that was 0.2 mM in lipid. The LG's fluorescence was monitored for 720 s at  $\lambda_{\text{ex}} = 372$  nm and  $\lambda_{\text{em}} = 504$  nm. At t = 30 s, 1  $\mu$ L of a 0.2 mM DMSO solution of the prodigiosene **2g** was added to the cuvette containing the EYPC solution. A pulse of 10 mM phosphate

(pH 6.5, 7.5 or 8.5), 1 M NaCl and 100 mM NaNO<sub>3</sub> was added at 60 s to get a final concentration of 100 mM NaCl in the cuvette. The influx of Cl<sup>-</sup>, facilitated by the transporter **2g** was characterized by a decrease in the LG's fluorescence. At t = 660 s, 0.05 mL of a solution of 10 % Triton-X detergent was added in order to lyse the liposomes and maximal fluorescence quenching of LG by Cl<sup>-</sup> was measured. Experiments were repeated thrice.

### 7.2.2 NMR Titrations

<sup>1</sup>H NMR experiments were performed at 25 °C using a Bruker AVIII-600MHz instrument. A mixture of two compounds in CD<sub>3</sub>CN was titrated with acid. Methanesulfonic acid (MeSO<sub>3</sub>H) was used. In a typical NMR experiment involving a mixture of two compounds, solutions were prepared containing 1 mM of each compound in a total volume of 0.8 mL. If the compound mixture was in the form of an HCl salt, then 2 μL of 0.4 M solution of tetraethylammonium bicarbonate (TEAB) was first added to the solution to create the free-base form of the compounds. Then, 2, 5 or 10 μL of a 0.08 M solution of MeSO<sub>3</sub>H in CD<sub>3</sub>CN was added to obtain 0.2, 0.5 or 1.0 eq, respectively of MeSO<sub>3</sub>H in the NMR tube. After each addition of MeSO<sub>3</sub>H, a <sup>1</sup>H NMR spectrum was recorded. Chemical shifts were referenced to the non-deuterated methyl group at δ 1.93 in the CD<sub>3</sub>CN solvent.

### 7.2.3 Determination of pK<sub>a</sub> Values for Prodigiosin **1** and Prodigiosene Ester **2f**

Based on the UV-vis titration spectra and ionization plots, pK<sub>a</sub> values were calculated to be 8.2 for prodigiosin **1**•H<sup>+</sup> and 6.5 for ester **2f**•H<sup>+</sup>. The UV-vis absorbance titration was performed in triplicate for each compound.

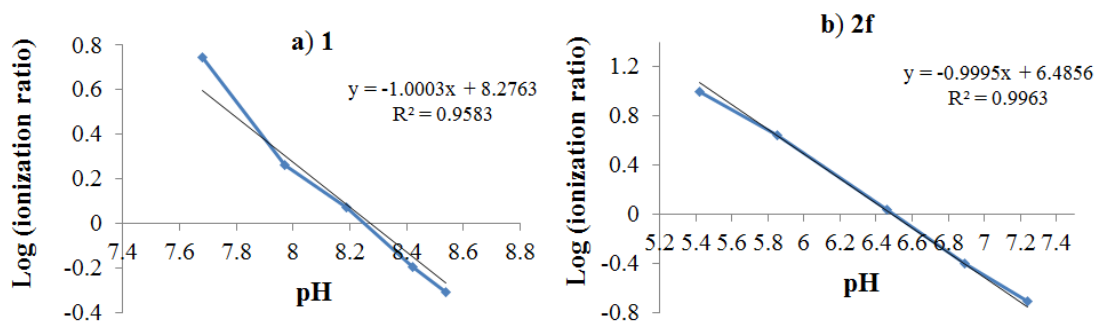


**Figure 7.5.** A plot of log (ionization ratio) vs. pH for prodigiosin **1** and ester analog **2f**.

### 7.3 Experimental Procedures for Chapter 3

#### 7.3.1 Determination of $pK_a$ Values for Prodigiosenes **3b**, **3d-f** and **3h**

The  $pK_a$  values were determined for protonated prodigiosenes **3b**, **3d-f** and **3h**.

Based on the UV-vis titration spectra and ionization plots,  $pK_a$  values were calculated.

The UV-vis absorbance titration was performed in triplicate for each compound.

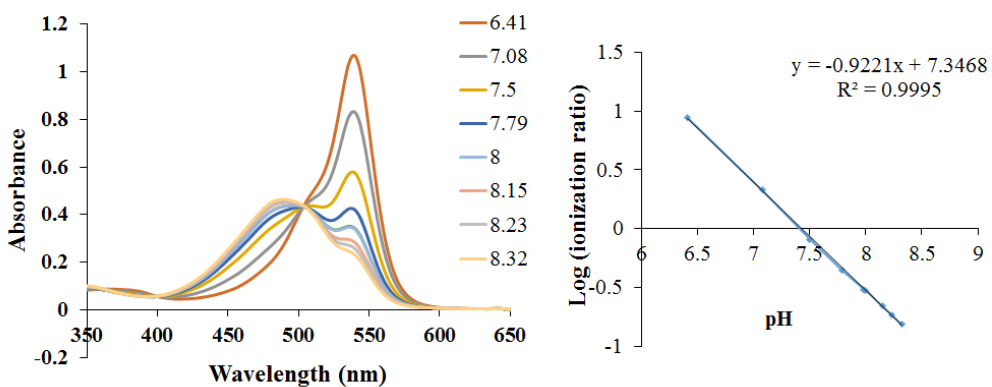


**Figure 7.6.** Absorbance spectra and ionization plot for **3e** (X = NMe<sub>2</sub>) as a function of pH.

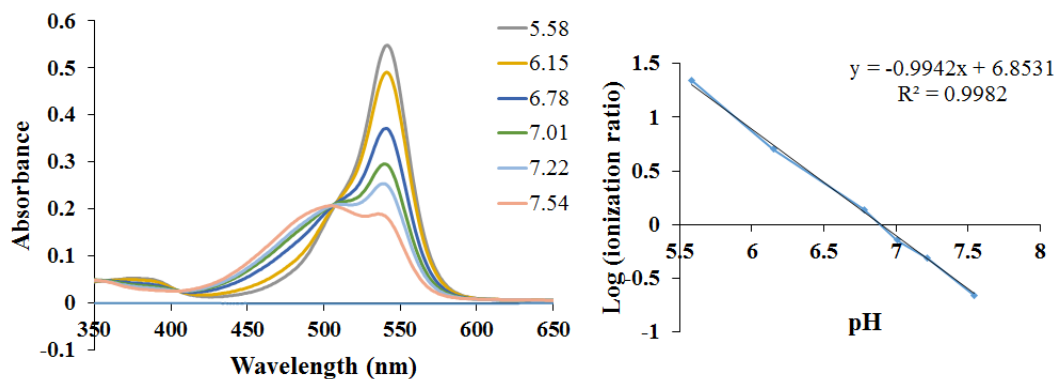


**Figure 7.7.** Absorbance spectra and ionization plot for **3h** (X = Cl) as a function of pH.

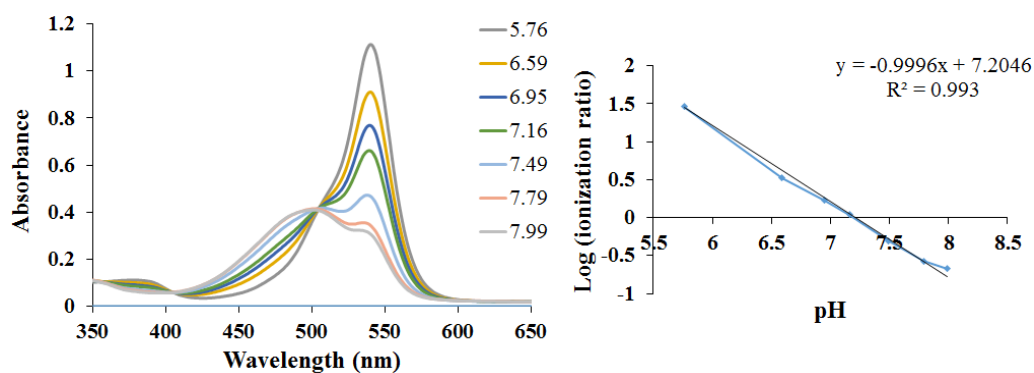


**Figure 7.8.** Absorbance spectra and ionization plot for **3b** (X = H) as a function of pH.

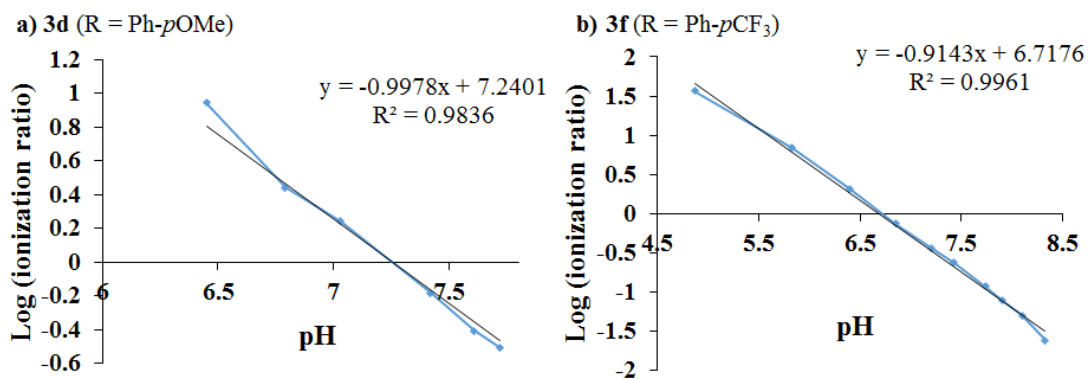


**Figure 7.9.** Ionization plots for **a) 3d** (X = OMe) and **b) 3f** (X = CF<sub>3</sub>) as a function of pH.

### 7.3.2 Anion Exchange Transport Assays

#### **Chloride-Nitrate Anion Exchange Transport Assay in EYPC Liposomes.**

Liposomes containing 1 mM LG, 20 mM HEPES and 100 mM NaCl buffer were prepared. In a typical experiment, 0.04 mL of the stock EYPC liposome solution was diluted into 2 mL of a solution of 20 mM HEPES (pH 7.4, 100 mM NaNO<sub>3</sub>) to give a solution that was 0.2 mM in lipid. The LG's fluorescence was monitored for 720 s with a  $\lambda_{\text{ex}} = 372$  nm and  $\lambda_{\text{em}} = 504$  nm. At  $t = 30$  s, 1  $\mu\text{L}$  of a 0.2 mM DMSO solution of the prodigiosene transporter was added to the cuvette containing the EYPC solution, giving a 1:125,000 ligand to lipid ratio (or 0.0008 mol% wrt lipid concentration). The efflux of Cl<sup>-</sup> facilitated by the transporter was characterized by an increase in the LG's fluorescence. At  $t = 660$  s, 0.05 mL of a solution of 10 % Triton-X detergent was added in order to lyse the liposomes and maximal fluorescence quenching of LG by Cl<sup>-</sup> was measured. Experiments were repeated in triplicate.

**Initial Rates and Half-Life.** For comparative purposes, the relative transport activity for various ionophores was expressed as the initial rate of LG fluorescence as chloride and nitrate were exchanged across the membrane. Addition of a transporter leads to movement of internal chloride across the membrane, which results in increase in fluorescence of LG. Rates are obtained by linear fitting of initial slopes of fluorescence traces. Half-life were calculated for each prodigiosene from fluorescence plots.

## 7.4 Experimental Procedures for Chapter 4

### 7.4.1 NMR Titrations

All experiments were performed with the Bruker AVIII-600 MHz instrument.  $^1\text{H}$  NMR experiments were performed at 25 °C on **3b**. Methanesulfonic acid ( $\text{MeSO}_3\text{H}$ ) was used as the acid source. In a typical NMR experiment, a 1 mM solution of **3b** was prepared. Then, 1 eq of  $\text{MeSO}_3\text{H}$  dissolved in  $\text{CDCl}_3$ , was added to the NMR sample. After adding 6 eq of  $\text{MeSO}_3\text{H}$ , a NOESY experiment was performed. Two sets of signals were resolved for each  $\alpha$  (•) and  $\beta$  (\*) conformer (**Figure 7.10**). 1D proton spectra of samples were recorded using pulsed-field gradient DPGSE for  $\text{H}_2\text{O}$  suppression.<sup>186</sup> Phase-sensitive NOESY spectra<sup>187,188</sup> were recorded with mixing times of 500 ms ( $T= 25$  °C). The relaxation delay was kept at 2s. Experiments were recorded using STATES-TPPI<sup>189</sup> procedure for quadrature detection. The time domain data consisted of 2048 complex points in f2 and 256 fids in f1 dimension. The NMR data were processed using TopSpin 3.0 software.



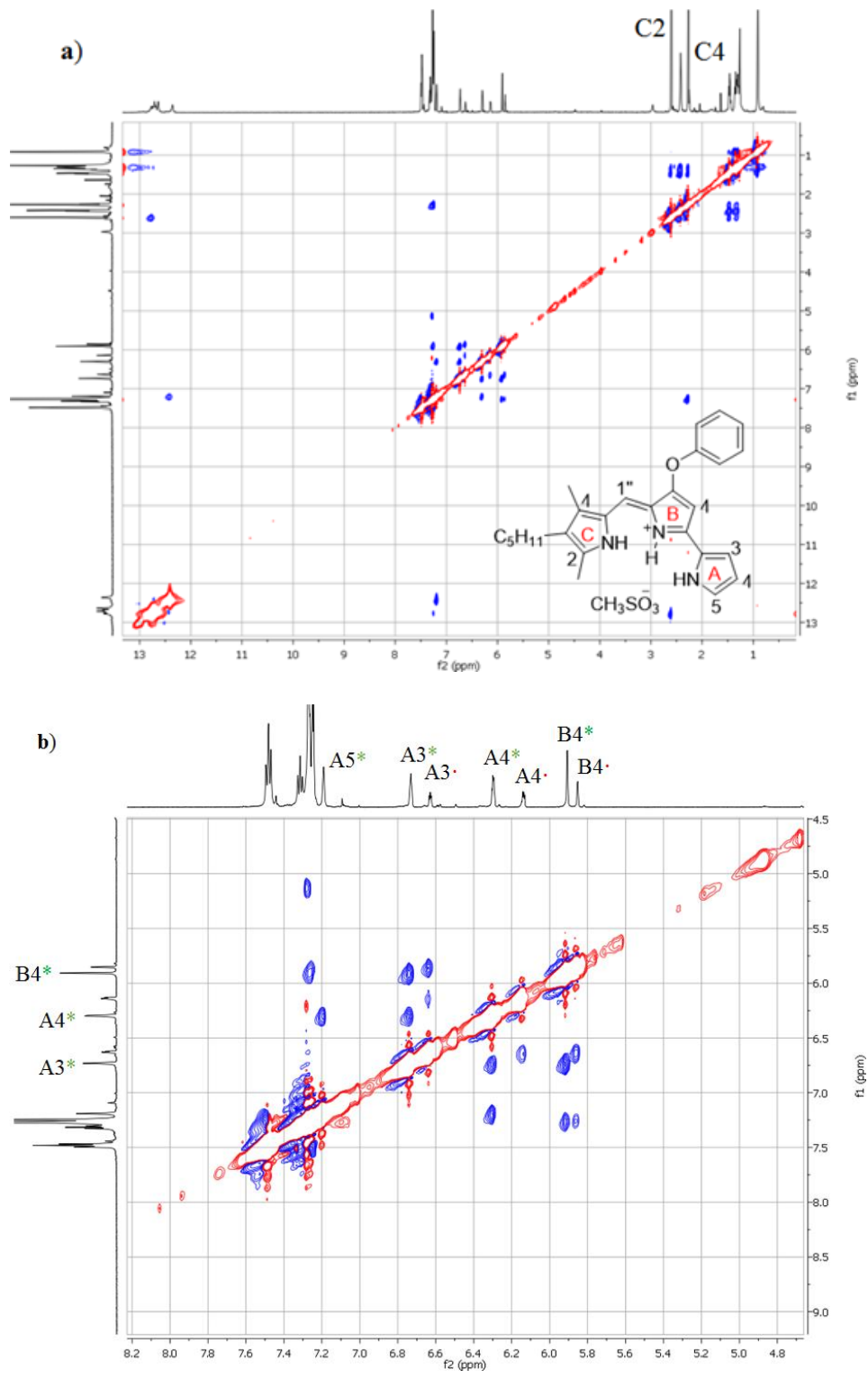


**Figure 7.10.** a) Full and b) expanded NOESY spectrum of **3b**•MeSO<sub>3</sub>H in CDCl<sub>3</sub>.

## 7.5 Experimental Procedures for Chapter 5

**Materials.** The oligonucleotide d(TGGGGT) was purchased from IDT Integrated DNA Technologies. Salts (> 99% purity) were purchased from Sigma-Aldrich and Acros Organics, and used as received. All fluorescence experiments were performed using a Hitachi F-4500 fluorescence spectrophotometer and UV-vis experiments were performed on a Shimadzu UV-1800 UV-visible spectrophotometer. NMR experiments were performed on different instruments - Bruker AVIII-600 MHz spectrometer at the Chemistry NMR facility; Bruker Avance III 600 MHz spectrometer with a CPTCI cryoprobe and Bruker Avance III HD 800 MHz spectrometer with a CPQCI cryoprobe at the Biomolecular NMR facility.

**Sample Preparation.** DNA solutions were prepared by dissolving solid lyophilized oligonucleotides in buffered solutions containing either chloride salt of  $K^+$  or  $Li^+$ . The  $K^+$  buffer used was 100 mM KCl, 10 mM Tris - 1 mM EDTA. The  $Li^+$  buffer was 100 mM LiCl, 10 mM Tris - 1 mM EDTA. Both buffer solutions were in 90%  $H_2O$ -10%  $D_2O$  at pH 7.0. DNA G-quadruplex  $d[TG_4T]_4$  was formed by heating the solutions to 95 °C for 5min. The solutions were then cooled slowly to room temperature and equilibrated overnight at 4 °C. Stock solution of prodigiosin **1** was prepared by dissolving it in  $d_6$ -DMSO. The concentration of oligonucleotide and prodigiosin solutions were determined by UV-vis absorption measurements using molar extinction coefficient ( $\epsilon$ ) values of 57,800 (260 nm) and 112,000 (535 nm; 95% EtOH-HCl)  $M^{-1} cm^{-1}$ , respectively.<sup>190,132</sup>

### **7.5.1 UV-vis titration**

Wavelength scans were measured at 37 °C in sub-micro spectrophotometer quartz cells of 1-cm path length from Starna Cells Inc. For UV-vis titrations, the DMSO stock solution of prodigiosin was diluted to 50 μM concentration in 200 μL volume in a cuvette. Buffer solutions used for dilution were 10 mM Tris - 1 mM EDTA containing either 100 mM KCl or 100 mM LiCl in 90% H<sub>2</sub>O-10% D<sub>2</sub>O at pH 7.0. The titration was performed by stepwise addition of aliquots of DNA solution (0.5 mM in tetraplex). After each addition of aliquot of DNA, absorbance of the sample was recorded. Each experiment was repeated three times.

### **7.5.2 Fluorescence titration**

Emission fluorescence scans were measured at 37 °C in semi-micro spectrophotometer quartz cells of 1-cm path length from Starna Cells Inc. For titrations, the DMSO stock solution of prodigiosin was diluted to 5 μM concentration in 400 μL volume in a cuvette. Buffer solutions used for dilution were 10 mM Tris - 1 mM EDTA containing 100 mM KCl in 90% H<sub>2</sub>O-10% D<sub>2</sub>O at pH 7.0. The excitation wavelength used was 520.0 nm at 5.0 nm slit size. The titration was performed by stepwise addition of aliquots of DNA solution (0.5 mM in tetraplex). After each addition of DNA, a fluorescence reading was taken. Each experiment was repeated three times.

### **7.5.3 <sup>1</sup>H-NMR titration**

All 2D and several 1D NMR experiments were performed in collaboration with Dr. Daoning Zhang at the Biomolecular NMR facility. G-quadruplex DNA NMR samples were prepared at a concentration of 2 mM (single-strand concentration) in 0.4

ml (H<sub>2</sub>O/D<sub>2</sub>O 9:1) buffer solution having 10 mM Tris, 100 mM KCl, and 1 mM EDTA, pH 7.0 or 10 mM Tris, 100 mM LiCl, and 1 mM EDTA, pH 7.0. Prodigiosin stock solutions were prepared in *d*<sub>6</sub>-DMSO. All experiments with G-quadruplex DNA were performed at 45 °C. <sup>31</sup>P chemical shifts were referenced relative to external phosphoric acid (> 99%). The acquired NMR data were processed using TopSpin version 3.0 or TopSpin version 3.2 software.

1D proton spectra of samples were recorded using excitation sculpting with gradients for H<sub>2</sub>O suppression.<sup>186,191</sup> Phase-sensitive 2D NOESY spectra with water suppression (pulseprogram: noesyegpph) were recorded with mixing times of 100 and 200 ms (T= 45 °C).<sup>191</sup> 2D NOESY experiments were recorded using STATES-TPPI procedure for quadrature detection.<sup>189</sup> The time domain data consisted of 2048 complex points in f2 and 256 fids in f1 dimension. A power-gated decoupling pulseprogram (zgpg30) was used to acquire 1D <sup>31</sup>P NMR spectrum. <sup>1</sup>H-<sup>31</sup>P HSQC correlation experiments (pulseprogram: na\_hsqcctf3gpxy) were recorded using XY16-CPMG with Echo/Antiecho-TPPI acquisition mode.<sup>192-194</sup> 1D selective TOCSY spectra using MLEV17 sequence were recorded with mixing times of 120 ms.<sup>195-198</sup> Saturation transfer difference experiments (STD, pulseprogram: stddiffesgp.3) used a shaped pulse sequence for saturation on f2 channel, alternating between on and off resonance.<sup>178, 191</sup> A spoil sequence was used to destroy unwanted magnetization and water suppression was achieved by using excitation sculpting with gradients. In all the experiments described above, the relaxation delay was kept at 2 s.

## Bibliography

1. Hearn, W. R.; Elson, M. K.; Williams, R. H.; Medina-Castro, J., Prodigiosene [5-(2-pyrryl)-2,21-dipyrrylmethene] and some substituted prodigiosenes. *J. Org. Chem.* **1970**, *35* (1), 142-146.
2. Regourd, J.; Al-Sheikh Ali, A.; Thompson, A., Synthesis and anti-cancer activity of C-ring-functionalized prodigiosin analogues. *J. Med. Chem.* **2007**, *50* (7), 1528-1536.
3. Diaz de Grenu, B.; Hernandez, P. I.; Espona, M.; Quinonero, D.; Light, M. E.; Torroba, T.; Perez-Tomas, R.; Quesada, R., Synthetic prodiginine Obatoclax (GX15-070) and related analogues: anion binding, transmembrane transport, and cytotoxicity properties. *Chem. - Eur. J.* **2011**, *17* (50), 14074-14083.
4. Smithen, D. A.; Forrester, A. M.; Corkery, D. P.; Dellaire, G.; Colpitts, J.; McFarland, S. A.; Berman, J. N.; Thompson, A., Investigations regarding the utility of prodigiosenes to treat leukemia. *Org. Biomol. Chem* **2013**, *11* (1), 62-68.
5. D'Alessio, R.; Bargiotti, A.; Carlini, O.; Colotta, F.; Ferrari, M.; Gnocchi, P.; Isetta, A.; Mongelli, N.; Motta, P.; Rossi, A.; Rossi, M.; Tibolla, M.; Vanotti, E., Synthesis and immunosuppressive activity of novel prodigiosin derivatives. *J. Med. Chem.* **2000**, *43* (13), 2557-2565.
6. Williamson, N. R.; Fineran, P. C.; Leeper, F. J.; Salmond, G. P. C., The biosynthesis and regulation of bacterial prodiginines. *Nat. Rev. Microbiol.* **2006**, *4* (12), 887-899.
7. Papireddy, K.; Smilkstein, M.; Kelly, J. X.; Salem, S. M.; Alhamadsheh, M.; Haynes, S. W.; Challis, G. L.; Reynolds, K. A., Antimalarial activity of natural and synthetic prodiginines. *J. Med. Chem.* **2011**, *54* (15), 5296-5306.
8. Marchal, E.; Uddin, M. I.; Smithen, D.; Hawco, C.; Lanteigne, M.; Overy, D.; Kerr, R.; Thompson, A., Antimicrobial activity of non-natural prodigiosenes. *RSC Adv.* **2013**, *3* (45), 22967-22971.
9. Davis, J. T., Anion binding and transport by prodigiosin and its analogs. *Anion Recognition in Supramolecular Chemistry*, Springer **2010**, 145-176.
10. Sessler, J. L.; Eller, L. R.; Cho, W. S.; Nicolaou, S.; Aguilar, A.; Lee, J. T.; Lynch, V. M.; Magda, D. J., Synthesis, anion-binding properties, and *in vitro* anticancer activity of prodigiosin analogues. *Angew. Chem., Int. Ed.* **2005**, *44* (37), 5989-5992.

11. Fürstner, A., Chemistry and Biology of Roseophilin and the Prodigiosin Alkaloids: A Survey of the Last 2500 Years. *Angew. Chem., Int. Ed.* **2003**, *42* (31), 3582-3603.
12. Daïri, K.; Yao, Y.; Faley, M.; Tripathy, S.; Rioux, E.; Billot, X.; Rabouin, D.; Gonzalez, G.; Lavallée, J.-F.; Attardo, G., A scalable process for the synthesis of the bcl inhibitor obatoclax. *Org. Process Res. Dev.* **2007**, *11* (6), 1051-1054.
13. O'Brien, S. M.; Claxton, D. F.; Crump, M.; Faderl, S.; Kipps, T.; Keating, M. J.; Viallet, J.; Cheson, B. D., Phase I study of obatoclax mesylate (GX15-070), a small molecule pan-Bcl-2 family antagonist, in patients with advanced chronic lymphocytic leukemia. *Blood* **2009**, *113* (2), 299-305.
14. Williamson, N. R.; Fineran, P. C.; Gristwood, T.; Chawrai, S. R.; Leeper, F. J.; Salmond, G. P., Anticancer and immunosuppressive properties of bacterial prodiginines. *Future Microbiology* **2007**, *2* (6), 605-618.
15. Stepkowski, S. M.; Erwin-Cohen, R. A.; Behbod, F.; Wang, M.-E.; Qu, X.; Tejpal, N.; Nagy, Z. S.; Kahan, B. D.; Kirken, R. A., Selective inhibitor of Janus tyrosine kinase 3, PNU156804, prolongs allograft survival and acts synergistically with cyclosporine but additively with rapamycin. *Blood* **2002**, *99* (2), 680-689.
16. Wrede, F.; Hettche, O., Über das Prodigiosin, den roten Farbstoff des Bacillus Prodigiosus (I. Mitteil.). *Berichte der deutschen chemischen Gesellschaft (A and B Series)* **1929**, *62* (9), 2678-2685.
17. Rapoport, H.; Holden, K. G., The Synthesis of Prodigiosin. *J. Am. Chem. Soc.* **1962**, *84* (4), 635-642.
18. Wasserman, H. H.; McKeon, J. E.; Smith, L.; Forgione, P., Prodigiosin. Structure and partial synthesis<sup>1</sup>. *J. Am. Chem. Soc.* **1960**, *82* (2), 506-507.
19. Lee, M. H.; Kataoka, T.; Magae, J.; Nagai, K., Prodigiosin 25-C suppression of cytotoxic T cells in vitro and in vivo similar to that of concanamycin B, a specific inhibitor of vacuolar type H(+)-ATPase. *Biosci Biotechnol Biochem* **1995**, *59* (8), 1417-1421.
20. Tsuji, R. F.; Magae, J.; Yamashita, M.; Nagai, K.; Yamasaki, M., Immunomodulating properties of prodigiosin 25-C, an antibiotic which preferentially suppresses induction of cytotoxic T cells. *J. Antibiot.* **1992**, *45* (8), 1295-1302.
21. Yamamoto, D.; Kiyozuka, Y.; Uemura, Y.; Yamamoto, C.; Takemoto, H.; Hirata, H.; Tanaka, K.; Hioki, K.; Tsubura, A., Cycloprodigiosin hydrochloride, a

H<sup>+</sup>/Cl<sup>-</sup> symporter, induces apoptosis in human breast cancer cell lines. *J. Cancer Res. Clin. Oncol* **2000**, *126* (4), 191-197.

22. Yamamoto, C.; Takemoto, H.; Kuno, K.; Yamamoto, D.; Tsubura, A.; Kamata, K.; Hirata, H.; Yamamoto, A.; Kano, H.; Seki, T., Cycloprodigiosin hydrochloride, a new H<sup>+</sup>/Cl<sup>-</sup> symporter, induces apoptosis in human and rat hepatocellular cancer cell lines in vitro and inhibits the growth of hepatocellular carcinoma xenografts in nude mice. *Hepatology* **1999**, *30* (4), 894-902.

23. Yamamoto, D.; Uemura, Y.; Tanaka, K.; Nakai, K.; Yamamoto, C.; Takemoto, H.; Kamata, K.; Hirata, H.; Hioki, K., Cycloprodigiosin hydrochloride, H<sup>+</sup>/Cl<sup>-</sup> symporter, induces apoptosis and differentiation in HL-60 cells. *Int. J. Cancer* **2000**, *88* (1), 121-128.

24. Manderville, R. A., Synthesis, proton-affinity and anti-cancer properties of the prodigiosin-group natural products. *Curr. Med. Chem.: Anti-Cancer Agents* **2001**, *1* (2), 195-218.

25. Ohkuma, S.; Sato, T.; Okamoto, M.; Matsuya, H.; Arai, K.; Kataoka, T.; Nagai, K.; Wasserman, H. H., Prodigiosins uncouple lysosomal vacuolar-type ATPase through promotion of H<sup>+</sup>/Cl<sup>-</sup> symport. *Biochem. J.* **1998**, *334* (3), 731-741.

26. Sudbeck, E. A.; Uckun, F. M., Recent advances in JAK3 kinase inhibitors. *IDrugs : The Investigational Drugs Journal* **1999**, *2* (10), 1026-1030.

27. Sato, T.; Konno, H.; Tanaka, Y.; Kataoka, T.; Nagai, K.; Wasserman, H. H.; Ohkuma, S., Prodigiosins as a new group of H<sup>+</sup>/Cl<sup>-</sup> symporters that uncouple proton translocators. *J Biol Chem* **1998**, *273* (34), 21455-62.

28. Tanigaki, K.; Sato, T.; Tanaka, Y.; Ochi, T.; Nishikawa, A.; Nagai, K.; Kawashima, H.; Ohkuma, S., BE-18591 as a new H<sup>+</sup>/Cl<sup>-</sup> symport ionophore that inhibits immunoproliferation and gastritis. *FEBS letters* **2002**, *524* (1), 37-42.

29. Gottlieb, R. A.; Nordberg, J.; Skowronski, E.; Babior, B. M., Apoptosis induced in Jurkat cells by several agents is preceded by intracellular acidification. *Proc. Natl. Acad. Sci.* **1996**, *93* (2), 654-658.

30. Konno, H.; Matsuya, H.; Okamoto, M.; Sato, T.; Tanaka, Y.; Yokoyama, K.; Kataoka, T.; Nagai, K.; Wasserman, H. H.; Ohkuma, S., Prodigiosins uncouple mitochondrial and bacterial F-ATPases: evidence for their H<sup>+</sup>/Cl<sup>-</sup> symport activity. *J. Biochem.* **1998**, *124* (3), 547-56.

31. Seganish, J. L.; Davis, J. T., Prodigiosin is a chloride carrier that can function as an anion exchanger. *Chem. Commun.* **2005**, (46), 5781-5783.

32. Davis, J. T.; Gale, P. A.; Okunola, O. A.; Prados, P.; Iglesias-Sanchez, J. C.; Torroba, T.; Quesada, R., Using small molecules to facilitate exchange of bicarbonate and chloride anions across liposomal membranes. *Nat. Chem.* **2009**, *1* (2), 138-144.
33. Melvin, M. S.; Tomlinson, J. T.; Park, G.; Day, C. S.; Saluta, G. R.; Kucera, G. L.; Manderville, R. A., Influence of the A-ring on the proton affinity and anticancer properties of the prodigiosins. *Chem. Res. Toxicol.* **2002**, *15* (5), 734-741.
34. Park, G.; Tomlinson, J. T.; Melvin, M. S.; Wright, M. W.; Day, C. S.; Manderville, R. A., Zinc and copper complexes of prodigiosin: implications for copper-mediated double-strand DNA cleavage. *Org. Lett.* **2003**, *5* (2), 113-116.
35. Fürstner, A.; Grabowski, E. J., Studies on DNA cleavage by cytotoxic pyrrole alkaloids reveal the distinctly different behavior of roseophilin and prodigiosin derivatives. *ChemBioChem* **2001**, *2* (9), 706-709.
36. García-Valverde, M.; Alfonso, I.; Quiñonero, D.; Quesada, R., Conformational analysis of a model synthetic prodiginine. *J. Org. Chem.* **2012**, *77* (15), 6538-6544.
37. Rizzo, V.; Morelli, A.; Pinciroli, V.; Sciangula, D.; D'Alessio, R., Equilibrium and kinetics of rotamer interconversion in immunosuppressant prodigiosin derivatives in solution. *J. Pharm. Sci.* **1999**, *88* (1), 73-78.
38. La, J. Q. H.; Michaelides, A. A.; Manderville, R. A., Tautomeric equilibria in phenolic A-ring derivatives of prodigiosin natural products. *J. Phys. Chem. B* **2007**, *111* (40), 11803-11811.
39. Melvin, M. S.; Ferguson, D. C.; Lindquist, N.; Manderville, R. A., DNA binding by 4-methoxypyrrolic natural products. Preference for intercalation at AT sites by tambjamine E and prodigiosin. *J. Org. Chem.* **1999**, *64* (18), 6861-6869.
40. Han, L.; Zhou, Y.; Huang, X.; Xiao, M.; Zhou, L.; Zhou, J.; Wang, A.; Shen, J., A multi-spectroscopic approach to investigate the interaction of prodigiosin with ct-DNA. *Spectrochim. Acta, Part A* **2014**, *123*, 497-502.
41. Montaner, B.; Castillo-Ávila, W.; Martinell, M.; Öllinger, R.; Aymami, J.; Giralt, E.; Pérez-Tomás, R., DNA interaction and dual topoisomerase I and II inhibition properties of the anti-tumor drug prodigiosin. *Toxicol. Sci.* **2005**, *85* (2), 870-879.
42. Bennett, J. W.; Bentley, R., Seeing red: The story of prodigiosin. *Advances in Applied Microbiology*, Academic Press **2000** Volume *47*, 1-32.



43. Perez-Tomas, R.; Montaner, B.; Llagostera, R.; Soto-Cerrato, V., The prodigiosins, proapoptotic drugs with anticancer properties. *Biochem. Pharmacol.* **2003**, *66* (8), 1447-1452.
44. Songia, S.; Mortellaro, A.; Taverna, S.; Fornasiero, C.; Scheiber, E. A.; Erba, E.; Colotta, F.; Mantovani, A.; Isetta, A.-M.; Golay, J., Characterization of the new immunosuppressive drug undecylprodigiosin in human lymphocytes: retinoblastoma protein, cyclin-dependent kinase-2, and cyclin-dependent kinase-4 as molecular targets. *J. Immunol.* **1997**, *158* (8), 3987-3995.
45. Boyd, M. R., The NCI in vitro anticancer drug discovery screen. *Anticancer Drug Development Guide*, Springer **1997**, 23-42.
46. Soto-Cerrato, V.; Llagostera, E.; Montaner, B.; Scheffer, G. L.; Perez-Tomas, R., Mitochondria-mediated apoptosis operating irrespective of multidrug resistance in breast cancer cells by the anticancer agent prodigiosin. *Biochem. pharmacology* **2004**, *68* (7), 1345-1352.
47. Montaner, B.; Navarro, S.; Piqué, M.; Vilaseca, M.; Martinell, M.; Giralt, E.; Gil, J.; Pérez-Tomás, R., Prodigiosin from the supernatant of *Serratia marcescens* induces apoptosis in haematopoietic cancer cell lines. *Br. J. Pharmacol.* **2000**, *131* (3), 585-593.
48. Montaner, B.; Perez-Tomas, R., Prodigiosin-induced apoptosis in human colon cancer cells. *Life Sci.* **2001**, *68* (17), 2025-2036.
49. Campas, C.; Dalmau, M.; Montaner, B.; Barragán, M.; Bellosillo, B.; Colomer, D.; Pons, G.; Pérez-Tomás, R.; Gil, J., Prodigiosin induces apoptosis of B and T cells from B-cell chronic lymphocytic leukemia. *Leukemia* **2003**, *17* (4), 746-750.
50. Aida Pharmaceuticals. <http://in.reuters.com/finance/stocks/companyProfile?symbol=AIDA.PK>.
51. Melvin, M. S.; Tomlinson, J. T.; Saluta, G. R.; Kucera, G. L.; Lindquist, N.; Manderville, R. A., Double-strand DNA cleavage by copper•prodigiosin. *J. Am. Chem. Soc.* **2000**, *122* (26), 6333-6334.
52. Andrieux, C. P.; Hapiot, P.; Audebert, P.; Guyard, L.; Dinh An, M. N.; Groenendaal, L.; Meijer, E. W., Substituent effects on the electrochemical properties of pyrroles and small oligopyrroles. *Chem. Mater.* **1997**, *9* (3), 723-729.
53. Guyard, L.; Hapiot, P.; Neta, P., Redox chemistry of bipyrroles: Further insights into the oxidative polymerization mechanism of pyrrole and oligopyrroles. *J. Phys. Chem. B* **1997**, *101* (29), 5698-5706.

54. Branum, M. E.; Que Jr, L., Double-strand DNA hydrolysis by dilanthanide complexes. *JBIC* **1999**, *4* (5), 593-600.
55. Povirk, L.; Neidle, S.; Waring, M., Molecular aspects of anti-cancer drug action. *Topics in Molecular and Structural Biology (Fourth Edition)*, 3Macmillan, London **1983**, 157-181.
56. Nelson, N.; Perzov, N.; Cohen, A.; Hagai, K.; Padler, V.; Nelson, H., The cellular biology of proton-motive force generation by V-ATPases. *J. Exp. Biol.* **2000**, *203* (1), 89-95.
57. Kataoka, T.; Muroi, M.; Ohkuma, S.; Waritani, T.; Magae, J.; Takatsuki, A.; Kondo, S.; Yamasaki, M.; Nagai, K., Prodigiosin 25-C uncouples vacuolar type H<sup>+</sup>-ATPase, inhibits vacuolar acidification and affects glycoprotein processing. *FEBS Letters* **1995**, *359* (1), 53-59.
58. Woo, J.-T.; Ohba, Y.; Tagami, K.; Sumitani, K.; Kataoka, T.; Nagai, K., Prodigiosin 25-C and metacycloprodigiosin suppress the bone resorption by osteoclasts. *Biosci., Biotechnol., Biochem.* **1997**, *61* (2), 400-402.
59. Maeshima, M.; Nakayasu, T.; Kawauchi, K.; Hirata, H.; Shimmen, T., Cycloprodigiosin uncouples H<sup>+</sup>-pyrophosphatase of plant vacuolar membranes in the presence of chloride ion. *Plant Cell Physiol.* **1999**, *40* (4), 439-442.
60. Nakayasu, T.; Kawauchi, K.; Hirata, H.; Shimmen, T., Demonstration of Cl<sup>-</sup> requirement for inhibition of vacuolar acidification by cycloprodigiosin *in situ*. *Plant Cell Physiol.* **2000**, *41* (7), 857-863.
61. Nakashima, T.; Tamura, T.; Kurachi, M.; Yamaguchi, K.; Oda, T., Apoptosis-mediated cytotoxicity of prodigiosin-like red pigment produced by  $\gamma$ -proteobacterium and its multiple bioactivities. *Biol. Pharm. Bull.* **2005**, *28* (12), 2289-2295.
62. Lagadic-Gossmann, D.; Huc, L.; Lecureur, V., Alterations of intracellular pH homeostasis in apoptosis: origins and roles. *Cell Death Differ.* **2004**, *11* (9), 953-961.
63. Griffiths, J., Are cancer cells acidic? *Br. J. Cancer* **1991**, *64* (3), 425.
64. Shannon, A. M.; Bouchier-Hayes, D. J.; Condron, C. M.; Toomey, D., Tumour hypoxia, chemotherapeutic resistance and hypoxia-related therapies. *Cancer Treatment Reviews* **2003**, *29* (4), 297-307.
65. Doyle, D. A.; Cabral, J. M.; Pfuetzner, R. A.; Kuo, A.; Gulbis, J. M.; Cohen, S. L.; Chait, B. T.; MacKinnon, R., The structure of the potassium channel: molecular basis of K<sup>+</sup> conduction and selectivity. *Science* **1998**, *280* (5360), 69-77.

66. Auld, V. J.; Goldin, A. L.; Krafte, D. S.; Marshall, J.; Dunn, J. M.; Catterall, W. A.; Lester, H. A.; Davidson, N.; Dunn, R. J., A rat brain Na<sup>+</sup> channel  $\alpha$  subunit with novel gating properties. *Neuron* **1988**, *1* (6), 449-461.
67. Deisenhofer, J.; Epp, O.; Miki, K.; Huber, R.; Michel, H., Structure of the protein subunits in the photosynthetic reaction centre of. *Nature* **1985**, *318*, 618-624.
68. Andreoli, T. E.; Tieffenberg, M.; Tosteson, D. C., The effect of valinomycin on the ionic permeability of thin lipid membranes. *J. Gen. Physiol.* **1967**, *50* (11), 2527-2545.
69. Poulsen, J. H.; Fischer, H.; Illek, B.; Machen, T. E., Bicarbonate conductance and pH regulatory capability of cystic fibrosis transmembrane conductance regulator. *Proc. Natl. Acad. Sci.* **1994**, *91* (12), 5340-5344.
70. Garcia, M. A. S.; Yang, N.; Quinton, P. M., Normal mouse intestinal mucus release requires cystic fibrosis transmembrane regulator-dependent bicarbonate secretion. *J. Clin. Invest.* **2009**, *119* (9), 2613-2622.
71. Simon, D. B.; Bindra, R. S.; Mansfield, T. A.; Nelson-Williams, C.; Mendonca, E.; Stone, R.; Schurman, S.; Nayir, A.; Alpay, H.; Bakkaloglu, A., Mutations in the chloride channel gene, CLCNKB, cause Bartter's syndrome type III. *Nat. Genet.* **1997**, *17* (2), 171-178.
72. Choi, J. Y.; Muallem, D.; Kiselyov, K.; Lee, M. G.; Thomas, P. J.; Muallem, S., Aberrant CFTR-dependent HCO<sub>3</sub><sup>-</sup> transport in mutations associated with cystic fibrosis. *Nature* **2001**, *410* (6824), 94-97.
73. Chen, T.-Y.; Hwang, T.-C., CLC-0 and CFTR: chloride channels evolved from transporters. *Physiol. Rev.* **2008**, *88* (2), 351-387.
74. Gale, P. A.; Perez-Tomas, R.; Quesada, R., Anion transporters and biological systems. *Acc. Chem. Res.* **2013**, *46* (12), 2801-2813.
75. Davis, J. T.; Okunola, O.; Quesada, R., Recent advances in the transmembrane transport of anions. *Chem. Soc. Rev.* **2010**, *39* (10), 3843-3862.
76. Shen, B.; Li, X.; Wang, F.; Yao, X.; Yang, D., A synthetic chloride channel restores chloride conductance in human cystic fibrosis epithelial cells. *PLoS ONE* **2012**, *7* (4), e34694.
77. Diaz, R. I. S.; Regourd, J.; Santacrose, P. V.; Davis, J. T.; Jakeman, D. L.; Thompson, A., Chloride anion transport and copper-mediated DNA cleavage by C-ring functionalized prodigiosenes. *Chem. Commun.* **2007**, (26), 2701-2703.

78. Legg, K. D.; Hercules, D. M., Quenching of lucigenin fluorescence. *J. Phys. Chem.* **1970**, *74* (10), 2114-2118.
79. Davis, A. P.; Sheppard, D. N.; Smith, B. D., Development of synthetic membrane transporters for anions. *Chem. Soc. Rev.* **2007**, *36* (2), 348-357.
80. Busschaert, N.; Karagiannidis, L. E.; Wenzel, M.; Haynes, C. J. E.; Wells, N. J.; Young, P. G.; Makuc, D.; Plavec, J.; Jolliffe, K. A.; Gale, P. A., Synthetic transporters for sulfate: a new method for the direct detection of lipid bilayer sulfate transport. *Chem. Sci.* **2014**, *5* (3), 1118-1127.
81. Veverkova, L.; Zaruba, K.; Kral, V., Study of receptor mediated selective anion transmembrane transport using parallel artificial membrane permeability assay. *Analyst (Cambridge, U. K.)* **2013**, *138* (10), 2804-2807.
82. Yamnitz, C. R.; Negin, S.; Carasel, I. A.; Winter, R. K.; Gokel, G. W., Dianilides of dipicolinic acid function as synthetic chloride channels. *Chem. Commun.* **2010**, *46* (16), 2838-2840.
83. Chen, L.; Si, W.; Zhang, L.; Tang, G.; Li, Z.-T.; Hou, J.-L., Chiral selective transmembrane transport of amino acids through artificial channels. *J. Am. Chem. Soc.* **2013**, *135* (6), 2152-2155.
84. Atkins, J. L.; Patel, M. B.; Daschbach, M. M.; Meisel, J. W.; Gokel, G. W., Anion complexation and transport by isophthalamide and dipicolinamide derivatives: DNA plasmid transformation in e. coli. *J. Am. Chem. Soc.* **2012**, *134* (33), 13546-13549.
85. Gehin, C.; Montenegro, J.; Bang, E.-K.; Cajaraville, A.; Takayama, S.; Hirose, H.; Futaki, S.; Matile, S.; Riezman, H., Dynamic amphiphile libraries to screen for the "fragrant" delivery of siRNA into HeLa cells and human primary fibroblasts. *J. Am. Chem. Soc.* **2013**, *135* (25), 9295-9298.
86. Cooper, J. A.; Street, S. T. G.; Davis, A. P., A flexible solution to anion transport: Powerful anionophores based on a cyclohexane scaffold. *Angew. Chemie., Int. Ed.* **2014**, *53* (22), 5609-5613.
87. Haynes, C. J. E.; Gale, P. A., Transmembrane anion transport by synthetic systems. *Chem. Commun.* **2011**, *47* (29), 8203-8209.
88. Brotherhood, P. R.; Davis, A. P., Steroid-based anion receptors and transporters. *Chem. Soc. Rev.* **2010**, *39* (10), 3633-3647.

89. Dutzler, R.; Campbell, E. B.; MacKinnon, R., Gating the selectivity filter in ClC chloride channels. *Science* **2003**, *300* (5616), 108-112.
90. Dutzler, R.; Campbell, E. B.; Cadene, M.; Chait, B. T.; MacKinnon, R., X-ray structure of a ClC chloride channel at 3.0 Å reveals the molecular basis of anion selectivity. *Nature* **2002**, *415* (6869), 287-294.
91. Liu, T.; Bao, C.; Wang, H.; Lin, Y.; Jia, H.; Zhu, L., Light-controlled ion channels formed by amphiphilic small molecules regulate ion conduction via cis-trans photoisomerization. *Chem. Commun.* **2013**, *49* (87), 10311-10313.
92. Si, W.; Li, Z. T.; Hou, J. L., Voltage-driven reversible insertion into and leaving from a lipid bilayer: Tuning transmembrane transport of artificial channels. *Angew. Chemie., Int. Ed.* **2014**, *53* (18), 4578-4581.
93. Tombola, F.; Pathak, M. M.; Isacoff, E. Y., How does voltage open an ion channel? *Annu. Rev. Cell Dev. Biol.* **2006**, *22*, 23-52.
94. Elie, C.-R.; Noujeim, N.; Pardin, C.; Schmitzer, A. R., Uncovering new properties of imidazolium salts: Cl<sup>-</sup> transport and supramolecular regulation of their transmembrane activity. *Chem. Commun.* **2011**, *47* (6), 1788-1790.
95. Chhun, C.; Schmitzer, A. R., A pseudorotaxane umbrella thread with chloride transmembrane transport properties. *MedChemComm* **2011**, *2* (10), 987-990.
96. Busschaert, N.; Bradberry, S. J.; Wenzel, M.; Haynes, C. J. E.; Hiscock, J. R.; Kirby, I. L.; Karagiannidis, L. E.; Moore, S. J.; Wells, N. J.; Herniman, J.; Langley, G. J.; Horton, P. N.; Light, M. E.; Marques, I.; Costa, P. J.; Felix, V.; Frey, J. G.; Gale, P. A., Towards predictable transmembrane transport: QSAR analysis of anion binding and transport. *Chem. Sci.* **2013**, *4* (8), 3036-3045.
97. Haynes, C. J. E.; Moore, S. J.; Hiscock, J. R.; Marques, I.; Costa, P. J.; Felix, V.; Gale, P. A., Tunable transmembrane chloride transport by bis-indolylureas. *Chem. Sci.* **2012**, *3* (5), 1436-1444.
98. van de Waterbeemd, H.; Pliska, V.; Testa, B., *Lipophilicity in drug action and toxicology*. VCH, **1996**.
99. Haynes, C. J.; Busschaert, N.; Kirby, I. L.; Herniman, J.; Light, M. E.; Wells, N. J.; Marques, I.; Félix, V.; Gale, P. A., Acylthioureas as anion transporters: the effect of intramolecular hydrogen bonding. *Org. Biomol. Chem.* **2014**, *12* (1), 62-72.

100. Kumar, B. V. V. S. P.; Rao, K. V.; Sampath, S.; George, S. J.; Eswaramoorthy, M., Supramolecular gating of ion transport in nanochannels. *Angew. Chemie., Int. Ed.* **2014**, *53* (48), 13073-13077.
101. Busschaert, N.; Elmes, R. B. P.; Czech, D. D.; Wu, X.; Kirby, I. L.; Peck, E. M.; Hendzel, K. D.; Shaw, S. K.; Chan, B.; Smith, B. D.; Jolliffe, K. A.; Gale, P. A., Thiosquaramides: pH switchable anion transporters. *Chem. Sci.* **2014**, *5* (9), 3617-3626.
102. Gerber, N. N., Prodigiosin-Like Pigments. *Crit. Rev. Microbiol.* **1975**, *3* (4), 469-485.
103. Boger, D. L.; Patel, M., Total synthesis of prodigiosin, prodigiosene, and desmethoxyprodigiosin: Diels-Alder reactions of heterocyclic azadienes and development of an effective palladium(II)-promoted 2,2'-bipyrrole coupling procedure. *J. Org. Chem.* **1988**, *53* (7), 1405-1415.
104. Wasserman, H. H.; Petersen, A. K.; Xia, M.; Wang, J., Pyrrole-singlet oxygen reactions leading to  $\alpha$ ,  $\alpha'$ -bipyrroles: Synthesis of prodigiosin and analogs. *Tetrahedron Lett.* **1999**, *40* (43), 7587-7589.
105. Wasserman, H. H.; Xia, M.; Wang, J.; Petersen, A. K.; Jorgensen, M.; Power, P.; Parr, J., Singlet oxygen reactions of 3-methoxy-2-pyrrole carboxylic acid *tert*-butyl esters. A route to 5-substituted pyrrole precursors of prodigiosin and analogs. *Tetrahedron* **2004**, *60* (34), 7419-7425.
106. Dairi, K.; Tripathy, S.; Attardo, G.; Lavallée, J.-F., Two-step synthesis of the bipyrrole precursor of prodigiosins. *Tetrahedron Lett.* **2006**, *47* (15), 2605-2606.
107. Jolicoeur, B.; Lubell, W. D., Prodigiosin synthesis with electron rich 2, 2'-bipyrroles. *Can. J. Chem.* **2008**, *86* (3), 213-218.
108. Ellington, A.; Rosenblum, M. Targeted chimeric molecules for cancer therapy. **2006** U.S. Patent Application 11/329,362.
109. Matsuya, H.; Okamoto, M.; Ochi, T.; Nishikawa, A.; Shimizu, S.; Kataoka, T.; Nagai, K.; Wasserman, H. H.; Ohkuma, S., Reversible and potent uncoupling of hog gastric ( $H^+K^+$ )-ATPase by prodigiosins. *Biochem. Pharmacol.* **2000**, *60* (12), 1855-1863.
110. Baldino, C. M.; Parr, J.; Wilson, C. J.; Ng, S.-C.; Yohannes, D.; Wasserman, H. H., Indoloprodigiosins from the C-10 bipyrrole precursor: New antiproliferative prodigiosin analogs. *Bioorg. Med. Chem. Lett.* **2006**, *16* (3), 701-704.

111. Hawco, C. L.; Marchal, E.; Uddin, M. I.; Baker, A. E.; Corkery, D. P.; Dellaire, G.; Thompson, A., Synthesis and biological evaluation of prodigiosene conjugates of porphyrin, estrone and 4-hydroxytamoxifen. *Bioorg. Med. Chem.* **2013**, *21* (19), 5995-6002.
112. Uddin, M. I.; Thirumalairajan, S.; Crawford, S. M.; Cameron, T. S.; Thompson, A., Improved synthetic route to C-ring ester-functionalized prodigiosenes. *Synlett* **2010**, *2010* (17), 2561-2564.
113. McNally, B. A.; Koulov, A. V.; Smith, B. D.; Joos, J.-B.; Davis, A. P., A fluorescent assay for chloride transport; identification of a synthetic anionophore with improved activity. *Chem. Commun.* **2005**, (8), 1087-1089.
114. Rastogi, S.; Marchal, E.; Uddin, I.; Groves, B.; Colpitts, J.; McFarland, S. A.; Davis, J. T.; Thompson, A., Synthetic prodigiosenes and the influence of C-ring substitution on DNA cleavage, transmembrane chloride transport and basicity. *Org. Biomol. Chem.* **2013**, *11* (23), 3834-3845.
115. Anslyn, E. V.; Dougherty, D. A., *Modern physical organic chemistry*. University Science Books, **2006**.
116. Stern, O.; Volmer, M., The extinction period of fluorescence. *Phys. Z* **1919**, *20*, 183-188.
117. Seganish, J. L.; Santacrose, P. V.; Salimian, K. J.; Fettinger, J. C.; Zavalij, P.; Davis, J. T., Regulating supramolecular function in membranes: Calixarenes that enable or inhibit transmembrane Cl<sup>-</sup> transport. *Angew. Chem., Int. Ed.* **2006**, *45* (20), 3334-3338.
118. Saggiomo, V.; Otto, S.; Marques, I.; Félix, V.; Torroba, T.; Quesada, R., The role of lipophilicity in transmembrane anion transport. *Chem. Commun.* **2012**, *48* (43), 5274-5276.
119. Busschaert, N.; Wenzel, M.; Light, M. E.; Iglesias-Hernandez, P.; Perez-Tomas, R.; Gale, P. A., Structure-activity relationships in tripodal transmembrane anion transporters: The Effect of Fluorination. *J. Am. Chem. Soc.* **2011**, *133* (35), 14136-14148.
120. Busschaert, N.; Gale, P. A.; Haynes, C. J. E.; Light, M. E.; Moore, S. J.; Tong, C. C.; Davis, J. T.; Harrell, W. A., Jr., Tripodal transmembrane transporters for bicarbonate. *Chem. Commun.* **2010**, *46* (34), 6252-6254.
121. NCI-60 DTP Human Tumor Cell Line Screen, Developmental Therapeutics Program, NCI/NIH. <http://dtp.cancer.gov>.

122. Valkenier, H.; Davis, A. P., Making a match for valinomycin: Steroidal scaffolds in the design of electroneutral, electrogenic anion carriers. *Acc. Chem. Res.* **2013**, *46* (12), 2898-2909.
123. Alfonso, I.; Quesada, R., Biological activity of synthetic ionophores: ion transporters as prospective drugs? *Chem. Sci.* **2013**, *4* (8), 3009-3019.
124. Oblatt-Montal, M.; Reddy, G. L.; Iwamoto, T.; Tomich, J. M.; Montal, M., Identification of an ion channel-forming motif in the primary structure of CFTR, the cystic fibrosis chloride channel. *Proc. Natl. Acad. Sci.* **1994**, *91* (4), 1495-1499.
125. Schlesinger, P. H.; Ferdani, R.; Liu, J.; Pajewska, J.; Pajewski, R.; Saito, M.; Shabany, H.; Gokel, G. W., SCMTR: a chloride-selective, membrane-anchored peptide channel that exhibits voltage gating. *J. Am. Chem. Soc.* **2002**, *124* (9), 1848-1849.
126. McNally, B. A.; Koulov, A. V.; Lambert, T. N.; Smith, B. D.; Joos, J.-B.; Sisson, A. L.; Clare, J. P.; Sgarlata, V.; Judd, L. W.; Magro, G.; Davis, A. P., Structure-activity relationships in cholapod anion carriers: Enhanced transmembrane chloride transport through substituent tuning. *Chem. – Eur. J.* **2008**, *14* (31), 9599-9606.
127. Koulov, A. V.; Lambert, T. N.; Shukla, R.; Jain, M.; Boon, J. M.; Smith, B. D.; Li, H.; Sheppard, D. N.; Joos, J. B.; Clare, J. P., Chloride transport across vesicle and cell membranes by steroid-based receptors. *Angew. Chem., Int. Ed.* **2003**, *42* (40), 4931-4933.
128. Gale, P. A.; Light, M. E.; McNally, B.; Navakhun, K.; Sliwinski, K. E.; Smith, B. D., Co-transport of H<sup>+</sup>/Cl<sup>-</sup> by a synthetic prodigiosin mimic. *Chem. Commun.* **2005**, (30), 3773-3775.
129. Pérez-Tomas, R.; Vinas, M., New insights on the antitumoral properties of prodiginines. *Curr. Med. Chem.* **2010**, *17* (21), 2222-2231.
130. Fűrstner, A., Chemistry and biology of roseophilin and the prodigiosin alkaloids: a survey of the last 2500 years. *Angew. Chem., Int. Ed.* **2003**, *42*, 3582-3603.
131. Marchal, E.; Rastogi, S.; Thompson, A.; Davis, J. T., Influence of B-ring modifications on proton affinity, transmembrane anion transport and anti-cancer properties of synthetic prodigiosenes. *Org. Biomol. Chem.* **2014**, *12* (38), 7515-7522.
132. Hearn, W. R.; Medina-Castro, J.; Elson, M. K., Colour change of prodigiosin. *Nature* **1968**, *220* (5163), 170-171.
133. Shoemaker, R. H., The NCI60 human tumour cell line anticancer drug screen. *Nat. Rev. Cancer* **2006**, *6* (10), 813-823.



134. Blake, A. J.; Hunter, G. A.; McNab, H., A short synthesis of prodigiosin analogues. *J. Chem. Soc., Chem. Commun.* **1990**, (10), 734-736.
135. Hua, Y.; Flood, A. H., Click chemistry generates privileged CH hydrogen-bonding triazoles: the latest addition to anion supramolecular chemistry. *Chem. Soc. Rev.* **2010**, 39 (4), 1262-1271.
136. Bryantsev, V. S.; Hay, B. P., Are CH groups significant hydrogen bonding sites in anion receptors? Benzene complexes with  $\text{Cl}^-$ ,  $\text{NO}_3^-$ , and  $\text{ClO}_4^-$ . *J. Am. Chem. Soc.* **2005**, 127 (23), 8282-8283.
137. Li, Y.; Flood, A. H., Pure C-H hydrogen bonding to chloride ions: A preorganized and rigid macrocyclic receptor. *Angew. Chem., Int. Ed.* **2008**, 47 (14), 2649-2652.
138. Sessler, J. L.; Cai, J.; Gong, H.-Y.; Yang, X.; Arambula, J. F.; Hay, B. P., A pyrrolyl-based triazolophane: A macrocyclic receptor with CH and NH donor groups that exhibits a preference for pyrophosphate anions. *J. Am. Chem. Soc.* **2010**, 132 (40), 14058-14060.
139. Hernando, E.; Soto-Cerrato, V.; Cortes-Arroyo, S.; Perez-Tomas, R.; Quesada, R., Transmembrane anion transport and cytotoxicity of synthetic tambjamine analogs. *Org. Biomol. Chem.* **2014**, 12 (11), 1771-1778.
140. Nager, U. F., Prodigiosin gluconate. **1954**, US Patent 2,673,855.
141. *Advanced Chemistry Development [ACD/Labs] Software VII.02*, © 1994-2014 ACD/Labs.
142. Dimitrov, D.; Boyanoff, A.; Todorov, T., A study of the association of prodigiosin, isolated from *Serratia marcescens*. *Zeitschrift fur Naturforschung. Teil B: Chemie, Biochemie, Biophysik, Biologie* **1970**, 25 (1), 46-48.
143. Gellert, M.; Lipsett, M. N.; Davies, D. R., Helix formation by guanylic acid. *Proc. Natl. Acad. Sci.* **1962**, 48 (12), 2013-2018.
144. Riou, J.-F., G-quadruplex interacting agents targeting the telomeric G-overhang are more than simple telomerase inhibitors. *Curr. Med. Chem.-Anti-Cancer Agents* **2004**, 4 (5), 439-443.
145. Ou, T. M.; Lu, Y. J.; Tan, J. H.; Huang, Z. S.; Wong, K. Y.; Gu, L. Q., G-quadruplexes: Targets in anticancer drug design. *Chemmedchem* **2008**, 3 (5), 690-713.

146. Neidle, S.; Balasubramanian, S., *Quadruplex nucleic acids*. Royal Society of Chemistry, **2006**, Vol. 7.
147. Davis, J. T., G-Quartets 40 years later: From 5'-GMP to molecular biology and supramolecular chemistry. *Angew. Chem., Int. Ed.* **2004**, *43* (6), 668-698.
148. Nakano, S.-i.; Miyoshi, D.; Sugimoto, N., Effects of molecular crowding on the structures, interactions, and functions of nucleic acids. *Chem. Rev.* **2013**, *114* (5), 2733-2758.
149. Burge, S.; Parkinson, G. N.; Hazel, P.; Todd, A. K.; Neidle, S., Quadruplex DNA: sequence, topology and structure. *Nucleic Acids Res.* **2006**, *34* (19), 5402-5415.
150. Bearss, D. J.; Hurley, L. H.; Von Hoff, D. D., Telomere maintenance mechanisms as a target for drug development. *Oncogene* **2000**, *19* (56), 6632-6641.
151. Alberti, P.; Lacroix, L.; Guittat, L.; Helene, C.; Mergny, J.-L., Nucleic acids as targets for antitelomerase agents. *Mini Rev. Med. Chem.* **2003**, *3* (1), 23-36.
152. Arola, A.; Vilar, R., Stabilisation of G-quadruplex DNA by small molecules. *Curr. Top. Med. Chem.* **2008**, *8* (15), 1405-1415.
153. Balasubramanian, S.; Neidle, S., G-quadruplex nucleic acids as therapeutic targets. *Curr. Opin. Chem. Biol.* **2009**, *13* (3), 345-353.
154. Mohanty, J.; Barooah, N.; Dhamodharan, V.; Harikrishna, S.; Pradeepkumar, P.; Bhasikuttan, A. C., Thioflavin T as an efficient inducer and selective fluorescent sensor for the human telomeric G-quadruplex DNA. *J. Am. Chem. Soc.* **2012**, *135* (1), 367-376.
155. Guo, Q.; Lu, M.; Marky, L. A.; Kallenbach, N. R., Interaction of the dye ethidium bromide with DNA containing guanine repeats. *Biochemistry* **1992**, *31* (9), 2451-2455.
156. Kim, M.-Y.; Vankayalapati, H.; Shin-ya, K.; Wierzba, K.; Hurley, L. H., Telomestatin, a potent telomerase inhibitor that interacts quite specifically with the human telomeric intramolecular G-quadruplex. *J. Am. Chem. Soc.* **2002**, *124* (10), 2098-2099.
157. Rosu, F.; Gabelica, V.; Smargiasso, N.; Mazzucchelli, G.; Shin-Ya, K.; De Pauw, E., Cation involvement in telomestatin binding to G-quadruplex DNA. *Journal of nucleic acids* **2010**, *2010*, Article ID 121259, 7 pages, doi:10.4061/2010/121259.

158. Martino, L.; Virno, A.; Pagano, B.; Virgilio, A.; Di Micco, S.; Galeone, A.; Giancola, C.; Bifulco, G.; Mayol, L.; Randazzo, A., Structural and thermodynamic studies of the interaction of distamycin A with the parallel quadruplex structure [d(TGGGGT)]<sub>4</sub>. *J. Am. Chem. Soc.* **2007**, *129* (51), 16048-16056.
159. Cocco, M. J.; Hanakahi, L.; Huber, M. D.; Maizels, N., Specific interactions of distamycin with G-quadruplex DNA. *Nucleic Acids Res.* **2003**, *31* (11), 2944-2951.
160. Wei, C.; Jia, G.; Yuan, J.; Feng, Z.; Li, C., A spectroscopic study on the interactions of porphyrin with G-quadruplex DNAs. *Biochemistry* **2006**, *45* (21), 6681-6691.
161. Anantha, N. V.; Azam, M.; Sheardy, R. D., Porphyrin binding to quadruplexed T<sub>4</sub>G<sub>4</sub>. *Biochemistry* **1998**, *37* (9), 2709-2714.
162. Nygren, J.; Svanvik, N.; Kubista, M., The interactions between the fluorescent dye thiazole orange and DNA. *Biopolymers* **1998**, *46* (1), 39-51.
163. Monchaud, D.; Allain, C.; Teulade-Fichou, M.-P., Development of a fluorescent intercalator displacement assay (G4-FID) for establishing quadruplex-DNA affinity and selectivity of putative ligands. *Bioorg. Med. Chem. Lett.* **2006**, *16* (18), 4842-4845.
164. Nakamoto, K.; Tsuboi, M.; Strahan, G. D., *Drug-DNA interactions: structures and spectra*. John Wiley & Sons, **2008**, Vol. 51.
165. Aboul-ela, F.; Murchie, A.; Lilley, D., NMR study of parallel-stranded tetraplex formation by the hexadeoxynucleotide d(TG<sub>4</sub>T). *Nature* **1992**, *360* (6401), 280.
166. Shi, X.; Mullaugh, K. M.; Fettingner, J. C.; Jiang, Y.; Hofstadler, S. A.; Davis, J. T., Lipophilic G-quadruplexes are self-assembled ion pair receptors, and the bound anion modulates the kinetic stability of these complexes. *J. Am. Chem. Soc.* **2003**, *125* (36), 10830-10841.
167. Forman, S. L.; Fettingner, J. C.; Pieraccini, S.; Gottarelli, G.; Davis, J. T., Toward artificial ion channels: A lipophilic G-quadruplex. *J. Am. Chem. Soc.* **2000**, *122* (17), 4060-4067.
168. Welsh, R. S., Nondegradative isolation of Desoxyribonucleic acid in subunit form from calf thymus nuclei. *Proc. Natl. Acad. Sci.* **1962**, *48* (5), 887-893.
169. Pommier, Y., Topoisomerase I inhibitors: camptothecins and beyond. *Nat. Rev. Cancer* **2006**, *6* (10), 789-802.

170. Aboul-ela, F.; Murchie, A. I.; Norman, D. G.; Lilley, D. M., Solution structure of a parallel-stranded tetraplex formed by d(TG<sub>4</sub>T) in the presence of sodium ions by nuclear magnetic resonance spectroscopy. *J. Mol. Biol.* **1994**, *243* (3), 458-471.
171. Wei, C.; Wang, L.; Jia, G.; Zhou, J.; Han, G.; Li, C., The binding mode of porphyrins with cation side arms to (TG<sub>4</sub>T)<sub>4</sub> G-quadruplex: Spectroscopic evidence. *Biophys. Chem.* **2009**, *143* (1), 79-84.
172. Wüthrich, K., *NMR of proteins and nucleic acids*. Wiley New York, **1986**, Vol. 155.
173. Negin, S.; Gokel, M. R.; Patel, M. B.; Sedinkin, S. L.; Osborn, D. C.; Gokel, G. W., The aqueous medium-dimethylsulfoxide conundrum in biological studies. *RSC Adv.* **2015**, *5* (11), 8088-8093.
174. Williams, A. C.; Barry, B. W., Penetration enhancers. *Adv. Drug Delivery Rev.* **2004**, *56* (5), 603-618.
175. Heddi, B.; Phan, A. T., Structure of human telomeric DNA in crowded solution. *J. Am. Chem. Soc.* **2011**, *133* (25), 9824-9833.
176. Mergny, J.-L.; De Cian, A.; Ghelab, A.; Sacca, B.; Lacroix, L., Kinetics of tetramolecular quadruplexes. *Nucleic Acids Res.* **2005**, *33* (1), 81-94.
177. Dalvit, C.; Bovermann, G., Pulsed-field gradient one-dimensional NMR selective ROE and TOCSY experiments. *Magn. Reson. Chem.* **1995**, *33* (2), 156-159.
178. Mayer, M.; Meyer, B., Characterization of ligand binding by saturation transfer difference NMR spectroscopy. *Angew. Chem., Int. Ed.* **1999**, *38* (12), 1784-1788.
179. Mayer, M.; Meyer, B., Group epitope mapping by saturation transfer difference NMR to identify segments of a ligand in direct contact with a protein receptor. *J. Am. Chem. Soc.* **2001**, *123* (25), 6108-6117.
180. Li, Q.; Xiang, J.-F.; Yang, Q.-F.; Sun, H.-X.; Guan, A.-J.; Tang, Y.-L., G4LDB: a database for discovering and studying G-quadruplex ligands. *Nucleic Acids Res.* **2013**, *41* (1), 1115-1123.
181. Hejazi, A.; Falkiner, F. R., *Serratia marcescens*. *J. Med. Microbiol.* **1997**, *46* (11), 903-912.
182. Sessler, J. L.; Weghorn, S. J.; Lynch, V.; Fransson, K., 5,15,25-tris-nor-Hexapyrrin: the first structurally characterized linear hexapyrrin. *J. Chem. Soc., Chem. Commun.* **1994**, (11), 1289-1290.

183. Chang, T. M.; Sinharay, S.; Astashkin, A. V.; Tomat, E., Prodigiosin analogue designed for metal coordination: Stable zinc and copper pyrrolyldipyrins. *Inorg. Chem.* **2014**, *53* (14), 7518-7526.
184. Bhosale, S.; Matile, S., A simple method to identify supramolecules in action: Hill coefficients for exergonic self-assembly. *Chirality* **2006**, *18* (10), 849-856.
185. Permyakov, E. A., *Luminescent spectroscopy of proteins*. CRC press, **1992**.
186. Piotto, M.; Saudek, V.; Sklenar, V., Gradient-tailored excitation for single-quantum NMR-spectroscopy of aqueous-solutions. *J. Biomol. NMR* **1992**, *2* (6), 661-665.
187. Jeener, J.; Meier, B.; Bachmann, P.; Ernst, R., Investigation of exchange processes by two-dimensional NMR spectroscopy. *J. Chem. Phys.* **1979**, *71* (11), 4546-4553.
188. Wagner, R.; Berger, S., Gradient-selected NOESY—a fourfold reduction of the measurement time for the NOESY experiment. *J. Magn. Reson., Series A* **1996**, *123* (1), 119-121.
189. Marion, D.; Ikura, M.; Tschudin, R.; Bax, A., Rapid recording of 2D NMR spectra without phase cycling. Application to the study of hydrogen exchange in proteins. *J. Magn. Reson.* **1989**, *85* (2), 393-399.
190. Cantor, C. R.; Warshaw, M. M.; Shapiro, H., Oligonucleotide interactions. III. Circular dichroism studies of the conformation of deoxyoligonucleolides. *Biopolymers* **1970**, *9* (9), 1059-1077.
191. Hwang, T.-L.; Shaka, A., Water suppression that works. Excitation sculpting using arbitrary wave-forms and pulsed-field gradients. *J. Magn. Reson., Series A* **1995**, *112* (2), 275-279.
192. Luy, B.; Marino, J. P., <sup>1</sup>H-<sup>31</sup>P CPMG-correlated experiments for the assignment of nucleic acids. *J. Am. Chem. Soc.* **2001**, *123* (45), 11306-11307.
193. Mulder, F. A.; Spronk, C. A.; Slijper, M.; Kaptein, R.; Boelens, R., Improved HSQC experiments for the observation of exchange broadened signals. *J. Biomol. NMR* **1996**, *8* (2), 223-228.
194. Davis, A. L.; Keeler, J.; Laue, E. D.; Moskau, D., Experiments for recording pure-absorption heteronuclear correlation spectra using pulsed field gradients. *J. Magn. Reson.* **1992**, *98* (1), 207-216.

195. Kessler, H.; Oschkinat, H.; Griesinger, C.; Bermel, W., Transformation of homonuclear two-dimensional NMR techniques into one-dimensional techniques using Gaussian pulses. *J. Magn. Reson. (1969)* **1986**, *70* (1), 106-133.
196. Stonehouse, J.; Adell, P.; Keeler, J.; Shaka, A., Ultrahigh-quality NOE spectra. *J. Am. Chem. Soc.* **1994**, *116* (13), 6037-6038.
197. Stott, K.; Stonehouse, J.; Keeler, J.; Hwang, T.-L.; Shaka, A., Excitation sculpting in high-resolution nuclear magnetic resonance spectroscopy: application to selective NOE experiments. *J. Am. Chem. Soc.* **1995**, *117* (14), 4199-4200.
198. Bax, A.; Davis, D. G., MLEV-17-based two-dimensional homonuclear magnetization transfer spectroscopy. *J. Magn. Reson.* **1985**, *65* (2), 355-360.